Nowicki, Stefan Andrzej (2016) *The metabolic and epigenetic effects of the isocitrate dehydrogenase-1 mutation in glioma*. PhD thesis.

http://theses.gla.ac.uk/7300/

Copyright and moral rights for this thesis are retained by the author

A copy can be downloaded for personal non-commercial research or study

This thesis cannot be reproduced or quoted extensively from without first obtaining permission in writing from the Author

The content must not be changed in any way or sold commercially in any format or medium without the formal permission of the Author

When referring to this work, full bibliographic details including the author, title, awarding institution and date of the thesis must be given

Glasgow Theses Service
http://theses.gla.ac.uk/
theses@gla.ac.uk

The Metabolic and Epigenetic Effects of the Isocitrate Dehydrogenase-1 Mutation in Glioma

Stefan Andrzej Nowicki

Thesis submitted to the University of Glasgow in accordance with the requirements for the degree of Doctor of Philosophy

CRUK Beatson Institute
Garscube Estate
Switchback Road
Bearsden, Glasgow

Institute of Cancer Science
College of Medical, Veterinary and Life Sciences
University of Glasgow
October 2015

Abstract

Cancer cells have been noted to have an altered metabolic phenotype for over ninety years. In the presence of oxygen, differentiated cells predominately utilise the tricarboxylic acid (TCA) cycle and oxidative phosphorylation to efficiently produce energy and the metabolites necessary for protein and lipid synthesis. However, in hypoxia, this process is altered and cells switch to a higher rate of glycolysis and lactate production to maintain their energy and metabolic needs. In cancer cells, glycolysis is maintained at a high rate, even in the presence of oxygen; a term described as "aerobic glycolysis". Tumour cells are rapidly dividing and have a much greater need for anabolism compared to normal differentiated cells. Rapid glucose metabolism enables faster ATP production as well as a greater redistribution of carbons to nucleotide, protein, and fatty acid synthesis, thus maximising cell growth. Recently, other metabolic changes, driven by mutations in genes related to the TCA cycle, indicate an alternative role for metabolism in cancer, the "oncometabolite". This is where a particular metabolite builds up within the cell and contributes to the tumorigenic process. One of these genes is isocitrate dehydrogenase (IDH)

IDH is an enzyme that forms part of the tricarboxylic acid (TCA) cycle and converts isocitrate to α-ketoglutarate (α-KG). It exists in three isoforms; IDH1, IDH2 and IDH3 with the former present in the cytoplasm and the latter two in the mitochondria. Point mutations have been identified in the IDH1 and IDH2 genes in glioma which result in a gain of function by converting α-KG to 2-hydroxyglutarate (2HG), an oncometabolite. 2HG acts as a competitive inhibitor of the α-KG dependent dioxygenases, a superfamily of enzymes that are involved in numerous cellular processes such as DNA and histone demethylation.

It was hypothesised that the IDH1 mutation would result in other metabolic changes in the cell other than 2HG production, and could potentially identify pathways which could be targeted for therapeutic treatment. In addition, 2HG can act as a potential competitive inhibitor of α-KG dependent dioxygenases, so it was hypothesised that there would be an effect on histone methylation. This may alter gene expression and provide a mechanism for tumourogenesis and potentially identify further therapeutic targets.

Metabolic analysis of clinical tumour samples identified changes associated with the IDH1 mutation, which included a reduction in α-KG and an increase in GABA, in addition to the increase in 2HG. This was replicated in several cell models, where ^{13}C labelled metabolomics was also used to identify a possible increase in metabolic flux from glutamate to GABA, as well as from α-KG to 2HG. This may provide a mechanism whereby the cell can bypass the IDH1 mutation as GABA can be metabolised to succinate in the mitochondria by GABA transaminase via the GABA shunt.

JMJ histone demethylases are a subset of the α-KG dependent dioxygenases, and are involved in removing methyl groups from histone tails. Changes in histone methylation are associated with changes in gene expression depending on the site and extent of chemical modification. To identify whether the increase in 2HG and fall in α-KG was associated with inhibition of histone demethylases a histone methylation screen was used. The IDH1 mutation was associated with an increase in methylation of H3K4, which is associated with gene activation. ChiP and RNA sequencing identified an increase in H3K4me3 at the transcription start site of the GABRB3 subunit, resulting in an increase in gene expression. The GABRB3 subunit forms part of the GABA-A receptor, a chloride channel, which on activation can reduce cell proliferation.

The IDH1 mutation was associated with an increase in GABA and GABRB3 subunit of the GABA-A receptor. This raises the possibility of GABA transaminase as a potential therapeutic target. Inhibition of this enzyme could reduce GABA metabolism, potentially reducing any beneficial effect of the GABA shunt in IDH1 mutant tumours, and increasing activation of the GABA-A receptor by increasing the concentration of GABA in the brain. This in turn may reduce cell proliferation, and could be achieved by using Vigabatrin, a GABA transaminase inhibitor licensed for use in epilepsy.

Table of Contents

List of Tables

List of Figures

Acknowledgement

I would like to thank Cancer Research UK for funding my three and a half year PhD at the Beatson Institute for Cancer research.

I would like to thank my supervisor Professor Eyal Gottlieb and advisor Professor Anthony Chalmers, for helping me develop a better understanding of basic science and how it relates to medicine. To Eyal, special thanks for giving me the chance to work with you and being part of an amazing lab. I very much enjoyed our discussions together and I feel very grateful for the opportunities you gave me.

I would like to thank everyone from R12 who have made this whole experience so enjoyable. In particular, I would like to thank Saverio for always having the time to listen and help me as well as teaching me how to gesture like an Italian! To Leon, Johann, Zach, Nadia, and Simone, the other post-docs in the lab, thank you for your continuous motivation and help. I would also like to thank the other PhD students in our lab; Barbara, Elodie and Laura for all the great conversation and coffees, and in particular, Jiska for being a great friend. I would also like to thank Henry, the clinical fellow, who always seemed to cheer me up while I was writing my thesis.

There are people I would like to thank outside of my lab. To Pearl, who worked beside me for her fantastic baking and conversation. To Alice for being great fun and making a long stint in tissue culture bearable. Also to the other oncology clinical fellows who started at the same time as me; Ross, Anne and Jen for going through this journey with me.

Finally, I would like to thank my family for all their love and support. In particular, to my children Xavier and Zane who always reminded me that there are more important things in life than work and to my wife Emma as without her continuous support this thesis would not have been possible.

Author's Declaration

I hereby declare that the worked presented in this thesis is the result of my own independent investigation unless otherwise stated. The introduction contains sections reproduced from a review written by me with the approval of the Federation of European Biochemical Societies (FEBS) journal [1].

This work has not hitherto been accepted for any other degree, nor is it being currently submitted for any other degree

Stefan Andrzej Nowicki

Definitions/Abbreviations

2HG – 2-hydroxyglutarate

5-hmC - 5-hydroxymethylcytosine

5-mC - 5-methylcytosine

ACLY - ATP-citrate lyase

ACSS2 - actyl-CoA synthetase short-chain family member 2

α-KG - α-ketoglutarate

AML - acute myeloid leukaemia

APS - ammonium persulfate

ASR – age standardised rate

BCAT1 - branch chain amino acid transferase 1

CIMP - CpG island methylator phenotype

CoA - coenzyme A

CT – computer tomography

D-2HGA - D-2-hydroxyglutaric aciduria

DMOG – dimethyloxaloylglycine

DMSO - dimethyl sulfoxide

DNMT - DNA methyltransferases

EDTA - ethylenediamine tetraacetic acid

EGFR – epidermal growth factor receptor

EGTA - ethylene glycol tetraacetic acid

EV – overexpressed empty vector MOG-GCCM cells

EV + 2HG - EV maintained ≥ 15 passages in 30 mM cell permeable 2HG-lactone

FAD - flavin adenine dinucleotide

FDG-PET - ^{18}F-deoxyglucose positron emission tomography

FH - fumarate hydratase

GABA – γ-aminobutyric acid

GABA-T – GABA transaminase

GABR(A1-6, B1-3, D, E, G1-3, P, Q, R1-3) – GABA-A receptor subunits α, β, δ, ε, γ, π, θ, and ρ, respectively

GAD - glutamate decarboxylase

GBM – glioblastoma multiforme

G-CIMP – glioma CpG island hypermethylation

GSH - glutathione

GSSG – glutathione disulfide

H6P - hexose-6-phophate

HA - haemaglutinin

HAT - histone acetyltransferases

HDAC - histone deacetylases

HDM - histone demethylases

HIF - hypoxia inducible factor

HLRCC - hereditary leiomyomatosis and renal cell cancer

HMT - histone methyltransferases

HPLC - high performance liquid chromatography

IDH1/2/3 – isocitrate dehydrogenase 1/2/3

JMJ - jumonji-C

LC-MS - liquid chromatography mass spectrometry

L-2HGA - L-2- hydroxyglutaric aciduria

LSD - lysine specific demethylase

MAPK – mitogen-activated protein kinase

MC3/9/10 – overexpressed $IDH1^{R132H}$ mutant MOG-GCCM clones

MOG-GCCM – anaplastic astrocytoma cell line

MRI – magnetic resonance imaging

MRSI – magnetic resonance spectroscopy imaging

mTHF – methylthetrahydrofolate

Mut - overexpressed $IDH1^{R132H}$ mutant immortalised astrocytes

NAA - N-acetylaspartate

NAAG - N-acetylaspartylglutamate

NSC – neural stem cell

OPC - oligodendrocyte precursor cell

PBS – phosphate buffered saline

PCL – parental cell line

PCV - procarbizine, lomustine and vincristine

PFA - paraformaldehyde

PI3K – phosphatidyl inositol-3-kinase

PDGFR – platelet derived growth factor receptor

PHD - prolyl hydroxylases

ROS - reactive oxygen species

SAM - s-adenylmethionine

SDH - succinate dehydrogenase

SDS - sodium dodecyl sulphate

SSA – succinate semi-aldehyde

TAE - Tris-acetate-EDTA

TEMED - tetramethylethylenediamine

TET - ten-eleven-translocation methylcytosine dioxygenase

TCA - tricarboxylic acid

THF – tetrahydrofolate

TSS - transcription start site

WHO – World Health Organisation

WT – overexpressed IDH1 wild-type immortalised astrocytes

VEGF - vascular endothelial growth factor

VHL - von Hippel-Lindau

Chapter 1 Introduction

1.1 Neurobiology

1.1.1 Neurons

The brain consists of two groups of cells; neurons and neuroglia. Neurons facilitate the transmission of information through electrical and chemical impulses. All neurons contain four distinct regions, each with their own unique function. These are the cell body, axon, axon terminal and the dendrites. The cell body is where all neuronal proteins and membranes are synthesised. Microtubules in axons facilitate the transport of these proteins to the axon terminal, and also the movement of damaged membranes and organelles back to the cell body. Each neuron has a single axon, which can extend along the whole length of the central nervous system. This region is where a specialised electrical impulse is transmitted, called the action potential. The action potential is propagated along the axon by a series of rapid depolarisation and repolarisation events across the plasma membrane [2]. The action potential travels from the cell body, down the axon, into small branches called axon terminals which form connections with other cells via synapses. Depending on the target cell, this may result in neuronal stimulation, muscle contraction, or hormone release.

Dendrites are extensions from the neuronal cell body that form part of the synapse with axon terminals. The most common type of synapse is the chemical synapse. In this case, the axon terminal contains vesicles of neurotransmitters, such as glutamate and γ-aminobutyric acid (GABA). These are released into the synaptic cleft in response to an increase in cytosolic Ca^{2+} induced by the arrival of an action potential. The dendrites convert the chemical signal into electrical signals through neurotransmitter receptors on the post-synaptic membrane. These propagate back to the cell body producing a new action potential if the change in membrane potential is large enough. Neurons have numerous dendrites that can stretch for long distances, allowing them to receive signals from a large number of other neurons, producing a complex electrical circuit within the nervous system.

1.1.2 Neuroglia

Over 150 years ago, Virchow created the term neuroglia to describe the cells that hold neurons together and create the structure of the brain [3]. Over the next 50 years these cells were further subdivided into astrocytes, oligodendrocytes, and microglia [4]. These cells were initially thought to have no other function than filling the space between neurons [5], but over the last century it has become increasingly evident that they possess more complex functions.

1.1.2.1 Astrocytes

The possibility of astrocytes providing a function other than scaffolding for neurons was first raised at the turn of the twentieth century by Carl Ludwig Schleich. He raised the concept of astrocytes modulating neuronal transmission through movement between nerve cells. We now know that astrocytes interact with neurons through the formation and maintenance of synapses, altering their potency and plasticity. They achieve this through the presence of numerous neurotransmitter receptors on their perisynaptic processes [6, 7]. This allows them to perceive synaptic transmission and respond by releasing neurotransmitters or altering neurotransmitter uptake, thus modulating the transmission dynamics in the synaptic cleft [8-10]. The type and number of these neurotransmitter receptors varies dependent on the neurons involved and the region of the brain. The complexity of the interaction between astrocytes and neurons is reflected in the number of connections between the two cell types. In rodents, every astrocyte is in contact with approximately 1×10^5 synapses, compared to approximately 2×10^6 synapses in a human brain [11]. This underlines the functional importance of astrocytes as cognitive complexity increases.

Astrocytes are important in maintaining neuronal function. They have perivascular end-feet allowing for regulation of vascular tone and thus the supply of nutrients to cells. In addition, they regulate the extracellular space by controlling ion and water movement. Astrocytes may have a neuroprotective effect through modulating extracellular pH and by acting as a major source of anti-oxidants, such as glutathione [12]. Astrocytes also have intrinsic signalling

properties in the form of Ca^{2+} waves, which can spread between cells and correlates with the release of glutamate [13, 14]. This may be facilitated by gap-junctions between astrocytes, and also between astrocytes and oligodendrocytes, providing a potential alternative signalling network [15]. Finally, some astrocytes have been shown to differentiate into other neural cells such as neurons or microglia, raising the possibility of stem cell properties [16].

1.1.2.2 Oligodendrocytes

The two other cell types that make up the neuroglia are oligodendrocytes and microglia. Oligodendrocytes act in a similar way to Schwann cells in the peripheral nervous system. They facilitate neuronal impulses through the formation of a myelin sheath, which acts to electrically isolate axons. This allows for the salutatory propagation of action potentials. Like astrocytes, they also possess neurotransmitter receptors, which can sense neuronal activity. This is thought to control the extent of myelination and oligodendrocyte differentiation [17-19].

1.1.2.3 Microglia

Microglia act as the defence system of the brain, responding to infection and damage [20]. They are present throughout the parenchyma of the brain, with each cell responsible for its own specific domain. Microglia are activated in the presence of purines, chemokines, and glutamate. This results in the controlled phagocytosis of pathogens and cellular debris. They also act as antigen-presenting cells, enabling a T-cell immune response. Conversely, neurons maintain the microglia “resting state” through the presence of immunoglobulins (CD200, CD47) on their cell surface and the release of neurotransmitters such as GABA. This enables tight regulation of microglial activity, preventing inadvertent damage to healthy structures [21].

1.2 Key metabolic pathways

1.2.1 Tricarboxylic acid cycle

The tricarboxylic acid cycle (TCA) is an essential pathway for cells in the metabolism of sugars, lipids and amino acids, as well as energy production

through oxidative phosphorylation. It begins with the condensation of acetyl-CoA with oxaloacetate, which forms citrate. This metabolite can be used as a precursor to lipid synthesis after exportation to the cytoplasm by the citrate transport protein, or it can be metabolised to isocitrate by aconitase. The first oxidative step of the TCA cycle then follows, with decarboxylation of isocitrate to α-ketoglutarate (α-KG) and the production of CO_2. αKG dehydrogenase then converts αKG to succinyl-CoA, which is further metabolised to succinate, with the release of another molecule of CO_2. Succinate dehydrogenase then oxidises succinate to fumarate. This enzyme also forms complex II of the respiratory chain, feeding electrons into oxidative phosphorylation and the production of ATP. The hydration of the double bond in fumarate is catalysed by fumarate hydratase, producing malate. Finally, malate is oxidised to oxaloacetate by malate dehydrogenase, completing the TCA cycle pathway (Figure 1-1) [22].

All the oxidation reactions are couple to the reduction of either NAD^+ or $NADP^+$ to NADH or NADPH respectively. The only exception is the oxidation of succinate to fumarate, which is couple to the reduction of FAD^+ to $FADH_2$. These in turn feed additional electrons to the electron transport chain, generating ATP. Many of these TCA metabolites are actively transported across the inner mitochondrial membrane and diffuse freely across the outer mitochondrial membrane, allowing for the production of amino acids and sugars. This generates pools of metabolites which are closely connected between the cytoplasm and the mitochondria, such that an increase in one pool is reflected by an increase in another [23].

One major mitochondrial transportation system is the malate/aspartate shuttle. This allows for the transportation across the inner mitochondrial membrane of NADH, generated from glycolysis, to the electron transport chain maximising ATP production. In addition it facilitates the movement of the key metabolites glutamate and α-KG between the mitochondria and the cytoplasm. It is composed of two sets of enzymes, which are located both in the mitochondria and the cytoplasm; malate dehydrogenase and aspartate aminotransferase. The process starts with cytoplasmic malate dehydrogenase catalysing the reaction of oxaloacetate and NADH to produce malate and NAD^+, which can be reduced again by glycolysis. Malate is then transported into the mitochondria by the

malate-alpha-ketoglutarate antiporter (Slc25a11) while exporting αKG into the cytosol. Mitochondrial malate dehydrogenase then metabolises malate back into oxaloacetate releasing NADH. Mitochondrial aspartate aminotransferase then converts oxaloacetate to aspartate by utilising glutamate producing αKG. The glutamate-aspartate antiporter (Slc25a13) then exports aspartate while importing glutamate. Aspartate is then converted back to oxaloacetate in the cytoplasm by cytosolic aspartate aminotransferase. This process can work in both directions, transporting NADH, glutamate and α-KG across the mitochondrial membrane [24].

1.2.2 Glutamate – Glutamine – GABA cycle

Astrocytes and neurons are closely connected metabolically through the glutamate-glutamine cycle [25]. This enables the metabolism of glutamate, the major excitatory neurotransmitter in the brain. Though the majority of tricarboxylic acid (TCA) cycle metabolites in neurons are derived from glucose, these cells also avidly take up glutamine from the synaptic space and convert it to glutamate using glutaminase. In turn, glutaminergic neurons release glutamate into the synaptic space, which results in activation of glutaminergic receptors on the post synaptic membrane, potentiating further neurotransmission. After their release, most of the neurotransmitter is taken up by astrocytes and converted back to glutamine [26, 27]. Glutamate accumulates in the astrocytic cytosol, where 85% is converted to glutamine by glutamine synthetase. The rest is oxidised in the TCA cycle after conversion to α-KG by glutamate dehydrogenase in the mitochondria [28].

Utilising a branch of glutamate metabolism called the GABA shunt, GABA can be metabolised via the glutamate-glutamine pathway. GABAergic neurons metabolise glutamate to GABA using glutamate decarboxylase (GAD). There are two GAD genes, GAD1 and GAD2, which encode the isoforms GAD65 and GAD67, respectively. The distribution of these enzymes differs throughout the brain, as well as within neuronal compartments, suggesting different functions for these isoforms. GAD65 is expressed mostly in the axon terminals, unlike GAD67 which is expressed mostly in the cell bodies, indicating that the former is more important in GABAergic neurotransmission. After metabolism from glutamate, GABA is released into the synaptic space producing post-synaptic inhibition via

activation of GABA receptors. There are two major types of GABA receptor; GABA-A and GABA-B. The GABA-A receptor exists as a pentameric assembly which can be formed from a combination of 19 different subunits (α1-6, β1-3, γ1-3, ρ1-3, δ, ε, θ and π), most commonly consisting of two α, two β, and one γ subunit [29]. It functions as an ionotropic receptor which on activation by GABA alters the cell membrane potential via an influx of Cl^- ions, hyperpolarising the cell and preventing action potential propagation [6, 30]. These differences in subunit composition are likely to alter the sensitivity of the receptor to GABA activation, as some subunits are specific to different regions of the brain and to different stages of development [31]. In contrast, the GABA-B receptor is a heterodimeric G-protein coupled receptor which is formed from three major subunits; $GABA_{B1a,}$ $GABA_{B1b,}$ and $GABA_{B2}$. Activation of these receptors leads to an increase in intracellular Ca^{2+} concentration, most likely from intracellular Ca^{2+} stores [32]. This in turn is linked to the opening of K^+ channels, hyperpolarising the cell and impairing action potential propagation [33, 34].

Subsequently, most of the GABA released by neurons is taken up again by neurons for recycling or by astrocytes where it is metabolised [35]. In astrocytes it accumulates in the mitochondria, where it is transaminated to succinate semi-aldehyde (SSA) by GABA transaminase (GABAT). α-KG acts as a donor for the amine group of GABA, reforming the GABA precursor, glutamate. SSA is then further oxidised to succinate by succininic semi-aldehyde dehydrogenase (SSADH), thus entering the TCA cycle [36, 37]. Both GABAT and SSADH are present in the brain only in the mitochondria, enhancing flux through the GABA shunt [36]. At this point the carbons derived from GABA may leave the TCA cycle as malate, where it is metabolised to pyruvate using the astrocyte specific cytosolic malic enzyme [38]. The pyruvate can then be completely oxidised after re-entering the TCA cycle. Alternatively, the carbons from GABA may continue through the TCA cycle to α-KG, where it is metabolised to glutamate and then glutamine. The glutamine is then released and taken up by neurons to complete the glutamate–glutamine cycle. GABA accounts for up to 20% of the flux through the glutamate–glutamine cycle [39] (Figure 1-1).

The GABA shunt is a highly conserved evolutionary metabolic pathway and occurs in bacteria and plants as well as mammals [40-42]. This is possibly due to the

ability of the GABA shunt to provide an alternative mechanism for supplying carbon to the TCA cycle, especially in the presence of mitochondrial dysfunction. The GABA shunt has been shown to be activated in the presence of hypoxia and reperfusion injury after stroke [43, 44]. There is also evidence for altered function in epileptic seizures [45]. This has resulted in the targeting of GABAT in epilepsy, by irreversibly inhibiting this enzyme the concentration of GABA in the brain can be increased reducing the threshold for seizures. Vigabatrin is a drug that irreversibly inhibits GABAT and has been used to treat refractory paediatric epilepsy [46, 47]. Conversely, impairment of GABA metabolism is a feature of Alzheimer's disease, though the connection with pathogenesis is not clear [48, 49]. These findings suggest that GABA metabolism may have an important role in maintaining the normal metabolic function of the human brain.

It is not known, however, if GABA is synthesised from glutamate in the mitochondria or in the cytoplasm and then transported into the mitochondria for subsequent metabolism into TCA metabolites. The latter seems more likely as mitochondrial GABA carriers have been identified in plants and micro-organisms, though not in mammals to date [50]. The lack of an identifiable GABA carrier in mammals may be due to the ability of GABA to passively diffuse across the mitochondrial membrane [51]. Isolated rat brain mitochondria, where GABA metabolism was inhibited, showed uptake of GABA with non-saturable kinetics up to 18 mM, which is in excess of normal physiological conditions [52]. Therefore, it seems feasible that a mitochondrial carrier is not required.

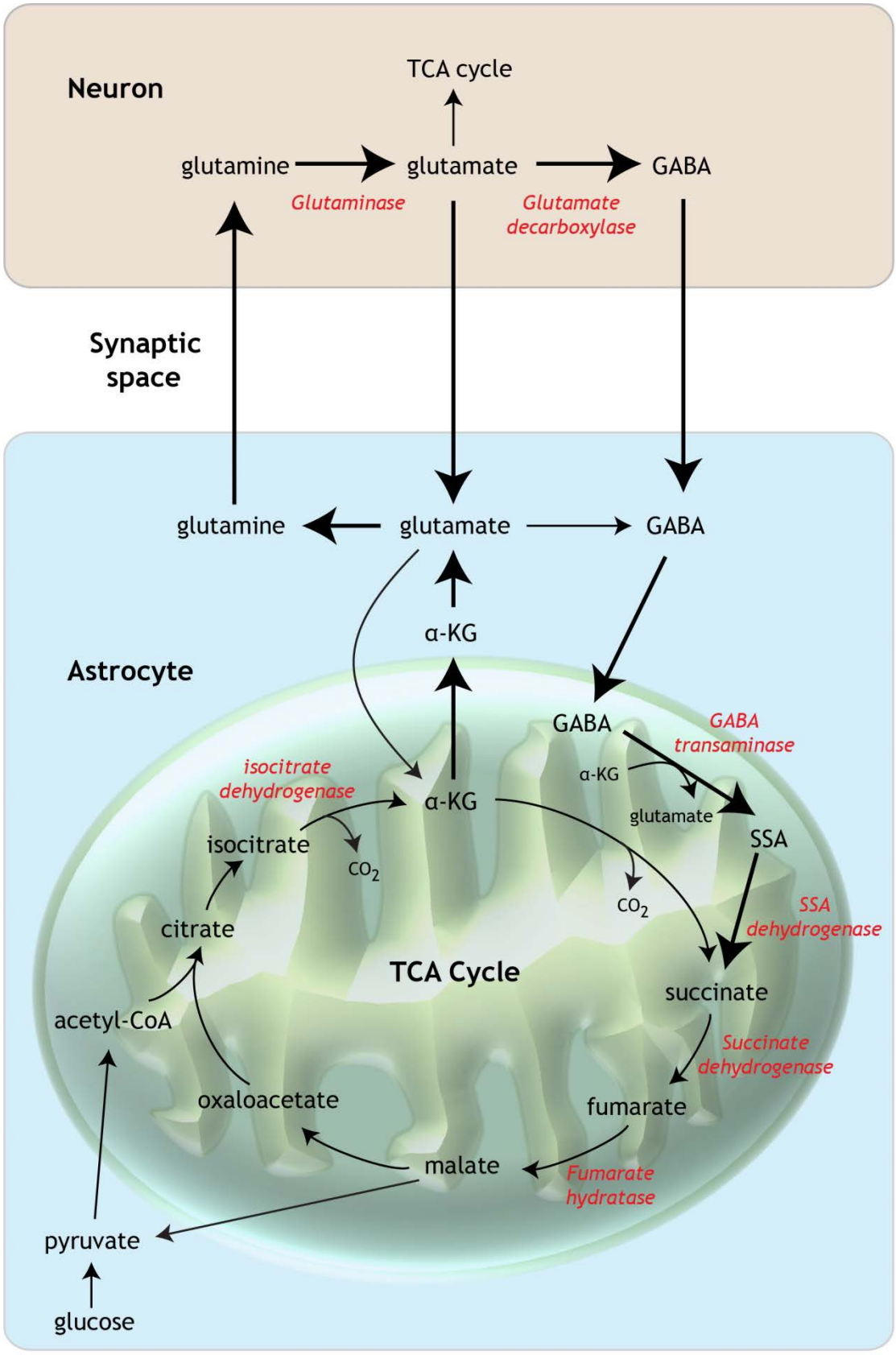

Figure 1-1 Glutamate - glutamine - GABA pathway
GABA and glutamate are released by neurons and taken up by astrocytes. Glutamate is metabolised to glutamine, while GABA enters the mitochondria where it is metabolised to succinate semi-aldehyde (SSA). SSA is metabolised to succinate which enters the TCA cycle. At this point it may leave the TCA cycle as malate, where it is metabolised to pyruvate, which can then be completely oxidised after re-entering the TCA cycle. Alternatively, the carbons from GABA may continue around the TCA cycle to α-KG, where it is metabolised to glutamate. Glutamate is then metabolised to glutamine, released and taken up by neurons. The larger arrows depict the direction of the major metabolic fluxes through this pathway. Key enzymes are depicted in red.

1.2.3 NAA and NAAG metabolism

There are two abundant aspartate derived metabolites in the central nervous system; N-acetylaspartate (NAA) and N-acetylaspartylglutamate (NAAG), both of which are predominantly synthesised in neurons. The former is the second most abundant amino acid derivative in the brain, and acts as a major osmolyte as well as a source of acetate for myelin synthesis by oligodendrocytes [53]. The importance of NAA as a source of acetate is evident in Canavan disease, where a non-functioning mutation in the gene for aspartocylase, the enzyme responsible for the metabolism of NAA to aspartate and acetate, results in demyelination and premature death in childhood [54]. NAA may also act as an acetate source for histone acetylation, potentially regulating oligodendrocyte differentiation [55, 56]. It is also required for the synthesis of NAAG, which is the third most common neurotransmitter in the brain. It is released by neurons and selectively stimulates the metabotropic glutamate receptor 3, which modulates excitatory neurotransmission by downregulating glutamate release [57-59]. NAAG, as well as NAA, have been shown to promote cell growth and inhibit differentiation of glioma stem-like cells, possibly by also acting as a source of acetate [60].

The metabolism of NAA and NAAG is unusual in that it requires the presence of three cell types, neurons, astrocytes, and oligodendrocytes. Typically, though not exclusively, NAA is synthesised in neurons by NAA synthase from acetyl-CoA and aspartate [61]. In some neurons, NAA is then converted into NAAG by NAAG synthase, using glutamate as a co-substrate [62]. NAA is primarily metabolised by oligodendrocytes to acetate and aspartate by aspartocylase [63]. The acetate can then be converted to acetyl-CoA for use in lipid synthesis, histone and protein acetylation and for use in the TCA cycle [64, 65]. The aspartate may be used for protein synthesis, or used to generate oxaloacetate for the TCA cycle [66]. NAAG is primarily metabolised on the surface of astrocytes by NAAG peptidase which catabolises NAAG to NAA and glutamate [67]. The glutamate can then be taken up by astrocytes, entering the glutamate-glutamine cycle [68]. NAA in turn is taken up by oligodendrocytes for further metabolism. Interestingly, the requirement for 3 cell types in the metabolism of NAA and NAAG indicates that these metabolites may have additional signalling functions that are yet to be determined [69].

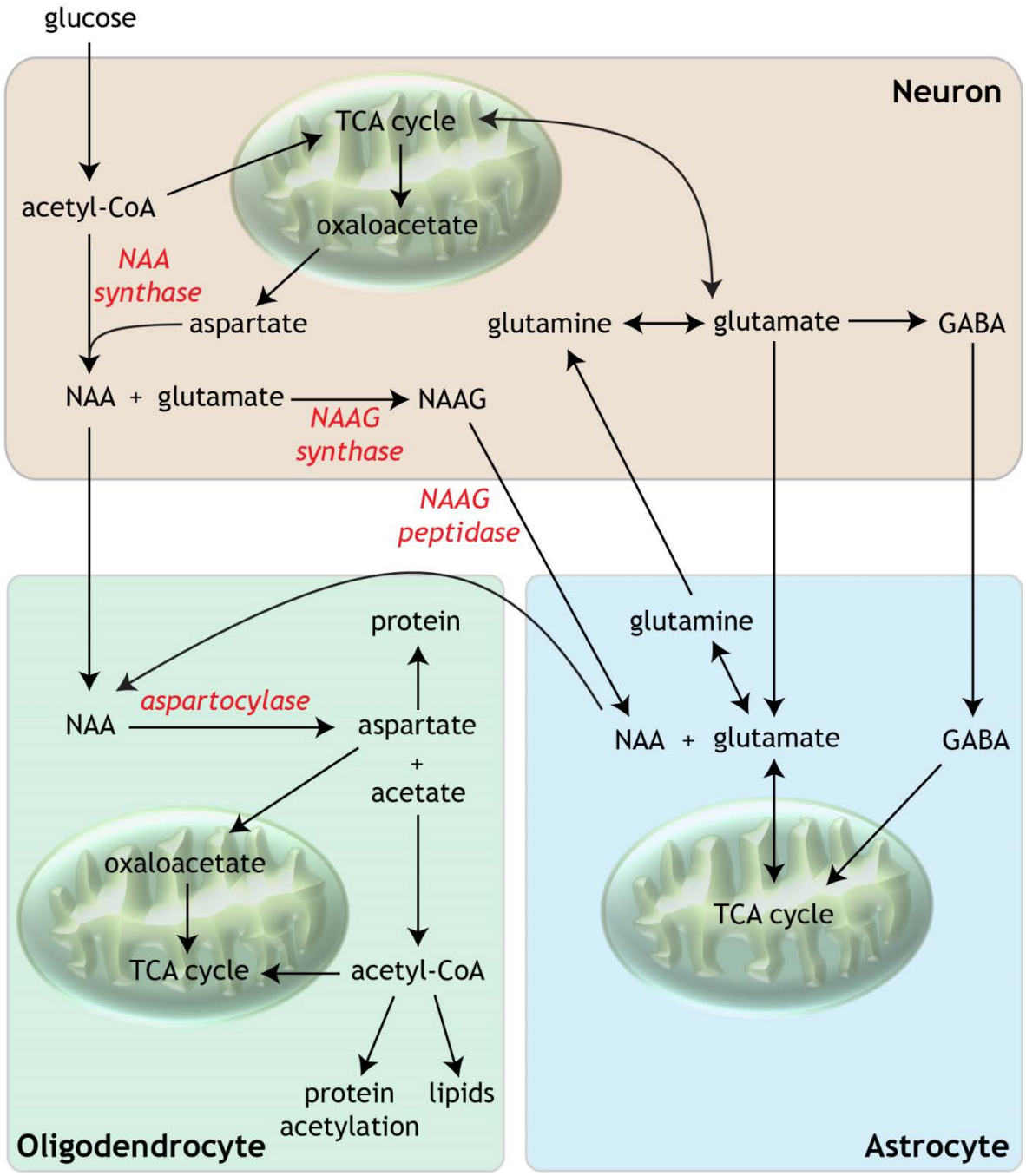

Figure 1-2 Metabolic pathways connecting neurons with glial cells.
Neurons are connected metabolically to other glial cells by the glutamate-glutamine-GABA cycle and NAA/NAAG. Glutamate and GABA are released by neurons and taken up by astrocytes. They are then metabolised to glutamine, which is released and taken up by neurons for recycling. In addition, NAA is synthesised in neurons by NAA synthase from acetyl-CoA and aspartate. NAA is then converted into NAAG by NAAG synthase, using glutamate as a co-substrate. NAA is primarily metabolised by oligodendrocytes to acetate and aspartate by aspartocylase. The acetate can then be converted to acetyl-CoA for use in lipid synthesis, histone and protein acetylation and for use in the TCA cycle. The aspartate may be used for protein synthesis, or used to generate oxaloacetate for the TCA cycle. NAAG is primarily metabolised on the surface of astrocytes by NAAG peptidase which catabolises NAAG to NAA and glutamate. The glutamate can then be taken up by astrocytes, entering the glutamate-glutamine cycle. NAA in turn is taken up by oligodendrocytes for further metabolism. Key enzymes are depicted in red.

1.3 Glioma

Gliomas are the commonest primary brain tumours, constituting 81% of brain and central nervous system malignancies [70]. Internationally, the age standardised rate (ASR) for incidence is 3.9 per 100,000 of population for all brain tumours. There is, however, a marked variation between countries, with a higher incidence in developed nations, potentially reflecting improved diagnosis (Figure 1-2). This compares to an incidence ASR for other solid tumours such as prostate, lung, and colorectal of 30.7, 34.2 and 20.6 per 100,000 of the population, respectively [71]. Though the incidence of primary brain tumours is lower than other solid tumours, it confers a very poor prognosis, which is reflected in a similar mortality ASR of 3 per 100,000 of the population (Figure 1-3) when compared to prostate, lung, and colorectal cancer. Factors that are associated with an increased incidence in glioma include increasing age, male gender, and non-Hispanic race [72].

Gliomas derive from two different cell types: oligodendrocytes and astrocytes. Gliomas are classified by the World Health Organisation (WHO) into four grades (I-IV). Increasing grade is associated with more aggressive cancer and worse prognosis. These tumours are described pathologically as an astrocytoma (WHO grade I-IV), oligodendroglioma (WHO grade I-III) or if they have features of both, an oligoastrocytoma (WHO grade II-III). Grade II tumours are classified as diffuse, while grade III are termed anaplastic. Finally, grade IV astrocytomas are also described as glioblastoma multiforme (GBM). Tumours which are WHO grade I-II are classed as low grade, while WHO grade III-IV are classed as high grade. The natural course for low grade tumours is to transform into high grade tumours after, on average, 4-5 years after diagnosis [73].

Astrocytomas are the most common glioma in adults, of which the majority constitute the highest and most aggressive form of the cancer, GBM (WHO grade IV). Less than 5% of these patients survive to 5 years from diagnosis. These tumours, as well as anaplastic astrocytomas (WHO grade III), are more common in the elderly with the highest incidence in the 75 – 85 year age group [74]. GBM can be divided into primary, if arising de novo, or secondary if arising as a result of transformation of a lower grade tumour (WHO grade II-III). Secondary tumours tend to occur in younger patients, with a median incidence age of 45 years

compared to 65 years for primary GBM [75]. Low grade glioma also occurs more commonly in younger patients, with the highest incidence in those aged 35 to 44 years old [74]. WHO grade I gliomas occur almost exclusively in children and young adults, and generally require only surgical intervention with an excellent prognosis. When comparing different types of glioma, oligodendroglioma tends to convey a better prognosis compared to astrocytoma on a grade to grade basis [74].

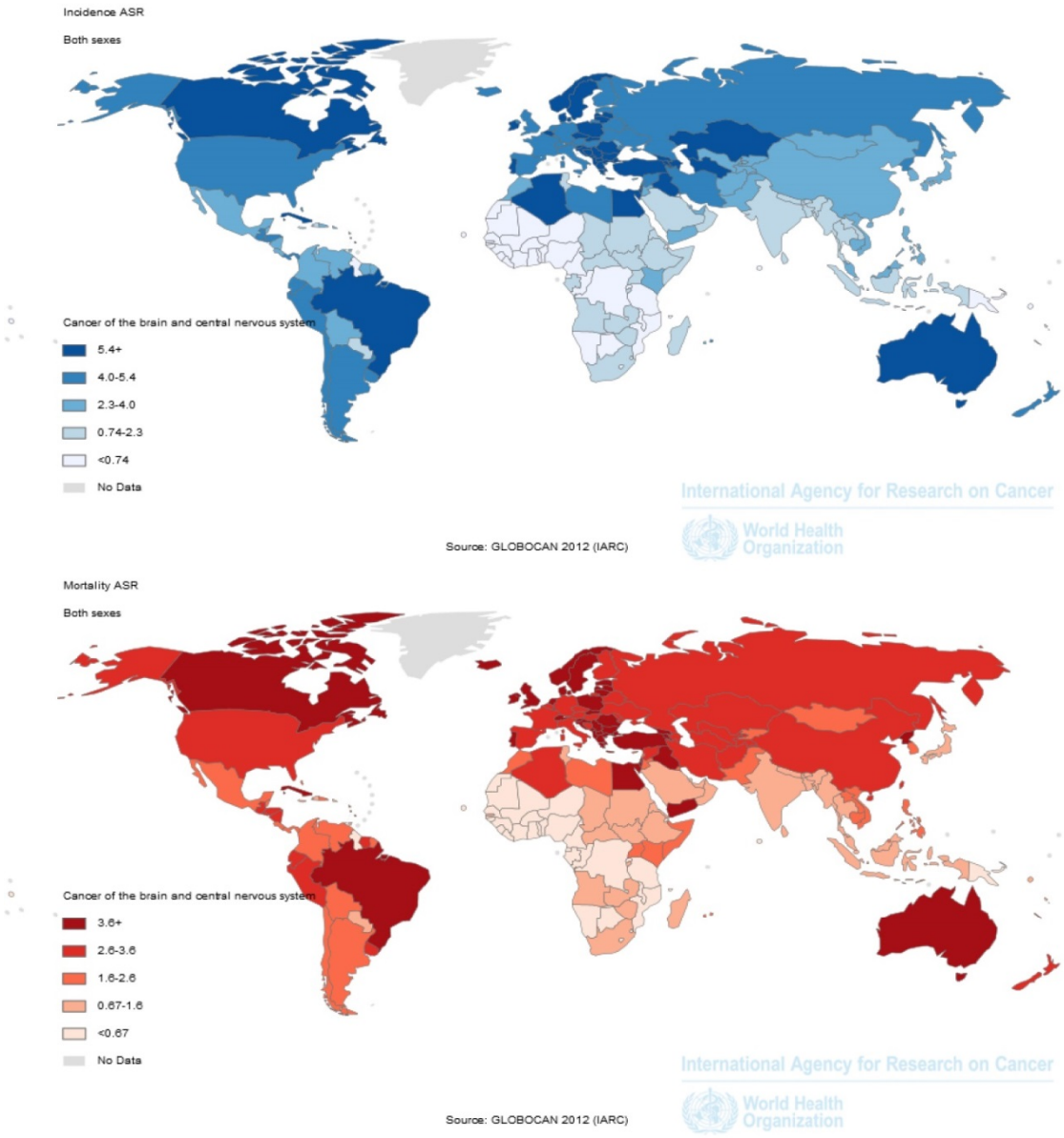

Figure 1-3 Brain tumour incidence and mortality
Age standardised incidence (blue) and mortality (red) rates of all brain tumours in the world, by country per 100,000 of the population (GLOBOCAN http://globocan.iarc.fr [76])

1.3.1 Cell origin of glioma

Gliomas were original thought to derive from normal brain glial cells as they shared numerous glial markers. This led to the assumption a century ago that astrocytomas were probably derived from astrocytes, and oligodendrogliomas from oligodendrocytes. However, more recently there has been emerging evidence that the cell of origin for these tumours is more complex, and several candidate cell types have been proposed. These include the astrocyte, neural stem cell (NSC), and the oligodendrocyte precursor cell (OPC).

1.3.1.1 Astrocyte

Astrocytes were initially thought to be the only dividing cells in the brain, which led them to become the first candidate for the glioma cell of origin [77]. The fact that GFAP was frequently detected in human glioma added weight to this hypothesis [78]. Astrocytes can de-differentiate to neural stem-like cells if exposed to transforming growth factor, and in turn can be induced to form high grade gliomas after irradiation in animal models [79]. A similar effect has also been shown when primary astrocytes, from new born *Ink4a/Arf*$^{-/-}$ mice, were cultured in media complimented with epidermal growth factor. These cells de-differentiated after ten days, as evidenced by a loss of GFAP, and the gain of nestin and A2B5, which are progenitor cell markers [80].

1.3.1.2 Neural stem cell

NSCs were first identified in mice in the 1990s, and later shown to also occur in humans [81, 82]. They are found predominantly in the subventricular zone and the dentate gyrus of the hippocampus, of which the former has been shown to be involved in over 90% of tumours [83]. In addition, signalling pathways that are required for differentiation, self-renewal, and proliferation in NSCs also occur frequently in gliomas. One such pathway is the phosphatidyl inositol-3-kinase (PI3K)/mitogen-activated protein kinase (MAPK), which mediates cell proliferation and survival. Epidermal growth factor receptor (EGFR), a positive regulator, is amplified or mutated in 45% of GBM, while PTEN, a negative regulator is mutated or deleted in 36% of GBM [84].

Additional evidence for NSCs as the glioma cell of origin comes from mouse models. Tumours induced by a germline mutation of *p53* in combination with a conditional knock-out of *Nf1* were initially located in the subventricular zone [85]. Also, high grade gliomas could be induced in *SCID* mice after implantation in the brain of NSC cultures, with a transduced EGFR mutation, grown from *Ink4a/Arf*$^{-/-}$ mice [86].

1.3.1.3 Oligodendrocyte precursor cell

OPCs are another dividing cell population in the brain and give rise to oligodendrocytes. They also have a wide distribution in the brain and occur in the subventricular zone, which makes them another good candidate for the glioma cell of origin. Similarly to NSCs, signalling pathways that are important to oligodendrocyte development are also altered in glioma. A good example of this is the platelet derived growth factor receptor (PDGFR), which is an activator of the PI3K/MAPK pathway, and important in the migration and proliferation of OPCs. It has been shown to be overexpressed in a range of glioma types [87].

Further evidence has been obtained from mouse models. Tumours derived from an S100β-vErb transgenic mouse model have been shown to have an OPC origin, and NSCs with sporadic *p53/Nf1* mutations only showed aberrant growth if they differentiated to OPCs, but not differentiation along other neural cell lineages [88, 89]. Conversely, gliomas could also be induced by in vitro transformation of OPCs through p53/Nf1 mutations [89].

1.3.2 Genetic origins of glioma

1.3.2.1 Common mutations in GBM

Three common pathways are mutated in over 75% of GBMs [84]. One third of these tumours have a mutation in p53, a tumour suppressor gene that is involved in regulating DNA repair, cell cycling, and apoptosis. The same effect is also achieved in some tumours by amplification of MDM2 or MDM4 [90]. Alternatively, cell cycling can be affected directly through several mechanisms. This includes amplification of cyclins or cyclin dependent kinases, loss of the retinoblastoma 1 gene, or mutation of the cell cycle inhibitors CDKN2A, CDKN2B, and CDKN2C [84]. These all act to impair cell cycle regulation, allowing cells with damaged

DNA to continue to proliferate. Lastly, changes in the phosphatidyl inositol-3-kinase (PI3K)/mitogen-activated protein kinase (MAPK) pathway, which is involved in mediating cell proliferation and survival, commonly occur in GBM. This include amplification of the epidermal growth factor receptor (EGFR), platelet derived growth factor receptor (PDGFR) or MET gene. Mutations in EGFR also occur in 20-30% tumours [91]. Downstream activation of this pathway can also occur by mutation of the neurofibromatosis 1 gene (NF1), KRAS, or the gene for PI3K, PI3KCA. Deletion or mutation of PTEN, an inhibitor of PI3K, can also facilitate pathway activation [84]. Less common mechanisms include gene translocation and fusion. Fusion of EGFR with SEPT14 occurs in 4% of GBM, while fusion of EGFR with PSPH occurs in 2% [92]. Translocation can also occur rarely between the FGFR and TACC1 or TACC3 genes [93].

1.3.2.2 Isocitrate dehydrogenase mutations

Isocitrate dehydrogenase (IDH) is an important metabolic enzyme that converts isocitrate to α-KG. α-KG is important as a substrate in the tricarboxylic acid cycle and acts as an important co-substrate for many cellular enzymes. It exists as 3 isoforms (IDH1/2/3), with IDH1 present in the cytoplasm and IDH-2/3 in the mitochondria. Recently point mutations in the IDH1 and IDH-2 genes have been identified in gliomas using genomic mutational screening [94, 95]. Over 300 gliomas of varying grades were analysed and showed the incidence in grade II and III gliomas ranged from 75-90% dependent on the pathological sub-type. Secondary GBM had an incidence of 85%, indicating that these mutations seem to be important early events in the development of gliomas. The clinical significance of an IDH mutation is apparent in the differential survival in the two groups. For anaplastic astrocytoma, the median overall survival for patients with IDH mutation was 65 months compared to 20 months for patients with wild type gene. This improved prognosis was also observed in GBM, where patients with IDH mutant tumours have a median overall survival of 31 months compared to 15 months for IDH wild-type tumours [95].

The IDH mutation, especially in oligodendrogliomas, is often followed by loss of the p-arm of chromosome 1 and the q-arm of chromosome 19 [96]. The consequence of this is inactivation of one copy of the Capicua transcriptional repressor (CIC) gene and the FUSE binding protein 1 gene. Subsequent mutation

of the remaining genes occurs in most (52%) grade II, and almost all (84%) grade III oligodendrogliomas [97]. The mechanistic consequences of this are not fully understood, but the presence of this co-deletion has prognostic significance in all types of glioma. Loss of 1p 19q is associated with an improved response to therapy and an increased overall survival compared to patients that do not have the co-deletion [98].

The IDH mutation is also associated with a hypermethylated genetic phenotype, with increased methylation at promoter sites resulting in gene silencing [99]. This is associated in particular with methylation of the promoter site for the enzyme, O6-methylguanine-DNA methyltransferase (MGMT). It is a DNA repair enzyme that is methylated in 36% of GBMs and 90% IDH mutant low grade tumours [100, 101] This has prognostic significance as it is predictive for improved response to chemotherapy and radiotherapy, which both act through DNA damage [102, 103].

1.3.2.3 Gene expression classification

It was first noted in the 1990's that genetic differences were present between certain types of glioma. It was discovered that amplification of the EGFR and the mutation of p53 were mutually exclusive in GBM. The latter occurred predominantly in secondary GBM and low grade glioma, while the former occurred mostly in primary GBM [104]. This prompted efforts to try and identify more genetic differences between the tumour types. When primary GBMs were stratified on survival, it was noted that a proneural gene expression profile was associated with a better prognosis. Conversely, patients with a worse prognosis could be divided into mesenchymal and classical subgroups [105]. In addition, further analysis of the Cancer Genome Atlas Network identified a fourth subset; the neural group [106]. This has led to the development of a molecular classification of adult GBM into four categories; proneural, neural, mesenchymal, and classical. Proneural is associated with alterations of PDGFRA with the TP53 and IDH1 mutation, neural with the expression of neuron markers such as NEFL, GABRA1, SYT1 and SLC12A5, mesenchymal with increased expression of genes in the tumour necrosis factor and NF-κB pathways, as well as mesenchymal markers such as CHI3L1 and MET, and classical with EGFR amplification and deletion of CDKN2A. The proneural subtype is associated with

secondary GBM and confers a better prognosis [106, 107]. In paediatric GBMs a further 2 subtypes have been identified, which correlate to histone H3.3 mutations, at two critical sites; K27(M) and G34(R/V). These both correspond to separate genetic and epigenetic profiles, and have not been observed in adults [108]. These new classification of GBM will hopeful allow for the development of new and more specific treatments for patients.

Low grade gliomas have also been further subdivided into three groups based on molecular markers; IDH wild-type, IDH mutant without 1p/19q co-deletion, and IDH mutant without 1p/19q co-deletion. This seems to form a better clinically predictive model than histological classification alone into astrocytoma or oligodendroglioma [109]. Low grade gliomas with an IDH mutation and 1p/19q co-deletion were associated with TERT activation, CIC and FUBP1 mutation, and activation of the PI3K pathway. Conversely, IDH mutation and no 1p/19q co-deletion were associated with TP53 and ATRX mutations. IDH1 wild-type tumours were molecularly similar to GBM and are clinically more aggressive. The presence of IDH mutation and 1p/19q co-deletion is associated with the best prognosis and IDH wild-type with the worst [109].

Anaplastic glioma can also be further sub-divided based on molecular markers that are independent of histology. This includes three groups; CIMP negative, non 1p 19q co-deleted CIMP positive, and 1p 19q co-deleted CIMP positive. This is helpful in management and determining prognosis as CIMP negative tumours behave like GBM, while the other two have a better prognosis and are more responsive to chemotherapy [110].

1.3.3 Treatment

1.3.3.1 Surgery

In comparison to other solid tumours, treatment of glioma is relatively limited and has changed little in the last 30 years. The initial treatment for newly diagnosed gliomas is surgery. Maximal resection results in the best outcome for patients. In GBM, a retrospective study showed that overall survival was increased to 11.3 months for a complete resection compared to 6.6 months with diagnostic biopsy only. Even a partial resection conferred an improved survival

benefit of 4 months compared to biopsy [111]. The benefits of complete surgical resection also extend to grade III glioma [112]. In low grade tumours, which are slow growing and where survival can extent to many years, early maximal resection also seems to confer survival benefit [113]. In addition, there is also an improvement in symptoms such as epilepsy [114]. This has to be to be weighed against the potential neurological complications of surgery. To guide management, several prognostic scores have been developed where the presence of high risk factors, such as large tumour size and astrocytic histology, predispose to early surgical intervention [115]. This has driven research into improved surgical techniques. Recent advances have involved using 5-aminolevulinic acid, a non-fluorescent prodrug that results in intracellular accumulation of fluorescent porphyrins, in high grade glioma cells. This allows for better visualisation of tumours intra-operatively resulting in a more complete resection [116].

1.3.3.2 Radiotherapy

Radiotherapy plays an important role in glioma management. In high grade astrocytoma, radiotherapy after surgery is associated with an improvement in overall survival. High dose irradiation of the brain post-operatively (>50 Gray), was associated with a doubling of survival compared to surgery alone [117, 118]. Escalating the radiotherapy dose to 60 Gray was shown to add an additional 2 months survival benefit with no significant differences in toxicity [117]. This seemed to be the limit of increasing radiotherapy dose however, as trials investigating further dose escalation resulted in radionecrosis of the brain. In addition, viable tumour was observed at autopsy in areas receiving up to 80 Gray, indicating no biological benefit from these higher doses [119].

The benefit of radiotherapy in low grade glioma is less clear cut, with an improved progression free survival but not overall survival [120]. In this circumstance the benefits of radiotherapy have to be weighed against the detrimental long term cognitive effects of treatment [121]. In this situation, radiotherapy after surgery is often deferred until there is evidence of disease recurrence or progression. Radiotherapy can be used as first line therapy in patients who are not medically fit for surgery or for tumours that are not amenable to surgical resection. These tumours also respond better to lower

doses of radiotherapy, with 50.4 Gray giving the same survival outcome as 64.8 Gray in a randomised phase III trial [122]. This lower dose radiotherapy regime is now the current standard of care.

Improved imaging techniques such as computer tomography (CT) and magnetic resonance imaging (MRI) allowed for better targeting of radiotherapy. Changing from whole brain radiotherapy to radiation fields that incorporate the tumour only, maintained survival outcome with reduced treatment toxicity [123]. New imaging techniques may allow for further improvement in guiding radiotherapy planning. Magnetic resonance spectroscopy imaging (MRSI) identifies tumour from normal cells based on the levels of metabolites such as choline, N-acetylaspartate, and lactate. This may allow for treatment of occult cancer and improved survival [124].

1.3.3.3 Chemotherapy

In the 1970s the first chemotherapy agent was used to treat glioma. It was a nitrosourea, called carmustine, and its cytotoxic effect was through DNA alkylation. Initial studies used this class of drug in the adjuvant setting after radiotherapy treatment. A meta-analysis showed a 10.1% improved overall survival in high grade gliomas at 1 year using this treatment combination. Interestingly, this effect was greater in anaplastic astrocytomas compared to the more aggressive glioblastoma multiforme [125]. This progressed to combination therapy in the 1990s with PCV (procarbizine, lomustine, and vincristine). Again, this combination showed an improved survival benefit when given after radiotherapy over single agent carmustine in anaplastic astrocytoma, but not the more aggressive glioblastoma. It doubled overall survival in anaplastic astrocytoma to 3 years [126]. Further progress in the chemotherapy treatment of glioma arose in the late 1990s with the development of temozolamide, a prodrug which can methylate the N-7 or O-6 positions of guanine residues on DNA resulting in tumour cell death. This had fewer side effects than previous chemotherapy regimens and also showed improved efficacy in conjunction with radiotherapy. Concurrent radiotherapy with temozolamide is associated with an improved overall survival, with a 2 year survival of 26.5% compared to 10.1% with RT alone. This treatment regime, with an additional 6 months of temazolamide after RT, now constitutes the gold-standard for initial

glioblastoma therapy [127]. Newer treatments developed in the last decade however have been disappointing. An example of this is Bevacizumab, an antibody that targets vascular endothelial growth factor (VEGF), acting as an angiogenesis inhibitor. It showed impressive results radiologically, but resulted in no survival benefit when used alone in recurrent GBM, or in combination with radiotherapy and temazolamide [128, 129]. Bevacucimab may however have a role in reducing cerebral oedema in re-irradiation therapy after tumour recurrence [130]. Targeting the VEGF receptor has also proved ineffective [131]. Researchers have also tried to target the EGFR and PDGF receptors, which are amplified in many GBM, using tyrosine kinase inhibitors. These agents have been well tolerated, but unfortunately have shown no efficacy even in combination with standard chemotherapy agents [132, 133]. Targeting downstream pathways such as mTOR have also failed to produce any meaningful results [134]. Novel use of older agents has however proved more successful, with the use of carmustine wafers to line the tumour bed after tumour resection. This can result in a survival benefit of up to 10% at 2 years in high grade glioma [135]. Low grade gliomas also show a response to the same chemotherapy agents as high grade glioma. Tumour response in both can be predicted by the use of molecular markers such as methylated MGMT and 1p 19q loss, which predict increased sensitivity to therapy.

Treatment for glioma has advanced markedly in the last few years, but in relation to most other solid tumours the treatment options are still very limited. The prognosis remains poor, especially for high grade tumours, with the mean overall survival for GBM remaining less than 18 months.

1.4 Cancer metabolism

It has now been over ninety years since it was first observed that cancer cells have an altered metabolic phenotype [136]. In the presence of oxygen, differentiated cells predominately utilise the tricarboxylic acid (TCA) cycle and oxidative phosphorylation to efficiently produce energy and the metabolites necessary for protein and lipid synthesis. However, in hypoxia, this process is altered and cells switch to a higher rate of glycolysis and lactate production to maintain their energy and metabolic needs. In cancer cells, glycolysis is maintained at a high rate, even in the presence of oxygen; a term described as

"aerobic glycolysis". This seems counterintuitive, as oxidative phosphorylation is much more efficient at energy production than glycolysis, producing 34 more units of ATP from the same molecule of glucose [137]. Tumour cells, however, are rapidly dividing and have a much greater need for anabolism compared to normal differentiated cells. Rapid glucose metabolism enables faster ATP production as well as a greater redistribution of carbons to nucleotide, protein, and fatty acid synthesis, thus maximising cell growth [138]. ^{18}F-deoxyglucose positron emission tomography (FDG-PET) utilises this feature of cancer by allowing visualisation of glucose uptake in patients, and has become an important tool in cancer diagnosis as well as measuring treatment response [139]. It has been used to confirm the correlation between glucose metabolism and cell proliferation rate in some human tumours [140-142]. Rapid glucose metabolism can also occur in normal cells where there is a need for rapid growth and proliferation, such during an immune response, wound healing and in utero [143-145]. In cancer cells, however, aerobic glycolysis can be deregulated in part due to genetic mutations, such as in the PI3K/AKT and Myc pathway [138]. In addition, increased expression of the M2 isoform of pyruvate kinase (PKM2), a glycolytic enzyme has been identified in cancer, which enables cells to shift metabolic flux from ATP generation to anabolic processes [146].

Recently, other metabolic changes, driven by mutations in genes related to the TCA cycle, indicate an alternative role for so-called "oncometabolites" [147]. In this instance, a particular metabolite builds up within the cell and contributes to the tumorigenic process. Mutations in fumarate hydratase (FH) and succinate dehydrogenase (SDH) follow the classic Knudson "two hit" model, with loss of gene function and subsequent accumulation of the substrates fumarate and succinate, respectively. Conversely, a single allele mutation in isocitrate dehydrogenase (IDH) confers a gain of function, leading to production of an excess of a new metabolite, 2-hydroxyglutarate [147]. These oncometabolites seem to have a common tumorigenic mechanism, namely the competitive inhibition of a superfamily of enzymes, the α-ketoglutarate (α-KG) dependent dioxygenases. These are important modulators of both the oxygen sensing machinery and epigenome, providing another link between metabolic dysfunction and altered gene expression in cancer.

1.5 Regulation of the epigenome

The epigenome consists of chemical changes that occur to DNA and histones without altering the DNA sequence. The structure of chromatin is important to understanding how the epigenome is regulated. It is organised into a histone core around which approximately 147 base pairs of DNA are folded, called a nucleosome. Each histone core is comprised of eight subunits; two each of histones H2A, H2B, H3 and H4. These histone are small globular (10-20 kDa) proteins, except for their histone tail, which protrudes from the surface. Nucleosomes are connected together by other proteins such as the linker histone H1, which condenses the DNA allowing it to fit within the nucleus. Epigenetic changes that alter gene expression can occur at either the DNA or histone level through cytosine methylation of DNA or chemical modification of histone tails, respectively. In normal healthy cells, these processes are essential in activating and suppressing genes to maintain cell differentiation and respond to environmental change.

1.2.4 DNA methylation

It has been observed for a long time that cancer is associated with changes in DNA methylation [148]. This modulation is effected by DNA methyltransferases (DNMT) and ten-eleven-translocation methylcytosine dioxygenase (TET) which add and remove methyl groups at the fifth position of the cytosine pyrimidine, respectively. TET enzymes achieve this by oxidising (hydroxylating) methyl groups, resulting in their removal. In cancer, large areas of the genome are hypomethylated compared to normal cells, especially in gene poor regions. This is associated with chromatin changes leading to genomic instability [149]. However, other regions called CpG islands are associated with hypermethylation in cancer. These sequences are over 200 base pairs long, have over 50% GC content, and are found near promoter sites where they are associated with gene silencing [150]. Distinctive patterns of hypermethylated CpG islands have been identified in glioma and colorectal cancer called CpG island methylator phenotype (CIMP) [107, 151]. CpG methylation at gene promoter sites interferes with enhancer interaction and transcription factor binding, resulting in gene repression [152].

1.2.2.6 DNA methyltransferases

DNMTs consist of two families of enzymes; DNMT1a and DNMT3. The former has a preference for hemi-methylated DNA and the latter consists of two enzymes, DNMT3a and DNMT3b, which are active on both unmethylated and hemi-methylated DNA. The different specificities of these enzymes can be explained by the classical model of DNA methylation [153, 154]. *De novo* DNA methylation occurs on both DNA strands, whereas maintenance of DNA methylation would require methylation of the complimentary DNA strand after replication. For this reason it was proposed that DNMT1a is a maintenance enzyme, and DNMT3a and DNMT3b are involved in *de novo* DNA methylation. However, recently it has been shown that co-operation between DNMT3 and DNMT1a are required to maintain DNA methylation, especially at CpG rich elements [155, 156], indicating that DNA methylation is a complex process than previously thought. The importance of this collaboration is emphasised in mammalian development as knocking down of any of these enzymes is embryonically lethal in mice [157, 158].

2.2.2.6 DNA demethylases

Initially, DNA demethylation was thought to be a passive process, but enzymes were recently identified which could actively remove methyl groups from DNA. This process is achieved by the TET family of enzymes, which has three members (TET 1-3) [159, 160]. These proteins belong to the dioxygenase family of enzymes and oxidise the methyl group on the cytosine residue (5-mC), generating hydroxymethylcystosine (5-hmC) [161]. Subsequent oxidation reactions by TET enzymes produce 5-formylcytosine (5-fC) and 5-carboxycytosine (5-caC) [162, 163]. Decarboxylation of 5-caC to cytosine is not a function of TET, but maybe an addition function of DNMT3 enzymes, providing a link between DNA methylation and demethylation [164]. This has led to an alternative dynamic stochastic model which incorporates the newly discovered TET enzymes. This describes a methylation steady-state that is altered by local rates of both DNMTs and TET, and may also be altered by other epigenetic mechanisms such histone marks [165].

1.2.5 Histone modification

Altering gene expression can also be achieved by changing chromatin structure through chemical modification of amino acid residues on histone tails. This changes the folding of DNA around the histone core, altering the extent to which the DNA is exposed to transcription factors and other proteins. This effect depends on the type, site, and extent of chemical modification and consists of a complex array of modifications. To date, there are twenty types of post-translational histone modifications, of which the most common are acetylation and methylation, but also include ubiquitination, phosphorylation, ADP-ribosylation, malonylation, hydroxylation, O-GlcNAcylation, and SUMOylation [166]. Acetylation on lysine residues are always associated with increased gene expression and is catalysed by histone acetyltransferases (HAT). Conversely, histone deacetylases (HDAC) remove the acetyl groups by hydroxylation. Histone methylation differs from acetylation in that more than one methyl group can be added to a single site and it can be associated with both activation and repression of genes. Up to three methyl groups can be added to lysine or arginine residues on histone tails, by a variety of histone methyltransferases (HMT), with different modifications potentially conferring different functions [167]. For example, methylation of H3K9 and H3K27 are associated with gene silencing, while methylation of H3K4 is associated with gene activation (H denotes histone subunit and K the lysine residue number) [168].

Histone modification is a dynamic process, with the activity of histone demethylases (HDM) as important as HMTs. There are two distinct families of HDM, the lysine specific demethylase (LSD) and the jumonji-C demethylases (JMJ), which contain the catalytic JMJC domain. LSD depends on a flavin adenine dinucleotide (FAD) based reaction to remove methyl groups and has two family members, LSD1 and LSD2 [166]. Interestingly, they can only demethylate mono- or di-methylated amino acid residues at H3K4 and H4K9 [169, 170]. JMJ demethylases form a much larger family of enzymes, with eighteen members so far identified with histone demethylase activity towards H3K4, H3K9, H3K27, H3K36, and H4K20. They are further divided into sub-groups, which share substrate specificity, such as JMJD2A-D which demethylate H3K9 and H3K36, and JARID1A-D which demethylate H3K4 [171]. The JMJ demethylases belong to a superfamily of enzymes called the α-KG-dependent dioxygenases, which require

Fe(II) and α-KG as co-factors [172]. Binding to methylated histones is facilitated by other domains such as PHD, TUDOR, and ARID [173]. In the case of JMJD2A, TUDOR domains allow the enzyme to target H3K4 and H4K20 [174]. In addition, both JMJ histone demethylases and LSDs can form large protein complexes with other proteins involved in chromatin modification, such as HDAC, allowing multiple histone modifications to occur at the same time [171]. The importance of these enzymes is evident by the embryonically lethal effect of the knock down of the LSD1/2 genes [175, 176]. Knocking down individual JMJ demethylases has a more varied effect from no detectable phenotype to embryonic lethality, probably dependent on the redundancy caused by the overlap in activity of these enzymes [177, 178].

1.2.6 Epigenetic modification in cancer

Traditionally, cancer has been thought to be driven by the accumulation of genetic mutations resulting in aberrant protein expression [179]. More recently, changes in epigenetic mechanisms have been shown to be a contributory factor in tumourogenesis [150, 180]. Genes involved in regulating the cell cycle and DNA repair have been observed to be hypermethylated in cancer, such as BRCA1/2 and PTEN [181]. In addition, MGMT, a gene coding for a DNA repair enzyme which is rarely mutated, is commonly silenced in glioma by promoter hypermethylation [180]. This can be driven my mutations in genes that regulate the epigenome, linking both processes, though the exact mechanism of tumourogensis is not known in most cases [182] (Table 1-1).

The most frequent gene mutated in cancer is TP53, followed by PIK3CA. However, this is closely followed by mutations in epigenetic regulatory genes [183]. Mutations in DNA methylation occur in both methyl transfer and demethylation genes. DNMT3A mutations occur frequently in AML [184]. DNMT3A plays an important role in cellular differentiation by silencing self-renewal genes in haematopoietic stem cells. Loss of function of DNMT3A therefore promotes tumourogenesis by preventing cellular differentiation [185, 186]. DNA methylation gene mutations also occur in solid tumours, with DNMT1 mutations occurring in colon cancer, and DNMT3B mutations in breast and lung [187, 188]. In addition to mutations in these enzymes there is also some evidence for overexpression of these genes in cancer, which may contribute to

hypermethylation phenotypes [189]. Conversely, mutations in TET proteins have also been identified in haematological malignancies, and seem to be mutually exclusive of IDH mutations [190, 191]. In addition, methyl-binding domain proteins (MBD), which may mediate transcription by binding to CpG sites, are found to be mutated in lung and breast cancer.

Changes in histone modifications are also a common occurrence in cancer. Mutations in HAT genes occur in colon, lung and leukaemias, and chromosomal translocations in haematological cancers often involve these genes [192]. Overexpression of HDACs has been observed in several cancers, which is probably related to their silencing of tumour suppressor genes [193, 194]. However, there is also evidence that in some situations they may do the opposite, maintaining chromatin structure and preventing tumourogenesis [195]. In addition, germline mutations in HDACs have also been associated with increased risk of lung and breast cancer [194]. It therefore seems likely that loss or gain of function mutations in HDACs could contribute to tumourogenesis in different tissue types. Mutations in genes associated with histone methylation have also been identified in cancer. The MLL gene, which codes for a HMT, is a site of chromosome translocation which commonly occurs in AML [196]. The fusion proteins generated are associated with a poor prognosis and results in aberrant H3K4me3 expression [197]. Mutations in MLL have also been identified in solid tumours, such as prostate and bladder [198, 199]. An increase in H3K27me3 has been observed in prostate breast and bladder cancer due to overexpression of EZH2, which may have a role in control of growth [200, 201]. Gain of function mutations in this same gene is also associated with poor prognosis in lymphoma [201]. In addition, another HMT, G9a, is mutated in several solid tumours including breast and ovary [202]. Mutations in both classes of histone demethylases have also been identified in cancer, with LSD1 mutations in prostate cancer, and KDM6A in brain, breast, bladder and lung cancer. The loss of function of the latter may enhance tumour cell proliferation [203].

DNA methylation		
Gene	Function	Tumour
DNMT1	DNA methyltransferase	colorectal, lung, pancreas, breast, gastric
DNMT3A	DNA methyltransferase	AML
DNMT3B	DNA methyltransferase	breast, lung
TET1	5'methylcytosine hydrolase	AML
TET2	5'methylcytosine hydrolase	AML, glioma
MBD1/2	methyl binding protein	breast, lung

Histone modification		
Gene	Function	Tumour
MLL1/2/3	Histone methyltransferase	Bladder, AML, lymphoma, prostate
G9a	Histone methyltransferase	Liver, breast, ovary, cervix
EZH2	Histone methyltransferase	Lymphoma, bladder, prostate , breast
LSD1	Histone demethylase	Prostate
KDM6A	Histone demethylase	Bladder, breast , lung, colon, brain
JARID1B/C	Histone demethylase	Breast, renal, testicular
CREBBP	Histone acetyltransferase	Gastric, colon, ovary, lung
PCAF	Histone acetyltransferase	Epithelial
EP300	Histone deacetyltransferase	Breast, pancreas, colon
HDAC2	Histone deacetyltransferase	Gastric, colon, endometrial
HDAC5/7A	Histone deacetyltransferase	Colon, prostate, breast

Table 1-1 Cancer mutations in genes involved in epigenetic modification.
Table depicting mutations in different genes involved in DNA and histone modification that have been associated with cancer. Indicates the tumour types where each mutation has been identified [182]. Abbreviations: AML, acute myeloid leukaemia.

1.2.7 Targeting epigenetics in cancer

These epigenetic changes have clinical significance with global changes in histone methylation and acetylation having important prognostic significance in colon, prostate and non-small cell lung cancer [204-206]. This has led to the development of drugs to target these epigenetic changes in cancer. The first successful targets were the DNMTs, with Decitabine and Azacitidine developed over 50 years ago. They were, however, limited to the treatment of myelodysplastic syndromes due to toxic side effects at high doses [207]. Vorinostat and Romidepsin are the only other drugs used in clinical practice, both of which inhibit HDACs and are used in the treatment of T-cell lymphoma, but again have issues of toxicity in other tumour types [208]. Targeting of HMTs has also not resulted in any clinical efficacy, which may be due to the broad activity and redundancy of these enzymes [209]. The difficulty in developing anti-cancer drugs targeting epigenetics may mean that greater clinical potential may be achieved by targeting some of the underlying metabolic causes.

1.6 The metabolic mechanism of epigenetic modification

Metabolism and epigenetics are linked through the processes of methyl and acetyl transfer, utilising s-adenylmethionine (SAM) and acetyl-CoA as substrates, respectively (Figure 1-4). SAM is generated from the coupled folate and methionine cycles, collectively called one carbon metabolism. This is also essential for the synthesis of nucleotides, protein, lipids, and glutathione, which maintains the redox state of the cell. For this reason, 1-carbon metabolism is often overactive in cancer [210], and is the reason why folate antagonists, such as methotrexate and pemetrexate, have proved to be successful in the clinic. Serine, glycine, methionine, and folic acid are important sources for one carbon metabolism and can be taken up by the cell. However, serine, glycine, and methionine can be synthesised de novo in the cell, which helps maintain one carbon metabolism when nutrients are scarce. Serine, which can be synthesised from 3-phosphoglycerate, an intermediate in glycolysis, donates a carbon to the folate cycle while producing glycine, and converting tetrahydrofolate (THF) to methylthetrahydrofolate (mTHF). In turn, glycine can also provide one carbon through the glycine cleavage system, producing mTHF. mTHF forms the link to the methionine cycle by providing the methyl group for betaine

hydroxymethylatransferase to catalyse the reaction of homocysteine to methionine. Methionine can in turn be utilised in protein and lipid synthesis or adenylated to SAM, the major methyl donor in the cell. SAM is then utilised by DNA and histone methyltransferases to methylate amino acid residues on DNA and histone tails, respectively.

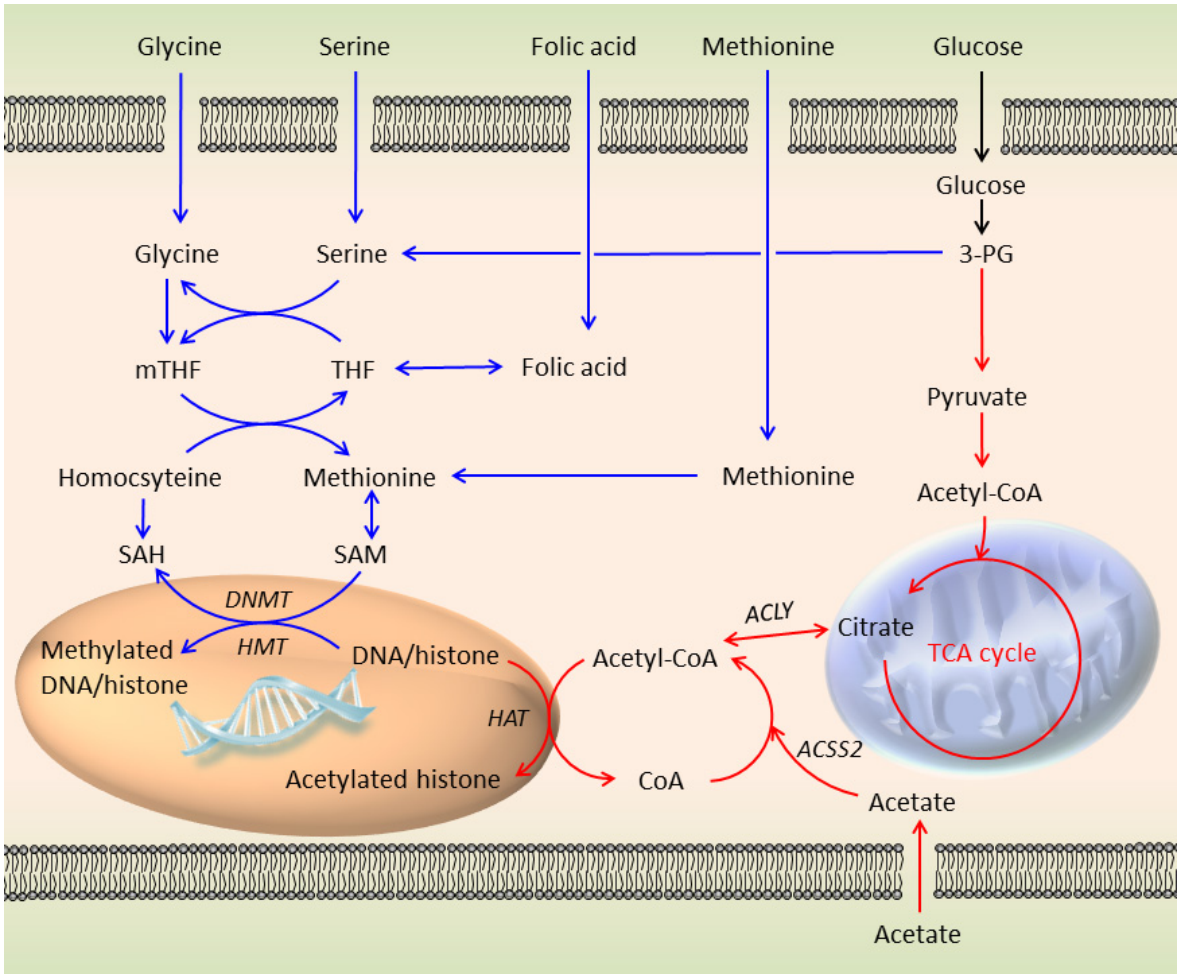

Figure 1-4 Methyl and acetyl transfer pathways
The blue pathway depicts one carbon metabolism and its generation of SAM, which provides a methyl group for histone and DNA methylation. Imported folate is reduced to THF and subsequently methylated to mTHF by the conversion of serine to glycine and the glycine cleavage system. The folate cycle is coupled to the methionine cycle by mTHF, donating a carbon to homocysteine converting it to methionine. Adenylation of methionine produces SAM, which acts as a co-substrate for DNMT and HMT, allowing transfer of its methyl group to DNA and histone tails respectively. The red pathway depicts acetyl transfer from acetyl-CoA. Acetyl-CoA which is derived from pyruvate, links glycolysis to the TCA cycle but is confined to the mitochondria. In the cytoplasm and nucleus, acetyl-CoA has to be derived by two alternative methods: firstly by ACLY, which utilises citrate from the mitochondrial TCA cycle, and secondly, ACSS2 which ligates acetate to CoA. Acetyl-CoA can then be utilised as a co-substrate by HAT, allowing transfer of the acetyl group to lysine residues on histone tails. Abbreviations: THF, tetrahydrofolate; mTHF, methyltetrahydrofolate; SAH, S-adenosylhomocysteine; SAM, S-adenosylmethionine; DNMT, DNA methyltransferase; HMT, histone methyltransferase; 3-PG, 3-phosphoglyceric acid; ACLY, ATP-citrate lyase; ACSS2, acetyl-CoA synthetase short-chain family member 2; HAT, histone acetyltransferase (reproduced from [1]).

Acetylation of histones is dependent on the acetyl donor, acetyl-CoA. Acetyl-CoA is an important link between glycolysis and the TCA cycle in the mitochondria, and is catalysed by pyruvate dehydrogenase. In the cytoplasm and nucleus, however, acetyl-CoA production is dependent on two different enzymes: ATP-citrate lyase (ACLY) and actyl-CoA synthetase short-chain family member 2 (ACSS2) (Figure 1) [211]. ACLY produces actyl-CoA from citrate, while ACSS2 ligates acetate to coenzyme A (CoA). Acetyl-CoA then acts as the acetyl donor for lysine acetylation on histone tails by HAT. While ACLY derives acetyl-CoA from the TCA cycle, ACSS2 is important as a scavenger of CoA from histone, protein, and lipid deacetylation reactions. Interestingly, it may also utilise exogenous acetate as a source of acetyl-CoA, especially during hypoxia [212, 213].

1.6.1 Oncometabolites and their effect on the epigenome

Changes in metabolism have been shown over the last 15 years to affect the epigenome. Regulators of major metabolic pathways such as AKT and PKM2 have been shown to alter histone acetylation. Global levels of histone acetylation correlates with phosphorylation of AKT in prostate cancer and glioma. This is likely due to the effect AKT has on citrate metabolism, with activation of AKT phosphorylating ACLY, resulting in an increase in histone acetylation *in vivo* [214]. PKM2 has also been shown to increase histone acetylation at the promoter regions of c-MYC and CCND1 (cyclin D1), by phosphorylating histone H3. This prevents the binding of HDAC, promoting H3K9 acetylation at these promoter sites, activating transcription and promoting cell growth [215, 216]. Histone methylation levels can also be affected in cancer cells by the overexpression of N-methyltransferase. This enzyme is involved in the catabolism of SAM to 1-methyl nicotinamide, which is highly stable and not utilised further by the cell. Overexpression of N-methyltransferase, results in a reduction in SAM with a corresponding decrease in histone methylation and an altered phenotype [217].

Mutations in metabolic genes can also promote epigenetic changes through a common mechanism, the accumulation of an “oncometabolite”. This acts as a competitive inhibitor of α-KG dependent dioxygenases, an ever-expanding superfamily of over 60 enzymes. Dioxygenases are involved in fatty acid metabolism, oxygen sensing, and collagen biosynthesis, as well as modulation of

the epigenome [172]. Chemically, they all share a common requirement for oxygen and α-KG as co-substrates. Hydroxylation of the primary substrate occurs in conjunction with the oxidative decarboxylation of α-KG to generate succinate and carbon dioxide (Figure 1-5).

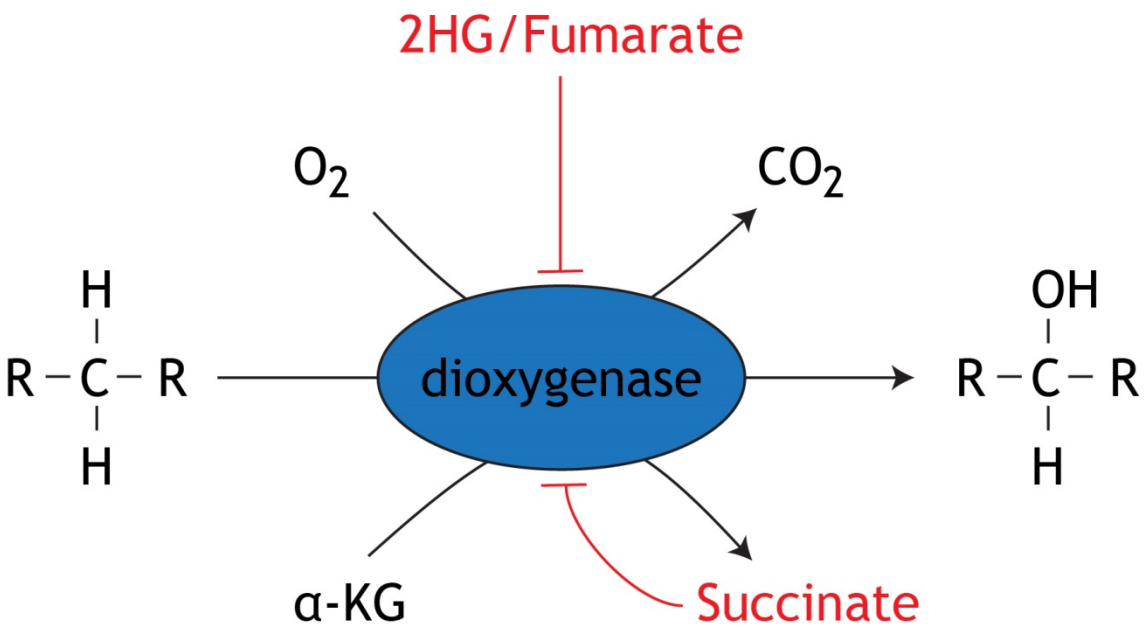

Figure 1-5 α-ketoglutarate (α-KG) dependent dioxygenases
This superfamily of enzymes uses oxygen and α-KG as co-substrates resulting in the hydroxylation of the primary substrate and the decarboxylation of α-KG producing succinate and CO2. These enzymes can be inhibited by elevated levels of 2-hydroxyglutarate, succinate and fumarate. This may occur by competing with the co-substrate α-KG, or potentially by product inhibition in the case of succinate and fumarate (adapted from [1]).

The first such effect was demonstrated for the loss of function of SDH in cancer. SDH loss was initially discovered in familial paraganglioma [218], but also occurs as spontaneous somatic mutations [219]. These tumours are of neuroendocrine origin and most commonly affect the carotid body, but can occur anywhere in the sympathetic and parasympathetic chain, as well as in the catecholamine-secreting chromaffin cells in the adrenal gland where it is called phaechromocytoma. SDH is a TCA cycle enzyme and also forms complex II of the electron transport chain. It oxidises succinate to fumarate with the transfer of an electron to ubiquinone, contributing to ATP production. The enzyme consists of 4 subunits, each of which can be mutated and cause a loss of function [218, 220-222].

Fumarate hydratase (FH) catalyses the next reaction in the TCA cycle: the hydration of fumarate to malate. It was also identified in a familial syndrome (Hereditary Leiomyomatosis and Renal Cell Cancer, HLRCC) resulting in smooth muscle tumours called leiomyomas and aggressive renal cell carcinomas [223]. They have subsequently been identified, like SDH mutations, in paragangliomas and phaechromocytomas [224]. In FH and SDH deficient tumours, there is the respective accumulation of fumarate or succinate, which confers a common function by competitively inhibiting α-KG dependent dioxygenases [225]. It seems likely that succinate and fumarate, which are structurally similar, inhibit these enzymes through product inhibition, as the effect of both metabolites can be reversed by the addition of excess α-KG in vitro and in vivo [226] (Figure 1-6).

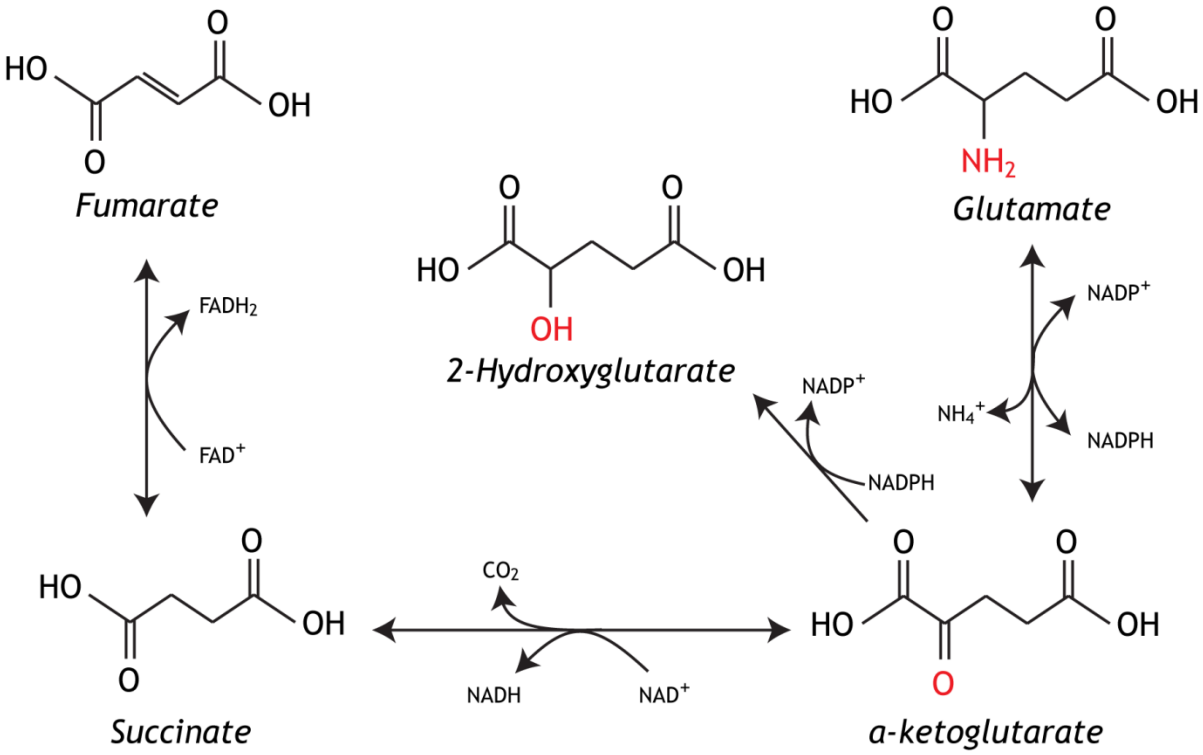

Figure 1-6 The metabolic structure of oncometabolites
Succinate, fumarate and 2-hydroxyglutarate (2HG) are closely linked both structurally and metabolically to α-ketoglutarate (α-KG). Succinate and fumarate differ from α-KG only by the presence of a hydroxyl group on C2 and the loss of C1. In addition, succinate and fumarate differ only in the presence of an ethylenic bond, which may explain their similar tumorigenic effects. 2HG differs from α-KG and glutamate only in the presence of a hydroxyl group instead of a ketone or amine group, respectively. This explains how 2HG can competitively inhibit α-KG by occupying the same enzymatic binding site (reproduced from [1]).

IDH is another TCA cycle related enzyme that has been implicated in tumorigenesis. Using genomic screening it was identified as a common mutation in gliomas as well as acute myeloid leukaemia (AML) [94, 95, 227]. Interestingly,

it is associated with a better prognosis in glioma, but a poorer prognosis in AML [228]. Subsequently, mutations have also been identified in other rare types of solid tumours, such as cholangiocarcinoma and chondrosarcoma [229, 230]. Isocitrate dehydrogenase exists as 3 isoforms (IDH1/2/3), with IDH1 present in the cytoplasm and IDH-2/3 in the mitochondria. IDH1 and 2 convert isocitrate to α-KG by oxidative decarboxylation with the production of NADPH from NADP+. IDH-3 is structurally different from the other two isoforms and utilises NAD+ to produce α-KG and NADH. It has not been found mutated in any cancer to date. The site of the mutation in IDH1/2 is at an equivalent arginine residue which is important to the active site for isocitrate binding [147]. There is an increased affinity instead for α-KG, and the mutated enzyme utilises NADPH in a partially reversed reaction to produce a new metabolite; 2-hydroxyglutarate (2HG) [147] (Figure 1-7). In gliomas, the arginine 132 (R132) is substituted for histidine (R132H) in 90% of IDH1 mutations, the rest consisting of arginine substituted with cysteine, serine, leucine or glycine. The corresponding arginine in the IDH2 mutation is R172, which is substituted for lysine. In AML, the substitution of arginine at R140 for glutamine has also been identified [95].

The IDH1 isoform accounts for 65% of cellular NADPH, which is an essential cofactor for the synthesis of glutathione (GSH), the most abundant intracellular antioxidant [231]. GSSG, the oxidised form of glutathione is reduced by glutathione reductase to GSH utilising NADPH. In this respect, the activity of IDH1 is important in maintaining the redox state of the cell. The IDH1 mutation results in the consumption of NADPH as opposed to production by the wild-type enzyme. It has been shown that overexpression of this mutation results in a fall in intracellular NADPH and glutathione, with a corresponding increase in reactive oxygen species (ROS) [232]. ROS has been shown to induce apoptosis, cause cell cycle arrest and reduce cell proliferation [233, 234]. The generation of ROS during chemotherapy and radiotherapy, coupled with the reduced ability to generate glutathione in IDH mutant tumours may explain in part the improved prognosis compared to wild-type gliomas [235].

Overexpression of IDH1 in cell lines has also been shown to result in other metabolic effects, which include a fall in α-KG and glutamate, as well as the increase in 2HG [236, 237]. This is presumably related to the increased consumption of α-KG by the IDH mutant enzyme. α-KG and glutamate are

structurally similar and are separated by a single metabolic reaction, via glutamate dehydrogenase, so are rapidly interchangeable. Glutamine is a major fuel for the cell and is metabolised to glutamate by glutaminase, so may provide a source of α-KG for the cell. This has led to a proposed model of glutamine addiction, as increased consumption of this metabolite may maintain α-KG levels in IDH mutant cells sufficiently to maintain cell growth [238]. However, inhibition of glutaminase in *in vitro* studies has only had a modest effect on IDH1 mutant cell proliferation, indicating that other metabolic pathways may be compensating for the fall in α-KG [239]. Low grade gliomas, which are predominantly IDH1 mutant, also express the excitatory amino acid transporter 2 (EAAT2), which is involved in the uptake of glutamate from the extracellular space [240, 241]. This raises the possibility that glutamate itself may be an important carbon source for α-KG production in IDH mutant tumours [242]. In addition, an IDH1 mutant oligodendroglioma xenograft model has been shown to maintain intracellular levels of α-KG compared to wild-type tumours, but with a marked increase in mitochondrial density and activity. This indicates another potential mechanism for maintaining α-KG production in IDH1 mutant cells, by increasing mitochondrial α-KG metabolism to compensate for a reduction in cytoplasmic production [243].

2HG is a five carbon dicarboxylic acid that is normally detectable in small amounts in the urine and amniotic fluid [244], but the exact physiological role of 2HG, if any, is not known. 2HG is structurally very similar to α-KG and glutamate; the only difference being the presence of a hydroxyl group instead of a ketone or amine group, respectively (Figure 1-6). It is this similarity that results in the competitive inhibition of α-KG dependent dioxygenases by 2HG, as it occupies the same binding site as α-KG [245]. The IDH1/2 mutation is associated with a decrease in α-KG potentially enhancing the inhibitory effect of 2HG on dioxygenases [236, 237]. 2HG occurs in two enantiomers, D-2HG and L-2HG, which are metabolised by FAD-linked 2HG dehydrogenases specific to each. Elevated levels of 2HG have been detected in two rare autosomal recessive genetic diseases, D-2-hydroxyglutaric aciduria (D-2HGA) and L-2- hydroxyglutaric aciduria (L-2HGA), where a markedly elevated level of 2HG is detectable in the urine. These diseases are caused by mutations in 2-HG dehydrogenases, as opposed to IDH in glioma. Both genetic conditions develop different phenotypes,

with variable severity, independently of the amount of 2HG secreted. D2HGA can cause early onset epileptic encephalopathy, cardiomyopathy and dysmorphic facial features [246] while L2HGA causes a progressive neurodegenerative disorder, and can predispose to brain tumours [247].

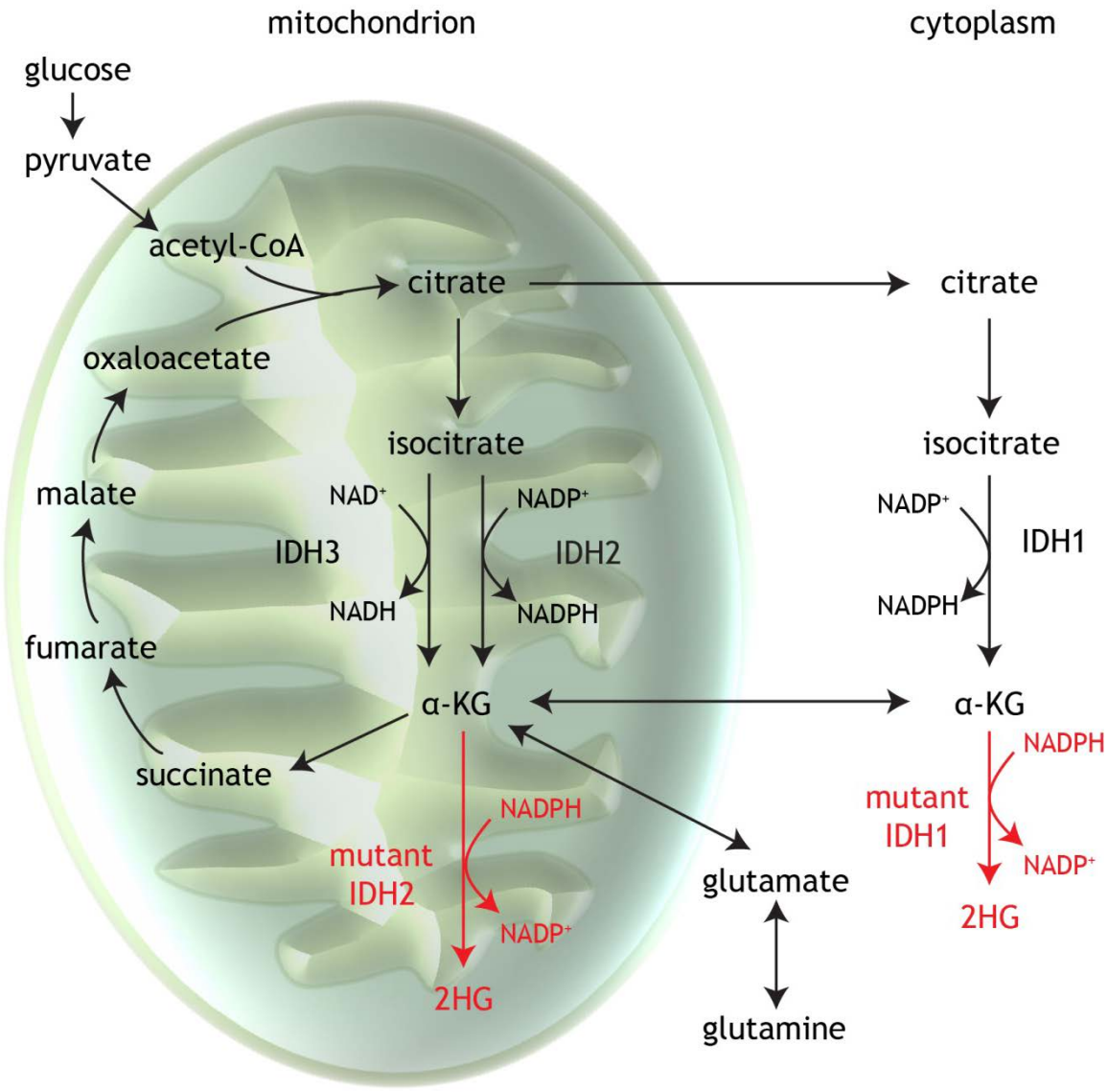

Figure 1-7 Isocitrate dehydrogenase mutation
Isocitrate dehydrogenase exists as 3 isoforms (IDH1/2/3), with IDH1 present in the cytoplasm and IDH-2/3 in the mitochondria. IDH1 and 2 convert isocitrate to α-KG by oxidative decarboxylation with the production of NADPH from NADP+. IDH-3 is structurally different from the other two isoforms and utilises NAD+ to produce α-KG and NADH. An equivalent point mutation on an arginine residue in IDH1/2 can occur at the active site for isocitrate binding. This results is an increased affinity instead for α-KG, and the mutated enzyme utilises NADPH in a partially reversed reaction to produce a new metabolite; 2-hydroxyglutarate.

It has been hypothesised that 2HG is a by-product of other cellular processes, and the 2HG dehydrogenases maybe acting as a "metabolite repair mechanism" [248]. L-2HG seems to be formed by mitochondrial L-malate dehydrogenase [248] and D-2HG by hydroxyacid-oxoacid transhydrogenase [249], but both at a much slower rate than their respective primary products. It is D-2HG that is produced by the IDH1/2 mutation.

A subgroup of α-KG dependent dioxygenases implicated in tumorigenesis are the prolyl hydroxylases (PHD), which play an important role in the degradation of hypoxia inducible factor (HIF) in normoxic conditions. HIF activates a range of genes in response to low oxygen to increase glycolysis and angiogenesis. In the presence of oxygen, PHD hydroxylates prolyl groups on HIF allowing it to bind to the von Hippel-Lindau (VHL) protein which tags HIF for ubiquitylation and degradation in the proteasome [250]. FH and SDH mutations cause a "pseudohypoxic" phenotype through the inhibition of PHDs that stabilises HIF. This promotes a hypoxic response even in the presence of oxygen causing increased glycolysis and angiogenesis [226, 251]. The effect of 2HG on PHDs is less clear, with conflicting evidence of an inhibitory as well as activating effect [245, 252-254]. This indicates variations between oncometabolites in their affinity towards different members of the α-KG dependent dioxygenase family of enzymes.

IDH, FH, and SDH mutations are associated with changes in DNA and histone methylation. A subset of gliomas has been identified that has a distinct pattern of CpG island hypermethylation (G-CIMP) [107], which has been replicated in mutant IDH1 overexpressed immortalised astrocytes, and a single copy IDH1 mutant knock-in colorectal cell line [255, 256]. IDH mutations in cholangiocarcinoma also replicate this hypermethylation pattern [257]. This is also likely to extend to SDH mutations, with similar patterns of DNA methylation observed in mouse derived SDH deficient chromaffin cells [258]. The underlying mechanism for these changes seems to be inhibition of TET, an α-KG dependent dioxygenase, which exists in three isoforms (TET 1-3). They hydroxylate 5-methylcytosine (5mC) to 5-hydroxymethylcytosine (5-hmC), allowing subsequent DNA demethylation. In human glioma tissue samples, levels of 5-hmC are markedly reduced in IDH mutant compared to IDH wild-type tumours [245]. In cell culture, this reduction in 5-hmC has been replicated by over expressing

mutant IDH1/2 in numerous cell lines including glioma, immortalised astrocytes and myeloblasts [190, 255]. The same effect has also been observed in FH and SDH mutant cell models [225]. Interestingly, in human AML samples, mutations in TET2 were found to be mutually exclusive to mutations in IDH, and produce similar DNA methylation patterns to IDH mutant AML [190]. Further genomic analysis of IDH1/2 mutant AML revealed increased methylation of promotor sites of genes associated with myeloid differentiation, producing a more stem-like phenotype [190]. Over-expression of IDH1, or exposure to exogenous cell permeable 2HG, was able to promote cytokine independence and block differentiation in a leukaemic cell line. This could be replicated by knockdown of TET2, providing a potential link between 2HG, TET inhibition, and tumorigenesis [259].

The jumonji-C (JMJ) histone demethylases are a sub group of histone demethylases that are members of the α-KG dependent dioxygenase family [172]. They initiate the first step in the removal of methyl groups by hydroxylation causing an increase or decrease in gene transcription dependent on the histone methylation site. JMJ histone demethylases are very sensitive to high levels of fumarate, succinate, and 2HG [260]. In the case of the IDH1/2 mutation, increases in histone methylation have been observed in human glioma samples for H3K9 and H3K27, both gene repressive marks [245, 261]. Interestingly, the IDH1 mutation was strongly correlated with H3K9me3 in oligodendrogliomas, but not astrocytomas, which are two different subtypes of glioma [262]. This implies that there is a differential effect of 2HG on different tumours even in the same tissue type. Murine 3T3-L1 fibroblasts, which can be differentiated into adipocytes, were used to prove a link between the repressive histone methylation marks, H3K9me3 and H3K27me3, and cellular differentiation. Over-expression of mutant IDH1 was associated with impaired adipogenesis due to an increase in both H3K9me3 and H3K27me3 at promoter sites for transcription factors responsible for adipocyte differentiation. Similar changes in histone methylation marks and impaired differentiation were also seen in IDH1 overexpressed primary murine neurospheres [261]. Increases in H3K27me3 and H3K9me3 have also been observed in SDH and FH mutant tumours and cell models [225, 258]. Interestingly, increased levels of H3K9me3 occur prior to increases in DNA methylation when mutant IDH1 is introduced to

immortalised astrocytes [261]. These histone methylation changes may therefore account for some of the changes in DNA methylation patterns [263].

1.6.2 Future therapies

There is now increasing evidence that mutations in metabolic enzymes are in part responsible for the epigenetic changes in some cancers. At least in AML there is reasonable evidence to suggest that the IDH1 mutation alone may be sufficient to induce leukoneogenesis by inhibiting genes responsible for cell differentiation through DNA hypermethylation [259]. For other tumours it is less clear, but at least in glioma, the IDH mutation seems to be an early event that is maintained throughout tumour progression [95]. It is also becoming evident that the presence of oncometabolites in tumours is not confined to malignancies with TCA gene mutations. Elevated levels of 2HG, driven by myc activation, have been identified in breast cancer resulting in DNA hypermethylation [264]. Interestingly, 3-phosphoglycerate dehydrogenase, which is the enzyme responsible for the first step in serine biosynthesis from the glycolytic intermediate 3-phosphoglycerate, has recently been shown to convert α-KG to 2HG by utilising NADH [265]. This provides a possible link between increased myc-driven glycolysis and 2HG production in some breast cancers. It seems likely that other tumours may also be affected, and new oncometabolites may be identified in the future. In fact, an *in silico* systems approach using 1700 genomes has already been used to identify potential new oncometabolites in a range of tumours [266].

The unique presence of 2HG in IDH1 mutant tumours raises the possibility of using non-invasive imaging techniques for diagnosis and monitoring of treatment response [267]. Magnetic resonance spectroscopy (MRS) allows for the measurement of metabolites within the brain using the same hydrogen protons used to make an anatomical image in magnetic resonance imaging (MRI), a widely used clinical technique. 2HG accumulates to a concentration of 5 to 35 mM in IDH1 mutant tumours, while normal tissue only contains trace levels of the metabolite [147]. In addition, the only other cause of raised 2HG is D-2HGA and L-2HGA; both very rare genetic disorders which have very specific phenotypes. This indicates that 2HG could be an ideal biomarker using MRS. The only complication is that the MRS spectra of NAA and glutamate overlap that of

2HG and may give a false negative result in tumours with low levels of the metabolite [268]. Further validation of the technique is warranted, but it has great potential in clinical practice.

The discovery of metabolic enzymes that can alter the epigenome has opened up a new exciting area for drug development. In only 5 years, IDH1 and IDH-2 small molecule inhibitors have been developed that are now entering clinical trials. AGI-5198, an IDH1 inhibitor, was tested in a heterozygous IDH1 mutant glioma cell line (TS603). It was able to reverse H3K9 trimethylation, promote cellular differentiation and delay growth, though interestingly it had no effect on DNA methylation [269]. Similarly, AGI-6780, a specific inhibitor of mutant IDH-2, induced leukaemic cell differentiation in primary human samples *ex vivo* [270]. Further investigation using a mutant IDH2 overexpressed leukaemic cell line showed reversal of both DNA and histone hypermethylation, inducing cell differentiation. Interestingly, histone methylation is rapidly reversed within days, while DNA methylation progressively changes over a period of weeks [271]. This is likely due to the fact that DNA methylation is highly stable compared to histone methylation, and less easily reversed [263], which may explain the lack of change in DNA methylation in TS603, and the slow change in DNA methylation in the mutant IDH2 overexpressed cell line. In addition, the TS603 cell line has an endogenous IDH1 mutation, so the epigenetic changes are likely to be long-standing and so maybe less easily reversed. This may explain the modest effect on cell growth of IDH1 inhibition in glioma pre-clinical models.

It will be interesting to see if these new drugs are equally efficacious in different types of IDH mutated tumours. In glioma, the presence of an IDH1 mutation is actually associated with a better prognosis compared to wild-type tumours. These tumours grow more slowly *in vitro* as well as *in vivo* [272]. The concern in glioma is that inhibiting 2HG production may potentiate tumour growth. Reduced expression of branch chain amino acid transferase 1 (BCAT1) in IDH1 mutated gliomas has been shown in part to be caused by hypermethylation of the BCAT1 promotor region. When BCAT1 is overexpressed in IDH1 mutant immortalised human astrocytes, some of the loss in cell proliferation is recovered [273]. This raises the concern that inhibition of the mutant IDH enzyme in glioma may increase cell proliferation, and further research is needed into the downstream effects of the IDH1 mutation. This is in direct contrast to

AML, where IDH mutations are associated with a worse prognosis and more aggressive disease, and where mutant IDH inhibitors may prove more beneficial.

1.7 Use of Stable Isotope Tracers

The extraction of metabolites from cells and medium can give useful information about changes in total metabolite levels. However, to demonstrate changes in related metabolic pathways it is important to use stable isotope tracing. When investigating changes in glycolysis, glutaminolysis, and the TCA cycle, $^{13}C_6$-glucose and $^{13}C_5$-glutamine are used as they are the major carbon sources for these pathways.

^{13}C stable isotopes tracers are non-radioactive compounds, where some or all of the ^{12}C atoms have been replaced by ^{13}C. Other atoms can also be replaced in this way such as ^{15}N for ^{14}N, an example of which is ^{15}N-GABA which was used in this study. In this thesis all the ^{13}C and ^{15}N isotopes are fully labelled. The metabolism of $^{13}C_6$-glucose and $^{13}C_5$-glutamine can be followed by measuring isotopologues of downstream intracellular metabolites over time. Isotopologues are similar molecular entities that differ only in their mass due to a different isotopic composition (Figure 1-7).

Steady state labelling was done by adding medium labelled with $^{13}C_6$-glucose or $^{13}C_5$-glutamine for 24 hours. In this situation, intracellular metabolites and metabolic fluxes are assumed to be constant as the cells are in an exponential growth phase. The contribution of labelled isotopologues for different metabolites can give an indication of qualitative changes in a particular pathway. An example of this would be looking at changes in abundance of the M+3 malate isotopologue from $^{13}C_6$-glucose, which would give an indication of relative differences in flux through pyruvate carboxylase. Dynamic labelling can give additional information on flux through a pathway by measuring how fast a labelled metabolite accumulates over time. The faster the labelled metabolite accumulates, the greater the flux to that metabolite from the labelled source. However, both methods cannot give absolute changes in flux as this would require complex computer modelling using data from labelling experiments, intracellular steady state concentration of each metabolite, and metabolite exchange between the medium and intracellular space.

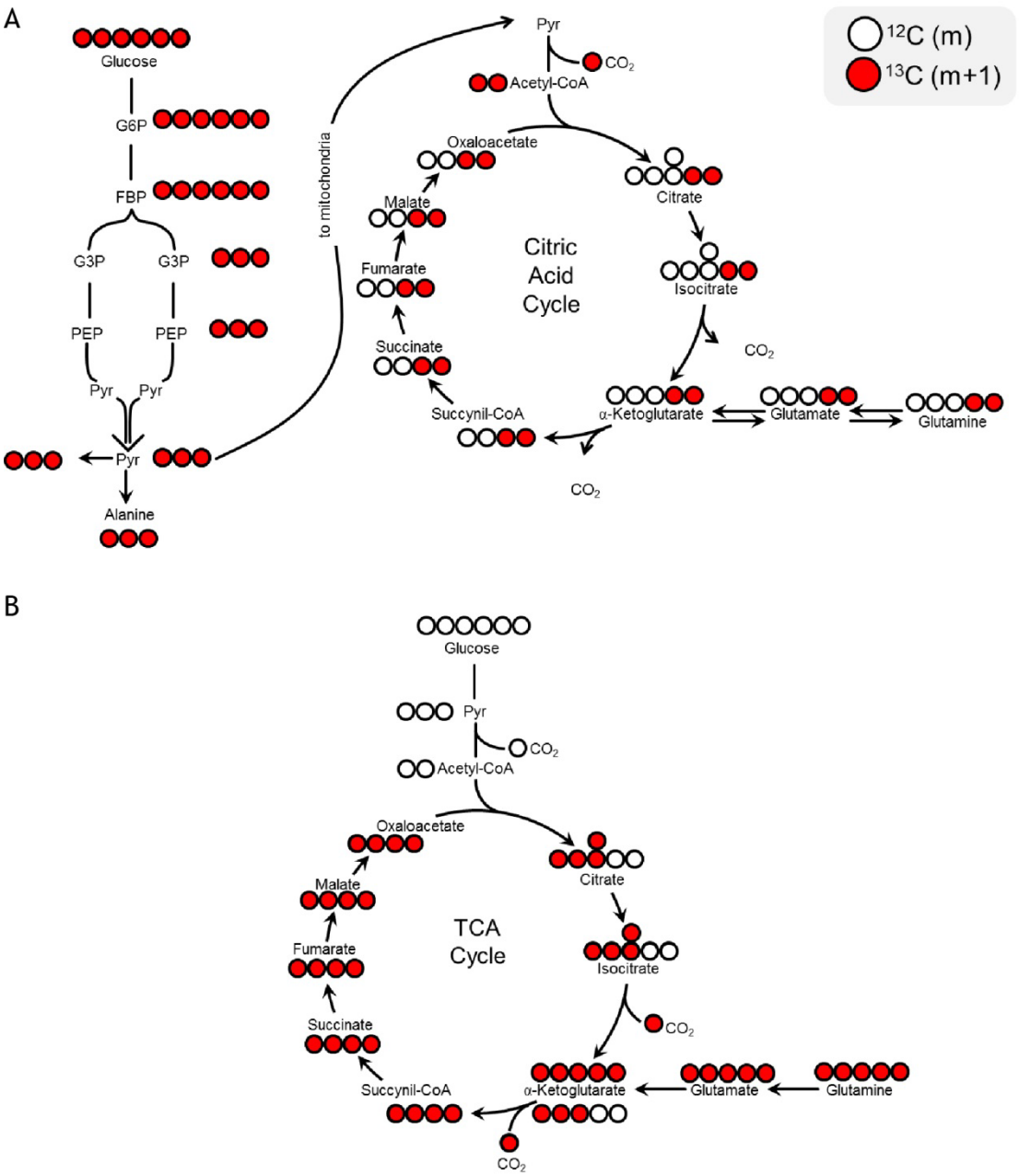

Figure 1-8 Metabolism of $^{13}C_6$-glucose and $^{13}C_5$-glutamine
Diagrams depicting how different isotopologues are generated from $^{13}C_6$-glucose (A) and $^{13}C_5$-glutamine (B) as they are metabolised around the TCA cycle. ^{12}C atoms are depicted in white and ^{13}C atoms in red.

Chapter 2 Materials and Methods

2.1 Materials

2.1.1 Reagents

Reagent	Supplier
Acetone	Fisher Scientific
Acetonitrile (HPLC grade)	VWR Chemicals
Acrylamide solution-30% acrylamide,37.5:1	Severn Biotech Ltd
Acrylamide solution-40% acrylamide,37.5:1	Bio-Rad
Agarose	Melford
4-aminobutyric acid-1-13C	ICON Isotopes
4-aminobutyric acid-1-15N	Sigma Aldrich
Ammonium persulfate (APS)	Fisher Scientific
Ampicillin	Sigma Aldrich
Baclofen	Sigma Aldrich
Bicuculline methiodide	Abcam
BSA	Calbiochem
Dimethyl 2-oxoglutarate	Sigma Aldrich
Dimethyloxaloylglycine (DMOG)	Sigma Aldrich
Dimethyl Sulfoxide (DMSO TC-grade)	Sigma Aldrich
DH5α competent cells	Invitrogen
DMEM (21969-035)	Invitrogen (GIBCO)
Dynabeads M-280 sheep anti-mouse IgG	Life Technologies
Ethanol	VWR Chemicals
Ethidium Bromide	Sigma Aldrich
Ethylenediamine tetraacetic acid (EDTA)	Sigma Aldrich
Ethylene glycol tetraacetic acid (EGTA)	Sigma Aldrich
Fast SYBR® Green Master Mix	Life Technologies
FBS	GE healthcare
Glutamine	Invitrogen
Glucose 13C	Cambridge Isotope Laboratories
Glutamine 13C	Cambridge Isotope Laboratories
Glycerol	Amersham Biosciences
G418S (Genetecin)	Formedium
HEPES	Invitrogen

Igepal CA-630	Sigma Aldrich
Methanol (General use)	Sigma Aldrich
Methanol (HLPC grade)	VWR Chemicals
Milk	Marvel
Muscimol	Sigma Aldrich
NaCl	Fisher Scientific
NaOH	Fisher Scientific
N-lauroylsarcosine	Sigma Aldrich
Paraformaldehyde (PFA)	Electron Microscopy science
Protease inhibitor cocktail solution	Sigma Aldrich
Puromycin	Sigma Aldrich
(R)-(-)-5-oxo-2-tetrahydrofurancarboxylic acid	Sigma Aldrich
Sodium deoxycholate	Sigma Aldrich
Sodium dodecyl sulphate (SDS)	Fisher scientific
SuperScript® VILO™ Master Mix	Life Technologies
Tetramethylethylenediamine (TEMED)	Sigma Aldrich
Triton X-100	Sigma Aldrich
Trypsin (10x)	Invitrogen
Tween-20	Sigma Aldrich
Vigabatrin	Sigma Aldrich

Table 2-1 Reagents

2.1.2 Kits

MODified histone peptide array, Histone purification mini kit (Active Motif**)**

MinElute PCR purification kit, RNeasy mini kit, QIAshredder, Qiaquick gel extraction kit (Qiagen)

Quibit RNA HS assay kit (Invitrogen**)**

Ribo-Zero magnetic kit (Epicentre)

Envision + system-HRP (DAB) (DAKO)

RNA 6000 Nano kit (Agilent)

2.1.3 General buffers and solutions

RIPA buffer: 50 mM Tris-HCl, 150 mM NaCl, 1% Triton x100, 1.0% NP-40, 0.1% SDS, 1:100 protease inhibitors cocktail, pH 8.0.

Metabolomics extraction buffer: 50% HPLC grade methanol, 30% HPLC grade acetonitrile, 20% milliQ water.

Phosphate buffered saline (PBS): 137 mM NaCl, 2.7 mM KCl, 10 mM Na_2HPO_4, 2 mM KH_2PO_4, pH 7.4.

4 X ProtoGel resolving buffer (Geneflow): 1.5 M Tris-HCl, 0.4% SDS, pH 8.8.

10% Acrylamide gel: 8 ml 4 X ProtoGel resolving buffer, 8 ml 40% acrylamide/bis, 16 ml H_2O, 320 µl APS, 20 µl TEMED.

15% Acrylamide gel: 8 ml 4 X ProtoGel resolving buffer, 12 ml 40% acrylamide/bis, 16 ml H_2O, 320 µl APS, 20 µl TEMED.

Stacking gel: 5.5 ml H_2O, 1.3 ml acrylamide/bis, 1 ml 1 M Tris (pH 6.8), 80 µl 10% SDS, 80 µl 10% APS, 12 µl TEMED.

1X Blotting buffer: 25 mM Tris, 192 mM glycine, 0.01% SDS, pH 8.3.

1X SDS-PAGE running buffer: 0.1% SDS, 192 mM glycine, 25 mM Tris-HCl pH 8.3

LB-Broth: 10 g/l tryptone, 5 g/l yeast extract, 10 g/l NaCl.

LB agar plates: LB medium, 15 g/l bacto agar.

4 X Laemlli buffer: 0.25 M Tris-HCl (pH 6.8), 40% glycerol, 8% SDS, 0.04% bromophenol blue, 0.2 M DTT.

Tris-acetate-EDTA 1X (TAE): 40 mM Tris, 20 mM acetic acid, 1 mM EDTA, pH 8.0.

PE: PBS, 0.01% EDTA.

Trypsin (1X): 10% 10 X trypsin, 90% PE.

PBST: PBS, 0.05% Tween-20.

Blocking buffer for western blot: 5% Milk in PBST.

Standard medium: high glucose DMEM, 10% FBS, 2 mM glutamine.

ChIP LB1: 50 mM Hepes-KOH (pH 7.5), 140 mM NaCl, 1 mM EDTA, 10% glycerol, 0.5% Igepal CA-630, 0.25% Triton-X 100.

ChIP LB2: 10 mM Tris-HCL (pH 8.0), 200 mM NaCl, 1 mM EDTA, 0.5 M EGTA.

ChIP LB3: 10 mM Tris-HCL (pH 8.0), 100 mM NaCl, 1 mM EDTA, 0.5 mM EGTA, 0.1% Na-Deoxycholate, 0.5% N-lauroylsarcosine.

RIPA buffer used in ChIP: 50 mM Hepes-KOH (pH 7.5), 500 mM LiCl, 1 mM EDTA, 1% Igepal CA-630, 0.7% Na-Deoxycholate.

ChIP elution buffer: 50 mM Tris-HCl (pH 8.0), 10 mM EDTA, 1% SDS.

TBS: 20 mM Tris-HCl (pH 7.6), 150 mM NaCl.

TBST: TBS + 0.05% Tween-20.

2.1.4 Plasmids

Plasmid	Supplier
pcDNA 3.1(+) wild type IDH1	Dr Mark Cockerill (Manchester University)
pcDNA 3.1(+) mutant IDH1 (R132H)	Dr Mark Cockerill (Manchester University)
pcDNA 3.1(+)	Invitrogen
pLKO.1	Addgene
pLKO.1 Scr	Addgene

Table 2-2 Plasmids

2.1.5 Antibodies

Primary Antibody	Concentration	Supplier
ABAT (ab108249)	WB 1/1000	Abcam
β-Actin (ab8226)	WB 1/5000	Abcam
GABAA Receptor β3 (ab98968)	WB 1/500, IHC 1/500	Abcam
H3K4me3 (9751S)	IHC 1/250	Cell Signalling
H3 (4499)	IF 1/200 WB 1:2000	Cell Signalling
H4 (ab10158)	IF 1/200 WB 1:1000	Abcam
H3K4me0 (CMA301)	IF 1/1000	H. Kimura
H3K4me1 (CMA302)	IF 1/500	H. Kimura
H3K4me2(CMA303)	IF 1/1000 WB 1/1000 IHC 1/500	H. Kimura
H3K4me3 (27B7)	ChIP 3 µg / Input WB 1:1000	H. Kimura
H3K4me3 (9751)	IHC 1/400	Cell signalling
H3K27me0 (37B4)	IF 1/500	H. Kimura
H3K27me1 (CMA 321)	IF 1/500	H. Kimura
H3K27me2 (CMA322)	IF 1/500	H. Kimura
H3K27me3 (CMA323)	IF 1/1000	H. Kimura
H3K27ac (CMA309)	IF 1/1000	H. Kimura
H3K9me0 (1C6)	IF 1/500	H. Kimura
H3K9me1 (CMA316)	IF 1/500	H. Kimura
H3K9me2 (CMA317)	IF 1/1000	H. Kimura
H3K9me3 (CMA318)	IF 1/1000	H. Kimura
H3K9ac (CMA310)	IF 1/1000	H. Kimura
H3K36me1 (CMA 331)	IF 1/500	H. Kimura
H3K36me2 (CMA332)	IF 1/500	H. Kimura
H3K36me3 (CMA 333)	IF 1/500	H. Kimura
H4K20me1 (15F11)	IF 1/500	H. Kimura
H4K20me2 (2E2)	IF 1/500	H. Kimura
H4K20me3 (27F11)	IF 1/500	H. Kimura
H4K20ac (6D6)	IF 1/500	H. Kimura
HA-probe (sc-7392)	3 µg / ChIP input	Santa Cruz
IDH1 (sc-49996)	WB 1/200	Santa Cruz
Myc-tag (9B11)	WB 1/1000	Cell Signalling
β-Tubulin (T5201)	WB 1:5000	Sigma Aldrich

Table 2-3 Primary antibodies
Antibodies for Western blot, immunohistochemistry, immunofluorescence and ChIP.

SecondaryAntibody	Concentration	Supplier
AlexaFlouro 488	IF 1/1000	Invitrogen
AlexaFlouro 555	IF 1/1000	Invitrogen
IR Dye 800CW donkey anti-goat	1/15000	LI-COR
IR Dye 800CW donkey anti-mouse	1/15000	LI-COR
IR Dye 680CW donkey anti-rabbit	1/15000	LI-COR
IR Dye 680CW donkey anti-mouse	1/15000	LI-COR
IR Dye 680CW donkey anti-rabbit	1/15000	LI-COR

Table 2-4 Secondary antibodies
Antibodies for immunofluorescence and Western blot.

2.1.6 Equipment

7500 Fast Real-Time PCR System (Applied Biosystems)

Odyssey CLx Infrared Imaging System (LI-COR Bioscience)

Agarose gel caster and tanks (Biorad)

SDS-PAGE mini-protean system (Biorad)

Exactive™ Plus Orbitrap Mass Spectrometer (Thermo Scientific)

CASY cell counter and analyser (Roche Applied Science)

Tissuelyzer bead-mill (Qiagen)

Agilent 2100 Bioanalyser

Qubit 2.0 flourometer (Invitrogen)

Bioruptor XL UCD-500 or Bioruptor Pico (Diagenode)

IncuCyte (Essen Bioscience)

SpectraMax Plus 384 spectrophotometer (Molecular Devices)

2.2 Experimental procedures

2.2.1 Metabolite extraction from clinical tumour samples

Clinical samples from brain tumours were obtained from 15 patients at the time of surgery at the Haukeland Hospital in Bergen, Norway. Fully labelled ^{13}C-glucose was administered prior to the start of surgery. Intravenous administration took 15 minutes and blood samples were taken during the operation (Figure 2-1). The blood samples were divided into 100 µl aliquots in 1.5 ml eppendorf tubes and stored at -80 ºC.

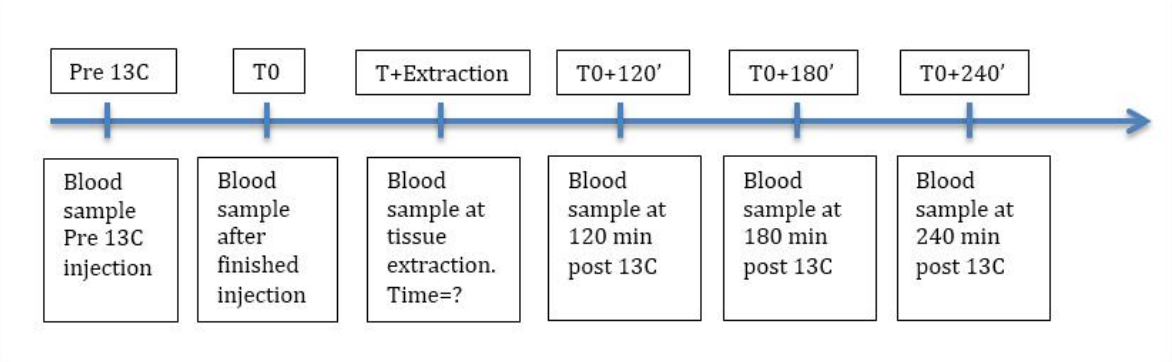

Figure 2-1 Flow diagram of blood sample collection during tumour removal
Samples were taken pre-^{13}C glucose injection, just after injection, at time of tumour removal, and every 60 minutes commencing 2 hours after injection.

The first 2 patients were given a 10 g $^{13}C_6$-glucose infusion over 20 minutes; all subsequent patients were given 20 g $^{13}C_6$-glucose. The surgeons stereotactically extracted roughly 200 mg tissue from the tumour core, contrast enhancing periphery, and non-enhancing oedema, if possible. After extraction, the samples were immediately snap-frozen in cryo-tubes. The tissues were further sub-divided, during one cutting session on ice, to yield fragments of roughly 15 mg, which were stored a -80 ºC. The weight of all tissue sub-fragments was determined accurately before the metabolite extractions, and metabolite extracts were generated from 1 replicate per region if possible. Metabolite extraction was done at the NORLUX lab in Luxembourg and samples were processed and analysed at the CRUK Beatson Institute, Glasgow. Informed consent was obtained from all human subjects prior to the start of the study. The administration of heavy isotopes and the collection of the surgical tissue

material was approved by the regional ethical committee at Haukeland University hospital, Bergen, Norway (REK 2010/130-2).

2.2.1.1 Extraction intracellular metabolites from brain tissue

During metabolite extraction the tissue and metabolite extraction buffer was kept on dry ice. 250 µL of metabolomics extraction buffer was added per 10 mg of tissue after it was placed in a 2 ml Eppendorf tube. The brain tissue was homogenised by mechanical disruption in a bead-mill (Retsch MM400 or Qiagen Tissuelyzer) using 5 mm beads added to the tissue and metabolite extraction buffer. The samples were then shaken for 2 cycles of 2 minutes at a frequency of 20 Hz. The samples were then transferred to an Eppendorf thermomixer at 4 ºC, vortexed at 1,400 rpm and spun down at 16,000 x g at 4 ºC for 15 minutes. The supernatant was then removed and stored at -80 ºC before analysis by liquid chromatography mass spectrometry (LC-MS).

2.2.1.2 Blood metabolite extraction

The blood samples were placed on dry ice and 300 µl of chilled metabolite extraction buffer (-20 °C) was added. As the blood thawed the samples were mixed by inverting the tube several times. The 1.5 ml tubes were placed in -20 °C chilled racks of the tissuelyzer, and homogenised by mechanical disruption in a bead-mill (Retsch MM400 or Qiagen Tissuelyzer) without the addition of beads. The samples were shaken for 2 x 2 minutes at a frequency of 20 Hz. Subsequently the samples were shaken for 12 minutes in an Eppendorf thermomixer (1,400 rpm at 4 °C). The clear supernatant was removed after centrifugation at 16,000 x g at 4 °C for 15 minutes. The samples were stored at -80 ºC before analysis by LC-MS.

2.2.2 Propagation of cell lines

2.2.2.1 MOG-GCCM

The MOG-GCCM cell line was propagated in 15 cm plates using high glucose DMEM with supplemented 2 mM glutamine and 10% FBS (heat inactivated at 56 °C for 45 minutes prior to use) in a humidified incubator at 37 °C and 5% CO_2. Cells were routinely split 1:3 every 3-4 days using 1 x trypsin. 600 µg/ml

geneticin was used to supplement the medium for cells transfected with the empty vector (EV) or IDH1 mutant plasmids. The EV + 2HG cells were EV cells maintained for at least 15 passages in medium containing 30 mM cell permeable 2HG-lactone [(R)-(-)-5-oxo-2-tetrahydrofurancarboxylic acid] unless otherwise stated.

2.2.2.2 Immortalised normal human astrocytes

The IDH1 wild-type and IDH1 mutant overexpressed immortalised astrocytes were kindly supplied by Sloan Kettering Institute for Cancer Research (SK2012-113) and were propagated in the same way as MOG-GCCM but with 400 µg/ml of geneticin.

2.2.2.3 NCH astrocytoma cell lines

Permission to use the NCH astrocytoma cell lines was given by Christel Herold-Mende, University of Heidelburg, and the cell lines were propagated at the NORLUX laboratories in Luxembourg. Five cell lines were used: two IDH1 wild-type GBM (NCH644, NCH421k) and three high grade endogenous IDH1 mutant (NCH1681, NCH551b, NCH612). The IDH1 mutant cell lines were derived from a secondary GBM, grade III astrocytoma, and a grade III oligodendroglioma, respectively. Metabolite extraction and protein quantification were done at the NORLUX laboratories and the samples were run and analysed at the CRUK Beatson Institute, Glasgow. These cell lines were grown as spheroids in the following medium: 400 ml DMEM, 100 ml BIT100 growth medium, 10 ml Pen-Strep, 17.5 mM glucose and 4 mM glutamax.

2.2.3 Freezing and thawing cells

The same procedure was used to freeze all cell stocks. Cells were detached using 1 x trypsin and pelleted by centrifuging at 1,000 x g for 5 minutes. The pellet was then re-suspended in freezing media (90% FBS, 10% DMSO) to give approximately $1x10^6$ cells/ml. 1 ml of the solution was then aliquoted into cryovials and placed into a polystyrene container at -80 °C overnight before transferring into a liquid nitrogen tank for long term storage.

The reviving of cell stocks required thawing of cells in a water bath at 37 °C before adding pre-warmed media and centrifuging at 1,000 x g for 5 minutes. The pelleting of the cells allowed for the removal of DMSO in the freezing media. Re-suspension of the pellet was done in fresh media and cells were transferred to a 10 cm plate for initial culturing.

2.2.4 Transfection of cell lines

Lipofectamine 2000 was used to transfect GCCM cells with EV and IDH1 mutant plasmids to produce stable cell clones. The procedure was as per manufacturer's guidelines. In brief, 5 x 10^4 MOG-GCCM parental cells were seeded into a 24 well plate with 500 µl medium without antibiotics to achieve 95% confluence after 24 hrs. For each well, 0.8 µg DNA was diluted in 50 µl Opti-MEM without serum. In addition, 2 µl Lipofectamine 2000 was diluted in a separate aliquot of 50 µl Opti-MEM without serum and incubated for 5 minutes at room temperature. Both solutions were then mixed together gently and incubated for 20 minutes at room temperature to allow for adequate complex formation. This was then added to the well and mixed gently by rocking. After 48 hrs, the cells were trypsinised and transferred to a 10 cm plate. The medium was changed after 24 hrs and the selective agent genetecin (600 µg/ml) was added. After 4 weeks, clones were removed using trypsin soaked sterile cloning disks (Sigma Aldrich) and propagated separately.

2.2.5 Cell proliferation assay

MOG-GCCM cells were seeded in triplicate at a density of 1 x 10^4 cells per well in 24 well plates. The next day, one plate was used to count cells at baseline. The medium was replaced in the remaining plates with 2.5 ml of standard medium. Plates were subsequently counted every 48 hrs for a minimum of 6 days. Counting was performed using a CASY cell counter and analyser (Roche Applied Science). Cell doubling time was calculated using exponential growth equation with least squares fit (Graphpad Prism software).

2.2.6 Clonogenic assay

MOG-GCCM cells were plated in triplicate at a density of 200 cells per well in a 6 well plate. The medium was changed every 5 days and the experiment

terminated at 16 days by fixing the cells in 4% paraformaldehyde for 15 minutes. The immortalised astrocytes were plated at the same density but the experiment terminated after 12 days. 1 ml of 0.05% crystal violet solution was then added to the wells for 30 minutes to stain the cellular protein. The plates were scanned using Epson perfection 4870 photo scanner. Quantification was done by counting colonies using Image J.

2.2.7 Metabolomics (Cell lines)

2.2.7.1 Metabolite extraction

MOG-GCCM: 2 x 10^5 cells were seeded per well of a 6-well plate, in triplicate. After 18 hrs the medium was replaced (1ml), and the metabolites extracted 24 hrs later, unless stated otherwise. For labelled metabolomics, ^{12}C-glucose or ^{12}C-glutamine was replaced in the medium by $^{13}C_6$-glucose or $^{13}C_5$-glutamine at the same concentration. In the experiments involving ^{15}N-GABA, this was added to the standard medium to a concentration of 500 µM. The cells were washed 3 times with ice cold PBS, and all residual PBS carefully aspirated after the final wash. To each well, 500 µl of metabolite extraction buffer (-20 $^{\circ}$C) was added. The plates were rocked for 10 minutes and the extraction buffer transferred to a 1.5 ml Eppendorf tube. After centrifuging at 4 $^{\circ}$C on full speed, the supernatant was removed and placed in glass HPLC vials and stored at -80 $^{\circ}$C until analysis by LC-MS. The 6-well plates were left to dry and protein was quantified by Lowry assay for each individual well.

To extract metabolites from the medium, the cells were plated as above. An extra triplicate of cells was plated at the same time to allow for calculation of protein concentration at the start of the experiment. To act as a reference, and to incorporate the effects of evaporation on metabolite concentration over time, medium was added to an additional 3 wells without cells. After 42 hours, 20 µl of medium was removed from each well and 980 µl of metabolite extraction medium (-20 $^{\circ}$C) added. The cells were shaken at 1400 rpm on a thermomixer at 4 $^{\circ}$C for 10 minutes. Subsequently, the samples were spun on a centrifuge at full speed at 4 $^{\circ}$C for 10 minutes and the supernatant transferred to glass HPLC vials and stored at -80 $^{\circ}$C. Normalisation was achieved using protein quantification using Lowry assay. To incorporate the effect of cellular

proliferation on metabolite consumption and secretion during the experiment, the average of the protein concentration from the end and the beginning of the experiment was used.

Immortalised normal human astrocytes: Metabolite extraction for both intracellular and extracellular metabolomics was achieved by the same method for the MOG-GCCM cell line with a few alterations. The number of cells seeded was 4 x 10^5 for all experiments and medium was removed after 24 hrs for extracellular metabolomics.

NCH cell lines: The cell lines were seeded in a 6-well plate. After 3 days growth in a 6 well plate format the spheroids were pipetted gently from the culture wells to 15ml tubes and centrifuged at 600 rpm to accelerate sedimentation. After this step, the medium was carefully aspirated (leaving 2-3 mm of medium above the pellet) and the spheroids were gently re-suspended in 1ml of medium. For labelled metabolomics, ^{12}C-glucose or ^{12}C-glutamine was replaced in the medium by $^{13}C_6$-glucose or $^{13}C_5$-glutamine at the same concentration. In the experiments involving ^{15}N-GABA, this was added to the standard medium to a concentration of 500 µM. The cells were then incubated for 24 hrs at 37 °C. After this incubation, the spheroids were transferred to 15ml tubes and centrifuged at 600 rpm for 3 minutes at 4 °C. The culture supernatant was transferred in a fresh tube for exometabolomic analysis, as described for MOG-GCCM above. The cell pellet was re-suspended in 0.9 ml of 0.9% NaCl solution at 4 °C. The suspension was transferred into 2 ml tubes and centrifuged at 800 rpm for 5 min at 4 °C. The supernatant was carefully removed and 300 µl of metabolite extraction buffer added with a bead (5 mm diameter) to the pellet for homogenization in a beadmill (1.0 minutes setting 20 Hz). The suspension was incubated at 4 °C for 20 minutes on a thermomixer before the removal of the metal bead and centrifugation at 13000 rpm for 15 minutes at 4 °C. The metabolite extract was transferred to a fresh 1.5 ml tube on dry ice and stored at -80 °C until analysis by LC-MS.

The cell pellet remaining after metabolite extraction was used to quantify the protein concentration. 200 µl of cell lysis buffer was added (30 mM Tris-HCl (pH 8.5), 8 M urea, protease inhibitor and phosphatase inhibitor) and dissociated in a beadmill for 1 minutes at 20 Hz. Samples were then incubated on a thermomixer

for 20 minutes at 4 °C, metal beads were removed, and samples were centrifuged in an Eppendorf benchtop centrifuge at 13,000 rpm for 15 minutes at 4 °C to obtain a clear protein solution. The protein concentrations of all replicates were determined using 2D-Quant kit (GE Healthcare) and used for normalization of the metabolite extracts.

2.2.7.2 LC-MS

Metabolites were separated by high performance liquid chromatography (HPLC) using a Sequant ZIC-pHILIC column (2.1 mm x 150 mm, 5 um polymeric beads, guard column Sequant Zic-pHILIC guard peek 2.1 mm x 20 mm, Millipore). The aqueous mobile phase solvent was 20 mM ammonium carbonate, adjusted to pH 9.4 with 0.1% ammonium hydroxide solution (25%), while 100% acetonitrile was used in the organic mobile phase. Detection of metabolites was performed using mass spectrometry (MS) in a Thermo Scientific Exactive (or Q-Exactive for NCH cell lines) high-resolution mass spectrometer with electrospray ionization, examining metabolites in both positive and negative ion modes over the mass range of 75-1000 m/z. The flow rate used was 200 µl / minute and the column temperature was 45 °C. Prior to injection, samples were maintained at 4°C in a chilled autosampler. The run time was 22.2 minutes. A previously in-house developed compound database, using commercial standards, was used to identify the appropriate retention time and mass for the targeted metabolites of interest. The peak area of the extracted ion chromatogram at the appropriate retention was then determined and subsequently peak areas between different samples compared. Data analysis was done using either Thermo Scientific TraceFinder or Thermo Scientific LC Quan software.

2.2.8 SDS-Page and Western Blot

Protein was obtained from cell lines by lysis with RIPA buffer. In the case of MOG-GCCM, 2 x 10^5 cells were seeded in a 6 well plate, the medium changed after 18 hours, and the cells lysed a further 24 hrs later using 100 µl RIPA buffer. The same protocol was used for the immortalised astrocytes, except 4 x 10^5 were seeded instead. The NCH cell lines were grown as spheroids for 3 days, centrifuged at 600 rpm, and the pellets lysed with 50 µl RIPA buffer. Samples were subsequently agitated using a thermomixer set at 1400 rpm at 4 °C for 30

minutes. This was followed by centrifugation at 12,000 rpm for 20 minutes at 4 °C. Protein quantification was done by BCA assay and 30 µg of protein was separated by SDS-Page. Prior to resolving using SDS-PAGE, 4 x Laemlli loading buffer was added to each sample, vortexed, and then heated for 5 minutes at 95 °C.

Histone protein extraction was done using the Active Motif histone purification mini kit, which utilises a spin column system to specifically remove histones from cells. After extraction, histone precipitation was achieved by adding perchloric acid to a final concentration of 4% and incubating overnight at 4 °C. The following day, the samples were spun at maximum speed in a centrifuge at 4 °C for 1 hour. Washing of the resultant pellet was done firstly with 4% perchloric acid, followed by acetone + 0.2% hydrochloric acid, and finally acetone. Each wash was done twice at 4 °C, with a 5 minutes maximum spin in a centrifuge after each wash. The pellet was finally air dried for 10-20 minutes and re-suspended in 50 µl sterile water. Protein quantification was done by BCA assay.

For SDS-PAGE, 10% or 15% polyacrylamide gels were used depending on the protein to be detected. After the gel was poured, a layer of water saturated butanol was added to maintain a level surface. After the gel had set, the remaining butanol was removed and the stacking gel poured on top. Wells were formed by inserting a 10 well gel comb. The comb was removed after setting of the stacking gel, and the gel transferred into the gel tank filled with 1 x SDS-PAGE running buffer. 7 µl of molecular weight marker (Full range rainbow molecular weight marker, GE healthcare Life sciences) was added to one of the wells alongside the protein samples. Protein separation was achieved by running each gel at 180 Volt for 1 hour.

Upon resolution by SDS-PAGE, proteins were transferred from the gel to a nitrocellulose membrane using the Biorad mini-protean apparatus, as per manufacturer's instructions. In brief, the gel and membrane were sandwiched between blotting paper and sponge and clamped together tightly. The chamber was filled with 1x blotting buffer and a container of ice to keep the apparatus cool during blotting. Transfer was performed at 100 V for 1 hour. The membrane was incubated briefly in ponceau solution to determine if the transfer was successful, followed by incubation in blocking buffer for 1 hour.

The membrane was incubated with primary antibody diluted in blocking buffer overnight at 4 °C. The following day, the membrane was washed three times in TBST and then the appropriate Licor fluorescent secondary antibody in blocking buffer was added and membranes were incubated for 1 hour at room temperature. The membrane was then washed again three times in TBST and proteins were visualised using Odyssey CLx Infrared Imaging System. Quantification of the bands was done using Image Studio v2.0 (LI-COR Bioscience).

2.2.9 Histone methylation screen

To screen for changes in histone methylation, a protocol was devised using the Operetta high throughput microscopy system. 7 x 10^4 cells were plated per well, in the central 60 wells, in a 96 well plate. One clone, or the MOG-GCCM parental cell line, was used per 96 well plate., The medium was replaced (200 µl) 18 hrs after seeding and half the wells incubated with 2 mM Dimethyloxaloylglycine (DMOG), an inhibitor of JMJ demethylases to act as a positive control. After 24 hours incubation the cells were washed once in PBS. The cells were fixed by adding 50 µl 4% paraformaldehyde to each well using a multi-dispenser pipette. After 15 minutes at room temperature the cells were washed in PBS 3 times (5 minutes per wash on a gyro-rocker). The cells were blocked and lysed by adding 50 µl of 5% BSA in PBS with 0.2% Triton X-100 for 5 minutes. After the cells were washed with PBS, 2 additional washes were done with PBST. Primary antibody was then added to each well after dilution in PBST (200 µl of 1:500 – 1:1000). The plate was left over night at 4 °C on a gyro-rocker in a box layered with wet tissue to prevent evaporation.

The next morning the cells were washed 3 times in PBST. The secondary antibody (1:1000) and DAPI (1:2000) were diluted in PBST + 5% BSA, and 200 µl added to each well. After 1 hour the cell were washed a further 3 times in PBST with 200 µl PBST pipetted into each well after the final wash. The plates were then imaged on the Operetta system.

The primary antibodies used were as follows: H3K4me0/1/2/3, H3K27me0/1/2/3/ac, H3K9me0/1/2/3/ac, H3K36me1/2/3, H3K36me1/2/3, H4K20me1/2/3/ac and H3K14ac. In addition, for each well a total H3 or H4

antibody derived from a different species was used as an internal control. 2 different fluorescent secondary antibodies were used (488 and 555 nM) to allow for differentiation between histone methylation and total H3/4 sites. DAPI fluoresces at a third wavelength and was used to identify individual cells. The average fluorescence per cell per well was calculated, and the value for each histone methylation site was divided by the total H3 or H4 measurement as appropriate. The data was then normalised to the EV clone. An example 96 well plate is shown in Figure 2-2.

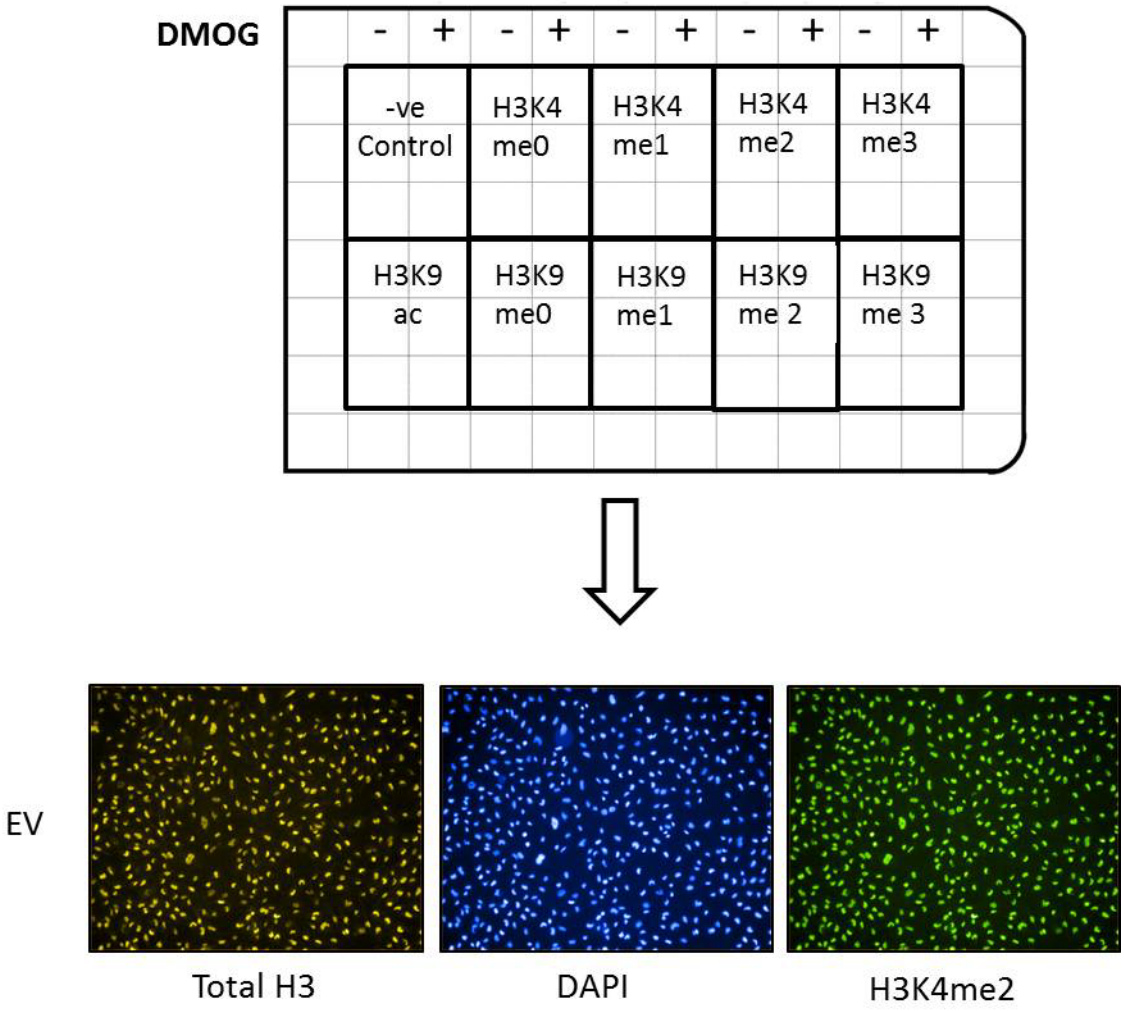

Figure 2-2 Plating method for high throughput microscopy screening using the Operetta
Cells were plated on a 96 well plate in triplicate for each methylation group of interest plus/minus DMOG, which acted as a positive control. To act as a negative control, an addition set of wells were used where only secondary antibody was added. Total H3 or H4 antibody was added to each well to act as an internal control. DAPI was used to identify the nucleus for fluorescence detection and cell counting. DMOG: Dimethyloxaloylglycine, EV: MOG-GCCM empty vector cells.

2.2.10 Immunohistochemistry

Paraffin fixed tumour samples were kindly provided by the Haukeland Hospital in Bergen, Norway. Firstly, paraffin was removed from the slides by submerging in 2 x 5 minutes in xylene, followed by 2 x 1 minutes in 100% ethanol, and finally 1 minute in 70% ethanol. The slides were subsequently washed in running tap water for 5 minutes. Antigen retrieval was done using a microwave method. 600 ml of water was placed in a pressure cooker, and 300 ml of antigen retrieval buffer into a slide holder. The pressure cooker, including the holder, was placed into a microwave with the lid loose and a weight placed on top. After 15 minutes on full power, ensuring the water was boiling, the slides were added and the lid locked. The microwave was placed on full power again for 2 minutes ensuring the pressure cooker valve was releasing steam. A further 9 minutes of heating at full power was done before the cooker was placed in a sink of cool water. The slides were then removed from the cooker and left to cool for 20 minutes. The slides were then washed for 2 x 5 minutes in TBST (all subsequent washes were for 5 minutes), and an area drawn around the tissue sections with a liquid repellent slide marker pen. Reagents and secondary antibodies from the Dako Envision + system-HRP (DAB) kit were used to stain the slides. This involved blocking endogenous peroxidase with hydrogen peroxide for 5 minutes, followed by 3 washes in TBST. The slides were then blocked using 5% BSA in TBST for 30 minutes, and washed twice in TBST. Primary antibody was added and incubated overnight at 4 °C. The next day, after 3 washes in TBST, the appropriate EnVision secondary antibody was added for 30 minutes. After 3 further washes, DAB was added for 5 minutes, and the slides placed in deionised water to wash. Counter-staining, dehydration, and mounting of slides by cover slips were done by the Beaston Histology services. Images were obtained using an Olympus BX51 microscope. The collection of human biopsy material was approved by the regional ethical committee at Haukeland University hospital, Bergen, Norway (REK 013.09).

To quantify the staining for H3K4me2/3 and GABRB3, the slides were scanned and analysed using SlidePath Tissue Image Analysis 2.0 (Leica microsystems). To generate a histoscore the stained cells algorithm was used for H3K4me2/3 and the stained area algorithm was used for the GABA-A receptor β3 subunit.

2.2.11 Chromatin immunoprecipitation (ChIP)

Chromatin pulled down by immunoprecipitation was used for ChiP Sequencing and ChIP-qPCR based on the procedure described by Schmidt and colleagues summarized below [274].

2.2.11.1 Cross Linking Cells

MOG-GCCM cells were plated at 1.5 x 10^6 cells in a 15 cm plate, for a total of 5 plates per experimental group. An additional plate was used to calculate cell number, so cells could be divided into pellets of 10 million cells. 5 million cells were used for each pull down. The medium was changed the next day, and the cells cross-linked 48 hours later. Cross-linkage was achieved by initially pouring off the medium from each plate and replacing it with a solution of 15 ml serum-free DMEM + 1ml 16% formaldehyde pre-warmed to room temperature. The plates were swirled briefly and left at room temperature for 9.5 minutes. The formaldehyde was quenched by adding 600 µl of 2.5 M glycine and mixed for 3 minutes on a gyro-rocker. Cells were rinsed twice with ice-cold PBS, then scraped using a cell scraper in 8 ml ice-cold PBS and transferred to a 50 ml Falcon tube. This was then centrifuged at 4 ˚C for 4 minutes at 1300 rpm. The supernatant was then removed, and the pellet transferred to a 2 ml tube by gently pipetting with 1ml of ice-cold PBS. Further centrifugation was done at 4 ˚C for 3 minutes at 8,000 rpm and the supernatant was removed again. The pellets were subsequently snap frozen in liquid nitrogen and stored at -80 ˚C.

2.2.11.2 Bead Preparation

100 µl of magnetic Dynabeads was used for each ChIP pull down. The beads were washed using 1 ml of blocking solution and collected using a magnetic stand. The supernatant was removed and the wash repeated two more times. 3 µg of antibody was added to each aliquot of magnetic beads in a final volume of 250 ml blocking solution. Two antibodies were used: H3K4me2, H3K4me3 (both IgG, anti-mouse) To act as a control, beads with no antibody were used in ChiP Seq, while an mouse IgG anti-haemaglutinin antibody was used for ChIP-qPCR. The solution was incubated overnight on a rotating platform at 4 °C. The next morning, the magnetic beads were briefly spun down in a centrifuge and washed as described above to remove unbound antibody (3 times in 1 ml block solution).

Each antibody was pulled into one tube, re-suspended in buffer LB3 allowing 150 µl to be aliquoted for each pull down.

2.2.11.3 Sonication

Each cell pellet was re-suspended in 1 ml of buffer LB1 in a 1.5 ml Eppendorf LoBind tube and kept on ice for 10 minutes. The solution was then spun at 2,000 g for 5 minutes at 4 ˚C. The supernatant was removed and the pellet re-suspended in 1 ml of buffer LB2, and kept on ice for a further 5 minutes. Centrifugation was repeated again at 2,000 g for 5 minutes at 4 ˚C. The supernatant was again removed and 300 µl buffer LB3 added, the pellet re-suspended and transferred to a polystyrene sonication 1.5 ml tube. The cells were then sonicated on Bioruptor Pico for 4 cycles of 30 sec on and 90 sec off. Cells used for ChIP-qPCR were sonicated using a Bioruptor XL UCD-500 for 24 min of 30 sec on 30 sec off. 5 µl of the whole cell extract was retained to ensure adequate sonication for each sample. The whole cell extract was centrifuged on the maximum setting for 10 minutes at 4 ˚C. The supernatant was mixed with 15 µl of Elution buffer and the crosslinks reversed by incubating at 65 °C overnight. The samples were then cooled down to room temperature before adding 20 µl of 1x TE plus 0.8 µl of 1 mg/ml RNaseA and incubating at 37 °C for 30 minutes. Proteinase K was then added (0.8 µl of 10 mg/ml) and the samples further incubated at 55 °C for 2 hours. Purification and concentration of the samples was achieved using the MinElute PCR purification kit so each sample was eluted into 10 µl of elution buffer. DNA fragmentation was visualised by running on 1.5% agarose gel for 30 minutes at 100V and stain with Sybr safe at 1:10,000 for 30 minutes. Adequate sonication was determined by identifying a smear limited to between 100 and 600 bp with a substantially reduced 2 kbp band.

2.2.11.4 Chromatin immunoprecipitation

The sonicated whole cell lysates were centrifuged at full speed for 10 minutes at 4 ˚C. 10% Triton-100 was added to the supernatant to achieve a final concentration of 1%. 5% of the whole cell extract was retained for Input and stored at -20 ˚C. The supernatant (LB3) was removed from the beads using a magnetic stand and re-suspended with the whole cell extract and rotated overnight at 4 ˚C. The beads are then briefly spun for a second and placed on a

magnetic stand on ice, discarding the supernatant. 1 ml of RIPA Buffer was added to each tube and agitated gently for 3 minutes to re-suspend the beads. The tubes are replaced in the magnetic stand and the supernatant removed. This process is repeated for a total of 6 times. The samples were then washed once with 1 ml 1 x cold TBS and the supernatant removed. The tubes are spun at 960 g for 3 minutes at 4 °C and any residual TBS buffer removed using a magnetic stand. 200 µl of Elution buffer was then added to each sample. The input whole cell extract is then thawed and elution buffer was added to a total volume of 200 µl. Reverse crosslinking was achieved by incubating in a water bath at 65 °C overnight for both immunoprecipitate and input. The beads are re-suspended in the first 15 minutes with brief vortexing every five minutes. Each ChIP sample and input was vortexed and spun at 16,000 g for 1 minute. 180 µl of supernatant was added to a DNA LoBind tube containing 200 µl of 1x TE + 8 µl of 1 mg/ml RNaseA, mixed and incubated at 37 °C for 30 minutes. 8 µl of 20 mg/ml proteinase K was added to the samples and incubated in a water bath at 55 °C for 1-2 hours. After cooling down to room temperature, small column purification was done using the MinElute PCR purification Kit. Each sample is eluted using 60 µl. Input samples were diluted 1/5 to make a total dilution of 1:100.

2.2.11.5 ChIP Sequencing

ChIP Sequencing was kindly performed at the CRUK Institute, Cambridge. DNA was quantified using Qubit HS and library preparation was done by using NEBNext Ultra DNA Library Prep Kit for Illumina (E7370), and run on an Illumina sequencer.

Analysis of the ChIP Sequencing data was done by Rafik Salama at CRUK Institute, Cambridge. For ChIP quantitative analysis, signal regions were first identified using both MACS and TPIC peak callers. 1 million random 2 Kb regions were then identified from the ENCODE Dnase II cluster to represent a sample from the background regions. The background signal was normalised using RPKM relying on the total count in the background regions. The counts in the signal along with the background were used to quantile normalise all the samples to a similar overall distribution. The last step was to normalise the background signal which is hypothesised to be of same mean

and variance. In doing so, the actual ChIP signal was also normalised. The mean signal across the 3 replicates was used to denote the expected signal of the peak in every condition. The log ratio was then calculated from those means.

2.2.11.6 ChiP-qPCR

GABRB3 Forward	5'-CCCAGTGTGAACGATCC-3'	Eurofins Operon MG
GABRB3 Reverse	5'-GTCTTAGGCGAATGTCGTAG-3'	Eurofins Operon MG
HK3 Forward	5'-CATCTAGGCCTACAACATCGAC-3'	Eurofins Operon MG
HK3 Reverse	5'-CATGGCTCACCTACAACTAGC-3'	Eurofins Operon MG
PGAM2 Forward	5'-TCACATAGTGTCTGCTGTGTAAA-3'	Eurofins Operon MG
PGAM2 Reverse	5'-GCAGGTTCAGCTCCATGAT-3'	Eurofins Operon MG

Table 2-5 DNA primer sequences for ChIP-qPCR

To validate ChIP Sequencing, ChIP qPCR was done for the gene of interest, GABRB3, and as a negative control 2 genes were used that showed no increase in H3K4me3 at the transcription start site (HK3, PGAM2). Primer sequences were derived from the first 1 kb of the gene sequence (Table 3). A standard curve was done to ensure efficiency between 90 – 110%. For qPCR analyses, 0.5 µM primers, 1 X Fast SYBR Green Master mix (AB, Life Technologies Corporation Carlsbad, California) and 3 µL of 1% input/ChIP extract were used. Real-time PCR was performed on the 7500 Fast Real-Time PCR System (Life Technologies Corporation Carlsbad, California) and the programme used was as follows: 20 seconds at 95 °C followed by 40 cycles of 3 seconds at 95 °C and 30 seconds at 60 °C. Finally the melting curve was performed to confirm the presence of single PCR products. Expression levels were calculated by the percentage input method. With this method, signals obtained from the ChIP are divided by signals obtained from an input sample. This input sample represents the amount of chromatin used in the ChIP. The input was adjusted to 100% by subtracting 6.644 ($\log_2$ of 100) from the Ct value of the diluted input. The percentage input was then calculated using the following formula:

$$100 * 2\text{^}[adjusted\ input - Ct(IP)]$$

2.2.12 Total mRNA isolation and qPCR

Actin Forward	5'-TCCATCATGAAGTGTGACGT-3'	Eurofins Operon MG
Actin Reverse	5'-TACTCCTGCTTGCTGATCCAC-3'	Eurofins Operon MG
GABRB3 Forward	5'-CTGCGCCCAGAGTGTGAAC-3'	Eurofins Operon MG
GABRB3 Reverse	5'-GGGTCTTAGGCGAATGTCGT-3'	Eurofins Operon MG

Table 2-6 Primers used for qPCR

mRNA was extracted for microarray analysis, RNA sequencing, and qPCR. 4 x 10^5 MOG-GCCM cells were plated in a 3 cm plate and lysed in RLT buffer (Qiagen, West Sussex, UK) 24 hrs after seeding. Lysates were passed through QiaShredder columns (Qiagen, West Sussex, UK) and mRNA was isolated using the RNAeasy kit (Qiagen, West Sussex, UK). For microarray analysis, the samples were sent to the Patterson Institute for Cancer Research, and data analysis done by Gabriela Kalna at the CRUK Beatson Institute, Glasgow using R software.

For RNA sequencing, rRNA was depleted from the samples by using the Ribo-Zero magnetic kit (Epicentre). Quality control both before and after rRNA depletion was done using the Agilent RNA 6000 Nano kit and Agilent 2100 Bioanalyser. Quantification was achieved using the Qubit RNA HS assay kit and the Qubit 2.0 flourometer. The samples were run on the Illumina Next Gen Sequencer and analysis was done by Rafik Salama at the CRUK Institute, Cambridge. The RNASeq data was processed using 2 R packages, DESeq2 and EdgeR. The data was normalised by the two packages and then differential genes significance was calculated. The calculated p-values from the two packages were then combined using Fisher method and adjusted using FDR.

For qPCR analyses 100 ng of mRNA was retro-transcribed into cDNA using SuperScript® VILO™ Master Mix as per manufacturer's guidelines. A negative control was used with no RNA added. The samples were incubated for 10 minutes at 25 °C, 60 minutes at 42 °C, and 85 °C for 5 minutes. The qPCR reaction consisted of 0.5 µM primers, 1X Fast SYBR Green Master mix (AB, Life Technologies Corporation Carlsbad, California) and 1 µL of cDNA in a final volume of 20 µL. Real-time PCR was performed on the 7500 Fast Real-Time PCR

System (Life Technologies Corporation Carlsbad, California) and expression levels of the indicated genes were calculated using the ΔΔCt method, using actin as the internal control. The PCR program used was 20 seconds at 95 °C, followed by 40 cycles of 3 seconds at 95 °C and 30 seconds at 60 °C. After the reaction was completed, a melt curve was performed to confirm the presence of single PCR products. A standard curve was done to ensure reaction efficiency of 90-110%. Analysis was done using 7500 software v2.0.5.

2.2.13 Scratch Assay

Cell migration was measured using a scratch assay on the IncuCyte imaging system (Essen Bioscience). 1 x 10^4 cells were seeded in a 96 well Essen Image lock plate. After 18 hours, medium was spiked with 0.5 mM GABA, 0.1 mM Bicuculline, or a combination of these compounds, as required. After 24 hours a scratch was produced using the 96 well Woundmaker (Essen Bioscience). The plate was then loaded into the IncuCyte, where it was kept at 37 °C and 5% CO_2. Images were taken of each well every 2 hours over 24 hours. Cell migration was measured by changes in wound confluence using the Incucyte software.

2.2.14 BCA protein assay

Protein concentration was determined in cell lysates using a BCA protein assay. This was performed as per manufacturer's instructions, with BSA standards used to generate a standard curve. Absorbance was measured for all samples and standards at 562 nm using the Molecular Devices SpectraMax Plus 384 spectrophotometer and SoftmaxPro software.

2.2.15 Lowry Assay

Protein quantification in cell lines was determined after metabolite extraction using a Lowry assay. A series of protein standards, consisting of a known concentration of protein in a 6 well plate, were used to produce a standard curve. After metabolite extraction, the experimental plates were allowed to dry. 500 µl of solution A (1 part Sodium Docusate, 2 parts 5 M NaOH and 7 parts water) was added to each well and agitated for 1 hour. 5 ml of solution B (0.5 g ethylenediaminetetraacetic acid copper disodium salt, 40 g $NaCO_3$, 8g NaOH in 2 L of distilled water) was then added for 10 minutes. Finally 500 µl Folin and

Ciocalteu's phenol reagent was added and the solution agitated for a further 1 hour. Protein quantification was determined using a Perkin Elmer Lambda 25 UV/VIS spectrometer at 750 nm and Perkin Elmer UV Winlab software.

2.2.16 Statistical analysis and data processing

For general statistical analyses, data were analysed and presented with Graphpad Prism 5.01 software (GraphPad Software Inc, CA, USA). The data (mean ± s.e.m.) are representative of 3 independent experiments, performed in technical triplicates, unless stated otherwise. Statistical significance was determined using 2-way ANOVA or student's t-test.

Chapter 3 The metabolic effect of the IDH1 mutation in glioma

3.1 Introduction

Brain tumours consist of a variety of histopathological diagnoses, of which glioma is the commonest. They are subdivided using the WHO classification into grades I to IV, with higher grades associated with more aggressive disease and poorer prognosis. The most common glioma in adults is GBM, a WHO grade IV tumour. GBM can be divided into two classes: primary GBM develops *de novo*, whereas secondary GBM arises as a result of transformation of a lower grade tumour. Currently, treatments for GBM are limited to combinations of surgery, chemotherapy and radiotherapy, with a median survival of 15 months [275].

Point mutations in the IDH1 and IDH2 genes have recently been identified in gliomas using genomic mutational screening. Over 90% of these mutations occurred in the IDH1 gene at R132. The rest occurred at R172 or R140 in the IDH2 gene [94, 95]. Up to 90% of WHO grade II, III and secondary GBM has the IDH1/2 mutation. This is in contrast to primary GBM which is 95% IDH wild-type [95].

IDH enzymes form an important part of the TCA cycle. The TCA cycle provides energy through ATP production by oxidative phosphorylation, contributes to lipid metabolism through citrate synthesis and to protein synthesis through amino acid production. The IDH enzyme exists as 3 isoforms (IDH1/2/3), with IDH1 present in the cytoplasm and IDH2/3 in the mitochondria. IDH1/2 catalyses the oxidative decarboxylation of isocitrate to produce α-ketoglutarate (α-KG) with the concurrent reduction of NAD(P)+ to NAD(P)H. IDH3 is structurally different from the other two isoforms and utilises NAD+ to produce α-KG and NADH. Interestingly, the IDH mutant enzyme does not possess the catalytic function of the wild type enzyme but rather uses α-KG to produce D-2-hydroxyglutate (2HG) [147]. 2HG has been implicated in tumourigenesis due to its structural similarity to α-KG. It can act as a competitive inhibitor of a superfamily of enzymes that rely on α-KG as a substrate, the α-KG dependent dioxygenases. These are important in a range of cellular processes, including epigenetic modification of DNA and histones, oxygen sensing and collagen formation [172].

The aim of the project was to identify whether the more commonly occurring IDH1 mutation, through the production of 2HG, is associated with changes in cellular metabolism.

3.2 Results

3.2.1 Identifying metabolic changes in clinical glioma samples

To investigate the effects of the IDH1 mutation on cellular metabolism *in vivo*, human samples were obtained post-operatively from patients with brain tumours. This was kindly undertaken by Mr Morten Lund-Johansen at Haukeland University Hospital in Norway. Initially fifteen patients were recruited to the study; thirteen patients had primary brain tumours and two had brain metastasis from a lung primary. Six of the primary brain tumours were IDH1 mutant and consisted of one GBM, one anaplastic astrocytoma, two anaplastic oligoastrocytomas, and two diffuse astrocytomas. The remaining seven primary brain tumours were IDH1 wild-type. All were GBM with the exception of a single gliosarcoma, which is rare sub-type of GBM (Table 3-1).

Pre-operative MRI imaging was used to aid stereotactic removal of tissue from the tumour core and periphery, as well as from the oedematous surrounding region. To investigate the metabolism of glucose within the tumour, 10-20g $^{13}C_6$ labelled glucose was given to the patient as a short 10-20 min infusion prior to the operation (Table 3-1). Additionally, blood samples were taken at regular intervals.

Patient	Diagnosis	IDH1 mutant	Gene Amplification	^{13}C glucose
1	Lung metastasis	negative		10g
2	GBM	negative		10g
3	GBM	negative	MYCN/PDGFRA/EGFR/MET	20g
4	GBM	negative	PDGFRA/EGFR	20g
5	Anaplastic oligoastrocytoma	positive		20g
6	GBM	positive	PDGFRA	20g
7	GBM	negative		20g
8	GBM	negative	EGFR	20g
9	Lung metastasis	negative		20g
10	gliosarcoma	negative		20g
11	Anaplastic astrocytoma	positive	CDK4	20g
12	GBM	negative		20g
13	Anaplastic oligoastrocytoma	positive		20g
14	Diffuse astrocytoma	positive	MYCN	20g
15	Diffuse astrocytoma	positive		20g

Table 3-1 Tumour sample data
Pathological diagnosis, IDH1 mutation status, gene amplification, and dose of $^{13}C_6$ glucose given to patients recruited to the clinical glioma ^{13}C glucose tracing study.

3.2.1.1 Analysis of tumour samples showed metabolic differences compared to surrounding oedematous tissue

Metabolites from the tumour core, periphery and oedematous tissue were analysed using LC-MS, after normalising to sample weight. Fifty-six specific metabolites were targeted from a database of metabolites verified at our metabolomics unit using known standards. The peaks were identified and checked using LCQuan software. For initial analysis, the isotopologues for each metabolite were summated to give a total peak area representative of the metabolic steady state levels in the tumours. These were then $\log_2$ transformed to improve normalisation of the data.

Principle component analysis was done to identify variation within the metabolic data. It showed clustering of the oedematous samples from the rest of the tumour samples. However, there was no evidence of clustering between the periphery and core (Figure 3-1A). When analysing only the periphery and core samples from the primary brain tumours there was evidence of clustering of IDH1

wild-type from IDH1 mutant samples (Figure 3-1B). To determine the composition of the oedematous tissue it was examined microscopically by a pathologist. Only two samples had tumour tissue present, one was 90% normal brain tissue, the other 65% normal brain tissue (data not shown). The other samples consisted of normal brain tissue only.

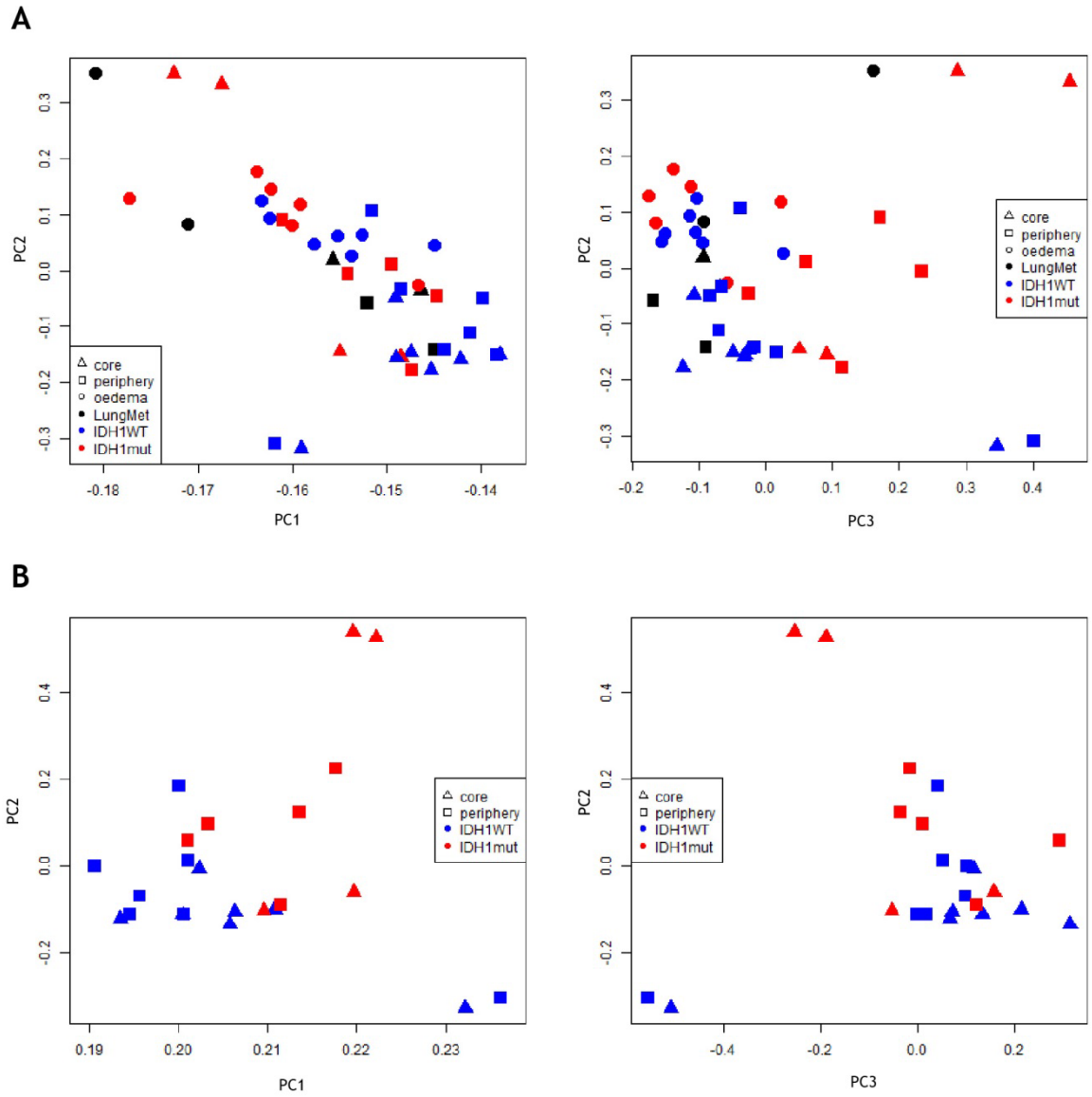

Figure 3-1 Principle component analysis of human brain tumour samples
A. Core, periphery and oedematous samples from lung metastasis and primary brain tumours, either IDH1 wild-type or IDH1 mutant. B. Core and periphery samples only from IDH1 wild-type and IDH1 mutant primary brain tumours. Symbols represent as follows: Triangles the core tumour samples, squares the periphery tumour samples and circles the samples from the surrounding oedema. Black depicts the lung cancer brain metastasis, red the IDH1 mutant samples, blue the IDH1 wild-type samples.

To investigate which metabolites were contributing to the differences seen in the principle component analysis, hierarchical clustering of the metabolic data was performed using Pearson correlation. Again, the majority of the oedematous brain tissue samples clustered together but not the core and periphery tumour samples. Differences were evident between the tumour and the oedematous normal brain, with tumour having increased levels of amino acids but lower levels of neurotransmitters, such as GABA, NAA, NAAG, and glutamate (Figure 3-2A).

When comparing the fold difference in metabolites between core and peripheral tumour samples, no significant differences were found between any of the metabolites analysed (data not shown). Therefore, core and peripheral samples were combined for each tumour and analysed together. Primary tumour samples were also divided into IDH1 wild-type and IDH1 mutant. For the purposes of this thesis the two brain metastasis were excluded from the subsequent analysis. In addition the gliosarcoma, a very rare form of glioma, was removed as it contains sarcomatous elements. As such, it behaves very differently from other gliomas by metastasising to other sites in the body [276]. This left six IDH1 wild-type and six IDH1 mutant patient samples.

Initially, IDH1 wild-type and IDH1 mutant samples were compared to the surrounding normal brain tissue. When comparing IDH1 wild-type tumours to normal brain, metabolic changes indicative of the need for tumours to increase their energy production and biomass for growth were observed. There was an increase in the level of essential amino acids histidine, leucine, isoleucine, lysine, valine and phenylanine, as well as the non-essential amino acids, asparagine, glycine, and proline. Glucose levels were increased, as well as α-KG, which is a TCA metabolite. There was also a marked increase in ornithine, which is generated in the urea cycle, allowing removal of excess nitrogen. Conversely, there was a reduction in neurotransmitters such as GABA, NAA and NAAG, and the amino acids from which they are synthesized, glutamate and aspartate (Figure 3-2B).

IDH1 mutant tumours showed similar levels of metabolites as IDH1 wild-type tumours when compared to normal brain. The major exception, as expected, was the large increase in the metabolite 2HG, which is produced by the mutant

IDH1 enzyme. However, there was also an increase in the essential amino acid threonine as well as the non-essential amino-acids serine, glutamine and arginine. In addition, there was also a reduction in glutamate, and the glycolytic metabolites pyruvate and lactate (Figure 3-2C).

A

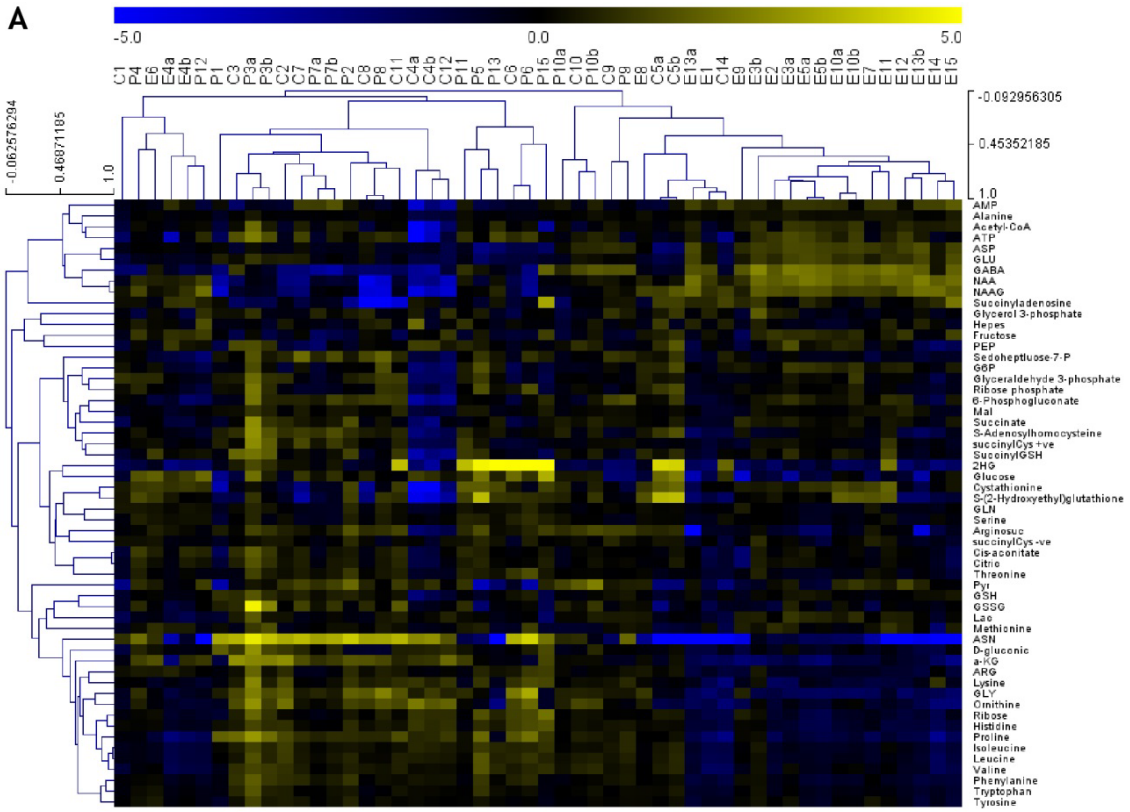

B

Metabolite	Log_2FC	p-value	Adj p-value
Asparagine	5.51	0.01	0.04
α-KG	2.56	6.82E -05	1.32E -03
Glycine	2.32	1.29E -04	1.49E -03
Proline	2.16	1.25E -04	1.49E -03
Ornithine	1.95	3.62E -04	3.00E -03
Glucose	1.71	0.01	0.02
Lysine	1.54	3.50E -03	0.02
GSSG	1.40	4.82E -03	0.02
2HG	1.14	0.07	0.14
Histidine	1.06	2.85E -03	0.02
Leucine	1.03	1.91E -03	0.01
Ribose	1.02	0.01	0.03
D-gluconic	1.00	4.55E -03	0.02
S-Adenosylhomocysteine	0.98	0.03	0.08
Isoleucine	0.96	2.85E -03	0.02
Valine	0.94	0.01	0.04
Sedoheptulose -7- phoshate	0.89	0.03	0.08
Phenylanine	0.80	0.01	0.02
Arginine	0.52	0.14	0.25
Glutamate	-0.50	0.14	0.25
S-(2-Hydroxyethyl) glutathione	-0.52	0.42	0.57
G6P	-0.56	0.16	0.27
Fructose	-0.80	0.03	0.08
AMP	-0.93	0.03	0.08
Cystathionine	-1.05	0.02	0.06
Aspartate	-1.12	1.14E -03	0.01
NAAG	-2.30	2.50E -04	2.41E -03
GABA	-2.49	5.76E -05	1.32E -03
NAA	-2.78	2.84E -06	1.65E -04
Succinyladenosine	-3.57	0.04	0.08

C

Metabolite	Log_2FC	p-value	Adj p -value
2HG	5.31	4.84E -09	2.81E -07
Glucose	2.07	1.08E -03	0.01
Arginosuccinate	1.92	1.58E -03	0.01
Proline	1.83	6.98E -04	4.50E -03
Histidine	1.46	1.32E -04	1.27E -03
Ribose	1.44	5.08E -04	3.68E -03
Glycine	1.35	0.01	0.04
Sedoheptulose -7- hosphate	1.30	2.95E -03	0.01
Leucine	1.25	3.06E -04	2.53E -03
S-(2-Hydroxyethyl) glutathione	1.16	0.08	0.15
Isoleucine	1.09	9.79E -04	0.01
Valine	1.08	4.70E -03	0.02
α-KG	1.06	0.06	0.11
PEP	0.94	0.02	0.04
Arginine	0.88	0.02	0.04
Asparagine	0.84	0.69	0.77
D-gluconic	0.80	0.02	0.04
Phenylanine	0.75	0.01	0.03
S-adenosylhomocysteine	0.73	0.10	0.16
Threonine	0.71	0.01	0.04
Ornithine	0.66	0.17	0.25
Ribose phosphate	0.63	0.08	0.15
Serine	0.54	0.02	0.04
Cystathionine	0.53	0.22	0.32
Glutamine	0.51	0.02	0.04
Fructose	-0.59	0.10	0.16
Lactate	-0.63	0.06	0.12
Acetyl -CoA	-0.88	0.04	0.09
AMP	-1.10	0.01	0.04
Pyruvate	-1.20	0.01	0.04
NAAG	-1.41	0.01	0.04
GABA	-1.44	0.01	0.03
Glutamate	-1.94	4.08E -06	5.92E -05
NAA	-2.17	7.81E -05	9.06E -04
Aspartate	-2.49	2.33E -08	6.76E -07

Figure 3-2 Metabolic differences between tumour core, periphery and oedema
A. Heat map depicting hierarchical clustering of targeted metabolites using Pearson correlation. C represents tumour core, P represents tumour periphery and E represents surrounding oedema. B. Table depicting metabolites with at least 0.5 log_2 fold change of metabolites between IDH1 wild-type and oedematous brain. C. Table depicting metabolites with at least 0.5 log_2 fold change of metabolites between IDH1 mutant and oedematous brain. Statistical analyses were performed using R statistical software.

3.2.1.2 IDH1 mutation is associated with changes in the TCA cycle and glutamate derived metabolites

To identify any metabolic differences caused by the IDH1 mutation in gliomas, the samples of wild-type and mutant tumours were compared. Figure 3-3 depicts the steady state metabolites which have a fold change of at least $\log_2$ 0.5. As expected the IDH1 tumours displayed higher levels of 2HG. In addition α-KG, which is converted to 2HG by the IDH1 mutant enzyme, was reduced in mutant tumours, but not other TCA metabolites. Glutamate was also reduced. Glutamate can be produced from α-KG by glutamate dehydrogenase, through transamination reactions, as well as from glutamine by glutaminase. Metabolites derived from glutamate were also altered. Ornithine and reduced glutathione (GSSG) were decreased. This was in contrast to GABA, the major inhibitory neurotransmitter in the brain, which was increased. Other neurotransmitters that were increased included N-acetyl-aspartate (NAA) and NAAG, though this was not significant (Figure 3-3, Figure 3-4, Figure 3-5)

Changes were also evident in other metabolic pathways. In glycolysis, the IDH1 mutation was associated with a decrease in steady state levels of pyruvate. In addition, a reduction was seen in the level of aspartate, which is derived from oxaloacetate, a TCA metabolite. Asparagine, a derivative of aspartate, was also reduced. Other metabolites that were increased included cystathionine, a precursor to cysteine that is generated from methionine and serine, and succinyladenosine, an intermediate in purine synthesis (Figure 3-3, Figure 3-4, Figure 3-5).

A

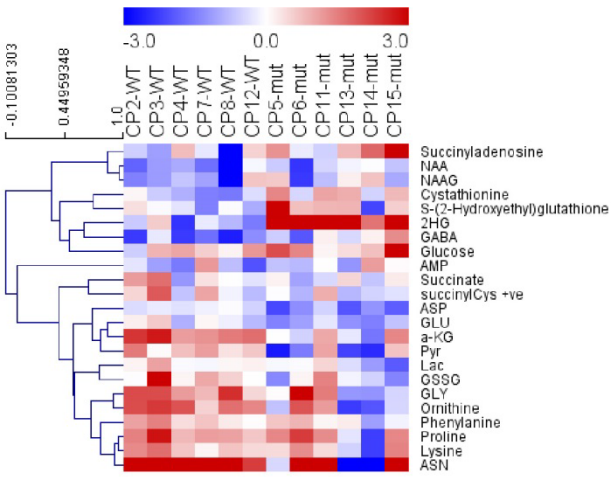

B

Metabolite	Log_2FC	p-value	Adj p-value
2HG	4.89	4.77E-07	1.38E-05
Succinyladenosine	4.06	0.05	0.23
GABA	1.54	0.02	0.14
Cystathionine	1.36	0.01	0.12
S-(2-Hydroxyethyl) glutathione	1.14	0.15	0.48
NAA	1.04	0.07	0.27
NAAG	1.01	0.13	0.44
Glucose	0.79	0.25	0.54
AMP	0.50	0.32	0.62
Succinate	-0.50	0.22	0.53
Phenylanine	-0.56	0.09	0.34
succinylcysteine	-0.58	0.17	0.49
Proline	-0.69	0.24	0.53
Lysine	-0.70	0.23	0.53
Lactate	-0.75	0.06	0.27
Glutamate	-0.90	0.03	0.18
GSSG	-1.21	0.04	0.19
Glycine	-1.23	0.06	0.25
Asparate	-1.24	2.42E-03	0.03
α-KG	-1.80	0.01	0.09
Pyruvate	-1.96	1.62E-03	0.02
Ornithine	-2.07	1.22E-03	0.02
Asparagine	-5.89	0.03	0.17

Figure 3-3 Metabolic differences between IDH1 mutant and IDH1 wild-type tumours
A. Heat map depicting metabolites with a log_2 fold change of greater or equal to 0.5 or -0.5 in IDH1 mutant compared to IDH1 wild-type tumours. B. Table representing the same data with log_2 fold change and associated p-values and adjusted p-values. Statistical analyses were performed using R statistical software.

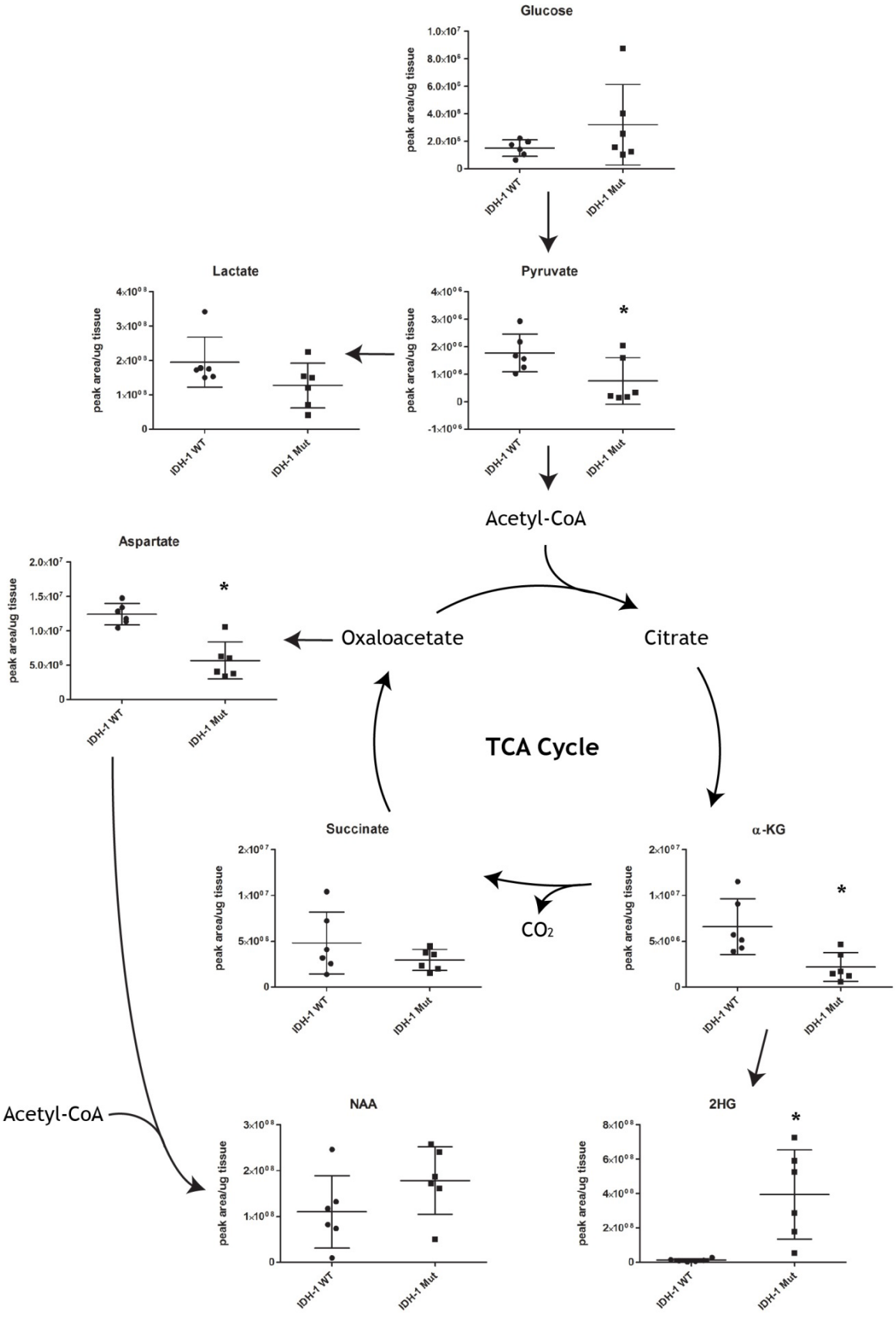

Figure 3-4 Change in steady state metabolites derived from glycolysis and the TCA cycle between IDH1 mutant and IDH1 wild-type tumours

Each point represents an average of core and peripheral tumour samples for one patient. Depicts mean +/- SD. * depicts a p value ≤ 0.05. Statistical analyses were performed using Student's t-test.

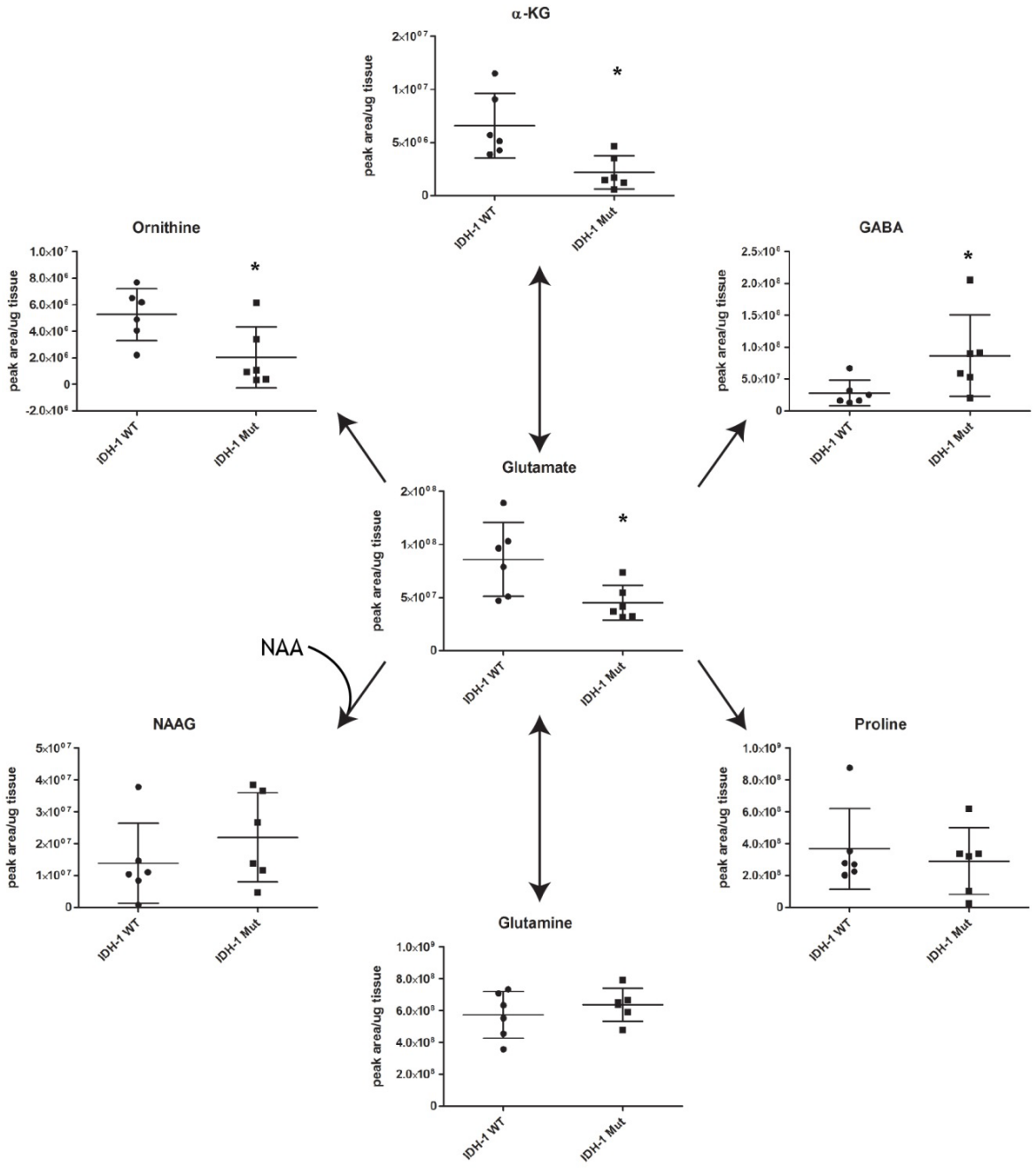

Figure 3-5 Change in steady state metabolites derived from glutamate metabolism between IDH1 mutant and IDH1 wild-type tumours

Each point represents an average of core and peripheral tumour samples for one patient. Depicts mean and SD. * depicts a p value ≤ 0.05. Statistical analyses were performed using Student's t-test.

3.2.2 Identifying changes in metabolic flux in IDH1 mutated glioma

Prior to tumour resection $^{13}C_6$-glucose was administered intravenously to each patient. Analysis of carbon labelling patterns in the tumour samples gave an indication of metabolic flux through different pathways using glucose-derived carbon. Blood samples were also taken at regular intervals to determine the pharmacokinetics of the $^{13}C_6$-glucose during the operation.

3.2.2.1 Serum sample analysis showed variation in $^{13}C_6$-glucose between patients at time of tumour extraction

Serum blood samples taken from each patient were analysed using LC-MS. Four of the patients, unfortunately, did not have blood samples taken at the time of tumour extraction. In the patients with serum samples available, there was a rapid increase in labelled glucose in the serum after infusion, which gradually decreased over time. Unlabelled serum glucose levels fell after $^{13}C_6$-glucose infusion, and gradually increased over time back to pre-infusion levels as the $^{13}C_6$-glucose was metabolised (Figure 3-6A). At the time of extraction, $^{13}C_6$-glucose levels were still maintained to at least 35 % of total glucose measured, but in some patients were over 55% (Figure 3-6C). This may be related to the variability in time to tumour resection after $^{13}C_6$-glucose infusion, which ranged from 15 to 90 minutes (Figure 3-6B). $^{13}C_3$- lactate levels, giving an indication of the systemic metabolism of the infused $^{13}C_6$-glucose, did not rise to above 20% of the total (Figure 3-6E). In addition, glucose can be metabolised to glutamine in other organs such as the liver, which can act as an alternative source of carbon for the TCA cycle in the brain. $^{13}C_5$-glutamine did not exceed 4% of the total glutamine level in the serum, indicating that glucose was the only major source of ^{13}C labelling of metabolites in the tumour (Figure 3-6D). Analysis of the tumour samples showed a large increase in 2HG in the IDH1 mutant tumours (Figure 3-4). However, the serum samples from IDH1 mutant and IDH1 wild-type tumours did not show any difference in 2HG levels (Figure 3-6F).

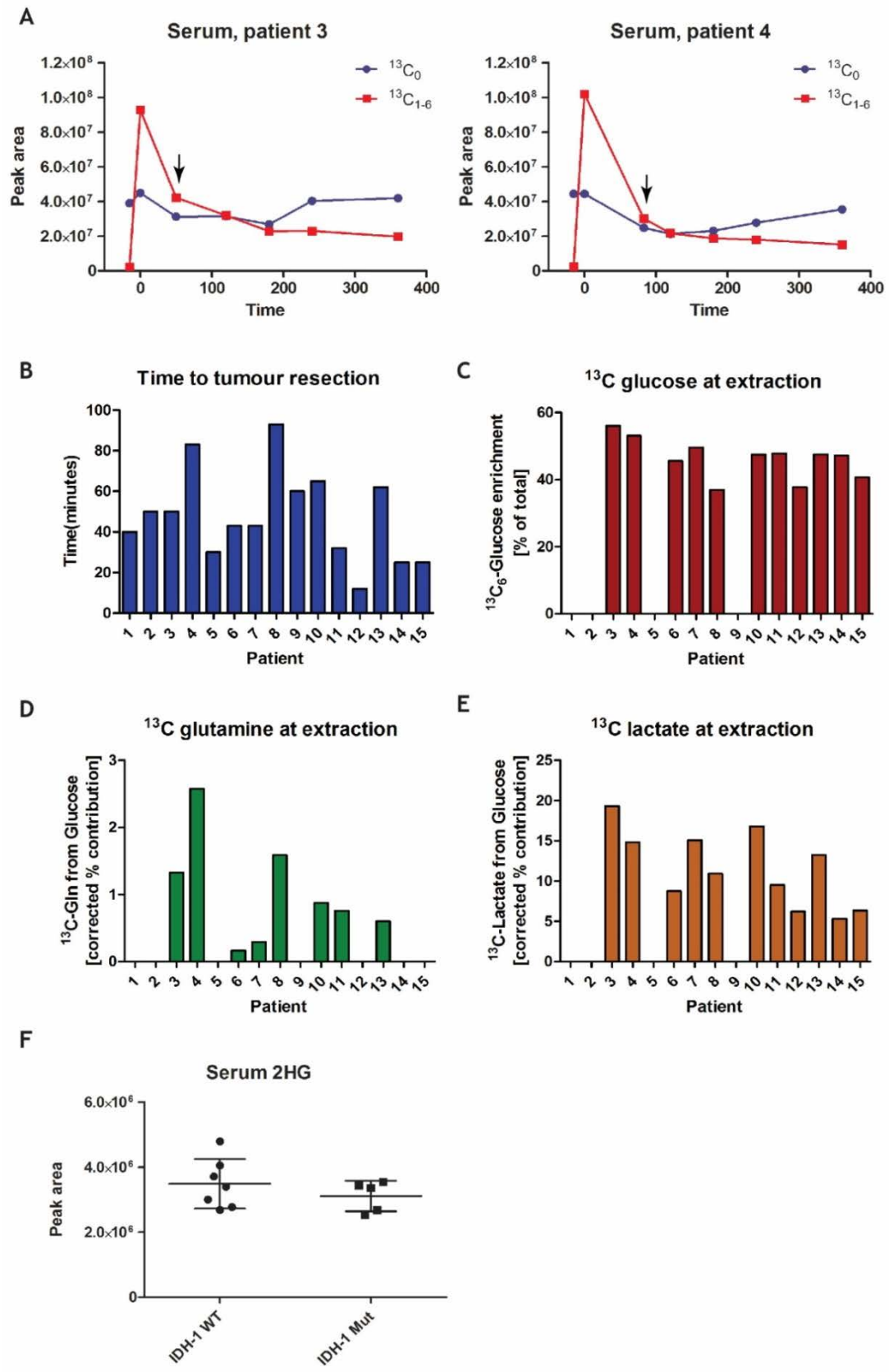

Figure 3-6 Analysis of metabolites from serum samples taken during surgery
A. Pharmacokinetics of $^{13}C_6$-glucose taken from 2 patients, in comparison to endogenous ^{12}C-glucose. Patient 3 is representative of an average surgical resection time. Patient 4 is representative of a long surgical resection time. Arrow depicts time of tumour extraction. B. Depicts time taken from completion of $^{13}C_6$-glucose infusion to surgical resection. C, D, E. Depicts the % contribution of ^{13}C labelled glucose, glutamine and lactate to total serum concentration at time of tumour extraction. Patients 1,2,5 and 9 did not have blood samples available from this time point. F Depicts the serum 2HG levels in patients with a primary brain tumour which is either IDH1 mutant or IDH1 wild-type.

3.2.2.2 IDH1 mutation may increase metabolic flux from glutamate to GABA as well as α-KG to 2HG

To identify changes in metabolic flux through different pathways utilizing glucose carbons, isotopologues generated from $^{13}C_6$-glucose were analysed in the tumour samples. As done previously, core and peripheral samples were averaged for each patient.

There was marked variability in the serum concentrations of $^{13}C_6$-glucose in the patients at the time of tumour extraction (Figure 3-6C). To reduce the effect of this variability, each metabolite of interest was normalized to fully labelled hexose-6-phophate (H6P). H6P is produced in the first step of glycolysis and forms a more consistent peak than glucose on LC-MS. It thus acts as a surrogate for glucose.

In the glycolytic pathway, there was a reduction in the ratio of fully $^{13}C_6$-labelled glyceraldehyde-6-phosphate from fully $^{13}C_6$-labelled H6P in the IDH1 mutant compared to the IDH1 wild-type tumours. This was also a reduction in alanine and lactate though the latter was not significant. There was a greater reduction in the ratio of $^{13}C_2$ labelled α-KG to fully labelled H6P in the IDH1 mutant tumours. In fact, the level of α-KG M+2 was undetectable in all the IDH1 mutant tumour samples. In contrast, the ratio of the downstream TCA metabolite malate M+2 to fully labelled H6P was unchanged between the IDH1 mutant and wild-type tumours. Interestingly, only 2 of the IDH1 mutant tumour samples showed an increase in ratio of 2HG+2 to fully labelled H6P compared to the IDH1 wild-type tumours. The other four tumours, like α-KG, had undetectable levels of 2HG+2. This implies an increase in flux from α-KG to 2HG in at least two of the IDH1 mutant tumours. The ratio of labelled glutamate to labelled H6P was similar to what was observed for α-KG, with a reduction in the IDH1 mutant compared to IDH1 wild-type tumours. Conversely, GABA, which is derived from glutamate, showed an increased ratio in the IDH1 mutant tumour samples, indicating a possible increased flux from glutamate (Figure 3-7).

Pyruvate carboxylase is highly expressed in astrocytes. It converts pyruvate to oxaloacetate, which can be utilised in the TCA cycle. Malate produced from oxaloacetate by malate dehydrogenase would generate malate M+3 from $^{13}C_6$-

glucose. To exclude the possibility that the reduction in M+2 metabolites in the TCA cycle in IDH1 mutant tumours was due to increased activity of pyruvate carboxylase a ratio of malate+3 to H6P+6 was calculated but showed no difference between the IDH1 mutant and IDH1 wild-type samples (Figure 3-7).

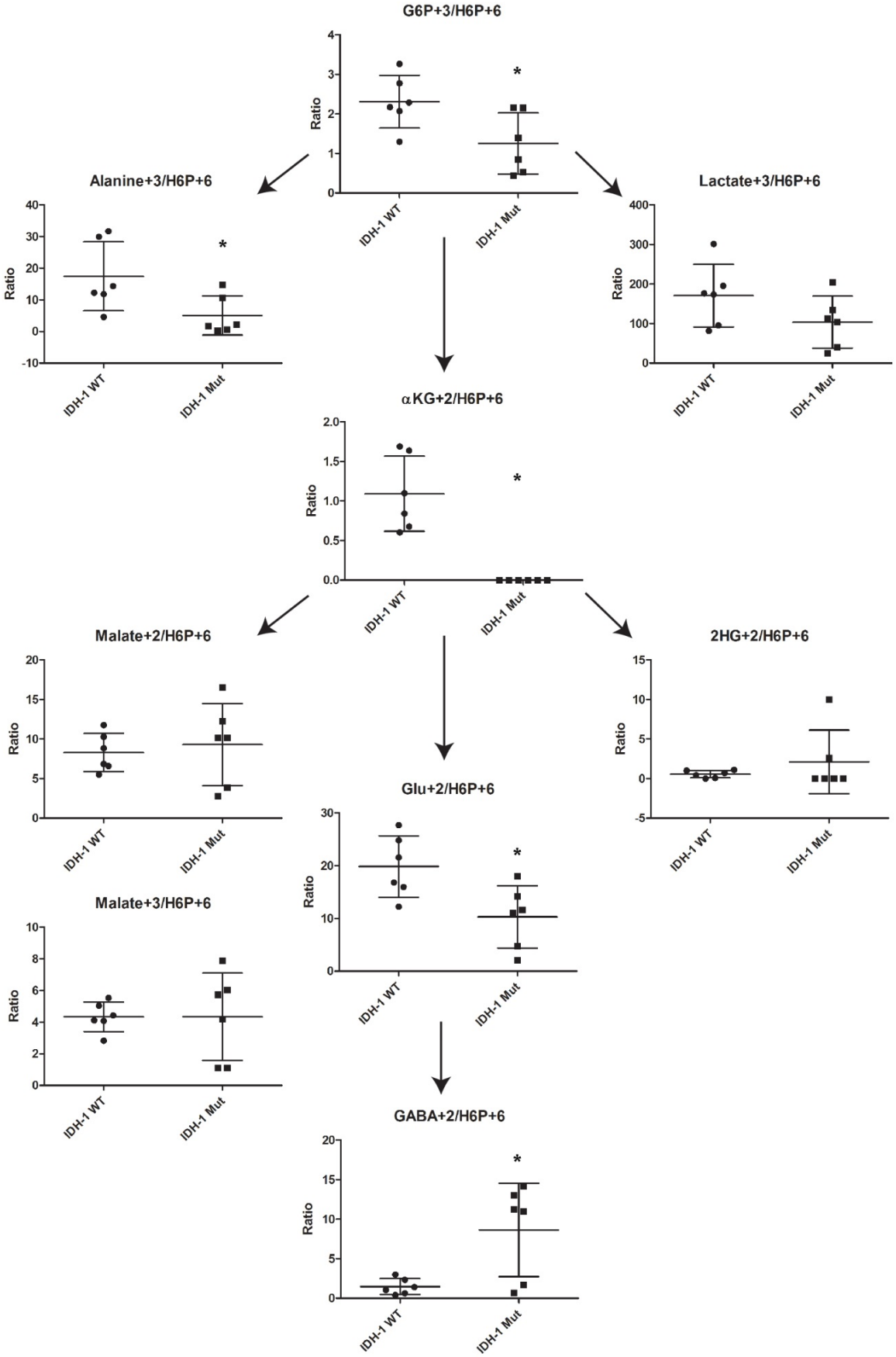

Figure 3-7 Ratio of labelled metabolites to fully labelled hexose-6-phosphate in IDH1 mutant compared to IDH1 wild-type tumours

Each point represents an average of core and peripheral tumour samples for one patient. Depicts mean +/- SD. * depicts a p value ≤ 0.05. Statistical analyses were performed using Student's t-test.

3.2.3 Metabolic effects of the IDH1 mutation in established cell lines

To determine whether the metabolic effects observed in the IDH1 mutated tumours could be replicated *in vitro*, we used cell lines kindly provided by Prof Christel Herold-Mende from Heidelberg University. The cell lines were grown from human glial tumours. They retained their endogenous IDH1 wild-type or mutation status and were maintained in culture for at least 60 passages. They were grown as spheroids in the Norlux laboratory in Luxembourg by our collaborator Dr Fred Fack. Two of the cell lines were IDH1 wild-type GBM (NCH644, NCH421), while three cell lines were high grade IDH1 mutant gliomas (NCH1681, NCH551b, NCH612).

In the following experiments, spheroids were plated and maintained for 3 days before the medium was replaced with either fully labelled ^{13}C glucose or ^{13}C glutamine and incubated for 24 hours before metabolite extraction. The experiments were performed in Luxembourg and the extracted metabolites were analysed using LC-MS at the CRUK Beatson Institute, Glasgow. The isotopologues for each metabolite were summated for each cell line to give a total steady state level. Changes in the levels of isotopologues for each metabolite between cell lines gave an indication of flux changes in metabolic pathways.

3.2.3.1 The IDH1 mutation results in changes in total steady state levels of TCA and glutamate derived metabolites

In the IDH1 mutant cell lines, 2HG levels were increased compared to the IDH1 wild-type cell lines. The mutant cell line with the lowest level of 2HG (NCH551b) still showed a two-fold increase over the highest 2HG level observed in the IDH1 wild-type cell line (NCH421), whereas the mutant cell line with the highest level of 2HG (NCH612) displayed a twenty-fold increase over the NCH421 cell line.

The IDH1 mutation resulted in changes in intracellular metabolites derived from glycolysis with increased serine levels in all IDH1 mutant cell lines compared to IDH1 wild-type. Alanine also showed an increase in the two IDH1 mutant cell lines with the highest levels of 2HG (Figure 3-8).

The IDH1 mutant enzyme utilises α-KG to produce 2HG. The intracellular levels of α-KG were lower in the two IDH1 mutant cell lines with the highest levels of intracellular 2HG (NCH16821, NCH612). Citrate, a precursor metabolite in the TCA cycle, was also higher in these two cell lines compared to the IDH1 wild-type GBM. Other TCA metabolites, such as succinate and malate, were not consistently different between the cell lines (Figure 3-8). However, aspartate, which is metabolised from oxaloacetate, was increased in the IDH1 cell line with the highest intracellular levels of 2HG (NCH612). Its derivative NAA was also increased when compared to the IDH1 wild-type cell lines (Figure 3-9).

α-KG can also be metabolised rapidly from glutamate. The levels of glutamate were increased in the cell line with the highest levels of intracellular 2HG (NCH612). Its precursor metabolite, glutamine, was also increased in the two cell lines with the highest intracellular 2HG levels. GABA, another metabolite derived from glutamate, was increased over ten times in the IDH1 mutant NCH551b cell line compared to the IDH1 wild-type controls (Figure 3-9).

3.2.3.2 The IDH1 mutation is associated with an increased flux from glutamine to 2HG

Comparing the relative contributions of different isotopologues generated from $^{13}C_6$ glucose or $^{13}C_5$ glutamine between the different cell lines can give an indication of changes in flux through different metabolic pathways.

Most of the contribution to the carbons in the TCA cycle in these cell lines comes from glutamine. When comparing glucose and glutamine labelled experiments there are more labelled isotopologues from glutamine than glucose. (Figure 3-8, Figure 3-9).

The IDH1 mutation converts α-KG to 2HG. In both the glucose and glutamine labelled experiments there is increased contribution of labelled 2HG in the IDH1 mutant compared to the IDH1 wild-type cell lines. With exception of α-KG, there was no difference in contribution from labelled glucose and glutamine in the TCA cycle, or for glutamate derived metabolites. This indicates an increased flux from α-KG to 2HG. In the IDH1 mutant cell lines, there is also more contribution from $^{13}C_5$ glutamine than $^{13}C_6$ glucose, indicating that most of the 2HG is derived from glutamine rather than glucose (Figure 3-8, Figure 3-9).

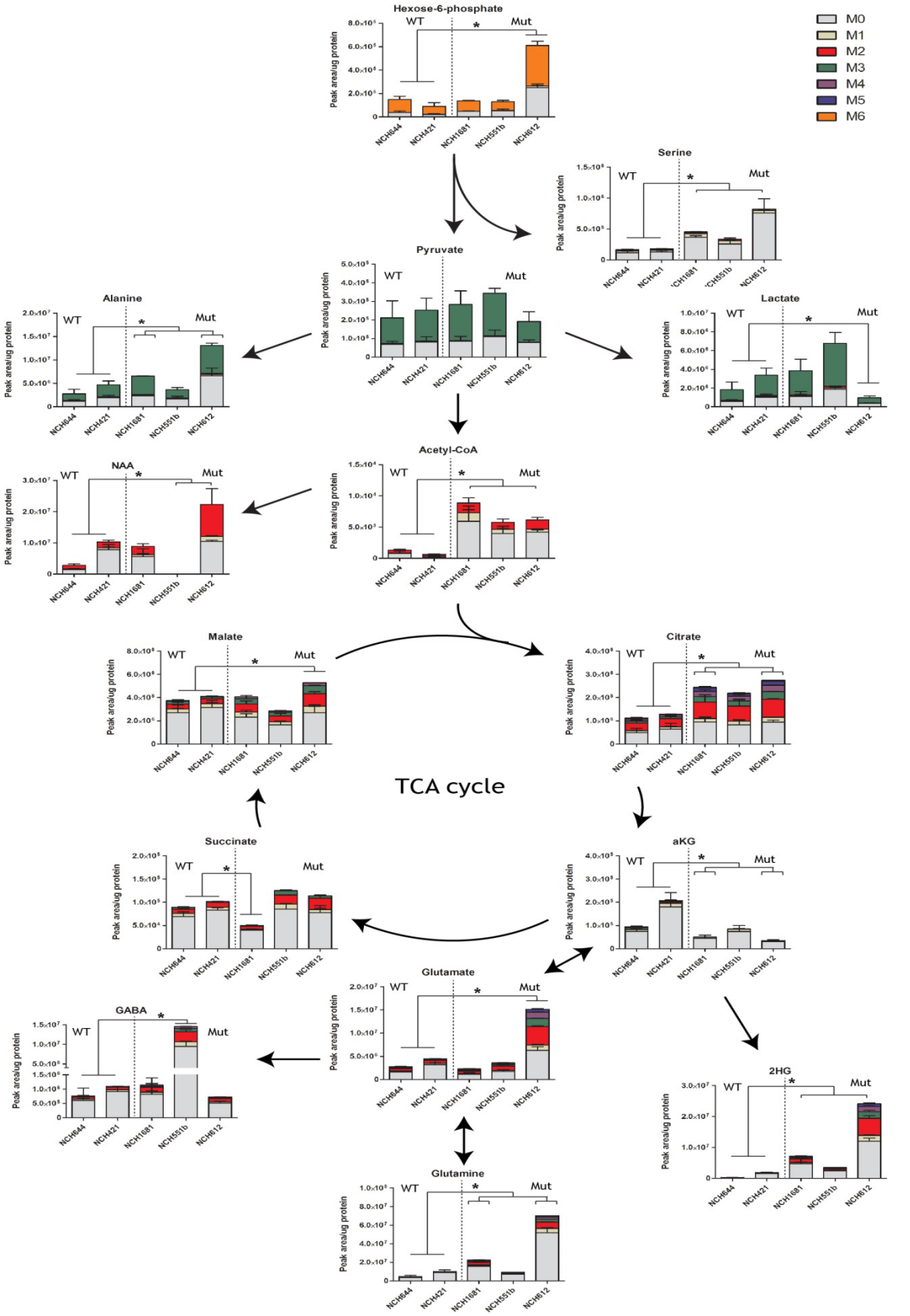

Figure 3-8 Metabolic isotopologues derived from glycolysis and the TCA cycle after the addition of $^{13}C_6$ labelled glucose

The first two cell lines depicted on the graph are IDH1 wild-type (WT) GBM (NCH644, NCH421), and the remaining three are high grade IDH1 mutant (Mut) glioma (NCH1681, NCH51b, NCH612). The different isotopologues are presented together for each metabolite in each cell line to depict total steady state metabolite levels. Results are from 2 independent experiments, mean +/- SEM. * depicts a p value ≤ 0.05 for total metabolite levels. Statistical analyses were performed using 2-way ANOVA.

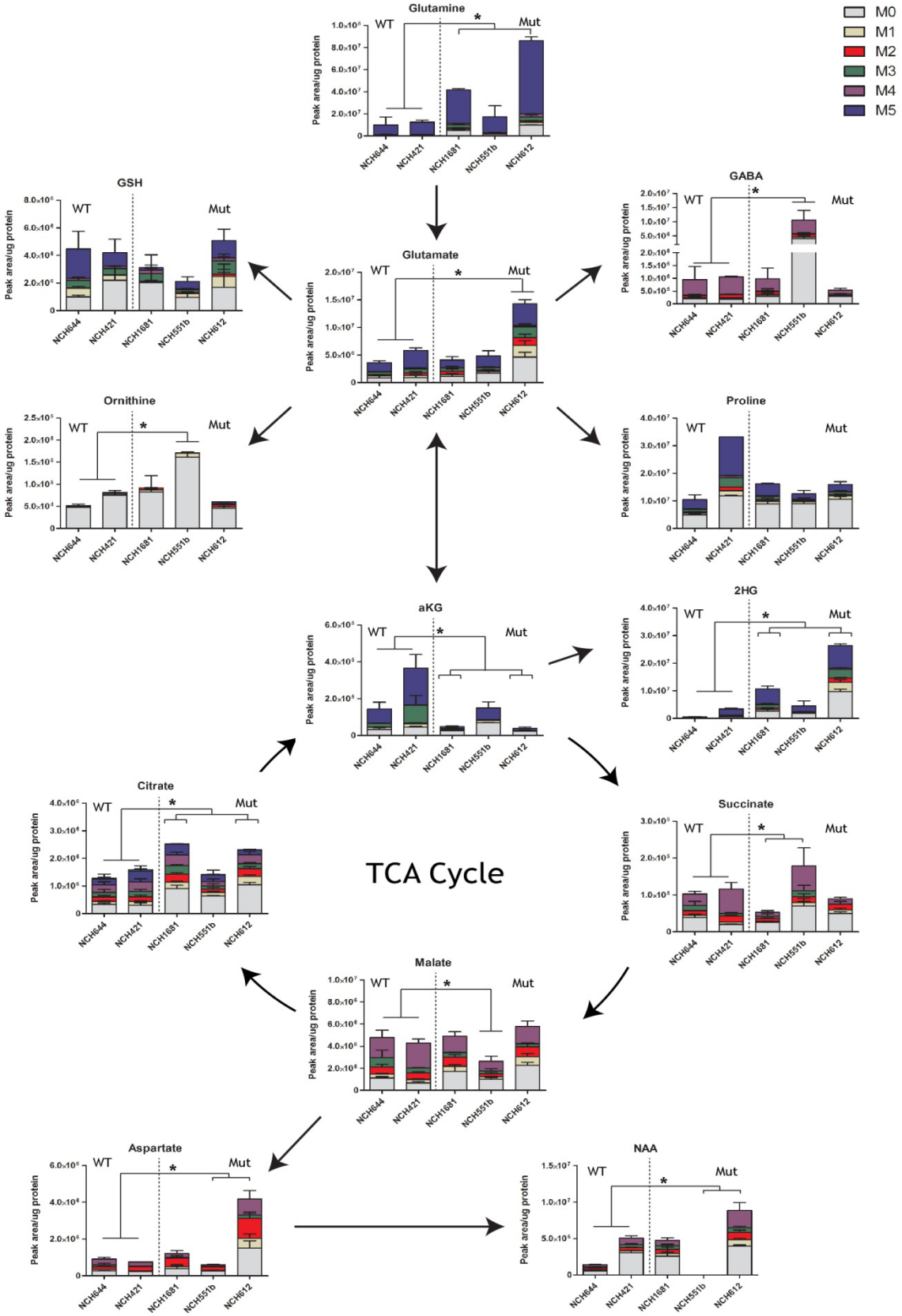

Figure 3-9 Metabolic isotopologues derived from glutamate metabolism after the addition of $^{13}C_5$ labelled glutamine

The first two cell lines depicted on the graph are IDH1 wild-type (WT) GBM (NCH644, NCH421), and the remaining three are high grade IDH1 mutant (Mut) glioma (NCH1681, NCH51b, NCH612). The different isotopologues are presented together for each metabolite in each cell line to depict total steady state metabolite levels. Results are from 2 independent experiments, mean +/- SEM. * depicts a p value ≤ 0.05 for total metabolite levels. Statistical analyses were performed using 2-way ANOVA.

3.3 Discussion

Tumour samples from patients taken at the time of surgery were analysed to understand the metabolic changes that occur due to the IDH1 mutation. Surrounding oedematous tissue was used as a control, which histologically contained mostly normal brain tissue. Two of the oedematous samples contained tumour (40% and 10%), which may have reduced the observed differences between the tumour and oedema samples. Both IDH1 mutant and IDH1 wild-type tumours showed metabolic changes which would be expected in a growing tumour, such as increases in amino acids required for protein synthesis and higher levels of glucose compared to normal brain. The IDH1 mutation results in the production of 2HG from α-KG. Unsurprisingly, the IDH1 mutant tumours showed a large increase in 2HG production compared to the surrounding normal brain. Conversely, both IDH1 wild-type and IDH1 mutant tumour samples had reduced levels of neurotransmitters, such as GABA, NAA, NAAG and glutamate. This is consistent with the lack of neuronal tissue in the tumours, which is the main source of these neurotransmitters. In addition, the high levels of 2HG produced by the IDH1 mutant tumours did not result in an increase in serum plasma levels compared to the wild-type controls. Though there is a high concentration of 2HG within the tumour, 2HG secreted into the extracellular space is probably negligible compared to the total volume of the circulation. The metabolite could also be rapidly metabolised by other tissues, such as the liver, if it entered the blood. This suggests that 2HG does not have a systemic effect, and serum 2HG measurements would not be an effective biomarker for monitoring disease.

When comparing IDH1 wild-type and IDH1 mutant primary brain tumours, there was again a marked increase in levels of 2HG in the mutant tumour. The substrate for the IDH1 mutant enzyme, α-KG, was reduced in the IDH1 mutant tumours, as were closely associated metabolites such as glutamate. Notably, there was a reduced contribution of labelling from glucose for α-KG in the IDH1 mutant samples compared to the wild-type. Interestingly, only 2 of the IDH1 mutant samples showed an increase in 2HG labelling from glucose compared to wild-type. This may be due to a technical issue with the LC-MS. We were not able to detect α-KG M+2, which may be explained by the low sensitivity to detect the levels of this isotopologue in these samples. This may also have been

the case for 2HG, explaining why only two of the tumours show increased flux from α-KG. Alternatively, as the IDH1 mutant enzyme is cytoplasmic it raises the possibility that 2HG production may be more dependent on other carbon sources, such as glutamine, rather than glucose in IDH1 mutant tumours, or that the turnover of 2HG is slow due to the high concentration of the metabolite in the cell. Also of note was the increased labelling contribution from glucose of GABA. The precursor to GABA is glutamate, which showed a decrease in labelling from glucose. This implies that there may be an increased flux from glutamate to GABA in the IDH1 mutant tumours compared to the IDH1 wild-type.

^{13}C glucose was given as a bolus which resulted in a marked increase in plasma glucose levels. The effect on metabolic rates of glucose compared to other carbon sources in the human brain in this situation is not known. However, an increase in plasma glucose has been shown to cause a corresponding increase in glucose phosphorylation in anaesthetised rats [277]. It could therefore be assumed that the increase in plasma glucose could result in an increase in glucose metabolism in the cell, altering the metabolic state of the tumour cells. This may overestimate the effect of glucose on TCA, NAA and GABA metabolism. In addition, the time taken to resect each tumour varied between patients, so the plasma level of ^{13}C glucose would differ in patients at the time of tumour extraction, potentially affecting the results. An infusion of ^{13}C glucose was considered as it would have given a more physiological and consistent plasma ^{13}C glucose level, but was not possible for practical reasons and cost.

The clinical study was limited due the small number of patients involved. There were only six IDH1 wild-type and six IDH1 mutant tumours. Also, while all the IDH1 wild-type tumours were GBM, the IDH1 mutant tumours were of various grades and histological types. There was only one IDH1 mutant GBM, 2 low grade diffuse astrocytomas, one high grade anaplastic astrocytoma, and two high grade anaplastic oligoastrocytomas. Unfortunately, this is due to the fact that IDH1 mutant tumours are common in WHO grade II to III tumours but rare in WHO grade IV GBM. The opposite is true for IDH1 wild-type tumours which are common in GBM but not in other lower grades of glioma. It raises the possibility that some of the metabolic changes we observed, such as lower levels of lactate and pyruvate, may be related to differences in tumour grade and histological sub-type rather than IDH1 mutant status. Low grade glial tumours grow over a

period of years, and these metabolic differences may in part be a reflection of lower metabolic activity compared to high grade rapidly growing GBM.

To try and replicate these results, established cell lines which retained their IDH1 mutant status were used. This included three IDH1 mutant high grade gliomas which were compared to two IDH1 wild-type GBM. To try and replicate *in vivo* conditions they were grown as spheroids and incubated with $^{13}C_6$-glucose or $^{13}C_5$-glutamine to give additional information on metabolic flux. In common with the *in vivo* tumour samples, there was an increase in 2HG and fall in α-KG in the IDH1 mutant samples. One of the IDH1 mutant cell lines also showed a marked increase in GABA. This was only present in one of the cell lines, which may reflect adaptation of the other IDH1 mutant cell lines to the medium, reducing the need for GABA metabolism, or that this effect is only observed in some IDH1 mutant tumours, as the cell lines were derived from different WHO grades of tumour. In addition, increased contribution of labelling from both $^{13}C_6$-glucose and $^{13}C_5$-glutamine in 2HG was observed, with a reduction in contribution for α-KG in the IDH1 mutant compared to IDH1 wild-type tumours. This also implies increased flux from α-KG to 2HG in the IDH1 mutant cell lines. Similarly to the *in vivo* tumour samples, only very low levels of α-KG M+2 could be detected in all the cell lines. Conversely, using $^{13}C_5$-glutamine labelling, the majority of the intracellular isotopologues of α-KG in the cell lines were labelled, indicating that most of the carbon contribution is from glutamine, which may explain the low levels of α-KG M+2 in the clinical samples.

There were discrepancies, however, between the data from the clinical samples and the cell lines. The IDH1 mutant cell lines, compared to the wild-type controls, had increased levels of citrate, acetyl-CoA, alanine, glutamine and glutamate, which was not evident from the clinical samples. This may be a consequence of the medium in which the cell lines were grown, which have much higher levels of glucose and glutamine then occur *in vivo*. This may result in increased consumption of these metabolites resulting in observed differences in glycolysis and glutamine metabolism which may not be physiologically relevant.

In summary, both the *in vivo* and cell line data suggests that in IDH1 mutant cells there is an increased metabolic flux towards 2HG from α-KG. This may in

turn have an effect on decreasing other metabolites associated with α-KG such as glutamate. In addition, there may be an increased flux from glutamate to GABA, increasing intracellular GABA levels as well as depleting glutamate. The decrease in α-KG, coupled with the increase in 2HG, raised the interesting possibility of the inhibition of α-KG dependent dioxygenases. These enzymes form a superfamily that is important in many cellular functions such as epigenetic modulation of DNA and histones, and oxygen sensing. Other enzymes, such as transaminases, are also dependent on α-KG as a co-substrate. Inhibition of these enzymes may also explain some of the other metabolic changes observed, such as the increase in GABA. Unfortunately, the endogenous IDH1 mutant cell lines were slow and problematic to grow in culture, so in order to investigate the metabolic, cellular, and epigenetic consequences of this increased 2HG/α-KG ratio we developed our own cell model by overexpressing an IDH1 mutant gene in an anaplastic astrocytoma cell line, as well as using an IDH1 wild-type and mutant overexpressed immortalised astrocyte cell line

Chapter 4 Investigating the metabolic effect of the IDH1 mutation *in vitro*

4.1 Introduction

In the previous chapter metabolic changes, caused by the IDH1 mutation, were reported in clinical glioma samples. In addition to the increase in 2HG, there was also a fall in α-KG and glutamate. Conversely, there was an increase in the level of the glutamate derived metabolite, GABA, which is the most common neuroinhibitor in the brain. This effect was also observed in cell lines with an endogenous IDH1 mutation. $^{13}C_6$ labelled glucose was administered to the patients prior to surgical excision of the tumour. The isotopologues generated from the metabolism of $^{13}C_6$ labelled glucose suggested an increased flux from α-KG to 2HG, and also from glutamate to GABA. Increased flux from α-KG to 2HG was observed with $^{13}C_6$ labelled glucose and $^{13}C_5$ labelled glutamine when comparing endogenous IDH1 mutant cell lines to IDH1 wild-type controls.

Endogenous IDH1 mutant cell lines are difficult to grow in culture, due to slow proliferation and loss of the IDH1 mutation over time. Currently, there is only one published glioma cell line, an anaplastic oligodendroglioma, with an endogenous IDH1 mutation [269]. Therefore, to further investigate the metabolic effects of the IDH1 mutation a cell model was developed using an anaplastic astrocytoma cell line.

4.2 Results

4.2.1 Developing a cell model

An anaplastic astrocytoma cell line MOG-GCCM, which is associated with p53 and MAPK pathway mutations, was used to develop a cell model. This is a type of glioma that has a high incidence of IDH1 mutation *in vivo*. This cell line is IDH1 wild-type, so the commonest IDH1 mutation was overexpressed using a pcDNA 3.1(+) plasmid with an IDH1 mutant R132H myc-tagged gene insert. Simultaneously, a separate population of cells from the same cell line was transfected with an empty vector (EV). This, in addition to the MOG-GCCM parental cell line (PCL), was used as a control (Figure 4-1A).

The transfected cells were kept as pools to maintain the genetic diversity of the cell line. Initially the IDH1 mutant pool had 2HG levels which were one hundred times the level of the EV control, while it was also noted that the IDH1 mutant pool exhibited slower cell proliferation, as the doubling time was ten hours longer than the EV control. Over time, the level of 2HG in the IDH1 mutant pool fell. At twenty passages, the level of intracellular 2HG was the same as the EV control. The IDH1 pool also displayed an increase in cell proliferation (Figure 4-1B). Immunofluorescence staining, with an antibody that detects both IDH1 wild-type and mutant protein, showed a sub-population of cells in the IDH1 mutant pool with high levels of IDH1 protein which was assumed to be IDH1 mutant, which did not occur in the EV pool. This additional flourescence was due to the over-expression of the IDH1 mutant protein and this decreased over time in conjunction with the fall in intracellular 2HG (Figure 4-1C).

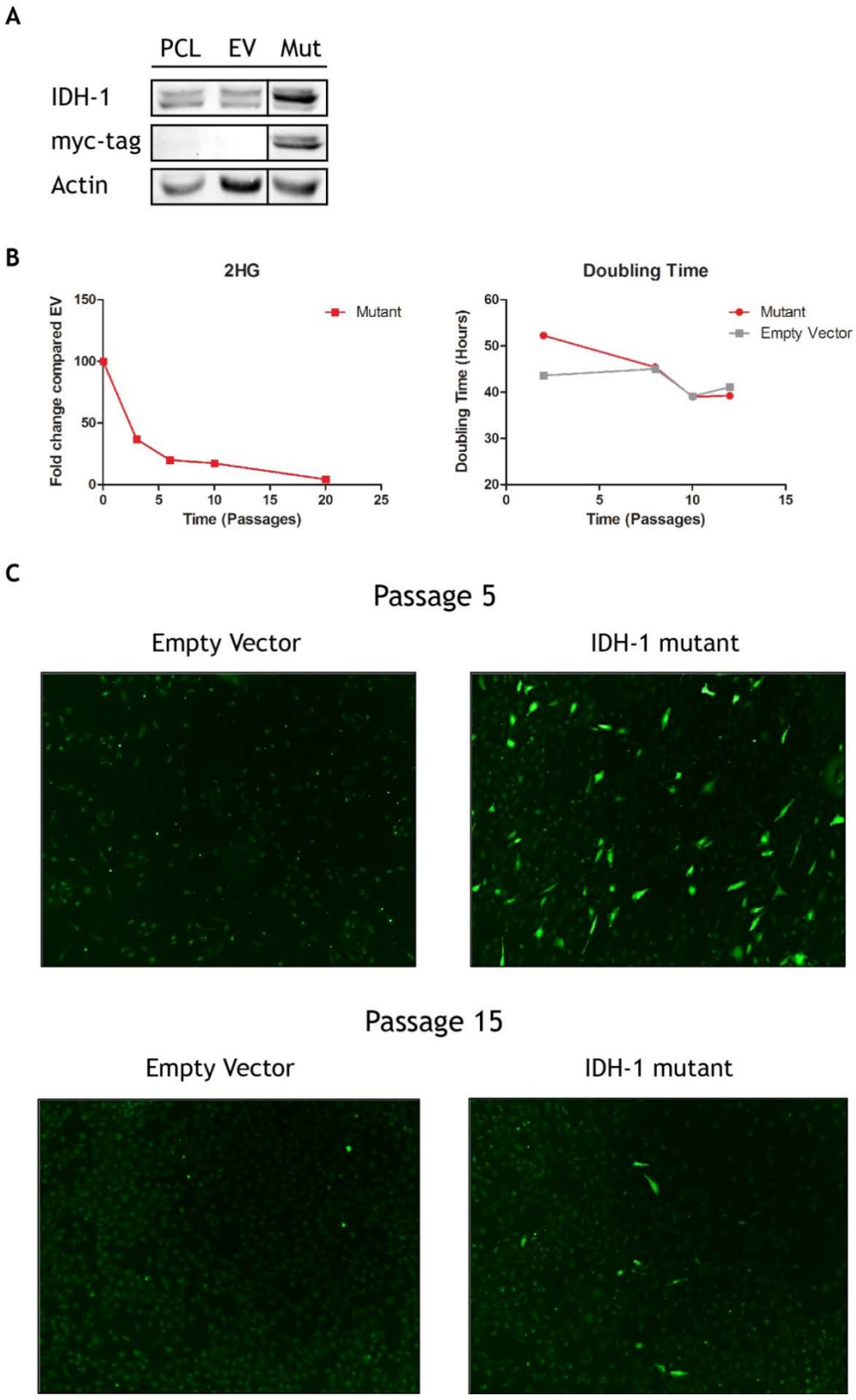

Figure 4-1 Developing a cell model

A. Western blot depicting protein expression of IDH1 in MOG-GCCM pools overexpressed with either a IDH1 R132H mutant plasmid (Mut) or empty vector (EV) plasmid. The IDH1 mutant gene was myc-tagged. PCL represents the MOG-GCCM parental cell line. Actin was used as an internal control. B. Ratio of 2HG in the IDH1 mutant pool compared to the EV pool over time. The effect on cell proliferation, depicted as cell doubling time, for the IDH1 mutant pool compared to the EV pool over time. C. Immunoflourescence microscopy images depicting non-specific IDH1 protein expression in IDH1 mutant pool and EV pool at 5 passages and 15 passages.

This led to the hypothesis that 2HG was responsible for decreased cell proliferation. This resulted in a loss of cells overexpressing mutant IDH1 from the cell pool, as cells with high levels of 2HG were outgrown. As 2HG is not cell permeable, exogenous 2HG-lactone was used in all future cell culture experiments, as it can easily cross the cell membrane. The lactone structure can spontaneously hydrolyses in water or it can be cleaved after it enters the cell by naturally occurring esterase [278]. After the addition of 2HG-lactone to the medium, high levels of intracellular 2HG-lactone and 2HG were observed (data not shown). The hypothesis that 2HG was responsible for decreased cell proliferation was tested and confirmed by the addition of exogenous 2HG-lactone to MOG-GCCM and LN18, a glioblastoma cell line established from an IDH1 wild-type tumour. Increasing concentrations of 2HG-lactone from 10 mM to 30 mM resulted in a dose dependent reduction in cell proliferation, confirming the negative effect of 2HG on cell growth (Figure 4-2D).

Clones were developed to decrease the possibility of 2HG loss after overexpression of the IDH1 mutation in the previously described pool format. These consisted of one EV clone and three IDH1 mutant clones with varying levels of expression: low, medium and high (MC3, MC10 and MC9 respectively, Figure 4-2A). Overexpression of IDH1 wild-type resulted in an increase in α-KG (data not shown), potentially affecting metabolism, α-KG-dependent dioxygenase activity and the epigenome, so were not used [255]. To identify whether the effect of the IDH1 mutation on cell proliferation was related to the production of 2HG an additional experimental group was added.This involved propagating the EV clone continuously in medium containing 30 mM 2HG-lactone for at least fifteen passages (EV + 2HG). This corresponded to an intracellullar 2HG level which was equivalent to the highest IDH1 mutant expression clone, MC9. In addition, the MOG-GCCM PCL was used as an additional control (Figure 4-2B). MC9 and MC10, which both exhibited the highest intracellular concentrations of 2HG, also showed increased cell doubling times when compared to the controls, confirming the inhibitory effect of 2HG on cell proliferation (Figure 4-2C).

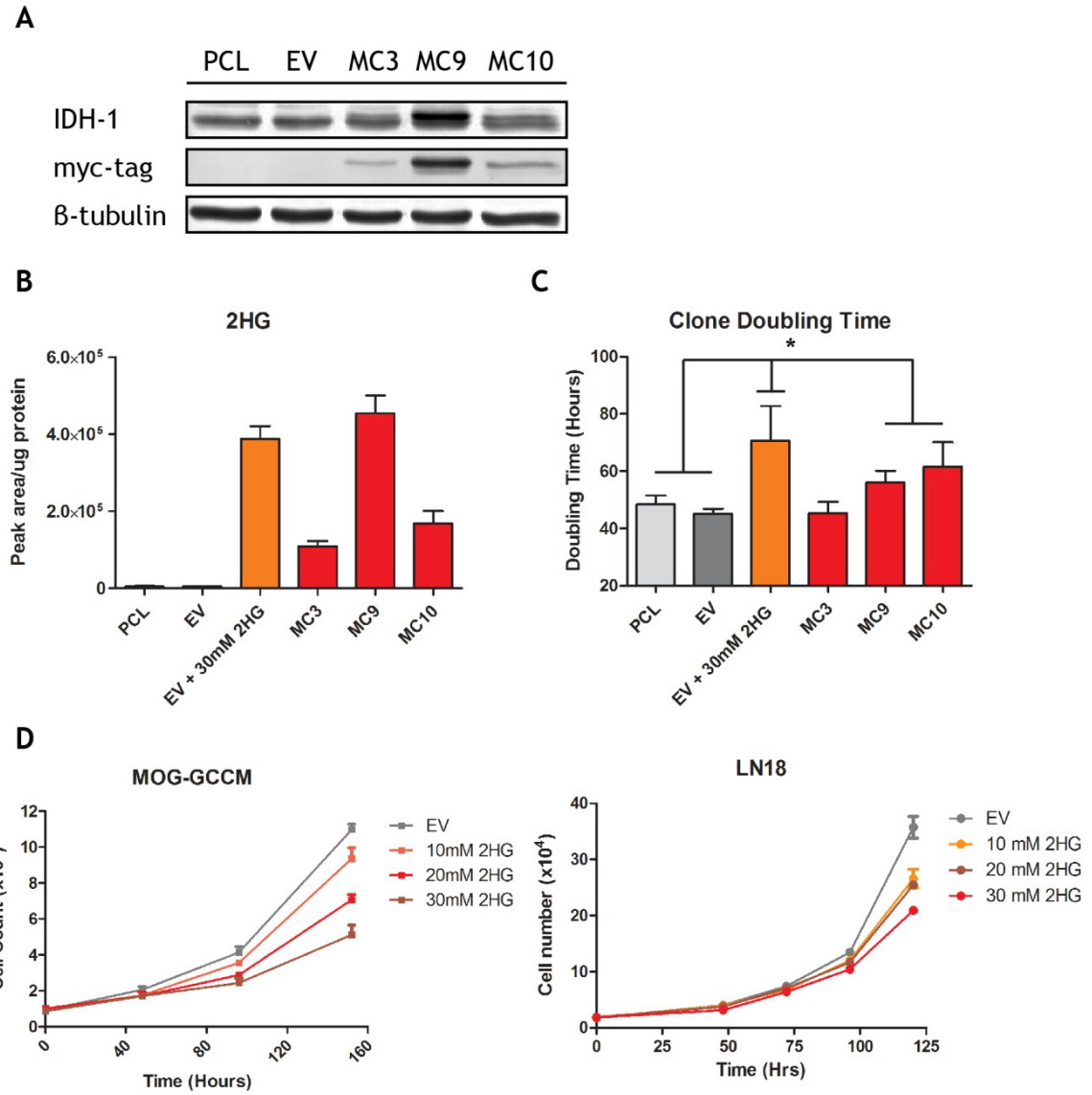

Figure 4-2 The effect of 2HG on cell proliferation

A. The Western blot depicts IDH1, and myc-tag protein expression in the MOG-GCCM PCL, EV and IDH1 mutant clones (MC3, MC9 and MC10). β-tubulin was used as an internal control. B. Intracellular levels of 2HG in the MOG-GCCM PCL, EV, EV + 2HG, and IDH1 mutant clones. C. Cell doubling time for IDH1 mutant clones, EV + 2HG, and EV and MOG-GCCM PCL controls. D. Cell proliferation assay depicting effect on cell growth of increasing concentrations of 2HG-lactone (2HG) in MOG-GCCM and LN18 cell lines. B + C depicts at least 3 independent experiments with mean +/- SEM. D depicts single cell proliferation experiment with mean +/- SD showing the effect of 2HG-lactone on MOG-GCCM and LN18 cell lines. * represents a p-value ≤0.05. Data were analysed using 2-way ANOVA.

4.2.1.1 The IDH1 mutation is associated with changes in mRNA expression

Affymetrix microarray experiments were performed to determine differences in gene expression between two of the IDH1 mutant clones (MC3 and MC9), EV + 2HG and the EV and MOG-GCCM PCL controls. The two IDH1 mutant clones were chosen to determine differences that occur both at high and low levels of intracellular 2HG. EV and MOG-GCCM PCL had a similar gene expression profile indicating that the EV was a good representation of the original MOG-GCCM PCL. However, differences were evident between the controls and the IDH1 mutant clones and EV + 2HG. MC3 and EV + 2HG had similar gene expression profiles, but the largest differences in gene expression were observed between the controls and the MC9 clone (Figure 4-3A).

The EV control was compared to the EV + 2HG and MC9 clone using Ingenuity Pathway Analysis. This identified the gene interaction pathways for the genes that were significantly different between the control and EV + 2HG or MC9. There were differences in pathways associated with cell proliferation and growth, and the cell cycle, consistent with the previously described experiments on cell growth (Figure 4-3B).

The top 50 genes upregulated in EV + 2HG and MC9 with the highest fold change included genes specific to neural function. Examples are KAL1, which is involved in cell adhesion and migration, UNC5C and ENAH, which are involved in axon guidance, and ZC4H2 and HEY1, which are involved in neurogenesis. GABRQ, a subunit of the $GABA_A$ receptor present on both astrocytes and neurons, was also upregulated. In addition, this group also included ALDOC and GPAM, which are genes involved in lipid metabolism. Several genes from the G-antigen family were also increased (GAGE12F, GAGE5, GAGE2E, GAGE8, GAGE10). These are normally expressed in normal testis, but have been associated with tumour growth and metastasis in some cancers [279] (Table 4-1). The top genes downregulated in EV + 2HG and MC9, compared to the EV, are shown in table 4-2.

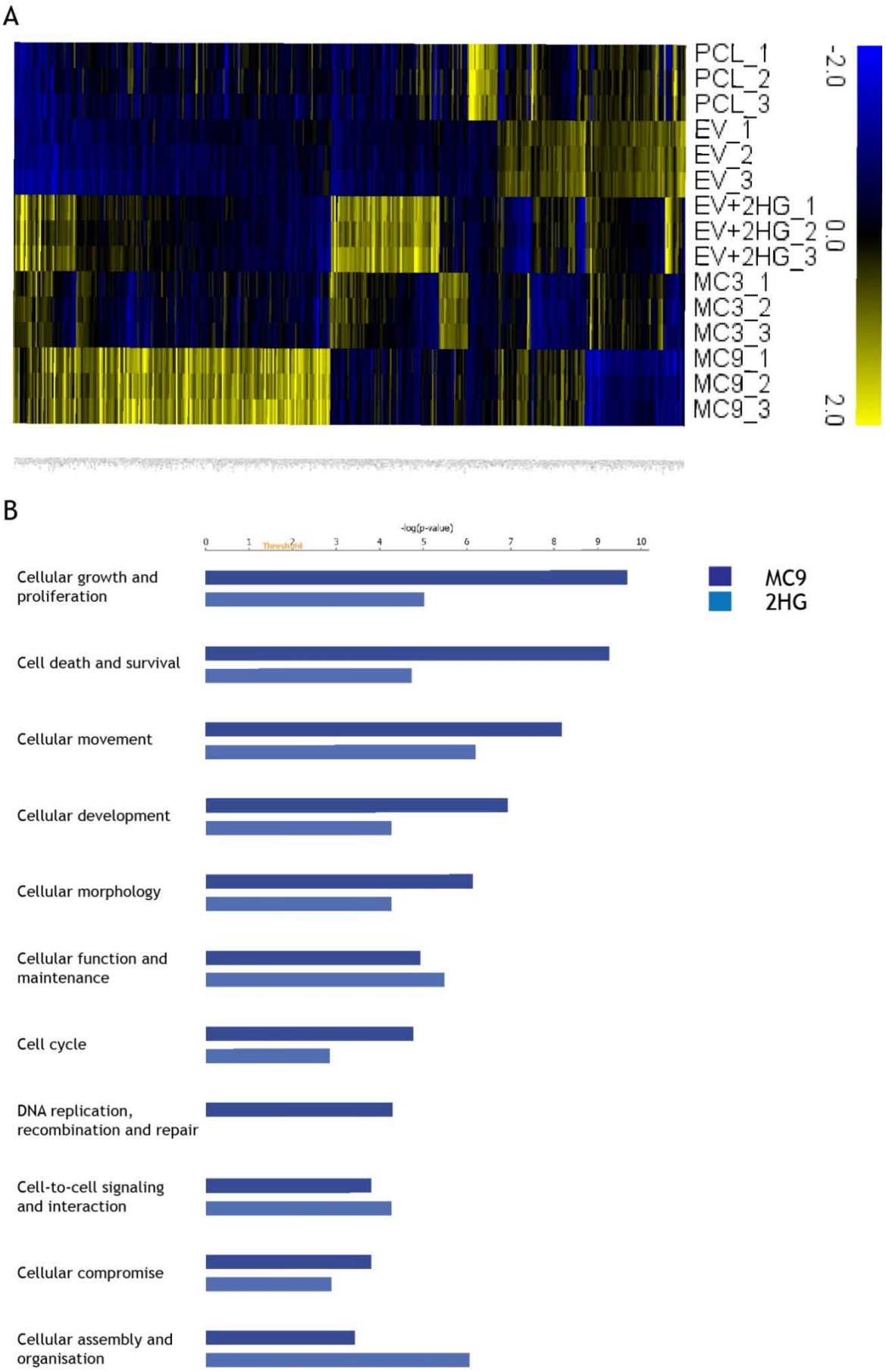

Figure 4-3 Changes in gene expression caused by the IDH1 mutation
A. Heatmap comparing genes differentially expressed in the EV compared to the MOG-GCCM PCL, IDH1 mutant clones (MC3 and MC9) or EV + 2HG. B. Ingenuity pathway analysis of genes represented in A. comparing EV to MC9 or EV + 2HG

	MC9			EV + 2HG		
Gene	FC	p-value	q-value	FC	p-value	q-value
THBS2	6.64	$7.70E^{-07}$	$2.73E^{-04}$	2.89	$2.17E^{-04}$	0.017
NID2	5.72	$2.12E^{-07}$	$1.24E^{-04}$	2.55	$1.11E^{-04}$	0.011
HMCN1	4.19	$8.94E^{-07}$	$3.01E^{-04}$	3.07	$1.10E^{-05}$	0.002
TMSB15A	4.06	$1.53E^{-04}$	$7.47E^{-03}$	3.38	$4.94E^{-04}$	0.028
PTPN13	3.92	$7.42E^{-09}$	$2.56E^{-05}$	2.06	$7.06E^{-06}$	0.002
GPAM	3.82	$6.02E^{-09}$	$2.38E^{-05}$	2.78	$1.25E^{-07}$	$1.39E^{-04}$
CPE	3.79	$3.58E^{-06}$	$7.16E^{-04}$	2.37	$2.21E^{-04}$	0.017
KAL1	3.59	$1.04E^{-05}$	0.001	6.29	$2.35E^{-07}$	$1.94E^{-04}$
DCN	3.47	$7.79E^{-06}$	0.001	3.18	$1.58E^{-05}$	0.003
MFAP4	3.20	$5.35E^{-07}$	$2.00E^{-04}$	2.59	$4.39E^{-06}$	0.001
IGF2BP1	3.18	$6.07E^{-05}$	0.004	2.41	$6.47E^{-04}$	0.032
RANBP3L	2.98	0.006	0.080	4.62	$5.89E^{-04}$	0.030
IGFBP7	2.91	$5.48E^{-04}$	0.017	3.11	$3.35E^{-04}$	0.022
TECTB	2.88	$2.35E^{-06}$	$5.59E^{-04}$	4.11	$1.06E^{-07}$	$1.28E^{-04}$
ZC4H2	2.83	$4.71E^{-07}$	$1.88E^{-04}$	1.71	$3.12E^{-04}$	0.021
C1R	2.82	$9.22E^{-06}$	0.001	1.80	$1.34E^{-03}$	0.049
PCSK1	2.62	$4.23E^{-08}$	$7.30E^{-05}$	2.71	$2.79E^{-08}$	$5.38E^{-05}$
GAGE12F	2.60	$3.21E^{-04}$	$1.20E^{-02}$	9.29	$6.97E^{-08}$	$9.17E^{-05}$
FN1	2.39	$1.86E^{-06}$	$4.80E^{-04}$	1.90	$4.05E^{-05}$	0.006
BFSP1	2.34	$5.12E^{-06}$	$8.52E^{-04}$	3.23	$1.69E^{-07}$	$1.48E^{-04}$
PCDHB10	2.31	$1.93E^{-06}$	$4.93E^{-04}$	1.50	$1.32E^{-03}$	0.049
ANKH	2.31	$1.05E^{-03}$	0.026	3.45	$3.66E^{-05}$	0.005
NR5A2	2.30	$2.89E^{-06}$	$6.48E^{-04}$	1.61	$5.04E^{-04}$	0.028
CADM1	2.27	$2.22E^{-07}$	$1.28E^{-04}$	2.19	$3.71E^{-07}$	$2.50E^{-04}$
RNF144B	2.24	$1.41E^{-03}$	$3.14E^{-02}$	4.44	$6.26E^{-06}$	0.002
CA11	2.23	$4.76E^{-07}$	$1.88E^{-04}$	1.55	$1.76E^{-04}$	0.015
PXDN	2.22	$3.48E^{-05}$	0.003	3.19	$7.93E^{-07}$	$4.17E^{-04}$
TMEM2	2.21	$4.01E^{-06}$	$7.43E^{-04}$	1.53	$1.06E^{-03}$	0.042
THBS3	2.19	$2.00E^{-05}$	$2.08E^{-03}$	3.36	$2.28E^{-07}$	$1.94E^{-04}$
GAGE5	2.13	$1.85E^{-05}$	0.002	9.75	$1.01E^{-10}$	$5.45E^{-07}$
GAGE2E	2.12	$2.01E^{-05}$	0.002	9.66	$1.13E^{-10}$	$5.45E^{-07}$
GABRQ	2.12	$2.77E^{-05}$	0.003	1.71	$5.47E^{-04}$	0.029
JAKMIP2	2.12	$2.33E^{-04}$	0.010	2.10	$2.55E^{-04}$	0.018
GAGE8	2.09	$8.50E^{-06}$	0.001	8.23	$7.66E^{-11}$	$5.45E^{-07}$
HNMT	2.05	$6.53E^{-05}$	0.004	1.74	$6.11E^{-04}$	0.031
C12orf53	2.05	$1.06E^{-06}$	$3.40E^{-04}$	2.03	$1.21E^{-06}$	0.001
HEG1	2.00	$5.74E^{-05}$	0.004	1.72	$4.91E^{-04}$	0.028
ALDOC	1.98	$5.00E^{-06}$	$8.45E^{-04}$	1.73	$4.38E^{-05}$	0.006
GAGE10	1.95	$1.77E^{-03}$	0.036	6.26	$1.34E^{-07}$	$1.42E^{-04}$
CDH6	1.95	$1.24E^{-04}$	0.006	3.31	$3.79E^{-07}$	$2.50E^{-04}$
BICC1	1.95	$1.39E^{-07}$	$1.14E^{-04}$	1.81	$4.80E^{-07}$	$2.95E^{-04}$
FNBP1L	1.92	$9.14E^{-06}$	0.001	1.58	$2.26E^{-04}$	0.017
KIAA1462	1.89	$1.61E^{-05}$	0.002	1.55	$4.53E^{-04}$	0.027
UNC5C	1.86	$5.58E^{-07}$	$2.05E^{-04}$	1.51	$3.25E^{-05}$	0.005
HLA-DMA	1.84	$2.60E^{-03}$	0.045	2.56	$8.31E^{-05}$	0.009
HEY1	1.83	$2.09E^{-04}$	0.009	2.20	$1.87E^{-05}$	0.003
S100A2	1.80	$4.58E^{-04}$	0.015	1.75	$6.80E^{-04}$	0.033
ENAH	1.80	$2.43E^{-09}$	$1.50E^{-05}$	1.56	$5.86E^{-08}$	$8.08E^{-05}$
ITGA10	1.80	$1.80E^{-04}$	0.008	1.68	$4.72E^{-04}$	0.027
HRCT1	1.78	$3.78E^{-05}$	0.003	1.73	$6.23E^{-05}$	0.008

Table 4-1 Genes upregulated in mRNA anaylsis
Top 50 genes upregulated both in the IDH1 mutant clone (MC9) and EV + 2HG compared to the EV. Includes genes with at least 1.5 fold change and a q-value ≤ 0.05.

	MC9			EV + 2HG		
Gene	FC	p-value	q-value	FC	p-value	q-value
ANPEP	-10.88	9.79E-10	1.35E-05	-2.15	1.53E-04	0.013
CPED1	-4.31	7.28E-06	0.001	-2.74	2.34E-04	0.017
GPR110	-4.32	5.12E-08	7.86E-05	-2.32	1.71E-05	0.003
SPP1	-3.82	6.99E-08	8.04E-05	-2.25	1.40E-05	0.003
RRAGD	-3.67	1.31E-06	3.78E-04	-3.51	1.88E-06	0.001
PMF1-BGLAP	-3.07	3.37E-04	0.012	-3.26	2.16E-04	0.017
G0S2	-2.89	9.64E-06	0.001	-1.84	1.25E-03	0.047
HAS2	-2.55	1.52E-05	0.002	-5.54	2.51E-08	5.38E-05
TM4SF1	-2.36	2.38E-05	0.002	-1.80	6.63E-04	0.033
HTR1F	-2.40	7.10E-05	0.005	-2.58	3.40E-05	0.005
PLAT	-2.26	4.78E-07	1.88E-04	-1.68	4.62E-05	0.006
PNP	-2.25	3.36E-07	1.64E-04	-1.60	7.95E-05	0.009
FGF5	-2.21	1.23E-07	1.14E-04	-1.67	1.15E-05	0.002
SLC43A3	-2.19	1.85E-07	1.16E-04	-2.23	1.48E-07	1.42E-04
AGPAT9	-2.18	3.58E-07	1.66E-04	-1.40	9.84E-04	0.041
PPFIA2	-2.13	4.84E-05	0.004	-1.76	5.92E-04	0.030
LYN	-2.07	1.25E-05	0.002	-2.14	8.32E-06	0.002
TMEFF2	-1.87	3.24E-04	0.012	-3.63	2.76E-07	2.22E-04
PRKCD	-1.77	9.42E-05	0.006	-1.59	5.34E-04	0.029
PM20D2	-1.77	1.13E-04	0.006	-1.76	1.16E-04	0.011
ETS2	-1.74	8.33E-05	0.005	-1.95	1.53E-05	0.003
HERC3	-1.74	5.50E-04	0.017	-1.73	6.15E-04	0.031
EPHB1	-1.74	1.90E-04	0.009	-1.91	4.48E-05	0.006
MAST4	-1.73	5.26E-05	0.004	-1.62	1.59E-04	0.014
SLC35D1	-1.71	1.59E-03	0.034	-1.75	1.23E-03	0.046
HMGA1P1	-1.70	1.96E-03	0.038	-1.77	1.15E-03	0.044
NEGR1	-1.70	3.38E-04	0.012	-1.68	4.25E-04	0.025
ELOVL6	-1.70	2.11E-03	0.04	-2.09	1.51E-04	0.013
BGN	-1.66	6.21E-05	0.004	1.80	1.60E-05	0.003
B4GALT6	-1.64	5.86E-05	0.004	-1.56	1.57E-04	0.014
IL1RAPL1	-1.63	7.77E-04	0.021	-1.66	5.91E-04	0.030
TMEM154	-1.63	6.49E-04	0.019	-1.62	7.22E-04	0.034
CNR1	-1.62	5.45E-04	0.017	-1.84	7.50E-05	0.009
POP1	-1.62	6.14E-04	0.018	-1.73	2.06E-04	0.016
NAV3	-1.60	1.19E-03	0.028	-2.19	1.42E-05	0.003
EPAG	-1.59	7.13E-04	0.020	-1.53	1.34E-03	0.049
CD55	-1.56	1.12E-05	0.001	-1.73	1.26E-06	0.001
FOSL1	-1.54	6.74E-04	0.019	-1.76	6.70E-05	0.008
FAH	-1.53	4.71E-04	0.015	-1.61	2.01E-04	0.016

Table 4-2 Genes downregulated in mRNA anaylsis

Top genes downregulated both in the IDH1 mutant clone (MC9) and EV + 2HG compared to the EV. Includes genes with at least 1.5 fold change and a q-value ≤ 0.05.

4.2.2 Metabolic changes caused by the IDH1 mutation

4.2.2.1 Overexpression of the IDH1 mutation is associated with changes in the TCA cycle and glutamate derived metabolites

To characterise the metabolic differences in IDH1 mutant clones compared to the controls, intracellular metabolites were extracted after propagation for 24 hours in fresh medium to generate data on steady state metabolomics. IDH1 wild-type and IDH1 R132H mutant overexpressed immortalised astrocytes (SK2012-113) were used to identify whether these effects could also occur in non-malignant cells. Metabolites were also extracted after 24 hours of cell propagation in fresh medium.

In the TCA cycle, there was a fall in α-KG levels in MC9 and MC10 compared to the controls. This was replicated in the EV + 2HG experimental group. Other TCA metabolites, such as succinate, malate, and citrate were also decreased in these clones. Again, this effect was repeated in the EV + 2HG group with the exception of succinate. The clone with the lowest intracellular levels of 2HG, MC3, had decreased levels of citrate and malate when compared to the controls (Figure 4-4). The IDH1 mutant astrocytes displayed an increase in intracellular 2HG and a reduction in α-KG and the downstream TCA metabolite succinate compared to IDH1 wild-type cells. Conversely, IDH1 mutant astrocytes had a small increase in intracellular levels of malate and citrate (Figure 4-5).

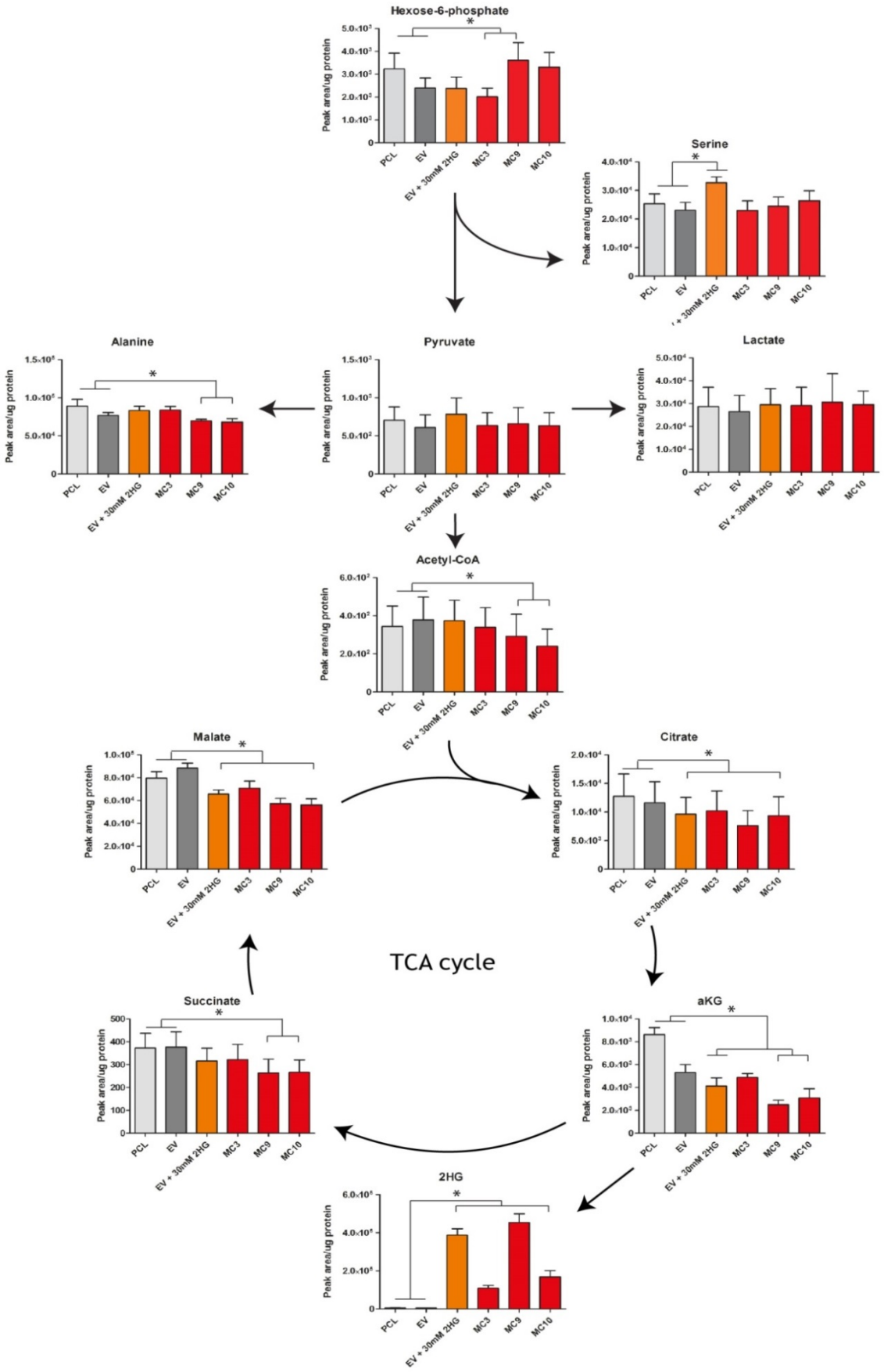

Figure 4-4 The metabolic effect of the IDH1 mutation on glycolysis and the TCA cycle in MOG-GCCM clones

IDH1 R132H overexpressed mutant clones are depicted in red (MC3, MC9, MC10), EV + 2HG is depicted in orange, and the controls in grey (EV and MOG-GCCM PCL). Data depicted as mean +/- SEM for 5 independent experiments. * represents a p-value ≤0.05. Data were analysed using 2-way ANOVA.

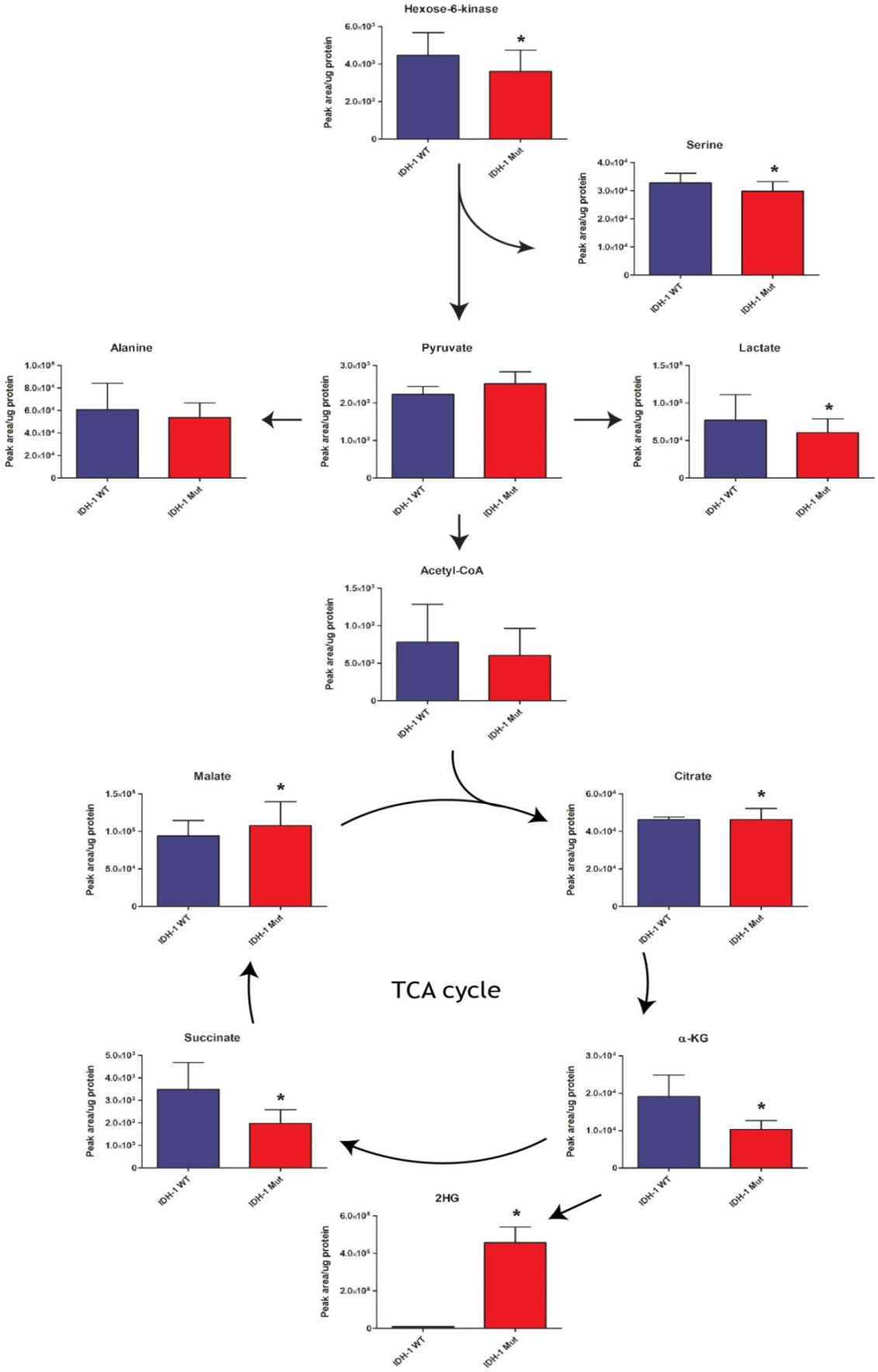

Figure 4-5 The metabolic effect of the IDH1 mutation on glycolysis and the TCA cycle in immortalised human astrocytes

IDH1 R132H overexpressed mutant pool is depicted in red and the IDH1 wild-type pool is depicted in blue. Data are displayed as mean +/- SEM for 3 independent experiments. * represents a p-value ≤ 0.05. Data were analysed using 2-way ANOVA.

Intracellular glutamate was decreased in two of the IDH1 mutant clones, MC3 and MC9, and EV + 2HG, when compared to controls. GSH, a glutamate derived metabolite, was also decreased in all the IDH1 mutant clones as well as EV + 2HG. Conversely, other glutamate derived metabolites were increased. This included GABA and NAA in all the IDH1 mutant clones while in MC3 and MC10, NAAG was also increased. Both NAA and NAAG were increased in EV + 2HG when compared to MOG-GCCM PCL and EV (Figure 4-6).

In the IDH1 mutant astrocytes, there was also a reduction in glutamate compared to wild-type cells. Metabolites derived from glutamate were also affected. When compared to the IDH1 wild-type astrocytes, there was a reduction in GSH and proline but an increase in NAAG in the IDH1 mutant cells. NAAG is produced from NAA as well as glutamate, and NAA, as well as its precursor aspartate, were increased in the IDH1 mutant astrocytes (Figure 4-7). A summary of the steady state metabolic changes caused by the IDH1 mutation or the addition of 2HG is depicted table 4-3.

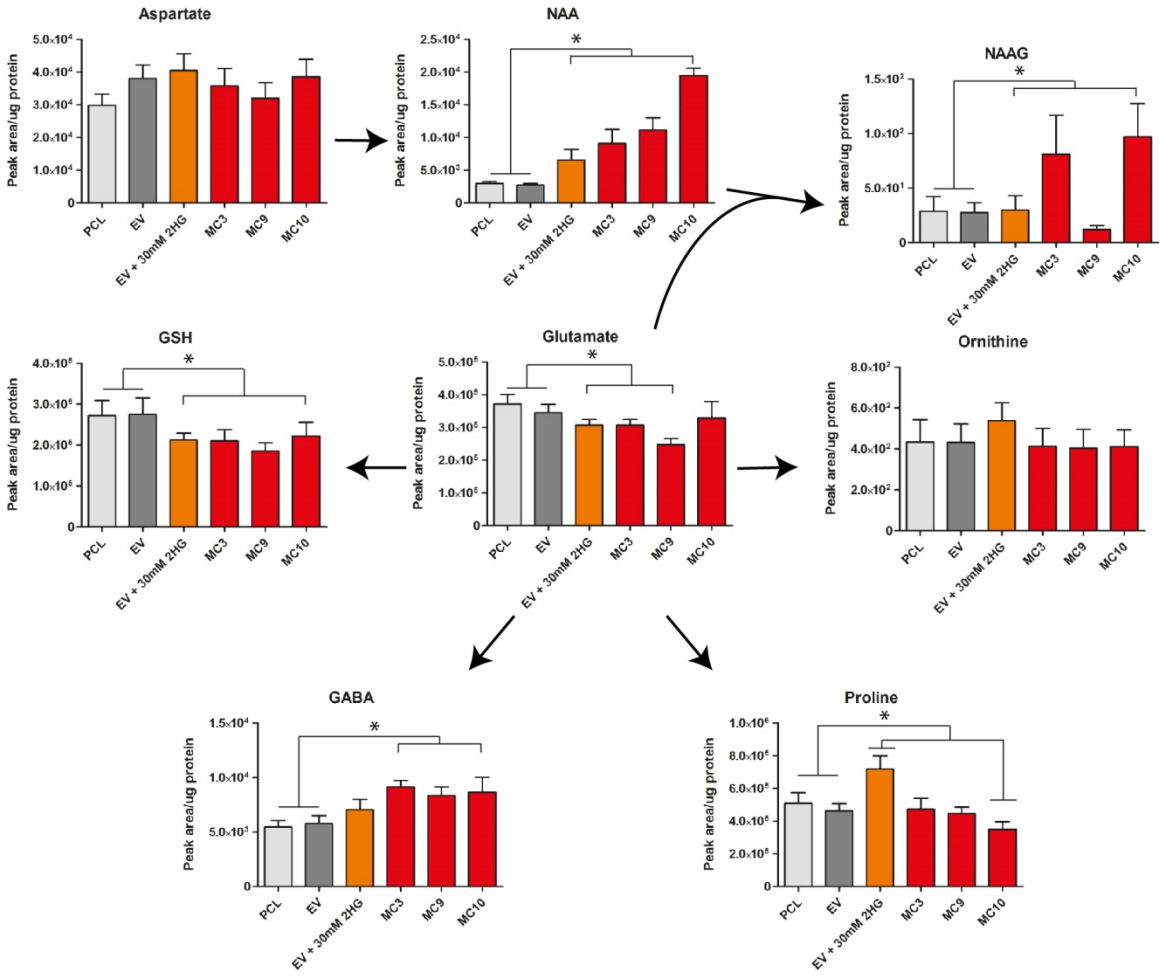

Figure 4-6 The metabolic effect of the IDH1 mutation on glutamate and its derivatives in MOG-CCM clones

The IDH1 R132H overexpressed mutant clones are depicted in red (MC3, MC9, MC10), EV + 2HG is depicted in orange, and the controls in grey (EV and MOG-GCCM PCL). Data depicted as mean +/- SEM for 5 independent experiments. * represents a p-value ≤0.05. Data were analysed using 2-way ANOVA.

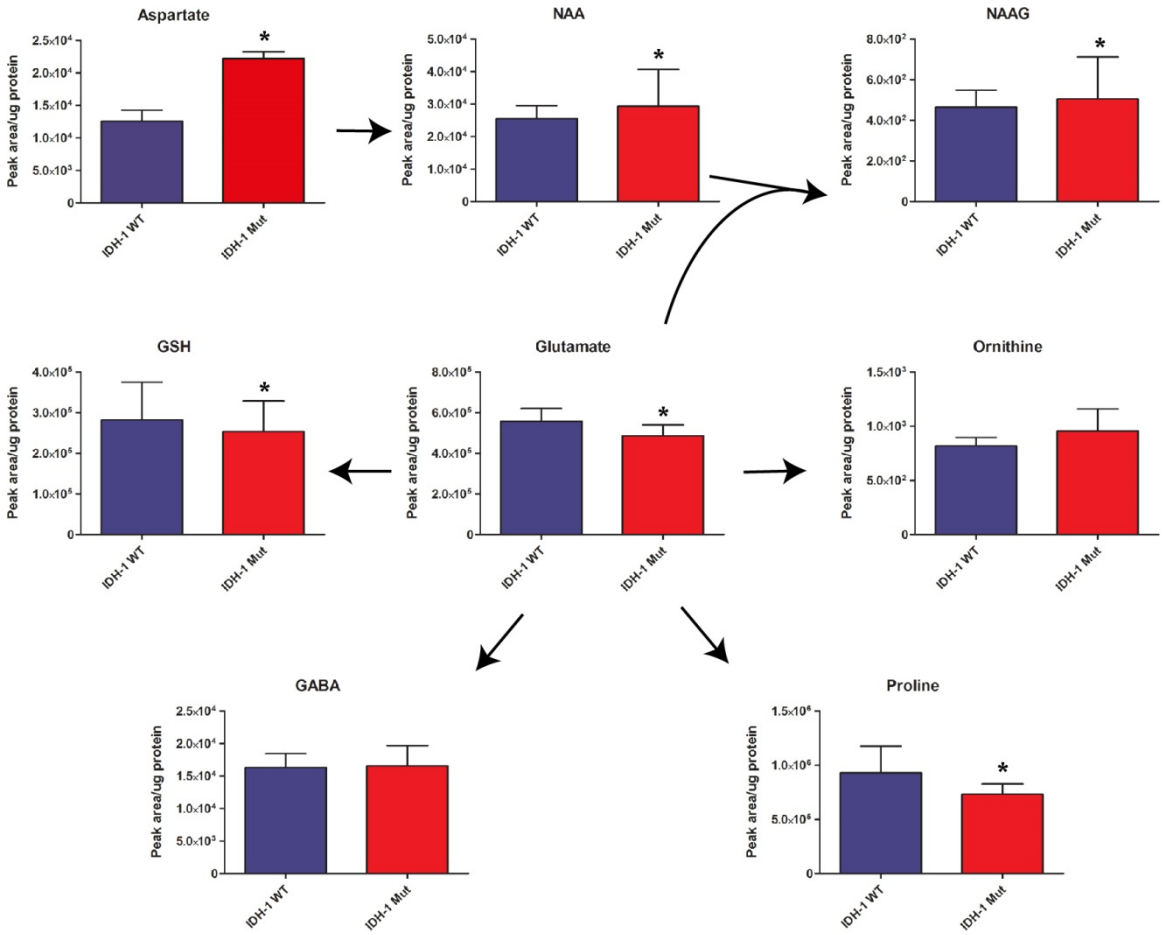

Figure 4-7 The metabolic effect of the IDH1 mutation on glutamate and its derivatives in immortalised human astrocytes
IDH1 R132H overexpressed mutant pool is depicted in red and the IDH1 wild-type pool is depicted in blue. Data are displayed as mean +/- SEM for 3 independent experiments. * represents a p-value ≤ 0.05. Data were analysed using 2-way ANOVA.

Metabolite	MOG-GCCM				Astrocytes
	EV + 2HG	MC3	MC9	MC10	Mutant
2HG	↑	↑	↑	↑	↑
α-KG	↓	↔	↓	↓	↓
citrate	↓	↓	↓	↓	↑
succinate	↔	↔	↓	↓	↓
malate	↓	↓	↓	↓	↑
glutamate	↓	↓	↓	↔	↓
NAA	↑	↑	↑	↑	↑
NAAG	↑	↑	↑	↑	↑
GSH	↓	↓	↓	↓	↓
GABA	↔	↑	↑	↑	↔

Table 4-3 Steady state metabolic changes caused by the IDH1 mutation
Changes in steady state metabolites compared to controls caused by the addition of 2HG (EV+2HG), and overexpression of the IDH1 mutation in MOG-GCCM (MC3,MC9,MC10) and immortalised astrocyte cell lines (Mutant).

To determine if these intracellular metabolic changes were the result of differences in metabolite consumption and secretion, medium was collected from the MOG-GCCM cells and astrocytes and compared to medium incubated without cells.

2HG was secreted from the IDH1 mutant MOG-GCCM clones. The highest level of 2HG secretion in MOG-GCCM cells was from the MC9 clone, which had the highest levels of intracellular 2HG. There was no difference in glucose consumption or lactate secretion between the experimental groups. Glutamine consumption was, however, slightly increased in MC3, MC9 and EV + 2HG compared to the controls. In addition, there was a small increase in glutamate secretion in MC9 and EV + 2HG (Figure 4-8A).

In the immortalised astrocytes, there was secretion of 2HG by the IDH1 mutant cells. There was no other difference in metabolite exchange between the mutant and wild-type cells, except for a small increase in lactate production in the IDH1 mutant astrocytes (Figure 4-8B).

The lack of major changes in exometabolomics indicates that intracellular changes in metabolites associated with glucose and glutamine were not due to exometabolomic differences between the cells. The secretion of 2HG into the medium by the IDH1 mutant cells indicates that 2HG secretion is an adaptive mechanism for removal of this metabolite from the cell.

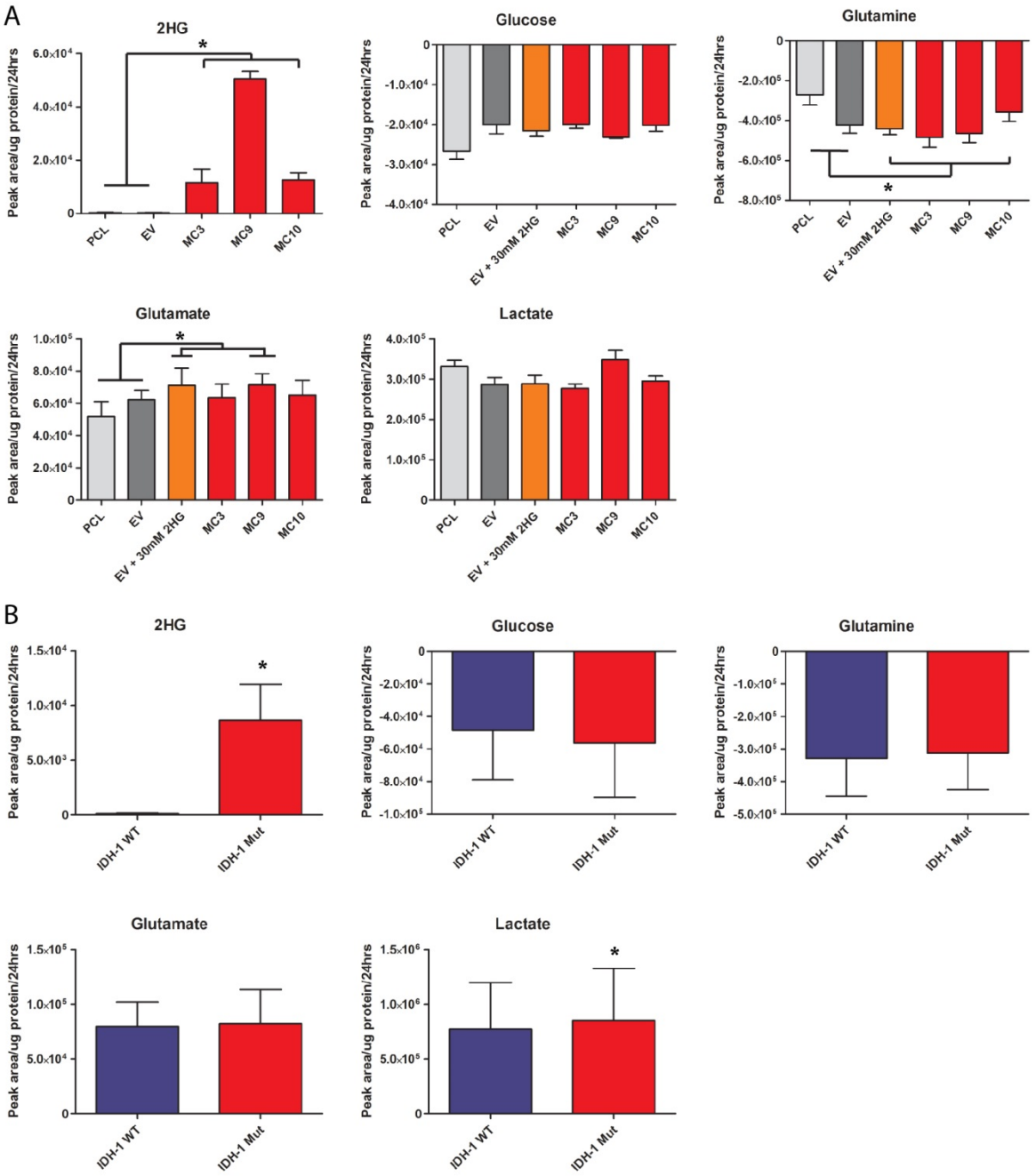

Figure 4-8 Exometabolomics of MOG-GCCM cell and immortalised astrocytes
A. MOG-GCCM and B. immortalised astrocytes. IDH1 mutant clones and astrocytes are represented in red, MOG-GCCM PCL and EV controls are represented in grey, and IDH1 wild-type astrocytes are represented in blue. EV + 2HG is represented in orange. Positive values on the y-axis represent metabolite secretion while negative values represent consumption. Data depicted as mean +/- SEM for 3 independent experiments. * represents a p-value ≤ 0.05. Data were analysed using 2-way ANOVA.

4.2.2.2 IDH1 mutation is associated with changes in metabolic flux in the TCA cycle and glutamine metabolism

To determine changes in metabolic flux through the TCA cycle and glutamate metabolism, MOG-GCCM cells and the astrocytes were incubated in $^{13}C_6$-glucose or $^{13}C_5$-glutamine for 24 hours. Intracellular metabolites were measured using LC-MS and normalised to cellular protein.

In the majority of metabolites there was no difference in contribution from labelled glucose and glutamine in glycolysis and the TCA cycle. However, in MOG-GCCM cells there was decreased labelling contribution from both $^{13}C_6$-glucose and $^{13}C_5$-glutamine in α-KG and succinate, compared to the EV and MOG-GCCM PCL controls (Figure 4-9, Figure 4-11). The IDH1 mutant astrocytes also had a decreased contribution from both $^{13}C_6$-glucose and $^{13}C_5$-glutamine in α-KG compared to the wild type (Figure 4-10, Figure 4-12). In both cell lines, there was increased labelling of 2HG from both $^{13}C_6$-glucose and $^{13}C_5$-glutamine in the IDH1 mutant cells (Figure 4-9,Figure 4-10). This was in contrast to glutamate which was the same in the IDH1 wild-type and mutant cells. The results suggest an increase in flux from α-KG to 2HG, resulting in a decrease in succinate and potentially other metabolites in the TCA cycle.

In both cell lines there was a similar contribution from $^{13}C_5$-glutamine to metabolites derived from glutamate, including GABA. As with the NCH cell lines in the previous chapter, most of the contribution to the carbons in the TCA cycle came from glutamine. In the IDH1 mutant cell lines, most of the 2HG was also derived from glutamine (Figure 4-11, Figure 4-12).

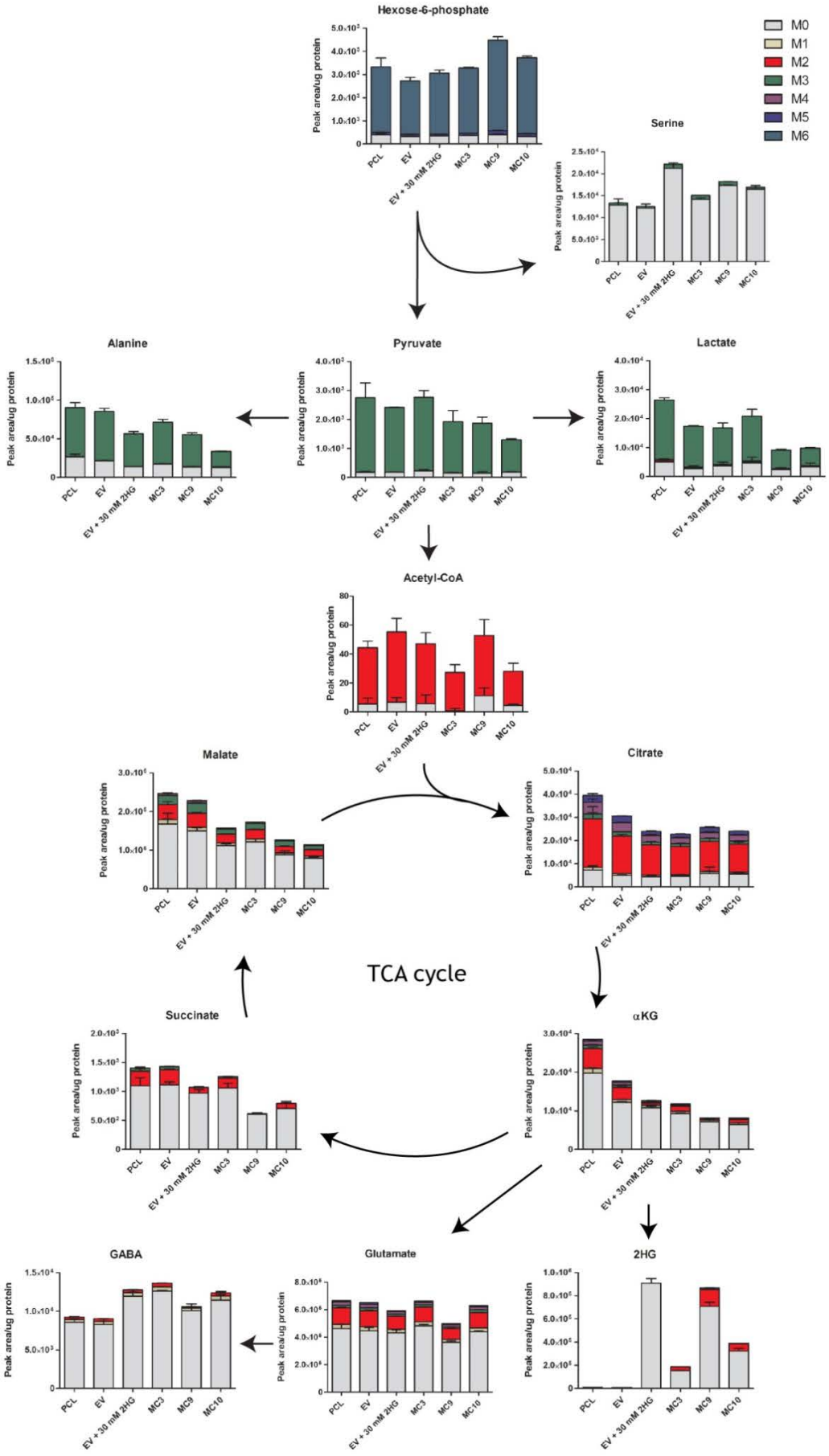

Figure 4-9 Steady state $^{13}C_6$-glucose labelled metabolomics for glycolysis and the TCA cycle in MOG-GCCM cells

The different isotopologues generated for each metabolite are presented as different colours which correspond to the legend in the figure. Single experiment depicting mean +/-SD.

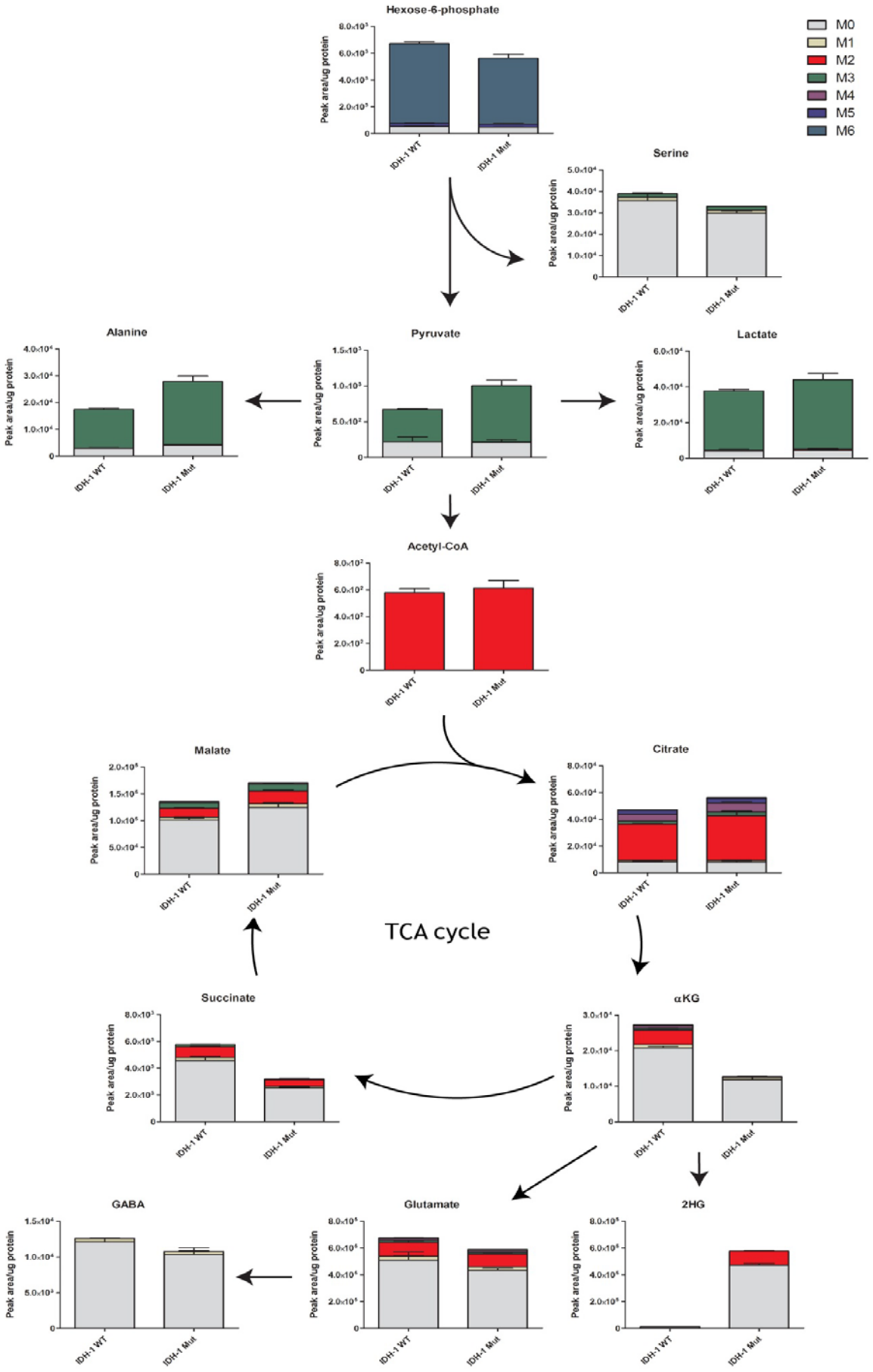

Figure 4-10 Steady state $^{13}C_6$-glucose labelled metabolomics for glycolysis and the TCA cycle in immortalised astrocytes

The different isotopologues generated for each metabolite are presented as different colours which correspond to the legend in the figure. Single experiment depicting mean +/-SD.

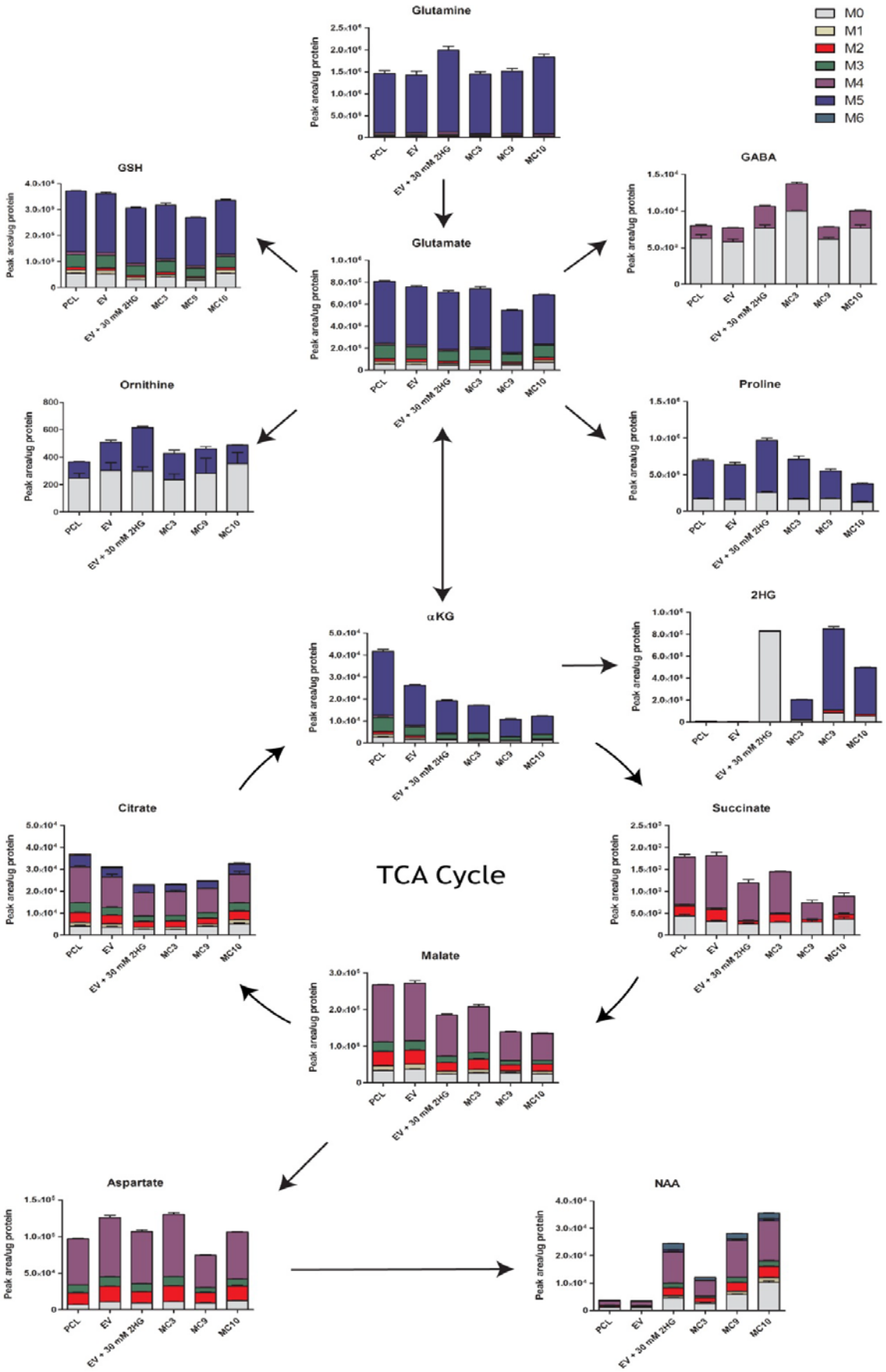

Figure 4-11 Steady state $^{13}C_5$-glutamine labelled metabolomics for glutamate metabolism and the TCA cycle in MOG-GCCM cells

The different isotopologues generated for each metabolite are presented as different colours which correspond to the legend in the figure. Single experiment depicting mean +/-SD.

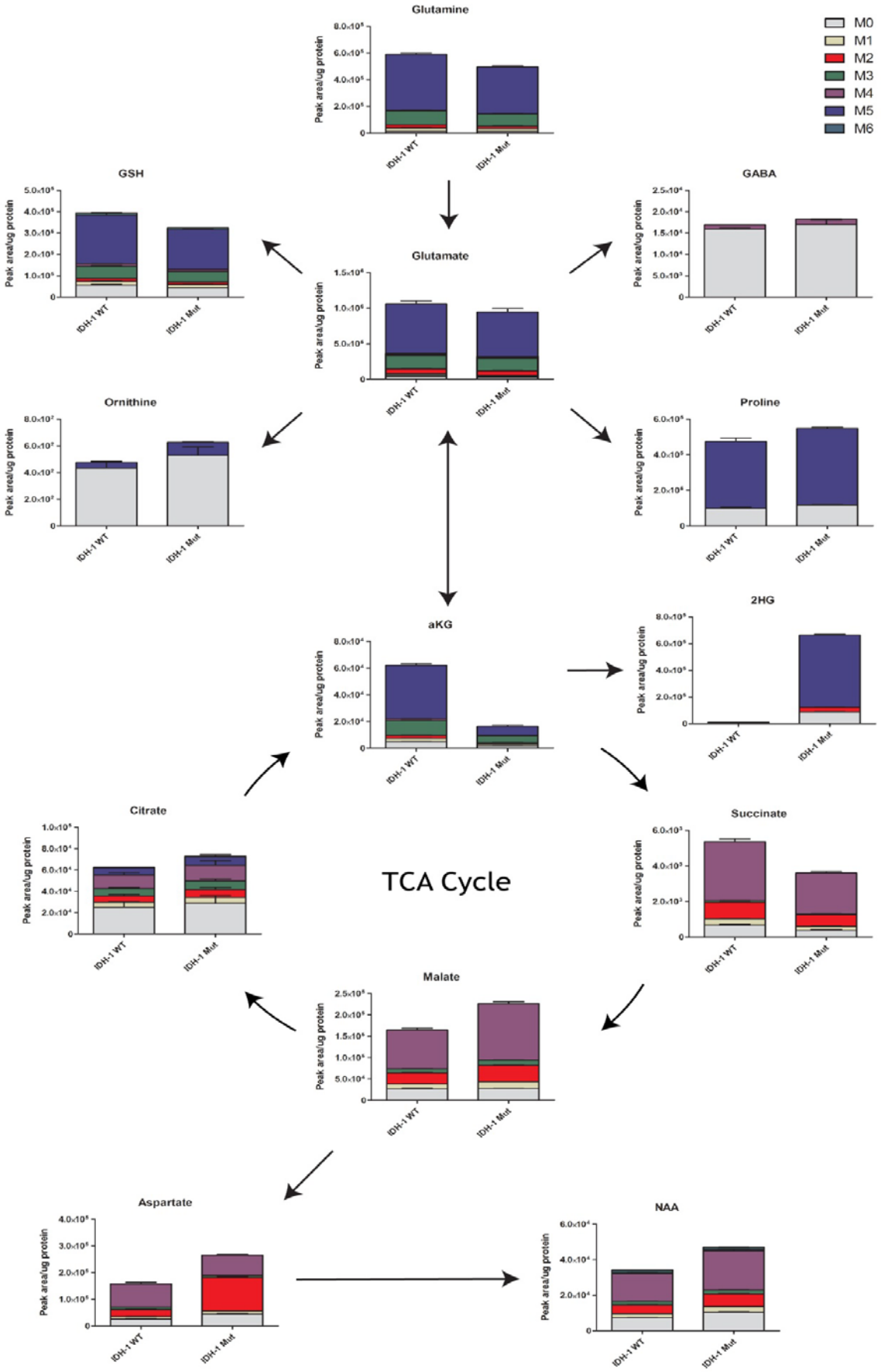

Figure 4-12 Steady state $^{13}C_5$-glutamine labelled metabolomics for glutamate metabolism and the TCA cycle in immortalised astrocytes

The different isotopologues generated for each metabolite are presented as different colours which correspond to the legend in the figure. Single experiment depicting mean +/-SD.

To confirm the effects observed with steady state labelling, dynamic labelling with $^{13}C_6$-glucose or $^{13}C_5$-glutamine was done using several time points for the MOG-GCCM clones and the immortalised astrocytes.

In the MOG-GCCM clones, there was an increased accumulation of labelled H6P, serine, and alanine in the MC9 clone compared to the EV after incubation with $^{13}C_6$-glucose. There were no differences between EV and MC9 for other metabolites related to glycolysis such as lactate and acetyl-CoA, indicating a possible increase in flux from glucose to serine and alanine (Figure 4-13). However, in the immortalised astrocytes, there was no difference in the accumulation of labelled metabolites from $^{13}C_6$-glucose in glycolysis or its associated metabolic pathways (Figure 4-14).

In the TCA cycle, there was decreased accumulation of labelled isotopologues for α-KG, succinate, and malate from both $^{13}C_6$-glucose and $^{13}C_5$-glutamine in the MC9 compared to EV. (Figure 4-13, Figure 4-15). In the astrocytes, there was a decreased accumulation of labelled α-KG and succinate from both $^{13}C_6$-glucose and $^{13}C_5$-glutamine in the IDH1 mutant compared to the IDH1 wild-type cells. There was no difference between the cell lines for the other TCA intermediates. 2HG displayed increased accumulation of labelled isotopologues from both $^{13}C_6$-glucose and $^{13}C_5$-glutamine in the IDH1 mutant astrocytes and MC9 compared to the wild-type controls (Figure 4-13, Figure 4-14, Figure 4-15, Figure 4-16), indicating an increased flux in both cell lines from α-KG to 2HG, caused by the IDH1 mutation, with a consequent reduction in downstream metabolites in the TCA cycle.

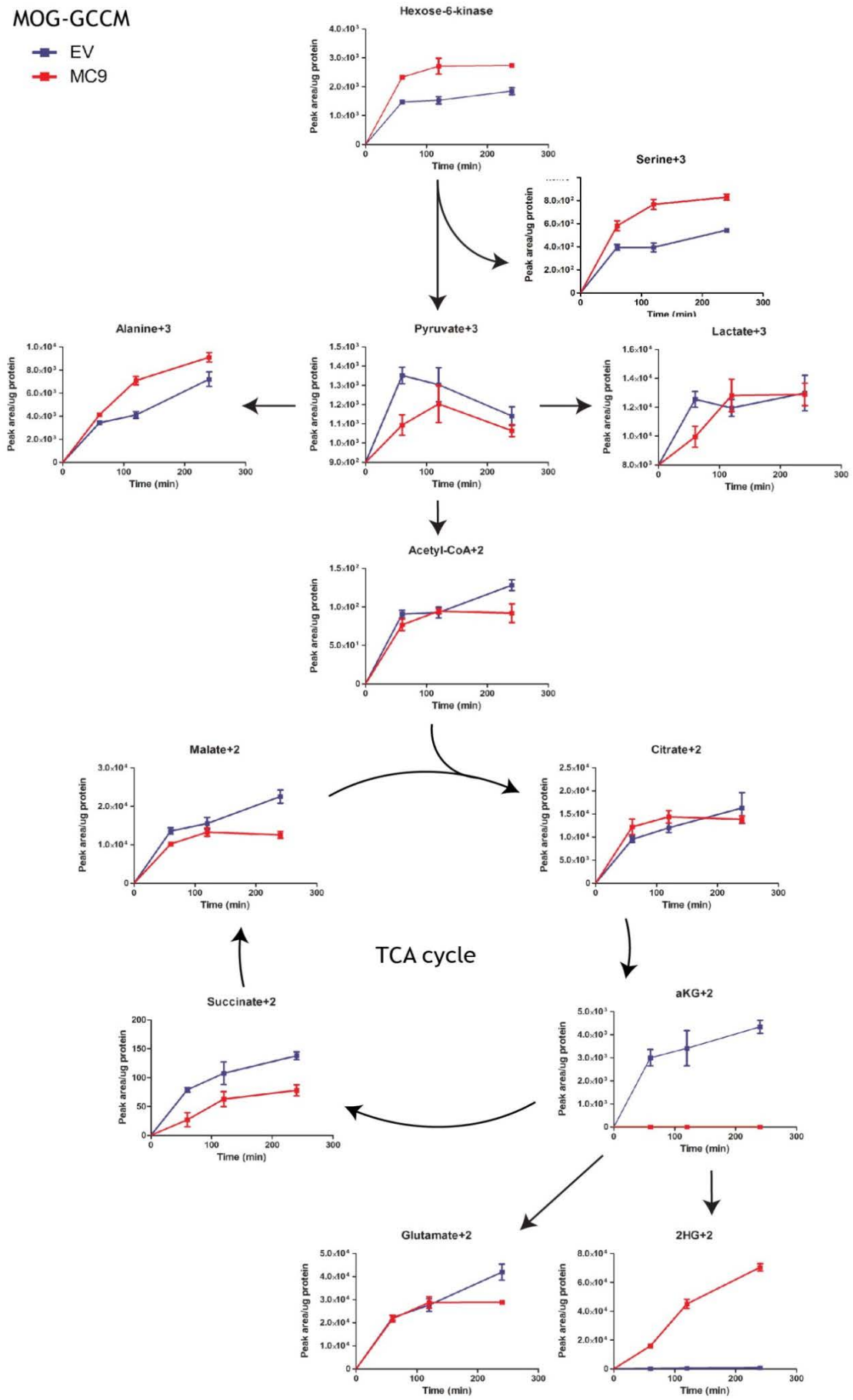

Figure 4-13 Accumulation in MOG-GCCM cells of labelled isotopologues from $^{13}C_6$-glucose in the TCA cycle and glycolysis

The red line represents the IDH1 mutant MC9 clone, while the blue line represents the empty vector (EV) control. Single experiment depicting mean +/-SD.

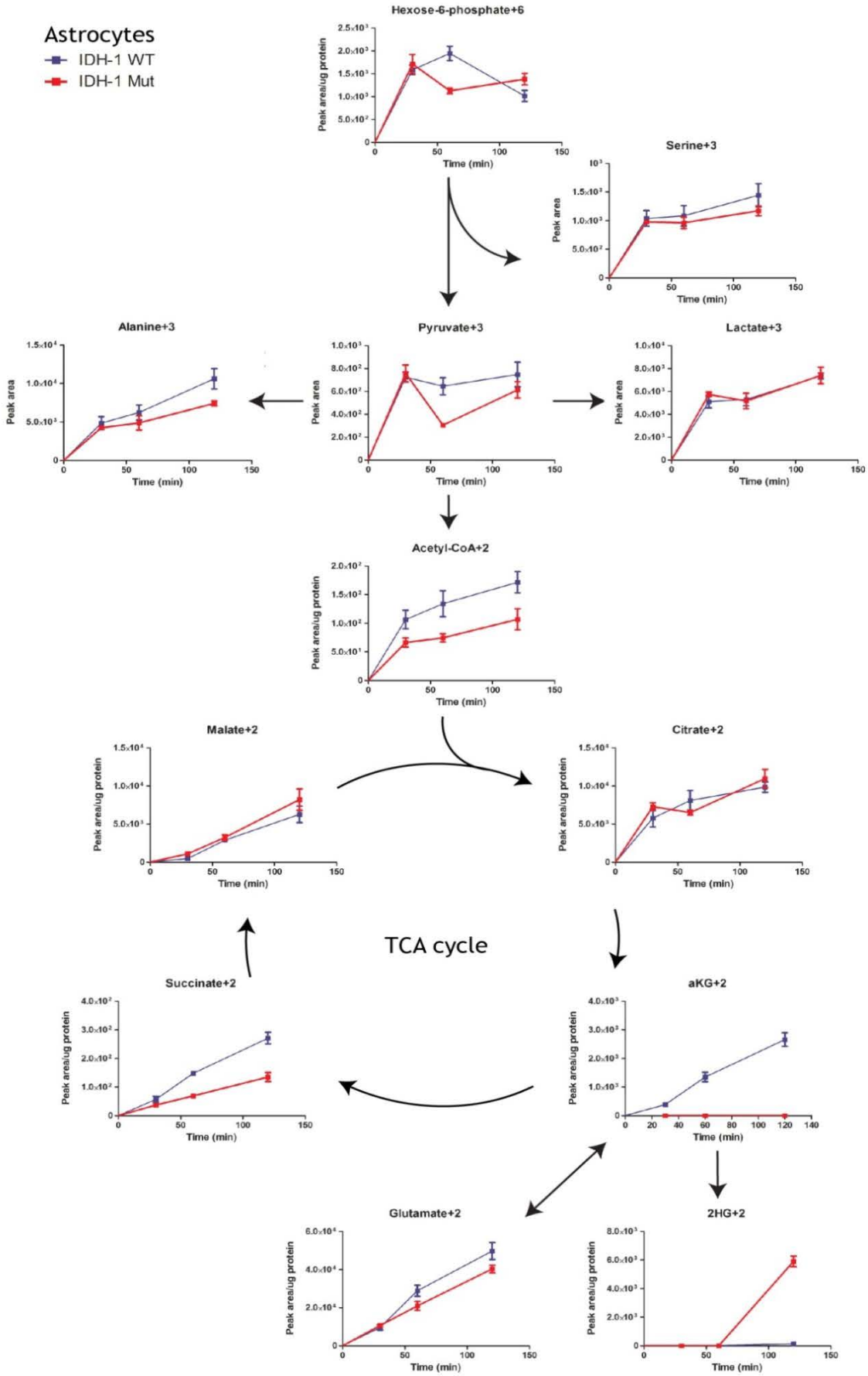

Figure 4-14 Accumulation in astrocytes of labelled isotopologues in the TCA cycle and glycolysis after incubation with $^{13}C_6$-glucose

The red line represents the IDH1 mutant astrocytes, while the blue line represents the IDH1 wild-type controls. Single experiment depicting mean +/-SD.

In the MOG-GCCM, differences between MC9 and EV were also observed in $^{13}C_5$-glutamine metabolism. There was decreased accumulation of the glutamate derivative GSH, in the IDH1 mutant MC9 clone compared to EV. Conversely, there was an increase in accumulation of labelled GABA in the MC9 clone. In addition, there was a reduction in the accumulation of aspartate, but an increase in NAA in the MC9 clone compared to the EV control (Figure 4-15).

In the astrocytes, no differences were observed in the accumulation of labelled glutamate, GSH, proline and ornithine from $^{13}C_5$-glutamine. Conversely, there was increased accumulation of labelled GABA, aspartate, and its derivative NAA in the IDH1 mutant compared to IDH1 wild-type astrocytes (Figure 4-16). This indicates in both cell models a potential increase in flux from glutamate to GABA, and NAA from aspartate and malate. Changes observed in metabolic flux caused by the IDH1 mutation is summarised in table 4-4.

Metabolic flux	MOG-GCCM	Astrocytes
	MC9	Mutant
Glucose to succinate	↓	↓
Glutamine to succinate	↓	↓
Glucose to 2HG	↑	↑
Glutamine to 2HG	↑	↑
Glucose to NAA	↑	↑
Glutamine to NAA	↑	↑
Glucose to GABA	↑	↑
Glutamine to GABA	↑	↑

Table 4-4 Changes in metabolic flux caused by the IDH1 mutation.
Table depicts changes in metabolic flux caused by the IDH1 mutation, from glutamine or glucose, when compared to controls.

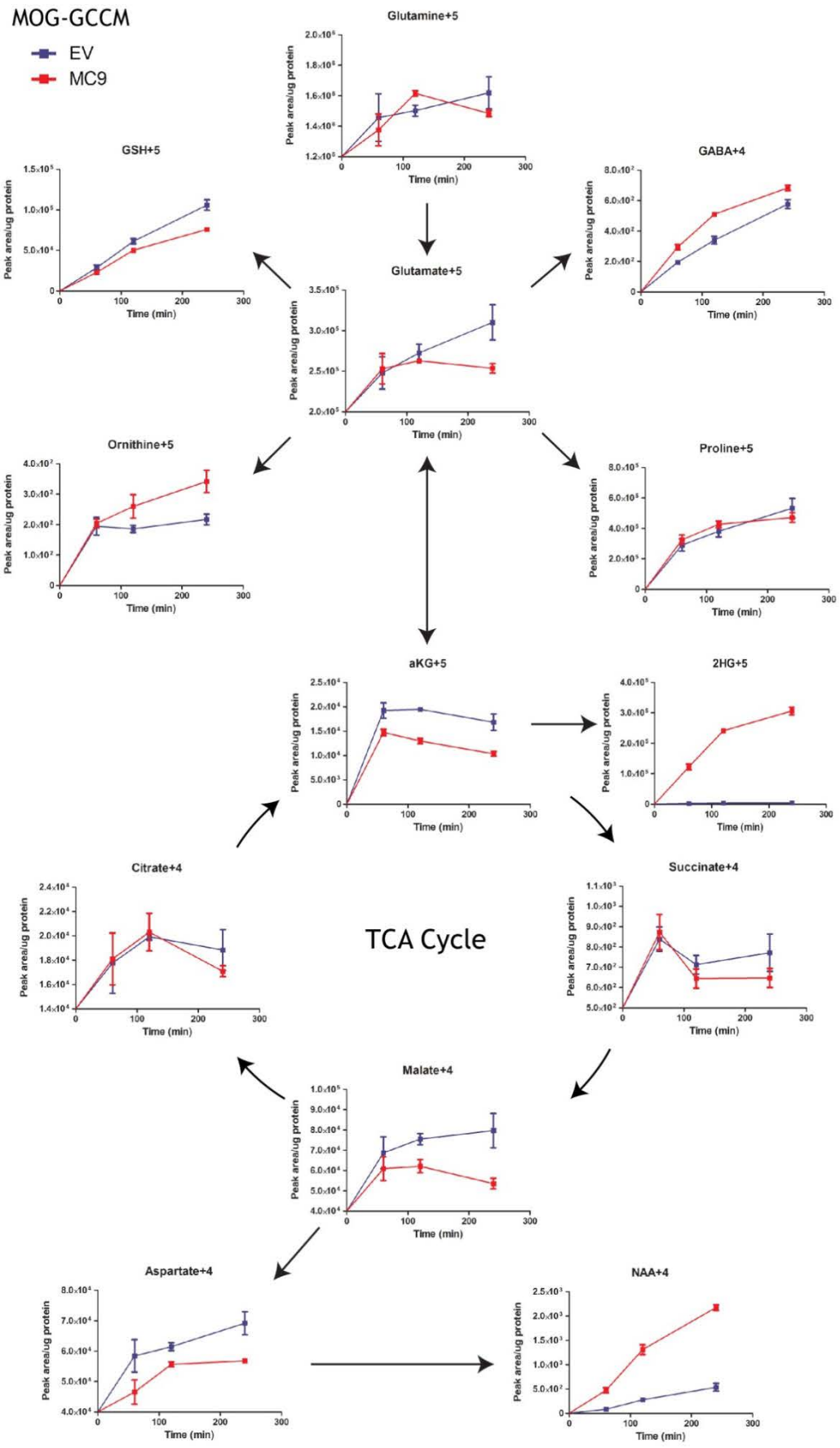

Figure 4-15 Accumulation in MOG-GCCM of labelled isotopologues from $^{13}C_5$-glutamine of metabolites in the TCA cycle and glutamate metabolism

The red line represents the IDH1 mutant MC9 clone, while the blue line represents the empty vector (EV) control. Single experiment depicting mean +/-SD.

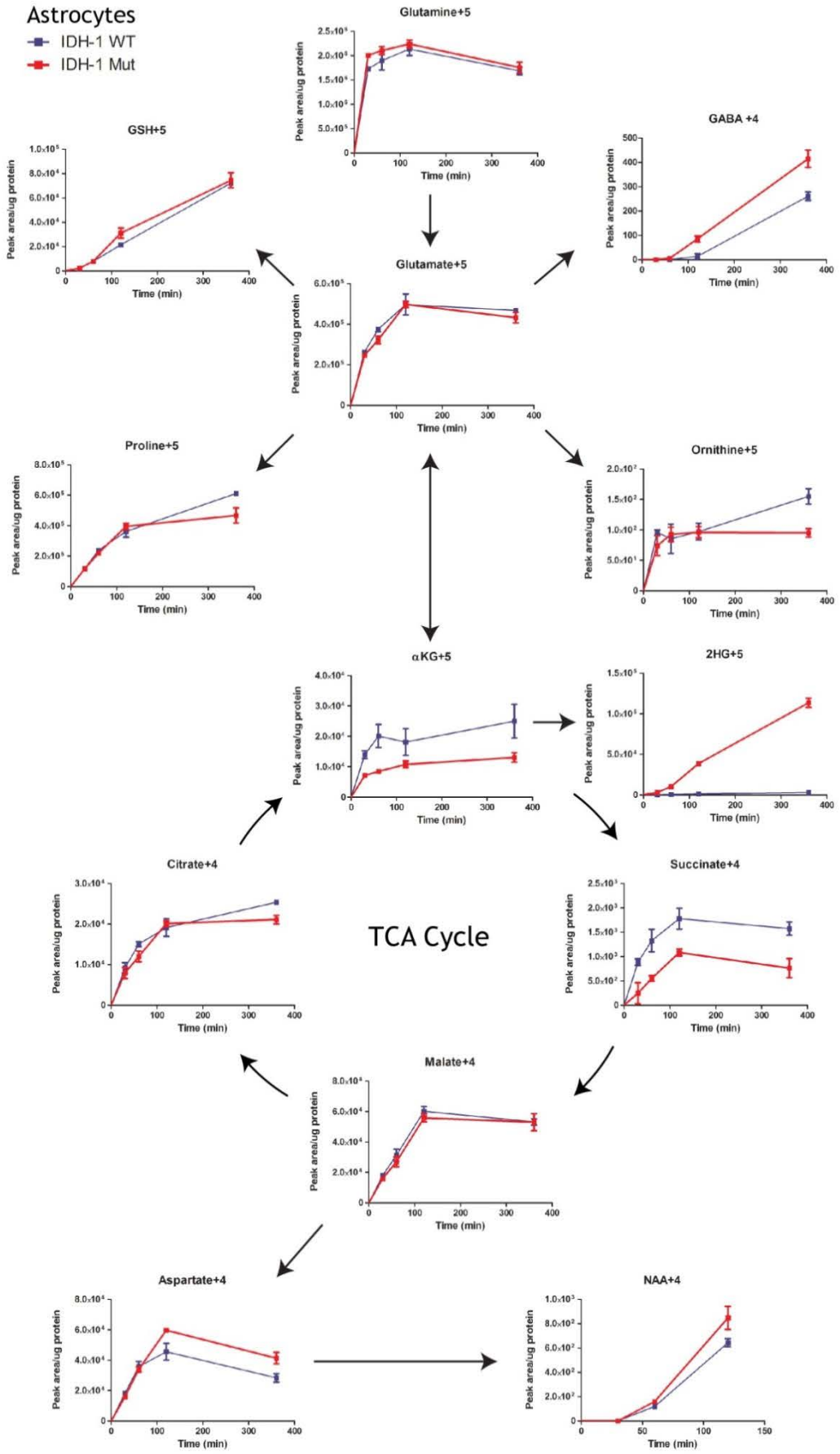

Figure 4-16 Accumulation in astrocytes of labelled isotopologues in the TCA cycle and glutamate metabolism after incubation with $^{13}C_5$-glutamine

The red line represents the IDH1 mutant astrocytes, while the blue line represents the IDH1 wild-type controls. Single experiment depicting mean +/-SD.

4.2.2.3 The IDH1 mutation is associated with an increase in GABA uptake

GABA is also taken up by astrocytes as part of the glutamine-glutamate-GABA cycle. This allows for the metabolism of GABA, after release by neurons, to glutamine. This is then released by astrocytes, taken up by neurons, and recycled back into neurotransmitters. The potential increase in metabolic flux from glutamine and glucose to GABA in the IDH1 mutant cell lines could indicate a potential benefit of GABA metabolism in these cells. This could also indicate a potential role also for exogenous GABA as a carbon source. To further investigate the role of GABA in the IDH1 mutant cell lines, 0.5 mM ^{15}N-GABA was added to the medium of EV, EV + 2HG, and MC9 MOG-GCCM cells and the immortalised astrocytes. The uptake of ^{15}N-GABA was assessed by determining the level of intracellular ^{15}N-GABA over time.

There was an increase in uptake of ^{15}N-GABA in the MC9 clone and EV + 2HG compared to the EV control. This was replicated in the immortalised astrocytes, where the IDH1 mutant cells showed faster accumulation of intracellular ^{15}N-GABA than the wild-type cells. In addition, the accumulation of ^{15}N-GABA was associated with a fall in intracellular serine in both the MOG-GCCM cells and the immortalised astrocytes (Figure 4-17A,B).

To investigate whether the fall in serine observed was due to the stimulation of GABA receptors, medium containing either 0.5 mM ^{15}N-GABA, 0.1 mM Muscimol ($GABA_A$ receptor agonist) or Baclofen ($GABA_B$ receptor agonist) was added to the EV and MC9 clones for 24 hours. $^{13}C_6$-glucose was also added to the medium to evaluate changes in endogenous serine synthesis. The addition of 0.5 mM ^{15}N-GABA resulted in a reduction in unlabelled levels of intracellular serine only, indicating that the reduction in serine was from an exogenous source. This was not observed with the addition of either Muscimol or Baclofen indicating that this effect was not GABA receptor mediated (Figure 4-17C).

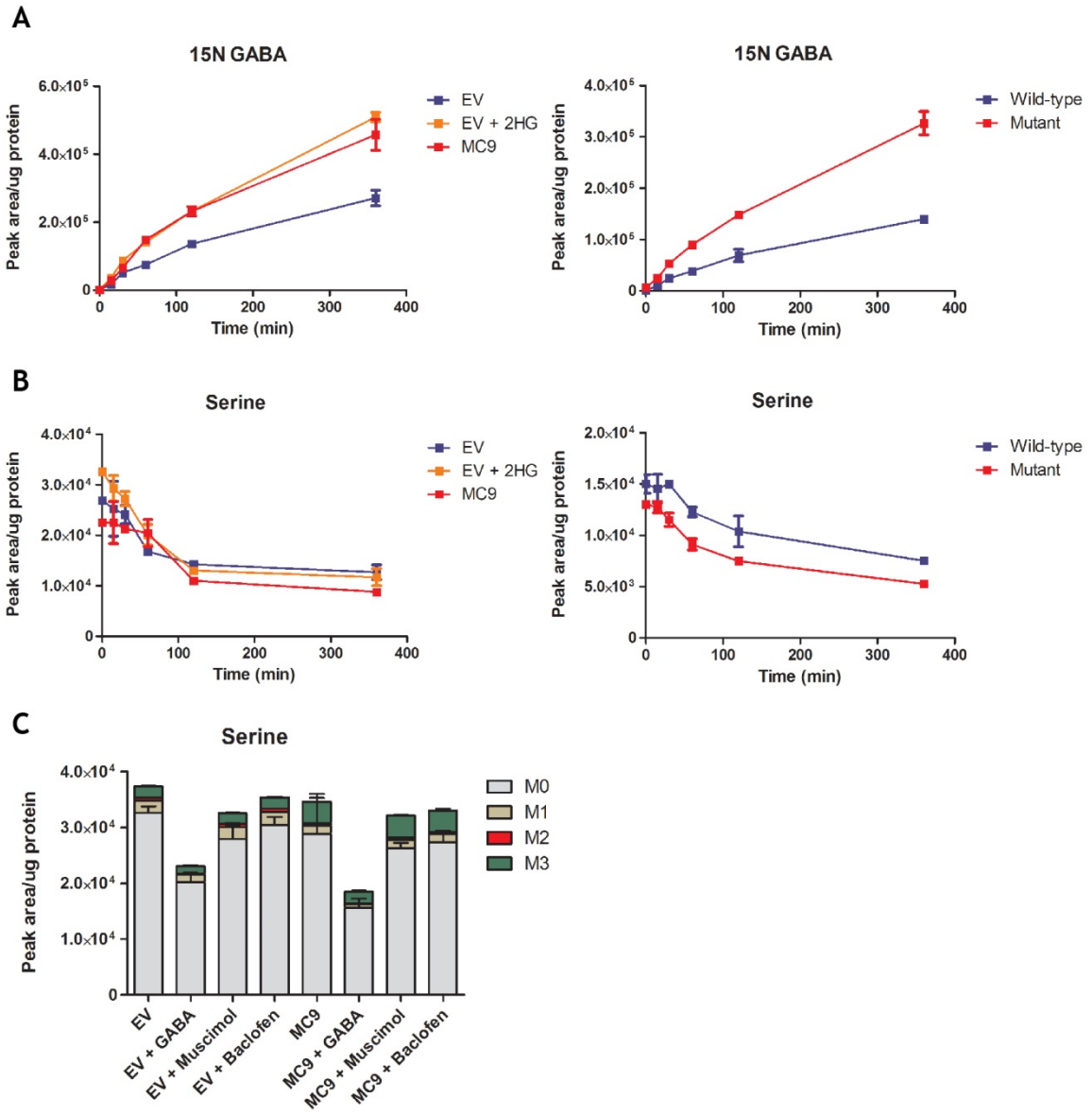

Figure 4-17 GABA and serine uptake in MOG-GCCM and astrocytes
A. Intracellular level of ^{15}N-GABA over time after incubation with DMEM plus 0.5 mM ^{15}N-GABA in both MOG-GCCM cells and immortalised astrocytes. B. Intracellular levels of serine after incubation with DMEM plus 0.5 mM ^{15}N-GABA in both MOG-GCCM cells and immortalised astrocytes. C. Intracellular levels of serine after incubation with $^{13}C_6$-glucose and either 0.5 mM GABA, 0.1 mM Muscimol ($GABA_A$ receptor agonist), or 0.1 mM Baclofen ($GABA_B$ receptor agonist) for 24 hours. In the MOG-GCCM cells, EV is depicted in blue, EV + 2HG depicted in orange, and MC9 depicted in red. The IDH1 wild-type astrocytes are depicted in blue and the IDH1 mutant astrocytes in red. Single experiment depicting mean +/-SD.

4.2.2.4 The IDH1 mutation does not inhibit GABA transaminase

The increased uptake of GABA, coupled with the potential increase in flux from glutamine to GABA in IDH1 mutant cells, led to the hypothesis that GABA may be an important source of succinate in the TCA cycle either exogenously or via the GABA shunt. GABA is metabolised in the mitochondria via GABA transaminase (GABA-T), utilising α-KG as a co-substrate, to SSA with glutamate as a co-product. SSA can then be further metabolised to succinate. In turn, succinate can enter the TCA cycle, bypassing α-KG and its metabolism to 2HG. As 2HG can act as a competitive inhibitor of α-KG, an alternative hypothesis is that the increase in steady state intracellular GABA is due to inhibition of GABA-T. Unfortunately, ^{13}C tracing is not useful in determining whether there is increased flux through the GABA shunt, as the same carbon is lost in the production of succinate via the TCA cycle as it is via the GABA shunt. To confirm increased flux through GABA-T an alternative method was devised, by following the metabolism of exogenous ^{15}N-GABA to ^{15}N-glutamate as an indication of the flux through the GABA-T enzyme.

To determine the flux through this pathway, 0.5 mM ^{15}N-GABA was added to the medium of MOG-GCCM and astrocytes for 24 hours. Unfortunately, ^{15}N-glutamate could not be detected above its natural abundance level in this cell model. Instead, the NCH cell lines cultured as spheroids, as previously described in chapter 3, were used. Two of these cell lines had endogenous IDH1 mutations (NCH551b, NCH612) while two were IDH1 wild-type (NCH 644, NCH421k). After incubation with ^{15}N-GABA, the IDH1 wild-type cell lines had higher levels of intracellular ^{15}N-GABA compared to the IDH1 mutant cell lines. In the IDH1 wild-type cell lines, labelled GABA constituted over 90% of the intracellular GABA. In the IDH1 mutant cell lines, endogenous unlabelled GABA constituted a higher percentage of total GABA compared to the labelled metabolite. This indicated maintenance of endogenous production even in the presence of high levels of exogenous ^{15}N-GABA (Figure 4-18A). However, there was no change in intracellular succinate levels after the addition of ^{15}N-GABA or Vigabatrin (Figure 4-18C). This may be due to the small peak area observed for succinate on LC-MS, making it difficult to identify differences between experimental groups.

Consumption of ^{15}N-GABA varied between the different cell lines (Figure 4-18B). To account for this, a ratio of ^{15}N-glutamate to ^{15}N-GABA was used to determine flux through GABA-T. The ^{15}N-glutamate/^{15}N-GABA ratio was highest in the IDH wild-type NCH412k and the IDH1 mutant NCH612 cell lines. The ^{15}N-glutamate/^{15}N-GABA ratio was decreased with the addition of 200 µM Vigabatrin, a specific GABA transaminase inhibitor, indicating that this enzyme is responsible for the observed effect in these cell lines (Figure 4-18D).

Alanine and aspartate are formed from transamination reactions that utilise glutamate as a source of nitrogen. The ratio of ^{15}N-labelled alanine and aspartate to ^{15}N-GABA was increased in the IDH1 mutant NCH612 compared to the wild-type cell lines. The other IDH1 mutant cell line, NCH551b, had a similar ratio to the wild-type cell lines of ^{15}N-labelled alanine and aspartate to ^{15}N-GABA. This indicates that 2HG does not inhibit GABA-T and in the NCH612 cell line could indicate an increased flux through the GABA transaminase enzyme (Figure 4-18E,F).

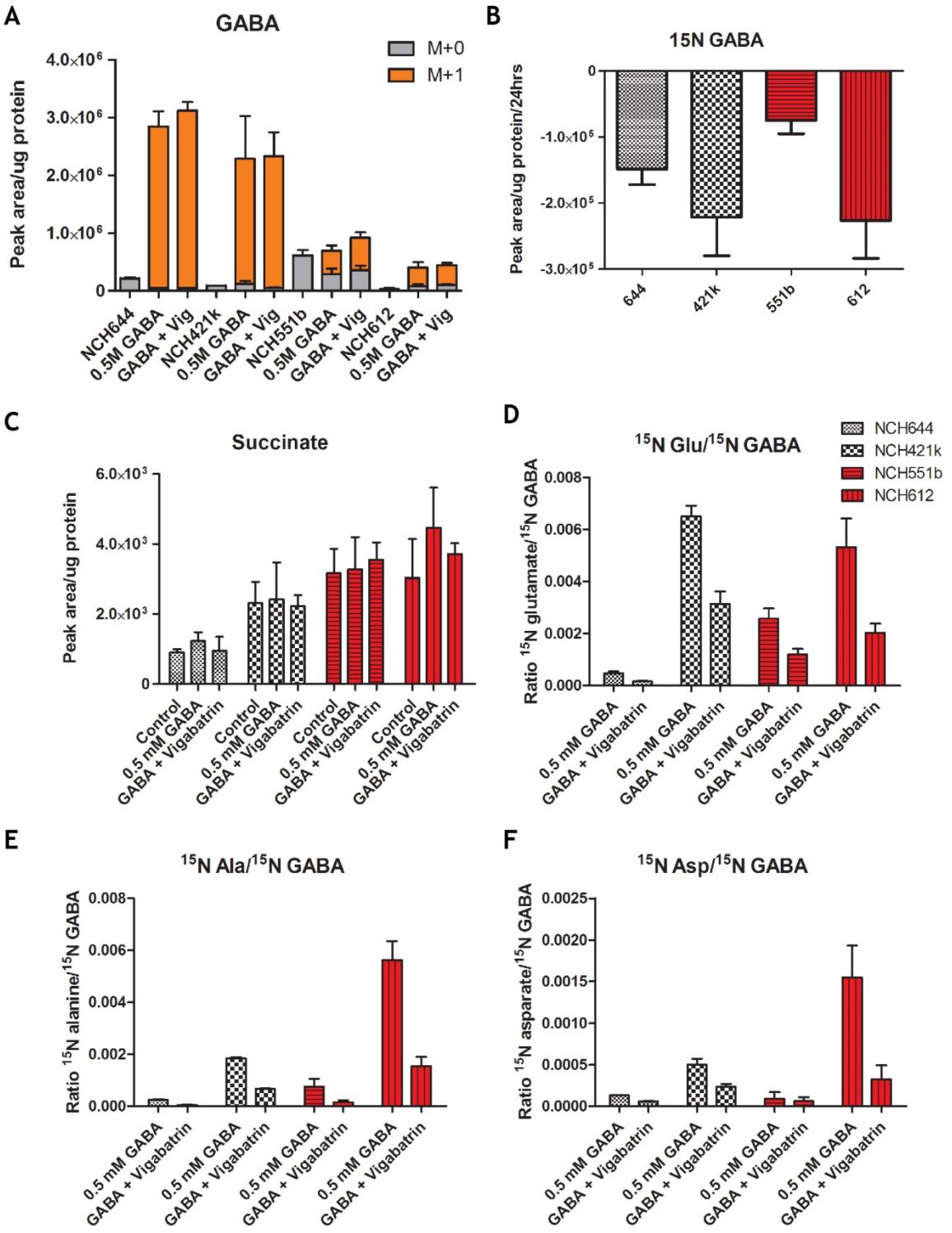

Figure 4-18 GABA metabolism in NCH cell lines

A. Intracellular levels of labelled and unlabelled GABA after incubation with 0.5 mM ^{15}N-GABA for 24 hours. B. Consumption of 15N GABA in NCH cell lines from the same experiment. C Ratio of ^{15}N-glutamate, ^{15}N-alanine, ^{15}N-aspartate, and ^{15}N-serine to ^{15}N-GABA. IDH1 wild-type cell lines depicted in white, IDH1 mutant cell lines depicted in red. Single experiment depicting mean +/-SD.

Glial tumours are typically resistant to radiotherapy and chemotherapy, and will recur after treatment. This often occurs in the irradiated regions of the tumour, and is thought to relate to the presence of a small number of individual cells that have survived treatment and have maintained an ability to reproduce. To replicate this environment, we used clonogenic assays to determine the effect of the IDH1 mutation on cell survival and proliferation in the MOG-GCCM cells and immortalised astrocytes. This involved the plating of several hundred cells and measuring the number of colonies produced over a set period of time. Cells that have managed to divide over 50 times are usually large enough to be counted as a colony. The addition of different agents to the colony assay determines their effect on cell survival as well as the ability to maintain proliferation. In the MOG-GCCM cells, the MOG-GCCM PCL grew numerous colonies of varing sizes. The clones had decreased clonogenicity compared to the MOG-GCCM PCL, with the EV producing the least number of colonies. In the immortalised astrocytes, the IDH1 mutant astrocytes exhibited decreased clonogenicity compared to the IDH1 wild-type cells (Figure 4-19).

The addition of 0.5 mM GABA, 0.2 mM Vigabatrin, or both, to the immortalised astrocytes had no effect on clonogenicity (Figure 4-20). In the MOG-GCCM EV and MC9 clones, the addition of 0.5 mM GABA also had no effect, but the addition of 0.2 mM Vigabatrin decreased the clonogenicity of both. This was reversed by the addition of 0.5 mM GABA in the MC9 clone (Figure 4-21).

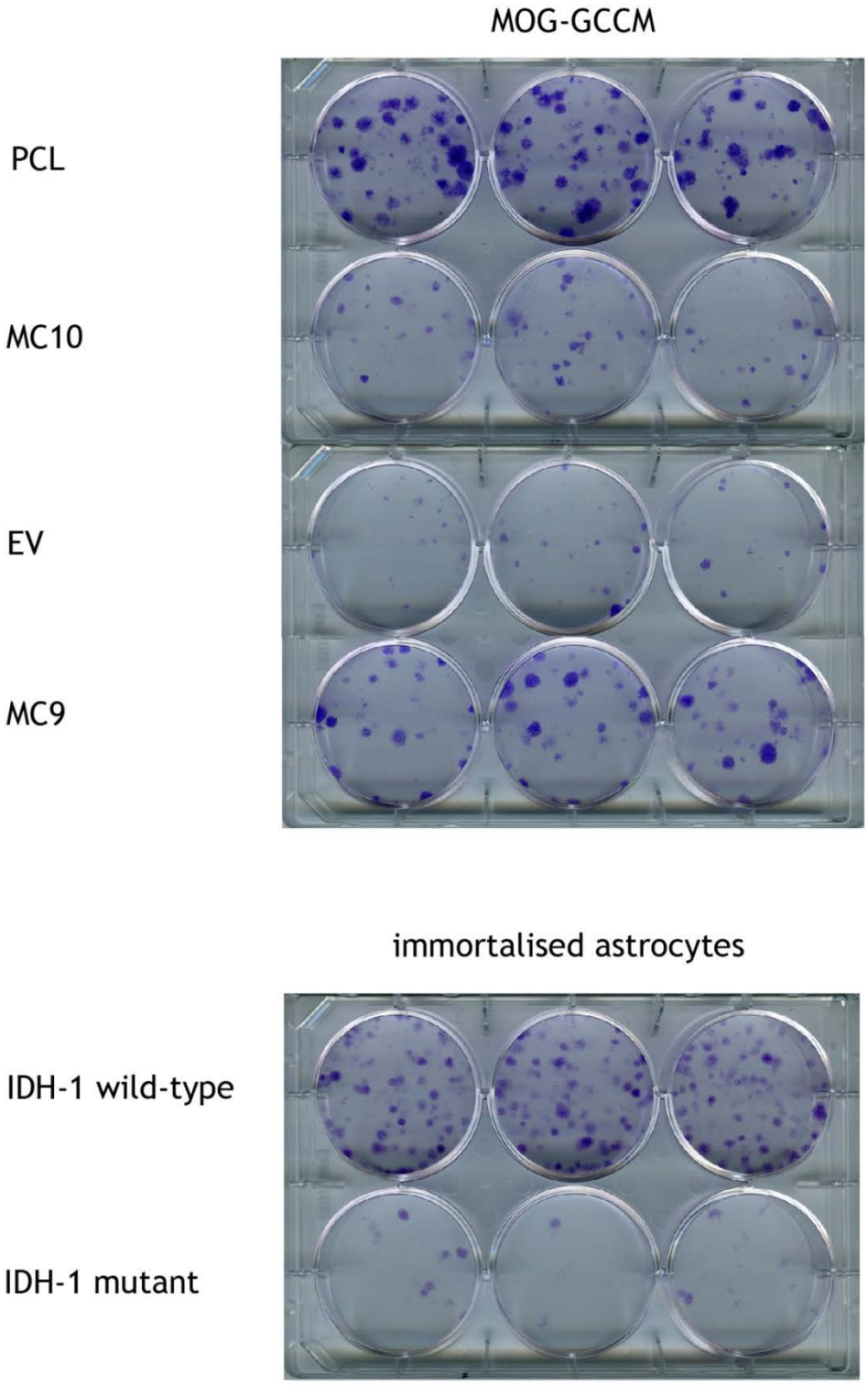

Figure 4-19 Clonogenic assay
A. Clonogenic assay of MOG-GCCM cells. B. Clonogenic assay of IDH1 wild-type and IDH1 mutant astrocytes. Representative of 2 independent experiments.

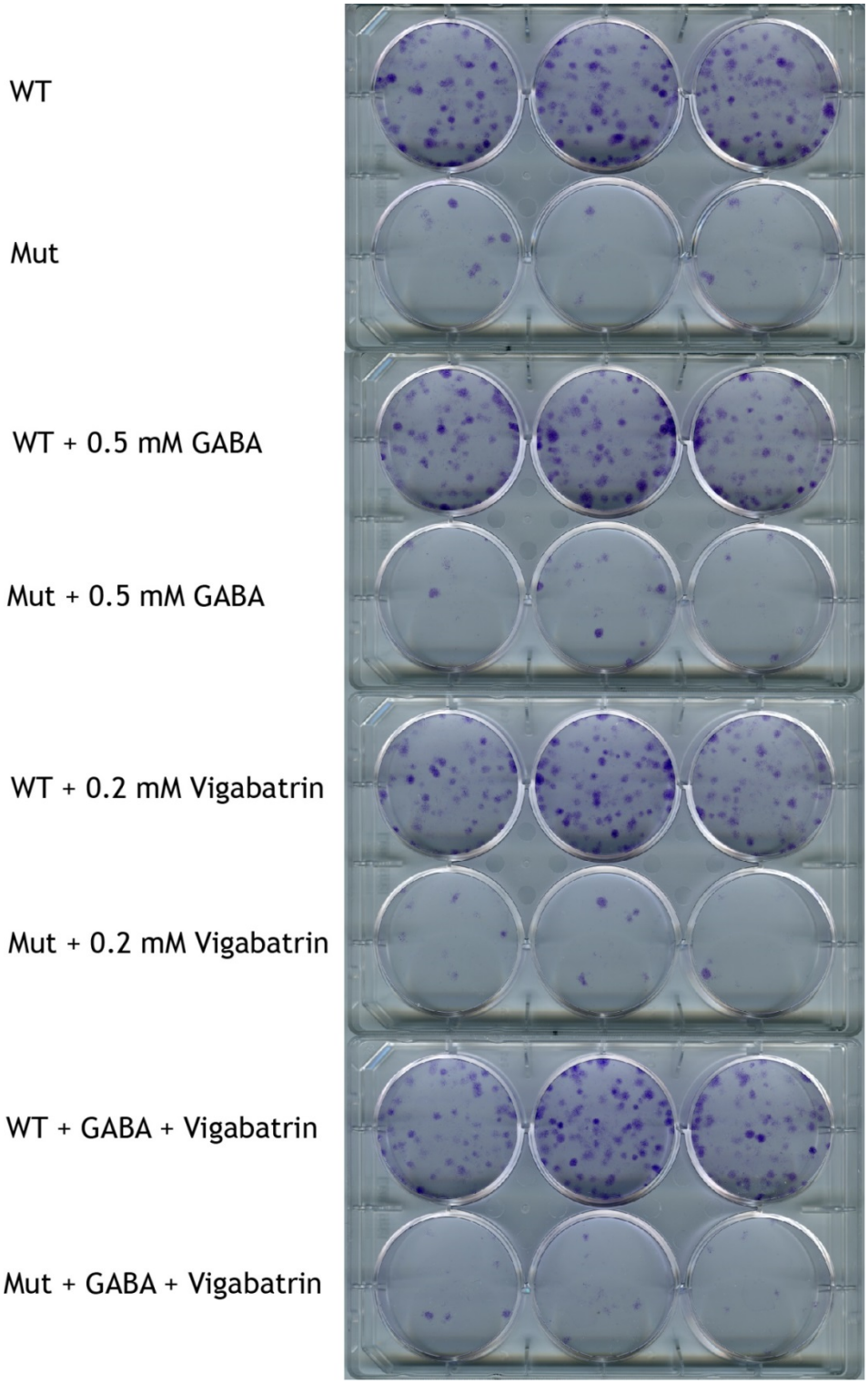

Figure 4-20 Effect on clonogenicity of GABA and Vigabatrin in astrocytes
Clonogenic assay of immortalised astrocytes with overexpressed IDH1 wild-type (WT) or IDH1 mutant (Mut) genes, incubated with 0.5 mM GABA, 0.2 mM Vigabatrin, or both. Representative of 2 independent experiments.

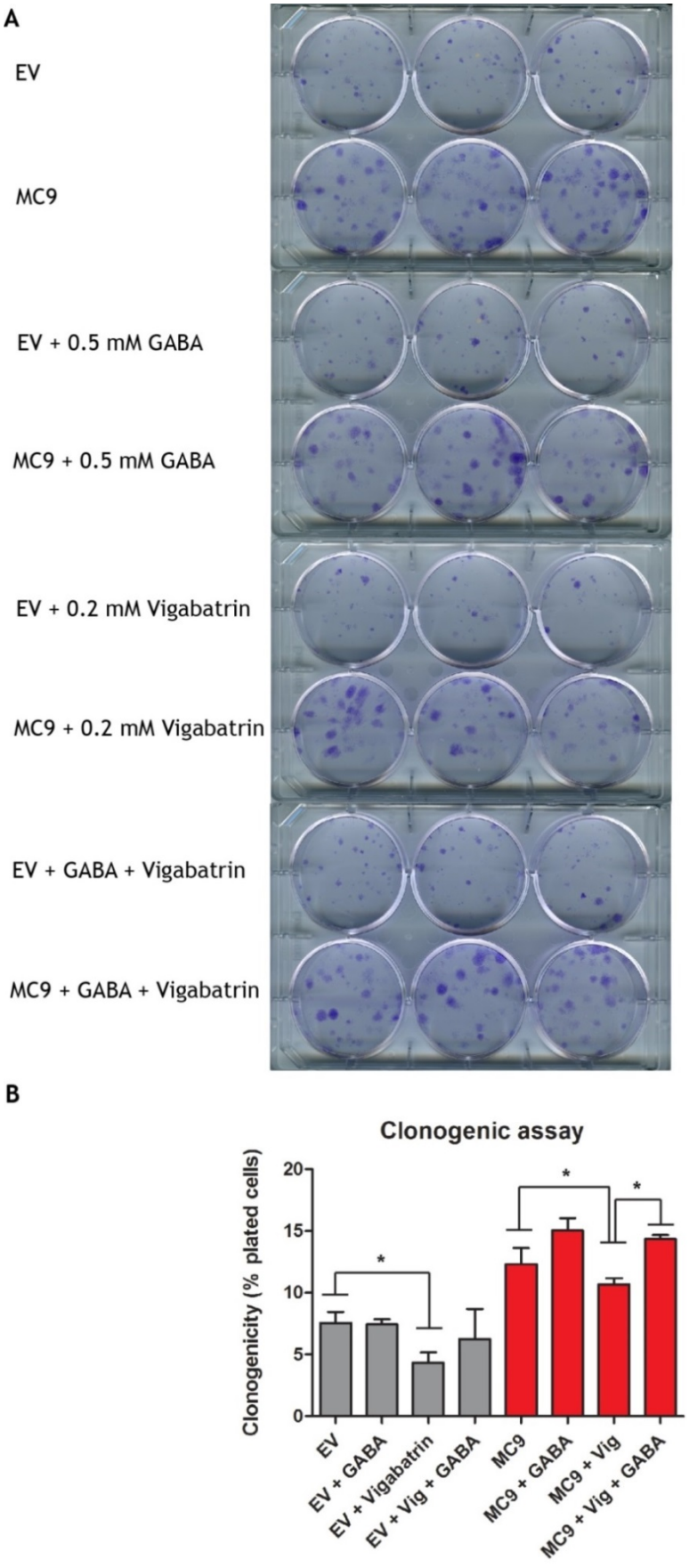

Figure 4-21 Effect on clonogenicity of GABA and Vigabatrin in MOG-GCCM cells
A. Clonogenic assay of MOG-GCCM empty vector (EV) or IDH1 mutant clone (MC9), incubated with 0.5 mM GABA, 0.2 mM Vigabatrin, or both. B. Quantification of 2 independent clonogenic experiments.

4.3 Discussion

To investigate the metabolic changes caused by the IDH1 mutation, a cell model was developed by overexpressing the IDH1 mutation in an anaplastic astrocytoma cell line, MOG-GCCM. The loss of intracellular 2HG from the IDH1 mutant overexpressed pools, and the increase in cell proliferation, led to the hypothesis that 2HG was responsible for decreased cell growth. As 2HG is not cell permeable, this hypothesis was tested and confirmed by the addition of exogenous cell permeable 2HG-lactone to MOG-GCCM and LN18, a glioblastoma cell line. In both cases, a dose dependent decrease in cell proliferation could be observed with increasing concentrations of exogenous 2HG-lactone. MOG-GCCM clones were developed to decrease the possibility of intracellular 2HG loss over time. The clones with the highest levels of intracellular 2HG were also associated with longer doubling times. The EV control was compared to the EV + 2HG and MC9 clone using Ingenuity Pathway Analysis. There were differences in pathways associated with cell proliferation and growth, and the cell cycle, consistent with changes in cell growth. This may explain the clinical pattern of the disease with an increase in overall survival associated with the IDH1 mutation [95].

Gene expression data using Affymetrix microarray showed similar expression profiles between the two controls, indicating that the EV was a good representation of the original MOG-GCCM PCL. The biggest differences in gene expression were seen between the MC9 clone and the controls. The EV + 2HG had similar intracellular levels of 2HG as the MC9 clone, but had a similar gene expression profile as MC3, the clone with lowest intracellular levels of 2HG. This indicates that factors other than intracellular 2HG level, such as α-KG level, may have contributed to the differences in gene expression profile observed in this experiment. Overexpression of the IDH1 mutation has been shown to cause epigenetic changes by increasing histone and DNA methylation over time [245]. It may be that the genetic variability observed is also in part a result of the increased number of passages of the IDH1 mutant clones compared to the EV + 2HG.

The IDH1 mutation resulted in changes in steady state levels of TCA cycle intermediates. There was a reduction in intracellular malate and citrate for all

IDH1 mutant clones and EV + 2HG. In addition, the two IDH1 mutant clones with the highest levels of intracellular 2HG, and EV + 2HG, had decreased levels of α-KG and succinate. In the immortalised astrocytes there was a reduction in intracellular α-KG and succinate in the IDH1 mutant compared to the IDH1 wild-type cells. Steady state and dynamic labelling from ^{13}C-glucose and ^{13}C-glutamine confirmed an increased flux from α-KG to 2HG in both cell models, resulting in a reduction in other TCA intermediates. However, the reduction in TCA metabolites does not seem to be solely due to the activity of the IDH1 mutant enzyme. The addition of 2HG to EV caused a reduction in α-KG, though not to the same extent as the MC9 and MC10 clones. This raises the possibility that other metabolic processes are affected by 2HG which results in reduced steady state levels of TCA metabolites. Conversely, the MOG-GCCM cell model showed a possible mechanism for increasing α-KG levels in the cell. Dynamic labelling of MC9 using ^{13}C-glucose showed an increase in accumulation of alanine and serine compared to the EV. Synthesis of these metabolites requires a transamination step, which utilises glutamate to produce α-KG as a co-substrate. The increased flux through these pathways may be a mechanism whereby the IDH1 mutant cell can replace the α-KG lost to 2HG production.

In both the MOG-GCCM and astrocyte cell models, the IDH1 mutant cells had lower intracellular levels of glutamate, when compared to controls. GSH, a glutamate derived metabolite, was also decreased. Steady state and dynamic labelling indicated that this decrease in GSH is due to the decreased intracellular levels of glutamate. GSH is the most common antioxidant in the cell, and decreased levels of GSH are associated with increased levels of reactive oxygen species (ROS). Increases in ROS are associated with cell cycle arrest and decreased cell proliferation [233]. Decreased GSH has been shown to inhibit cell proliferation in an IDH1 overexpressed GBM cell line because of increased ROS, and may provide an explanation for the decreased cell proliferation caused by 2HG in MOG-GCCM [232].

Conversely, the glutamate derived metabolite NAAG, and its precursor NAA, were increased. The same metabolic changes were also observed in EV + 2HG. Dynamic labelling suggested that the increase in NAA was due to an increased flux from malate and aspartate. NAA, after glutamate, is the most abundant

amino acid derivative in the brain and is synthesised mostly by neurons. It is also the most abundant source of acetate in the brain and is required for the production of NAAG. Both NAA and NAAG can act as neurotransmitters activating metabotropic glutamate receptors. Interestingly, NAAG is metabolised almost exclusively by astrocytes to NAA, which in turn is metabolised back to glutamine by oligodendrocytes and released into the extracellular space for neuronal uptake [69]. These two metabolites may have a role in tumorigenesis as they have been shown to replicate a feature of IDH1 mutant cells, namely the prevention of cellular differentiation, and may help to promote cell growth [60, 261].

GABA, another glutamate derived neurotransmitter, was also increased in the IDH1 mutant clones in the MOG-GCCM model. Dynamic labelling from $^{13}C_5$-glutamine in the IDH1 mutant MOG-GCCM and immortalised astrocytes indicated a possible increased flux from glutamate. IDH1 mutant cells, and EV + 2HG, also showed increased uptake of ^{15}N-GABA when compared to wild-type controls. Interestingly, there was also an associated fall in intracellular serine levels, and decreased serine uptake from the medium, which was not a GABA receptor associated effect. However, these experiments were only done once, though in two different models, so would need to be repeated to confirm these observations. GABA has been implicated in mitochondrial nucleoside salvage, which may decrease the need for nucleotide synthesis by serine via one-carbon metabolism [280]. This may account for the reduction in serine uptake causing a fall in intracellular serine as GABA levels increase.

The increased uptake of GABA, coupled with the increase in flux from glutamine to GABA in IDH1 mutant cells, led to the hypothesis that GABA may be an important source of succinate in the TCA cycle. GABA-T is an α-KG dependent enzyme, so the increase in GABA could be due to inhibition of this enzyme. The metabolism of ^{15}N-GABA to ^{15}N-glutamate in the NCH cell lines was used as a measure of flux through GABA-T. There was no inhibition of GABA-T by 2HG but potentially an increased flux from GABA to succinate in one of the IDH1 mutant cell lines. This may provide a mechanism for the cell to bypass α-KG in the TCA cycle. Though GABA-T utilises α-KG as a co-substrate to produce SSA and glutamate, the glutamate produced could be utilised in the production of alanine, aspartate and serine producing α-KG, potentially preventing an overall

net loss of α-KG in the cell. The increased uptake of GABA in the MOG-GCCM and immortalised astrocytes raises the possibility of GABA as an alternative carbon source for the TCA cycle which could maintain production of TCA intermediates such as malate and citrate.

Unfortunately, there was no benefit to the addition of GABA to colony formation in the IDH1 mutant astrocytes and MOG-GCCM compared to the IDH1 wild-type cells. However, in the MOG-GCCM cells there was a reduction in colony formation after the addition of Vigabatrin in the IDH1 wild-type EV and IDH mutant MC9 clones. This was rescued with the addition of GABA in the MC9 cells. It may indicate that in this cell line, GABA transaminase is important for cell proliferation and survival, but is not specific to the IDH1 mutation. Alternatively it may be an off target toxic effect of the drug in this cell line. However, investigating the effect on cell proliferation in NCH cell lines would give a better indication of the importance of the GABA shunt, as the activity of GABA transaminase in the cell lines was measurable unlike the MOG-GCCM and astrocyte cell models.

There were limitations of the MOG-GCCM and astrocytoma cell models used, principally that they were developed using overexpression of an IDH1 mutant vector. This does not accurately reflect the physiological expression of the protein in tumour cells, where there is one IDH1 mutant allele and one IDH1 wild-type allele. The majority of the IDH1 mutant protein forms a complex with the IDH1 wild-type protein and this may not have been the case in the cell models depending on the expression levels of wild-type and mutant proteins [281]. This in turn may have effects on the production of metabolites such as α-KG and 2HG, altering the potential effects on α-KG dependent dioxygenases and gene expression. An example of this is that the IDH1 mutation is associated with downregulation of branch chain aminotransferase (BCAT) in vivo [273], but there was no observed change in leucine, isoleucine and valine in these cell models (data not shown) which would be expected if there was a loss of this enzyme. As this could potentially affect glutamate and α-KG synthesis, it may have had an indirect effect on the glutamine-glutamate-GABA cycle. However, many other metabolic changes were consistent in these cell models with the IDH1 mutant endogenous cell lines, when compared to controls, indicating that they were able to replicate many of the changes present in endogenous IDH1 mutant cell

lines. The latter cell lines were difficult to grow in culture so the MOG-GCCM and astrocyte cell lines were reasonable alternatives to investigate the effects of the IDH1 mutation on metabolomics and gene expression.

There were also limitations to the metabolic analysis of the cell lines. Intracellular compartments exist within the cell in the form of organelles such as mitochondria and peroxisomes, and can result in metabolic processes which are separate from the rest of the cell. Most metabolites are present in more than one compartment, and the concentrations of these metabolites may change separately in one compartment compared to another under different cellular stresses. Unfortunately, with current techniques only the average metabolite level and labelling pattern can be measured within the cell [282]. This raises the possibility that the changes observed in α-KG and GABA may only occur in one compartment. In the case of α-KG this could have implications on enzymes which are restricted to certain compartments such as TET and histone demethylases. However, as these metabolites can be transferred between compartments it seems likely that a change in one compartment is reflected in another [24, 51]. This could potentially be investigated further in the future, if a method to extract metabolites successfully from organelles is developed.

In summary, the IDH1 mutation results in an increased flux from α-KG to 2HG, and potentially from glutamate to GABA and aspartate to NAA. This increase in GABA is not the result of inhibition of GABA transaminase by 2HG, but potentially due to increased flux through the GABA shunt. The most striking metabolic change, however, is the increase in the 2HG/ α-KG ratio in the IDH1 mutant cells. This could potentially have an effect on α-KG-dependent dioxygeneses, which have a role in DNA and histone methylation.

Chapter 5 Epigenetic changes associated with the IDH1 mutation

5.1 Introduction

The epigenome consists of a range of alterations that change gene expression without affecting the DNA sequence. Several components of the chromatin structure can be modulated to alter gene expression. This includes DNA and histones, around which the DNA is folded to form a nucleosome. Histones are comprised of eight subunits; two each of H2A, H2B, H3 and H4. Modulation of gene expression can occur epigenetically by chemical modification at the DNA nucleotide level or on histone tails. DNA modification occurs through methylation of cytosine residues, while histone tails can undergo several modification processes which include methylation and acetylation. DNA methylation results in gene suppression, while histone tail modification can result in either gene activation or repression depending on the site and chemical modification. These processes are important in healthy tissues to maintain cellular differentiation and adapt to environmental change.

In the previous chapter, the IDH1 mutation was associated with an increase in intracellular 2HG and a fall in intracellular α-KG. 2HG has been shown to act as a competitive inhibitor of α-KG dependent dioxygenases. These include enzymes involved in modulation of DNA and histone methylation. To identify specific changes related to 2HG inhibition of histone methylation in particular, a histone methylation screen was devised using the MOG-GCCM cell line discussed in the previous chapter.

5.2 Results

5.2.1 Increased 2HG/α-KG ratio with IDH1 mutation

The IDH1 mutation was associated with increases in intracellular 2HG and a fall in α-KG, its precursor metabolite. 2HG can act as a competitive inhibitor of α-KG dependent enzymes, which include dioxygenases and transaminases. The fall in α-KG associated with 2HG production would potentially exacerbate the inhibitory effect of 2HG on these enzymes. The 2HG/α-KG ratio in the clinical samples

ranged from 50 to almost 600 in the IDH1 mutant tumours. In comparison the IDH1 wild-type tumours had a 2HG/α-KG ratio that was close to zero. A similar effect was seen in the endogenous IDH1 mutant NCH cell lines, with a 2HG/α-KG ratio up to 600. The IDH1 mutant over-expressed cell lines also had increased 2HG/α-KG ratios. In the MOG-GCCM IDH1 mutant clones, the 2HG/α-KG ratio went up to 200, and up to 50 in the IDH1 mutant astrocytes (Figure 5-1A).

5.2.2 The IDH1 mutation is associated with changes in histone methylation

The α-KG dependent dioxygenases are a family of enzymes which rely on α-KG as a co-substrate. Prolyl hydroxylases (PHD) are a subgroup of α-KG dependent dioxygenases that have been implicated in tumorigenesis. They play an important role in the degradation of hypoxia inducible factor (HIF) in normoxic conditions. HIF activates a range of genes in response to low oxygen to increase glycolysis and angiogenesis. In the presence of oxygen, PHD hydroxylates prolyl groups on HIF allowing it to bind to the von Hippel-Lindau (VHL) protein which tags HIF for ubiquitination and degradation in the proteasome. HIF can be stabilised by inhibition of PHDs, which occurs in tumours with other TCA metabolite mutations, namely succinate dehydrogenase and fumarate hydratase. To investigate whether this same effect occurs in IDH1 mutant tumours, protein was extracted from the MOG-GCCM cells and levels of HIF-1α were determined. To act as a positive control, the EV was incubated in either 2 mM dimethyloxaloylglycine (DMOG), an α-KG dependent dioxygenase inhibitor, or 0.1% oxygen for 24 hrs. The IDH1 mutant clones, and EV + 2HG, did not show any increase in HIF-1α expression compared to the EV and PCL controls, indicating that 2HG doesn't inhibit PHDs (Figure 5-1B).

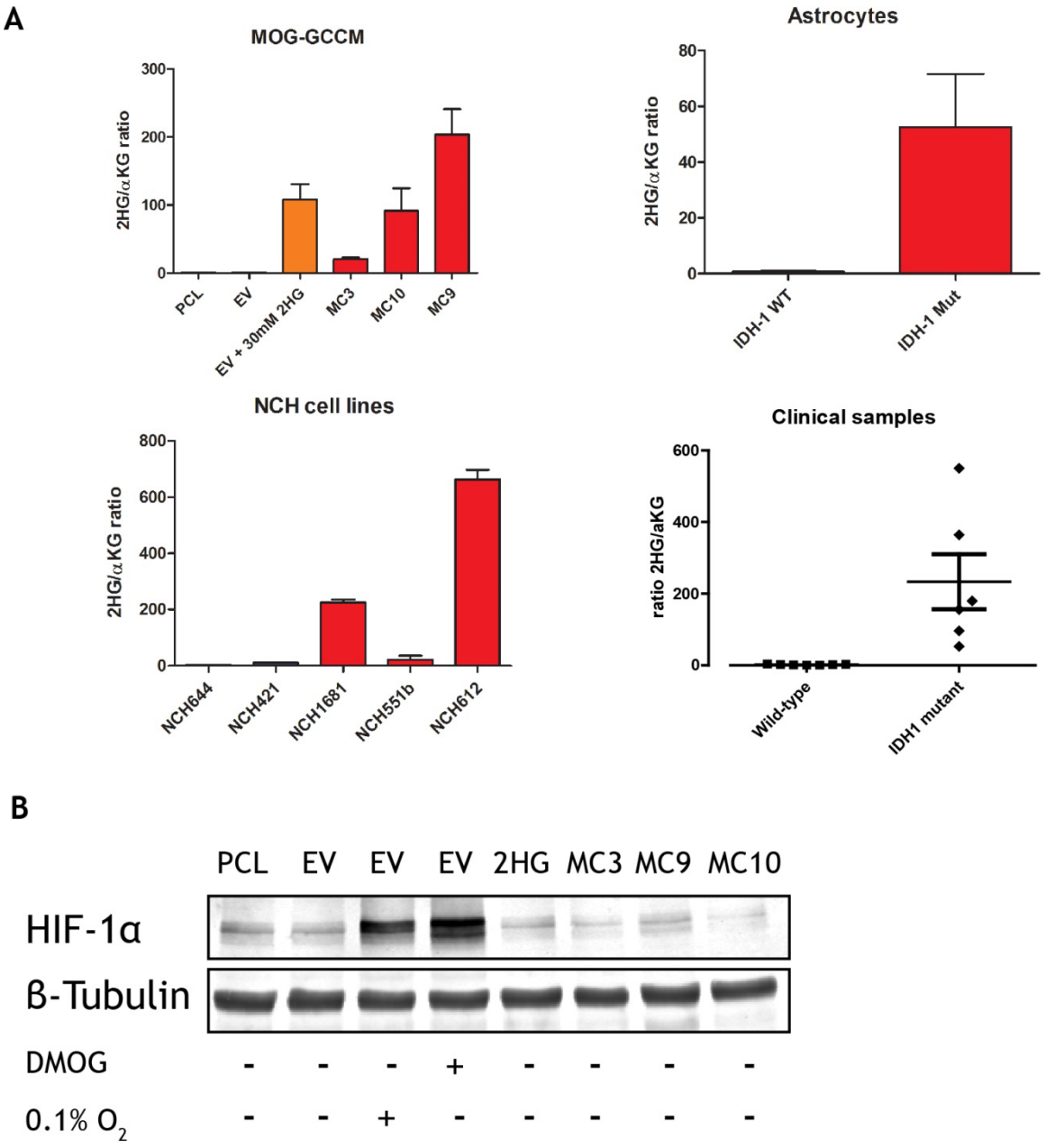

Figure 5-1 The effect of the IDH1 mutation on the 2HG/α-KG ratio and HIF1α expression
A. 2HG/α-KG ratio for the MOG-GCCM cell lines, immortalised astrocytes, NCH cell lines and clinical tumour samples. The IDH1 mutant samples are depicted in red and the EV + 2HG in orange. B. Western blott depicting protein expression of hypoxia inducible factor 1α (HIF1α) in MOG-GCCM cells. 2 mM dimethyloxaloylglycine (DMOG) and incubation in 0.1% oxygen were used as positive controls. Β-tubulin was used as an internal control.

Histone JMJ demethylases are another sub-group of the α-KG dependent dioxygenases, which are involved in the removal of methyl groups from histone tails. The number and site of these methyl groups determines whether it leads to gene activation or suppression. To determine whether there was any change in histone methylation with the IDH1 mutation, a histone methylation screen was devised using immunofluorescence and a high throughput microscopy screening method. This involved using antibodies obtained from Dr H. Kimura, University of Osaka, for different histone methylation sites with either a total H3 or H4 antibody as an internal control. Ratios of the fluorescence of the histone methylation sites with total H3 or H4 was used to compare the IDH1 mutant clones with the IDH1 wild-type controls. Cells were also incubated in 2 mM DMOG for 24 hrs to act as a positive control.

The histone methylation screen showed an increase in H3K4me2, H3K4me3, H4K20me2, H4K20me3, and H3K27me3 in the IDH1 mutant clones and EV + 2HG, compared to the EV and MOG-GCCM PCL controls. Other histone methylation sites screened, such as H3K36 and H3K9, showed no difference between the IDH1 mutant clones and the IDH1 wild-type controls (Figure 5-2, Figure 5-3). Of these histone methylation sites, H3K4 methylation, a marker associated with gene activation, had the most consistent dose response when related to the intracellular levels of 2HG of the different IDH1 mutant clones and EV + 2HG. To confirm the specificity of H3K4me2 and H3K4me3 a MODified histone peptide array was used (Active Motif). Both antibodies had a specificity factor of over 20, compared to a specificity factor of less than 4 for other histone methylation sites (Figure 5-4).

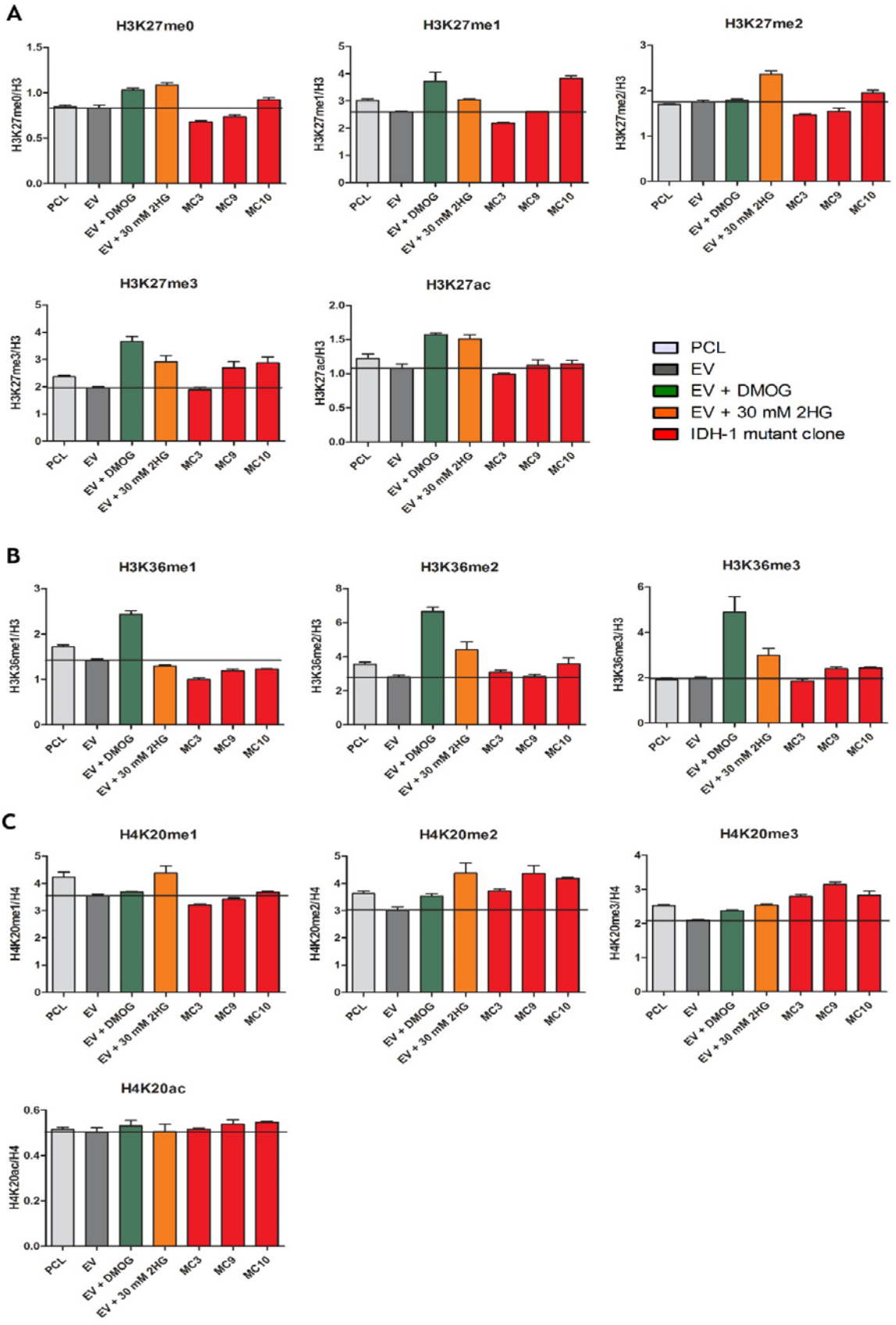

Figure 5-2 Histone methylation screen for H3K27, H3K36 and H4K20

A immunoflourescence screen was used to detect histone methylation and acetylation levels at H3K27 (A), H3K36 (B), and H4K20 (C) in MOG-GCCM cells. Comparison of different experimental goups was done by producing a ratio of the histone methylation site to the appropriate total histone (H3 or H4). EV and PCL controls are represented in grey. The IDH1 mutant clones are represented in red, and EV + 2HG is represented in orange. EV + 2 mM dimethyloxaloylglycine (DMOG), a jumonji histone demethylase inhibitor, is represented in green. Single experiment depicting mean +/- SD.

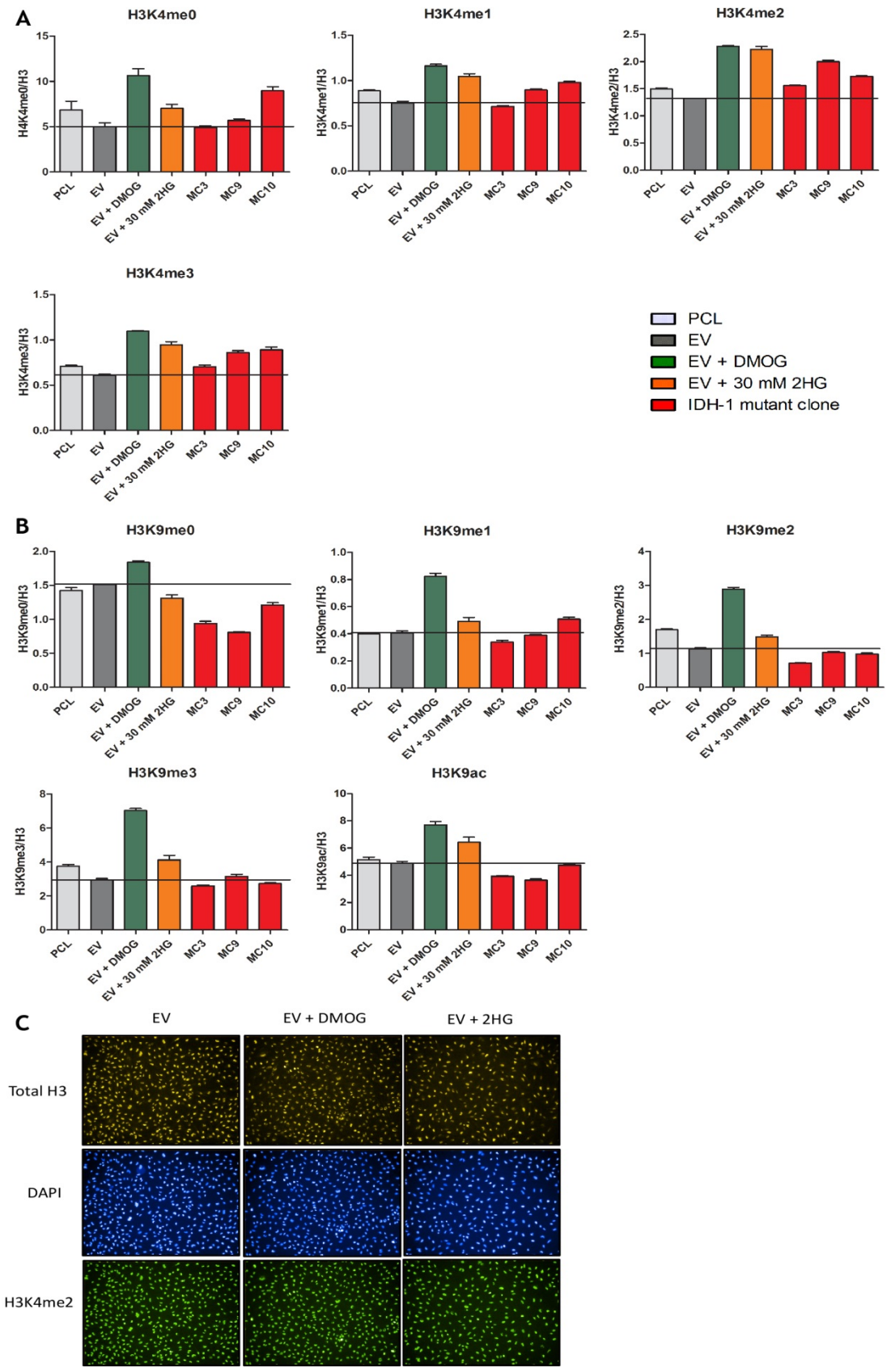

Figure 5-3 Histone methylation screen for H3K4 and H4K9
A immunoflourescence (IF) screen was used to detect histone methylation and acetylation levels at H3K4 (A) and H4K9 (B) in MOG-GCCM cells. Comparison of different experimental goups was done by producing a ratio of the histone methylation site to the appropriate total histone (H3 or H4). The EV and PCL controls are represented in grey. The IDH1 mutant clones are represented in red, and EV + 2HG is represented in orange. EV + 2 mM dimethyloxaloylglycine (DMOG) is represented in green. Single experiment depicting mean +/- SD. (C) Example of images obtained using IF screen.

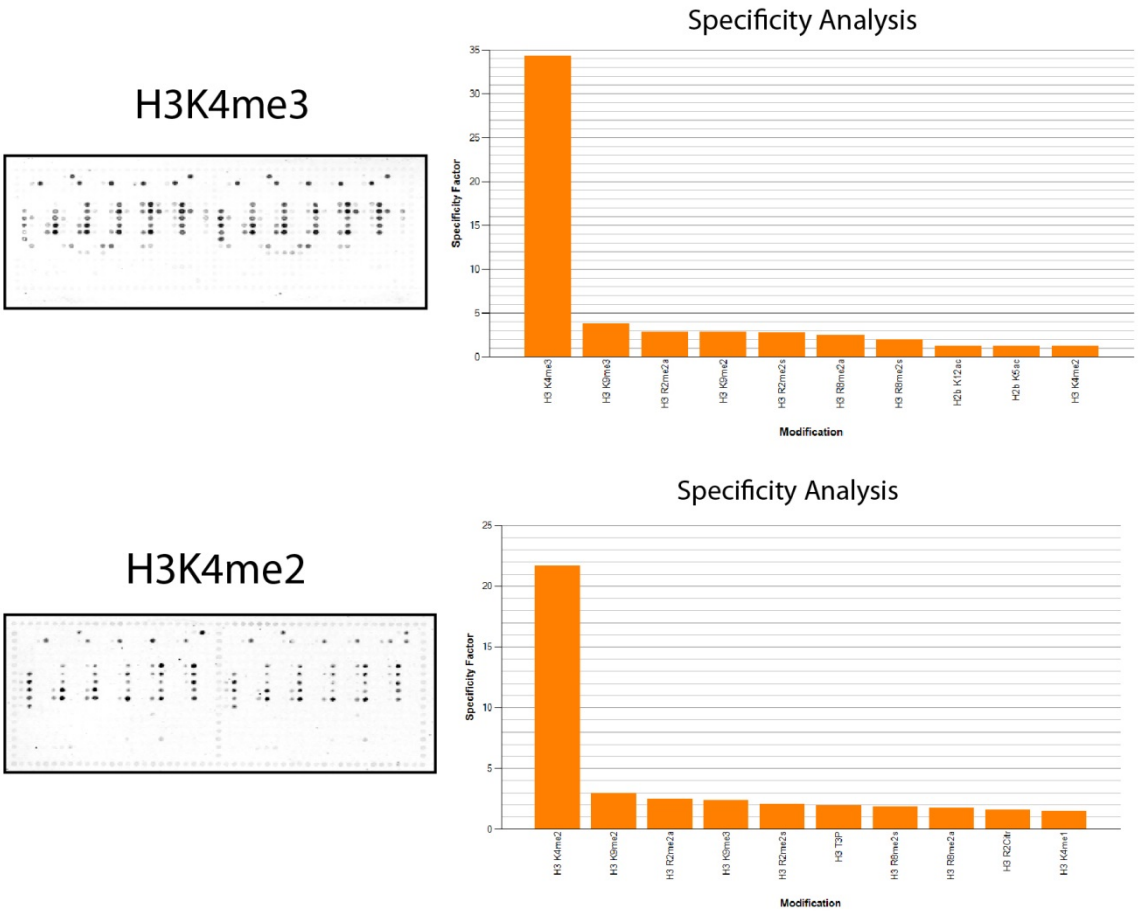

Figure 5-4 MODified histone peptide arrays
MODified histone peptide arrays (Active Motif) were used to determine the specificity of antibodies used to detect H3K4me3 and H3K4me2. Specificity factor was determined using software provided with the product.

5.2.3 IDH1 mutation is associated with an increase in H3K4 methylation

To validate the histone methylation screen, histones were extracted from the NCH cell lines, MOG-GCCM cells and the immortalised astrocytes. When compared to IDH1 wild-type cell lines, H3K4me3 was increased in the IDH1 mutant NCH cell line with the highest 2HG/α-KG ratio (NCH612). This was not the case in the other two endogenous IDH1 mutant cell lines, which may indicate that a minimal 2HG/α-KG ratio is required to increase H3K4 methylation, or that this change in histone methylation mark not be present in all IDH1 mutant tumours. However, the MOG-GCCM IDH1 mutant clones and EV + 2HG also had increased presentation of H3K4me2 and H3K4me3 compared to the EV and PCL controls. A similar effect was seen in the immortalised astrocytes with increased expression of H3K4me3 in the IDH1 mutant compared to the IDH1 wild-type cells (Figure 5-5 A,B,C).

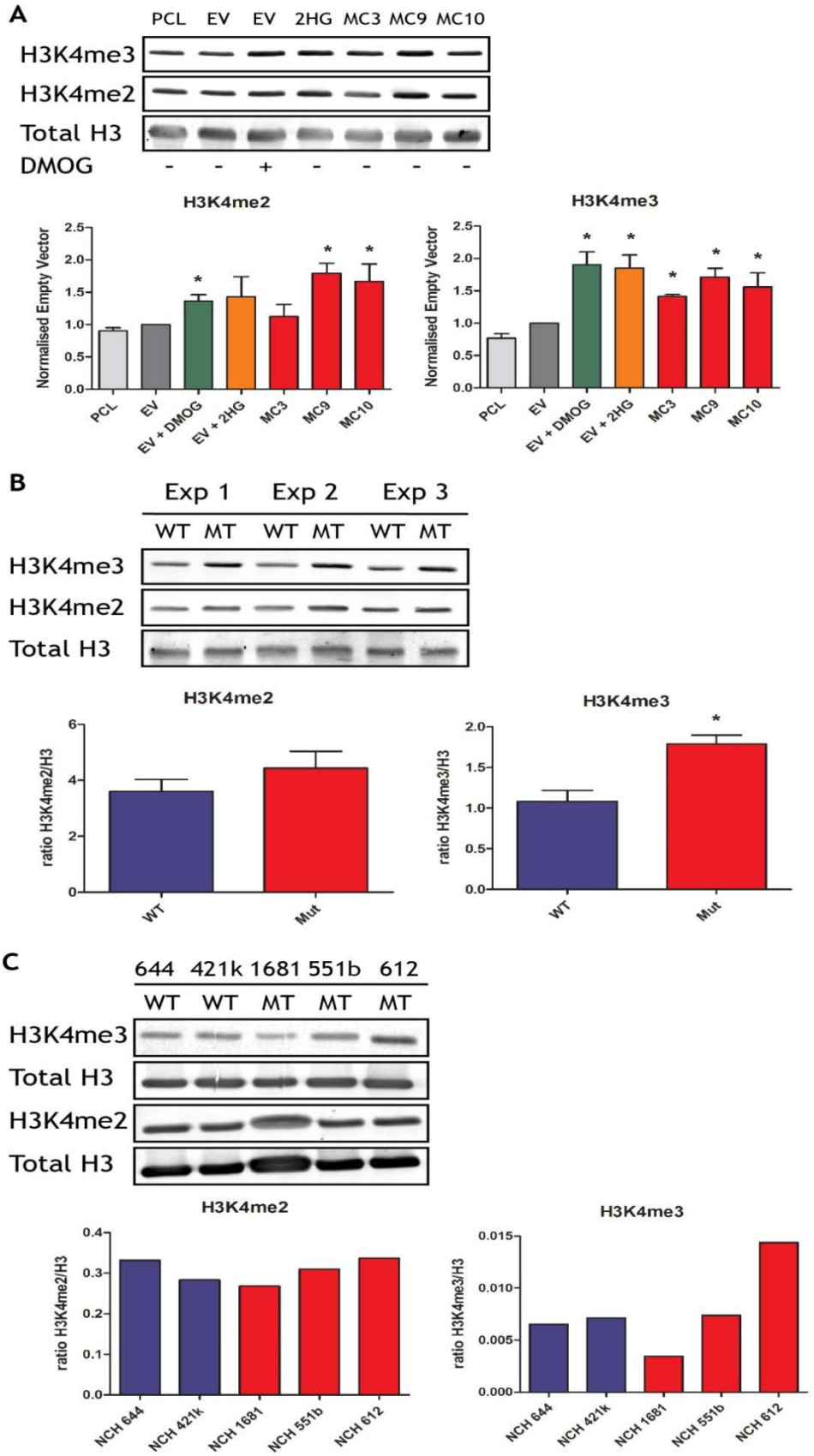

Figure 5-5 H3K4me2 and H3K4me3 presentation in cell lines
Western blot depicting H3K4me2 and H3K4me3 presentation in A. MOG-GCCM PCL, EV, EV propagated in 30 mM 2HG-lactone (2HG), and IDH1 mutant clones (MC3, MC9, MC10) B. immortalised IDH1 wild-type (WT) and IDH1 mutant (MT) astrocytes and C. endogenous IDH1 wild-type (644, 421k) and endogenous IDH1 mutant (1681, 551b, 612) cell lines. EV + 2 mM dimethyloxaloylglycine (DMOG), a JMJ histone demethylase inhibitor, was used as a positive control. Graphs depict quantification of Western blot from 3 independent experiments (A + B) or a single experiment (C). Data were analyzed using Students t-test. * depicts $p \leq 0.05$.

To identify whether this change in histone methylation also occurred *in vivo*, ten IDH1 wild-type and ten IDH1 mutant glioblastoma tumours were stained for H3K4me2 and H3K4me3 expression. To quantify the staining for H3K4me2/3, the slides were scanned and analysed using SlidePath Tissue Image Analysis 2.0 (Leica microsystems). To generate a histoscore the stained cells algorithm was used on the whole section for each slide. An increase in both H3K4me2 and H3K4me3 was seen in IDH1 mutant compared to IDH1 wild-type tumours (Figure 5-6D,E).

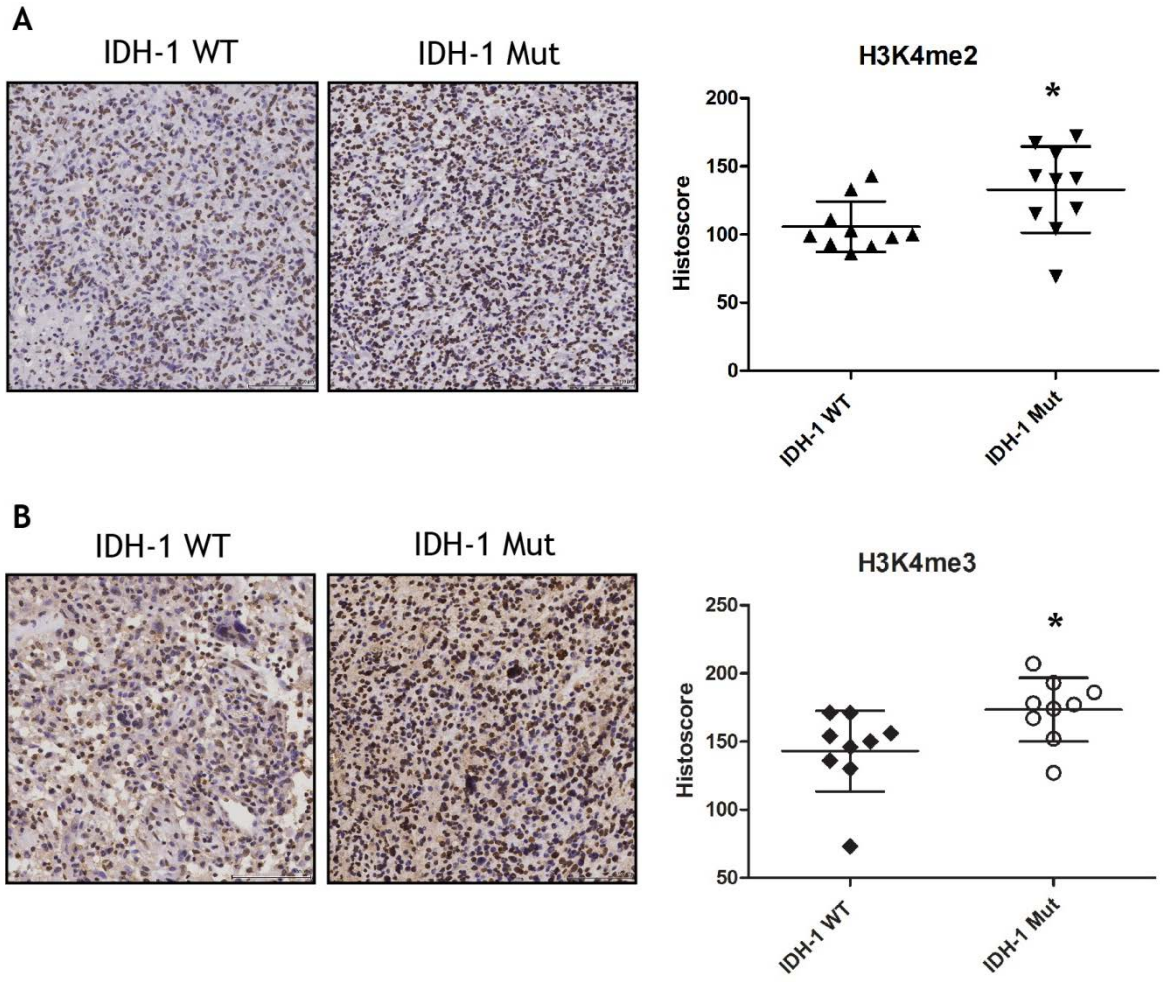

Figure 5-6 H3K4me2 and H3K4me3 presentation in clinical samples
Immunohistochemistry for presentation of H3K4me2 (D) and H3K4me3 (E) in 10 IDH1 wild-type (WT) and IDH1 mutant (Mut) glioblastoma samples. Graphs depict quantification of these samples by generating a histoscore using Leica SlidePathTissue Analysis 2.0. Data were analyzed using Students t-test. * depicts $p \leq 0.05$.

5.2.4 ChIP sequencing shows an increase in peaks for H3K4me2 and H3K4me3 caused by the IDH1 mutation.

H3K4me2 and H3K4me3 are associated with increases in gene expression. Chromatin immunoprecipitation sequencing (ChIP Seq) was used to identify the genes with an increase in these histone marks. Specific antibodies were used to extract chromatin bound to H3K4me2 and H3K4me3 which was then precipitated and sequenced against the human genome to identify genes that were associated with this histone methylation site. ChIP sequencing was used to investigate the effects of increased methylation of H3K4 in the MOG-GCCM EV, EV + 2HG, and MC9 clones.

Analysis of the ChIP Seq data showed that there were more peaks from H3K4me2 than H3K4me3. In addition, the EV + 2HG, and MC9 cells had more peaks of H3K4me2 and H3K4me3 than the EV control (Figure 5-7A). When the H3K4me2 and H3K4me3 peaks were compared, there was almost a complete overlap between these histone methylation states in all three groups (Figure 5-7B). Peaks were then analysed to determine their position relative to the transcription start site (TSS). The peak distribution for H3K4me3 was predominantly around the TSS, but for H3K4me2 this was spread across the gene region, with most of the peaks away from the TSS (Figure 5-8A, B).

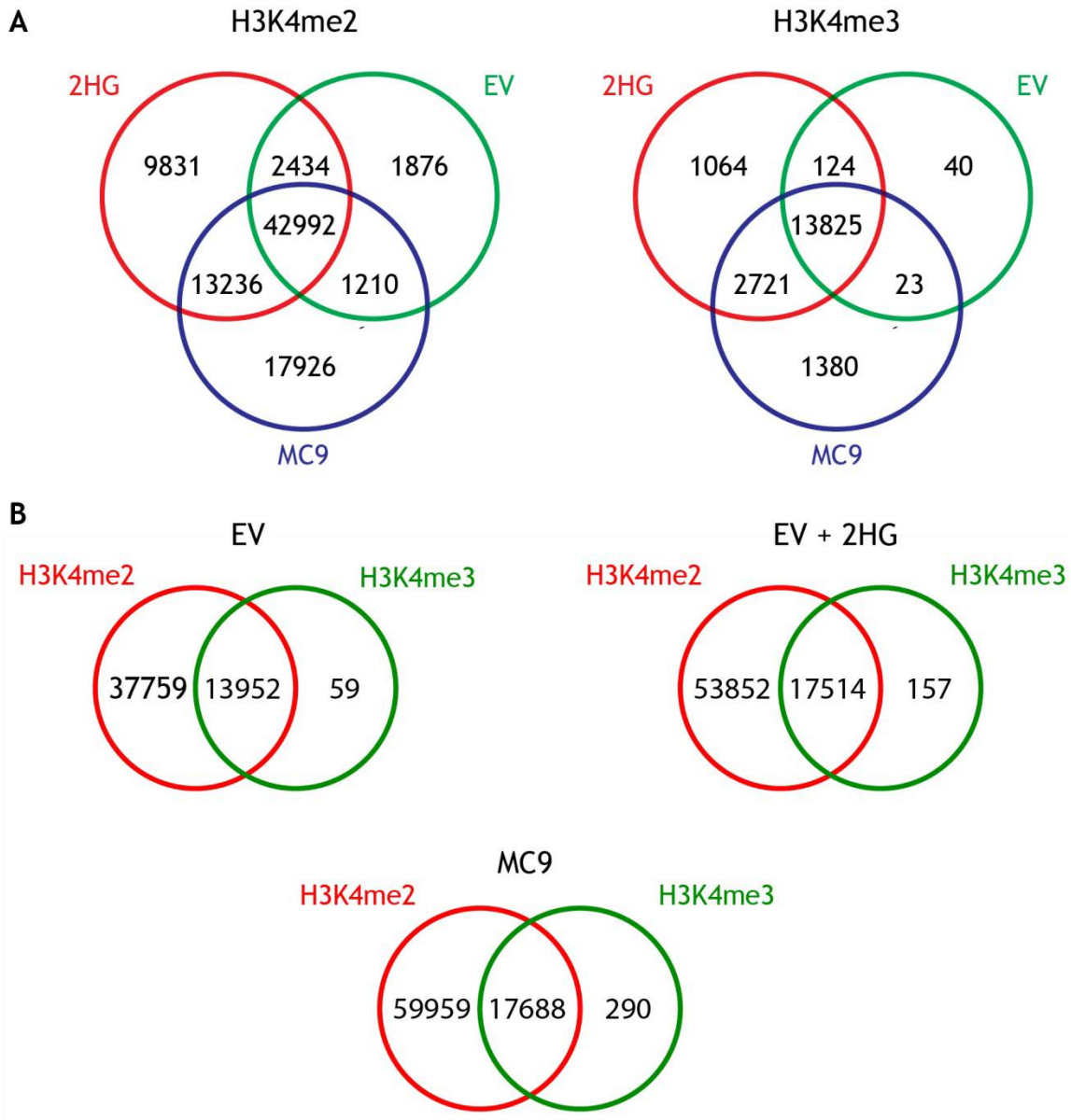

Figure 5-7 Venn diagrams depicting ChIP Seq peaks associated with either H3K4me2 or H3K4me3

A. Diagram representing distribution of peaks between EV, EV + 2HG, and MC9. B. Distribution of peaks between H3K4me2 and H3K4me3 for EV, EV + 2HG, and MC9. 2HG, and IDH1 mutant clone by MC9.

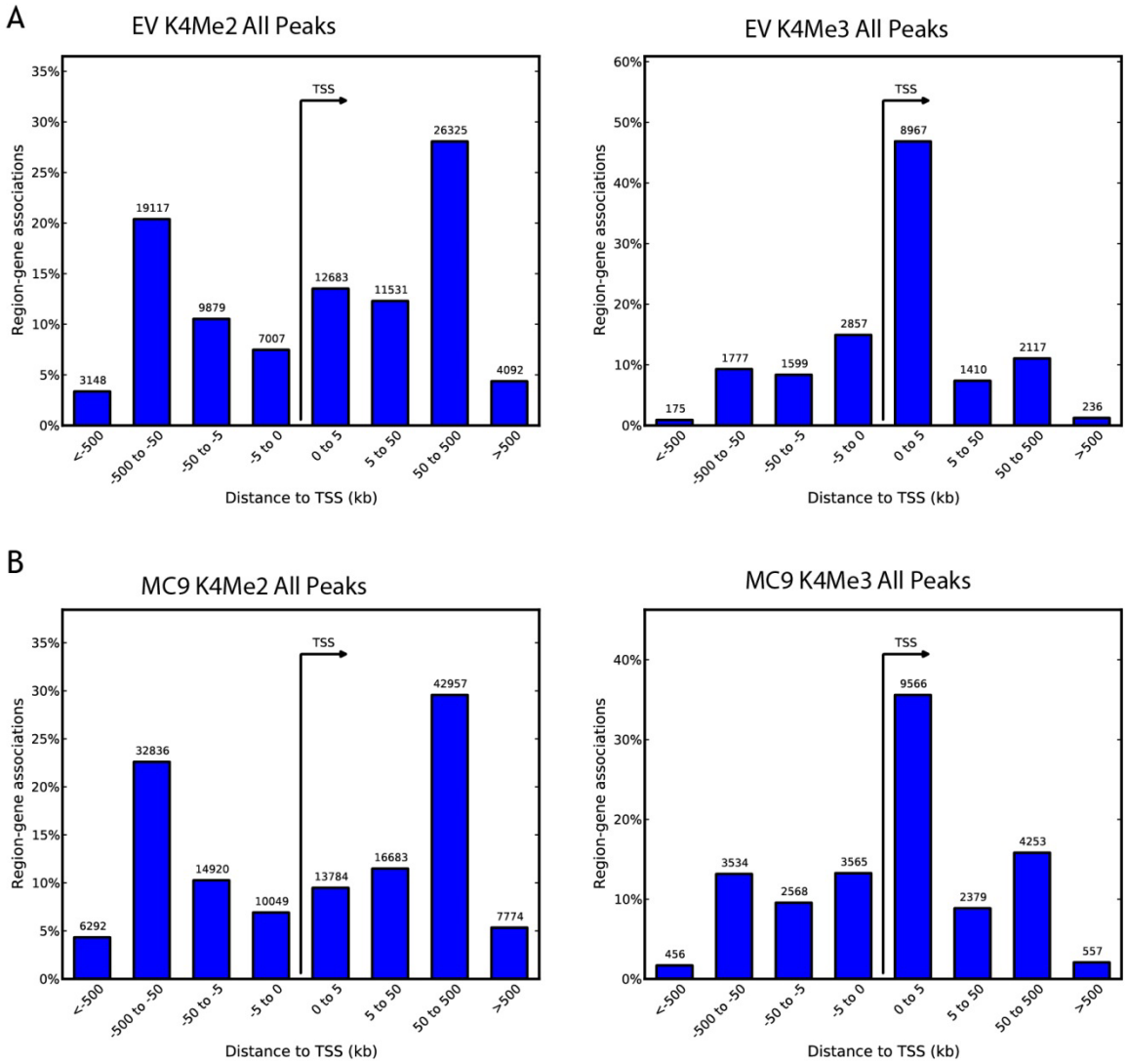

Figure 5-8 All ChIP Seq peaks
Graphs depict the proportion of peaks present within a specified distance from the transcription start site (TSS) for A. H3K4me2 and B. H3K4me3 in EV and IDH1 mutant MC9 clone.

Peaks that were new to the EV + 2HG or MC9 cells compared to the EV control were further examined. There were more new peaks in the MC9, compared to the EV + 2HG cells. The majority of new peaks for H3K4me2 and H3K4me3 were situated over 50 kbps from the TSS for both EV + 2HG, and MC9. However, a bigger proportion of new peaks were associated with the TSS for H3K4me3 compared to H3K4me2 (Figure 5-9A,B).

Focusing on H3K4me3, there was a strong correlation between peaks around the TSS that were significantly different from the EV for EV + 2HG compared to MC9. This corresponds to an increase in reads for H3K4me3 around the TSS for MC9 and EV + 2HG (Figure 5-9C,D). The top 50 genes that had increased reads for H3K4me3 at the TSS, common to EV + 2HG and MC9 compared to EV, are depicted in Table 5-1.

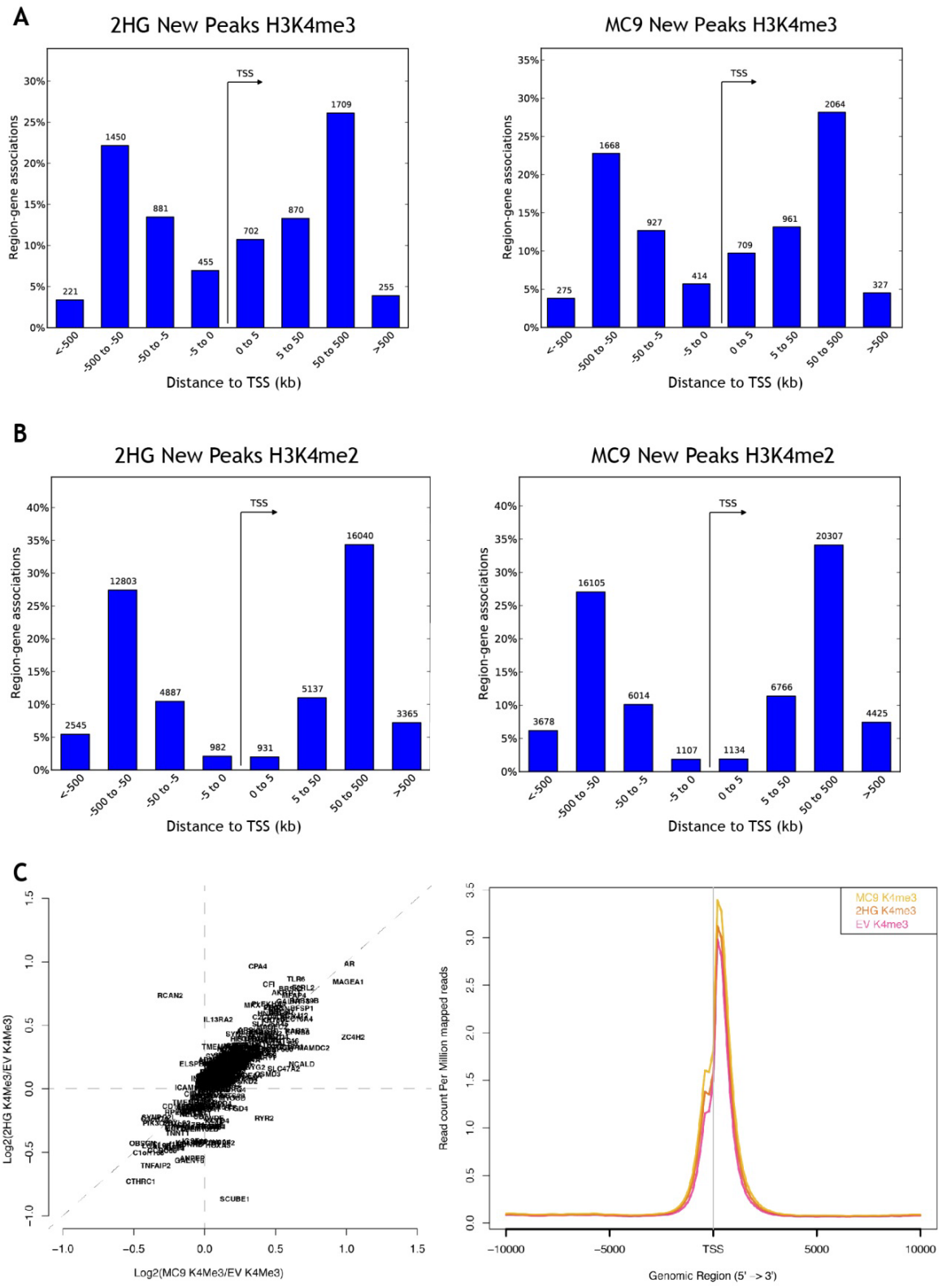

Figure 5-9 New Chip Seq peaks

Graphs depicting the proportion of new peaks present within a specified distance from the transcription start site (TSS) for A. H3K4me2 and B. H3K4me3 in EV + 2HG and IDH1 mutant MC9 clone when compared to the EV control. C. Graph depicting the correlation between ChIP peaks of EV + 2HG and MC9 when compared to the EV. D. Comparison of ChIP Seq peak locations relative to the nearest transcription start site for EV, EV + 2HG and MC9.

	MC9			EV + 2HG		
Gene	FC	p-value	Adj p-value	FC	p-value	Adj p-value
CPA4	4.61	5.82E-22	1.16E-19	1.46	0.067	0.374
AR	4.42	1.74E-30	7.29E-28	4.32	2.29E-37	4.32E-34
TLR6	4.01	2.98E-21	5.54E-19	2.40	6.68E-08	3.57E-06
MAGEA1	3.89	2.43E-21	4.56E-19	3.95	3.80E-37	7.01E-34
MKX	3.87	1.44E-19	2.21E-17	1.84	0.003	0.034
RAB39B	3.85	2.47E-24	6.11E-22	3.79	4.85E-26	3.26E-23
MFAP4	3.85	3.27E-16	3.54E-14	2.80	1.83E-10	1.61E-08
GALNT15	3.77	4.78E-16	5.12E-14	2.80	5.54E-11	5.45E-09
PLEKHA4	3.77	3.72E-22	7.62E-20	2.49	1.29E-07	6.45E-06
BFSP1	3.66	1.22E-13	9.41E-12	3.37	2.27E-16	5.28E-14
HNMT	3.44	2.26E-15	2.22E-13	2.55	2.82E-07	1.29E-05
KRT80	3.41	5.21E-13	3.69E-11	2.88	4.51E-10	3.74E-08
CFI	3.34	1.43E-13	1.09E-11	1.31	0.004	0.049
SLC16A4	3.26	3.85E-09	1.46E-07	2.90	1.02E-12	1.34E-10
SRRM3	3.23	1.79E-07	4.89E-06	2.71	1.02E-06	4.06E-05
IL13RA2	3.20	9.59E-10	4.05E-08	0.68	0.934	1
SSC5D	3.20	6.12E-18	8.24E-16	3.03	3.61E-17	9.15E-15
AKR1C1	3.12	1.01E-11	5.92E-10	1.50	8.57E-06	2.65E-04
ALX4	3.09	6.85E-16	7.18E-14	3.16	2.86E-20	1.08E-17
CALB2	3.01	7.77E-04	0.008	3.48	6.06E-15	1.12E-12
F2RL2	2.96	3.53E-11	1.88E-09	1.80	7.13E-08	3.79E-06
EFNB3	2.85	7.07E-07	1.72E-05	3.24	1.59E-23	8.22E-21
COL15A1	2.81	0.002	0.016	3.40	6.11E-17	1.52E-14
SYNPO2	2.75	2.57E-07	6.81E-06	1.46	0.057	0.337
FAM19A2	2.70	3.81E-06	7.85E-05	2.33	1.64E-05	4.76E-04
MAMDC2	2.55	0.011	0.066	4.03	8.40E-33	9.72E-30
SLC43A3	2.33	0.187	0.508	0.73	0.720	1
BRSK2	2.29	1.50E-49	2.01E-46	1.87	6.21E-26	4.14E-23
NCALD	2.24	0.445	0.859	3.65	1.21E-26	8.85E-24
SLC25A45	2.24	2.82E-13	2.05E-11	2.04	6.03E-10	4.91E-08
MAGEC2	2.22	5.32E-12	3.23E-10	2.16	2.80E-12	3.44E-10
MTMR11	2.22	0.275	0.648	1.97	3.28E-04	0.006
RGL3	2.19	2.97E-28	1.02E-25	2.06	8.03E-20	2.94E-17
NRGN	2.02	8.63E-32	3.96E-29	1.82	1.31E-19	4.65E-17
ZIM2	2.01	2.46E-30	1.01E-27	1.72	8.73E-16	1.85E-13
PEG3	2.01	3.02E-30	1.22E-27	1.72	1.03E-15	2.15E-13
CPA4	1.99	0.053	0.213	1.89	1.13E-06	4.44E-05
KCNJ12	1.96	2.15E-18	3.01E-16	2.07	4.92E-24	2.70E-21
RAB17	1.81	0.001	0.010	1.97	2.79E-09	2.03E-07
ZNF560	1.78	0.004	0.028	2.20	8.05E-13	1.08E-10
C2CD4C	1.75	1.06E-19	1.67E-17	1.50	9.70E-11	9.09E-09
CTSH	1.69	2.78E-11	1.51E-09	1.64	1.74E-10	1.54E-08
APOE	1.63	0.107	0.350	1.46	3.66E-04	0.007
ALS2CL	1.47	5.07E-15	4.76E-13	1.20	6.37E-06	2.05E-04
HIST1H3J	1.43	1.23E-05	2.23E-04	1.28	4.98E-04	0.009
LYNX1	1.43	0.276	0.649	1.40	0.008	0.086
CBLN2	1.40	0.014	0.081	1.60	7.59E-08	4.00E-06
AKR1C3	1.38	4.30E-05	6.71E-04	1.20	0.003	0.039
HIST1H3C	1.38	1.06E-08	3.70E-07	1.16	3.83E-04	0.007

Table 5-1 Genes associated with changes in ChIP Seq
Top 50 genes with increased H3K4me3 over the TSS common to EV + 2HG and MC9 compared to EV with $\log_2$ fold change ≥ 0.5 and adjusted p value ≤ 0.05.

5.2.5 Increased abundance of H3K4me3 is associated with increased expression of GABRB3

To obtain additional information on gene expression for the EV, EV + 2HG, and MC9 cells, RNA was extracted and sequenced using an Illumina next generation sequencer. Differential expression was calculated for EV + 2HG and MC9 compared to EV.

The MC9 clone and EV + 2HG had different gene expression profiles compared to the EV control. There were both increases and decreases in gene expression in a large number of genes for the EV + 2HG and MC9 clone compared to EV, with the biggest changes seen in the MC9 clone (Figure 5-10A). When these differences in gene expression were compared between the EV + 2HG and MC9, there was a strong correlation between these two experimental groups (Figure 5-10B). A heatmap generated from the genes that were significantly different between the EV + 2HG or MC9 when compared to the EV, which showed a similar pattern between the EV + 2HG and MC9 (Figure 5-10C).

The top 50 upregulated genes with the highest fold change common to EV + 2HG and MC9, compared to the EV, included ZC4H2 and EFNB3 which are involved in neurogenesis and brain development, respectively. In addition, there were upregulated genes, such as CACNA1G and CACNA2D3, which encode calcium channel subunits involved in neurotransmitter release. ALDF3A1, a gene involved in neurotransmitter metabolism was also increased in the EV + 2HG and MC9 when compared to the EV. Finally, there was an increase in the GABRB3 gene, which is a subunit of the GABA-A receptor and involved in GABA signalling in the brain (Table 5-2).

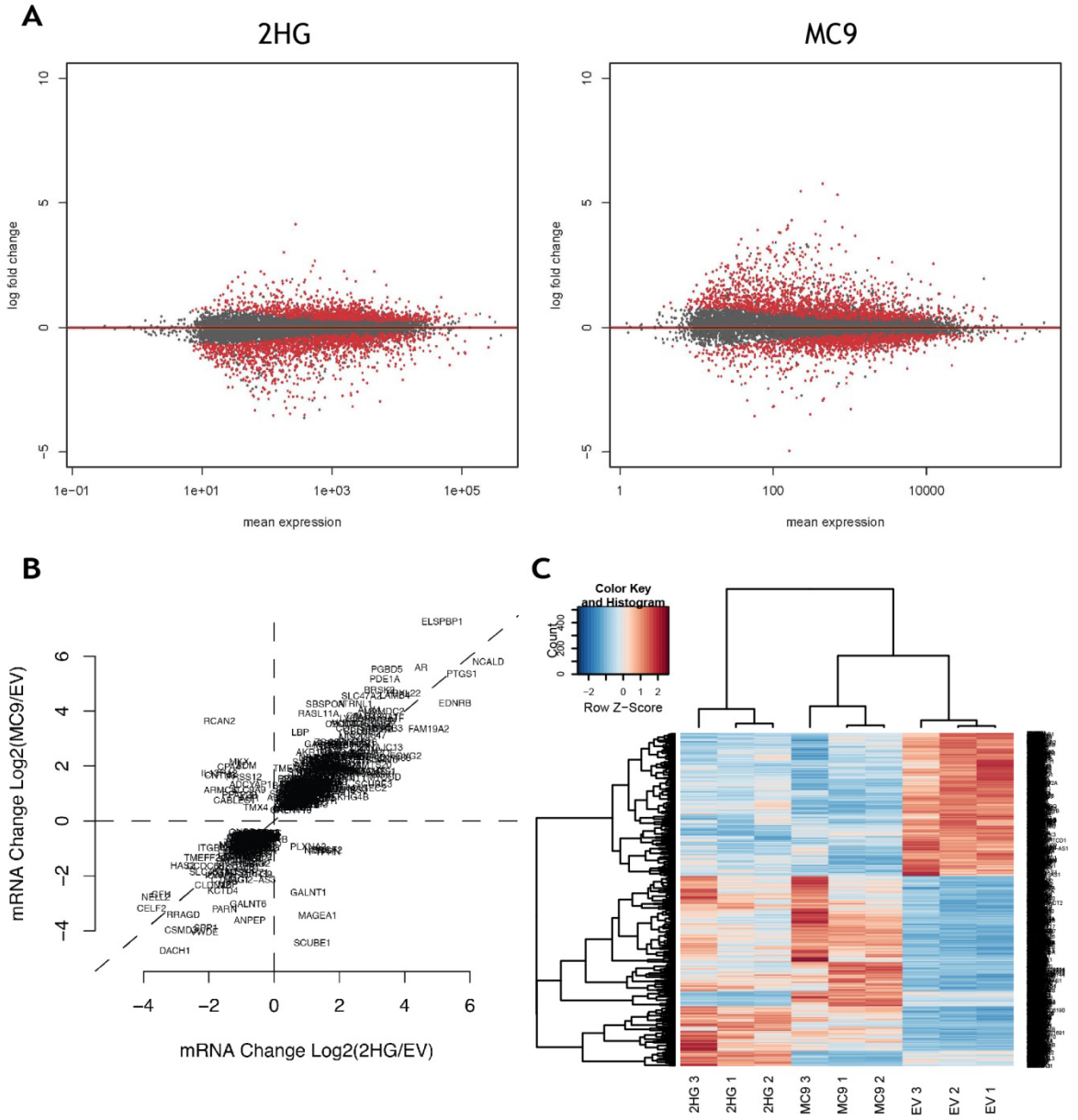

Figure 5-10 RNA Seq data

A. MA plot of gene expression versus their log_2 fold change for either EV + 2HG or IDH1 mutant MC9 clone compared to the EV control. Each dot represents a single gene. Red dots depict genes with adjusted p value ≤ 0.05, while grey dots represent genes with an adjusted p value > 0.05. B. Graph depicting the correlation between differential gene expression of EV + 2HG and MC9 when compared to the EV. C. Heatmap of the genes represented in A with a statistically significant difference between the EV + 2HG or MC9 compared to the EV control.

	MC9			EV + 2HG		
Gene	Log_2FC	p-value	Adj p-value	Log_2FC	p-value	Adj p-value
CLCA2	5.32	$7.14E^{-117}$	$5.07E^{-113}$	0.97	0.002	0.01
AR	4.29	$8.68E^{-51}$	$7.71E^{-48}$	2.48	$1.44E^{-16}$	$1.46E^{-14}$
PGBD5	4.08	$8.23E^{-43}$	$4.33E^{-40}$	2.07	$2.49E^{-12}$	$1.37E^{-10}$
PDE1A	3.97	$2.94E^{-44}$	$1.74E^{-41}$	2.19	$1.80E^{-14}$	$1.40E^{-12}$
BRSK2	3.93	$1.54E^{-51}$	$1.68E^{-48}$	2.06	$1.23E^{-12}$	$7.11E^{-11}$
ELSPBP1	3.91	$3.53E^{-32}$	$9.30E^{-30}$	1.19	$4.14E^{-05}$	0.0004
CACNA1G	3.81	$5.08E^{-32}$	$1.31E^{-29}$	0.89	0.003	0.017
SLC47A2	3.75	$2.74E^{-45}$	$1.77E^{-42}$	1.9	$4.36E^{-12}$	$2.30E^{-10}$
CACNA2D3	3.68	$1.91E^{-96}$	$6.78E^{-93}$	0.72	0.010	0.043
SBSPON	3.67	$5.74E^{-51}$	$5.44E^{-48}$	1.23	$7.50E^{-07}$	$1.44E^{-05}$
RASL11A	3.32	$3.93E^{-38}$	$1.65E^{-35}$	1.05	$5.18E^{-05}$	0.001
ALDH3A1	3.31	$4.05E^{-30}$	$8.72E^{-28}$	0.97	0.001	0.008
PPP2R2B	3.24	$1.09E^{-24}$	$1.63E^{-22}$	1.03	0.001	0.005
LY6E	3.20	$1.90E^{-39}$	$8.20E^{-37}$	1.78	$5.58E^{-12}$	$2.93E^{-10}$
LAMB4	3.18	$4.57E^{-24}$	$6.56E^{-22}$	1.81	$3.19E^{-09}$	$1.04E^{-07}$
HSD11B1	3.16	$1.28E^{-20}$	$1.40E^{-18}$	0.53	0.004	0.022
AKR1C2	3.03	$7.12E^{-33}$	$2.02E^{-30}$	2	$1.58E^{-24}$	$3.94E^{-22}$
PEG3	3.02	$1.37E^{-30}$	$3.24E^{-28}$	2.78	$3.39E^{-36}$	$1.49E^{-33}$
ST3GAL5	3.00	$2.00E^{-25}$	$3.12E^{-23}$	0.96	0.0008	0.005
C2CD4C	2.97	$1.40E^{-30}$	$3.25E^{-28}$	1.71	$3.10E^{-12}$	$1.68E^{-10}$
SRRM3	2.97	$1.09E^{-35}$	$4.07E^{-33}$	2.27	$2.04E^{-17}$	$2.34E^{-15}$
ICOSLG	2.96	$3.74E^{-24}$	$5.43E^{-22}$	1.15	0.0001	0.002
FAM89A	2.95	$2.59E^{-23}$	$3.58E^{-21}$	0.93	0.002	0.014
COL15A1	2.94	$3.37E^{-35}$	$1.20E^{-32}$	1.79	$7.45E^{-11}$	$3.14E^{-09}$
PDZD4	2.92	$1.06E^{-24}$	$1.61E^{-22}$	2.56	$1.27E^{-27}$	$4.08E^{-25}$
CD163L1	2.91	$1.73E^{-26}$	$2.85E^{-24}$	1.71	$9.09E^{-09}$	$2.73E^{-07}$
ALX4	2.87	$3.34E^{-19}$	$3.34E^{-17}$	2.25	$3.85E^{-19}$	$5.52E^{-17}$
ATRNL1	2.83	$7.67E^{-18}$	$6.77E^{-16}$	1.28	$3.11E^{-05}$	0.0004
RYR2	2.82	$1.12E^{-27}$	$2.07E^{-25}$	2.79	$2.93E^{-40}$	$1.70E^{-37}$
LBP	2.77	$2.06E^{-28}$	$3.96E^{-26}$	0.73	$4.15E^{-05}$	0.0004
FAM189A1	2.74	$4.74E^{-19}$	$4.65E^{-17}$	1.67	$3.89E^{-08}$	$1.02E^{-06}$
CALB2	2.73	$8.47E^{-18}$	$7.41E^{-16}$	1.74	$1.68E^{-09}$	$5.75E^{-08}$
LTF	2.72	$5.16E^{-18}$	$4.67E^{-16}$	2.81	$9.13E^{-27}$	$2.70E^{-24}$
KCNC1	2.72	$1.15E^{-19}$	$1.19E^{-17}$	0.87	0.004	0.021
LINC00847	2.68	$4.52E^{-27}$	$7.65E^{-25}$	1.9	$8.32E^{-12}$	$4.25E^{-10}$
COLEC12	2.63	$1.90E^{-19}$	$1.93E^{-17}$	0.8	0.008	0.036
ZC4H2	2.62	$4.55E^{-38}$	$1.85E^{-35}$	1.44	$1.17E^{-11}$	$5.82E^{-10}$
ADAMTS16	2.56	$1.96E^{-31}$	$4.87E^{-29}$	2.08	$6.52E^{-24}$	$1.52E^{-21}$
GPAM	2.54	$1.20E^{-49}$	$9.49E^{-47}$	1.56	$1.52E^{-20}$	$2.51E^{-18}$
KIAA1462	2.51	$9.51E^{-30}$	$1.99E^{-27}$	1.92	$3.40E^{-18}$	$4.42E^{-16}$
PPM1H	2.51	$3.53E^{-34}$	$1.11E^{-31}$	1.38	$6.08E^{-09}$	$1.91E^{-07}$
ACTBL2	2.50	$4.69E^{-24}$	$6.67E^{-22}$	0.71	0.004	0.023
HECW2	2.45	$1.87E^{-12}$	$9.15E^{-11}$	0.85	0.003	0.020
F2RL2	2.44	$7.35E^{-26}$	$1.17E^{-23}$	1.53	$4.01E^{-11}$	$1.79E^{-09}$
RGCC	2.41	$1.28E^{-11}$	$5.53E^{-10}$	0.86	0.004	0.021
RSAD2	2.40	$1.69E^{-18}$	$1.57E^{-16}$	1.06	0.0005	0.004
FBXL22	2.38	$1.45E^{-11}$	$6.21E^{-10}$	2.00	$4.75E^{-11}$	$2.09E^{-09}$
GABRB3	2.38	$8.32E^{-21}$	$9.39E^{-19}$	1.24	$1.01E^{-07}$	$2.42E^{-06}$
GPR116	2.32	$1.29E^{-11}$	$5.56E^{-10}$	0.8	0.007	0.037
EFNB3	2.31	$1.12E^{-12}$	$5.62E^{-11}$	2.15	$2.44E^{-13}$	$1.59E^{-11}$

Table 5-2 Changes in gene expression from RNA Seq
Top 50 genes with increased expression common to EV + 2HG and MC9 compared to EV with adjusted p value ≤ 0.05

To identify genes associated with changes in H3K4me3 in the EV + 2HG and MC9 cells versus the EV, the RNA seq and ChIP seq data were analysed together. Genes with significant differential expression (q value ≤ 0.001) in the RNA Seq were used for further analysis. Promoters (First TSS +/- 5kb) of differentially expressed genes that were common across EV + 2HG and MC9 were used to check the K4Me3 change across samples.

The top 20 genes associated with an increase in H3K4me3 and gene expression for both EV + 2HG and MC9 compared to EV are shown in Table 5-3. This included the androgen receptor (AR), which regulates gene transcription; BRSK2 which plays a role in axonogenesis and the cell cycle; LAMB4 which is involved in the PI3K-Akt signaling pathway; and PEG3 which mediates the neuronal death pathway activated by DNA damage. However, one of these genes was GABRB3, a subunit of the GABA-A receptor. This receptor is activated by GABA, which was increased intracellularly in the *in vivo* and *in vitro* metabolomic data described in the previous two chapters. Therefore, the GABRB3 subunit and its interaction with GABA was investigated further and validated. The other targets have not yet been validated.

	MC9		EV + 2HG	
Gene	Gene FC	ChIP FC	FC	ChIP FC
AR	4.29	4.42	2.48	4.32
PDE1A	3.97	0.82	2.19	0.67
BRSK2	2.00	2.29	2.06	1.87
SLC47A2	3.75	1.25	1.9	1.84
LAMB4	3.18	0.71	1.81	0.38
PEG3	3.02	2.01	2.78	1.72
C2CD4C	2.97	1.75	1.71	1.5
SRRM3	2.97	3.23	2.27	2.71
COL15A1	2.94	2.81	1.79	3.4
PDZD4	2.92	1.06	2.56	1.31
ALX4	2.87	3.09	2.25	3.16
LBP	2.77	1.07	0.73	1.69
FAM189A1	2.74	0.9	1.67	0.98
CALB2	2.73	3.01	1.74	3.48
LTF	2.72	0.77	2.81	0.92
ZC4H2	2.62	1.33	1.44	3.28
ADAMTS16	2.56	0.98	2.08	1.33
F2RL2	2.44	2.96	1.53	1.80
GABRB3	2.38	0.64	1.24	0.55
EFNB3	2.31	2.85	2.15	3.24

Table 5-3 Genes with increased expression and H3K4me3 presentation
Top 20 genes with increased H3K4me3 over the TSS and increased gene expression common to EV + 2HG and MC9 compared to EV with $\log_2$ fold change ≥ 0.5 and adjusted p value ≤ 0.001.

Differences in the expression of the GABRB3 subunit in MC9 and EV + 2HG, compared to the EV, were validated using qPCR. The expression of GABRB3 was three times higher in the EV + 2HG, and eight times higher in the MC9 clone compared to the EV control. Validation of the ChIP Seq data for the same gene was done using ChIP qPCR. This showed a % input that was double in the EV + 2HG and four times higher in the MC9 clone compared to the empty vector control (Figure 5-11).

RNA seq and Affymetrix microarray analysis showed that other subunits of the GABA-A receptor were also upregulated in the EV + 2HG and MC9 clone compared to the EV control. In both methods, there was an increase in gene expression for GABRA3, GABRE, and GABRQ (Table 5-4).

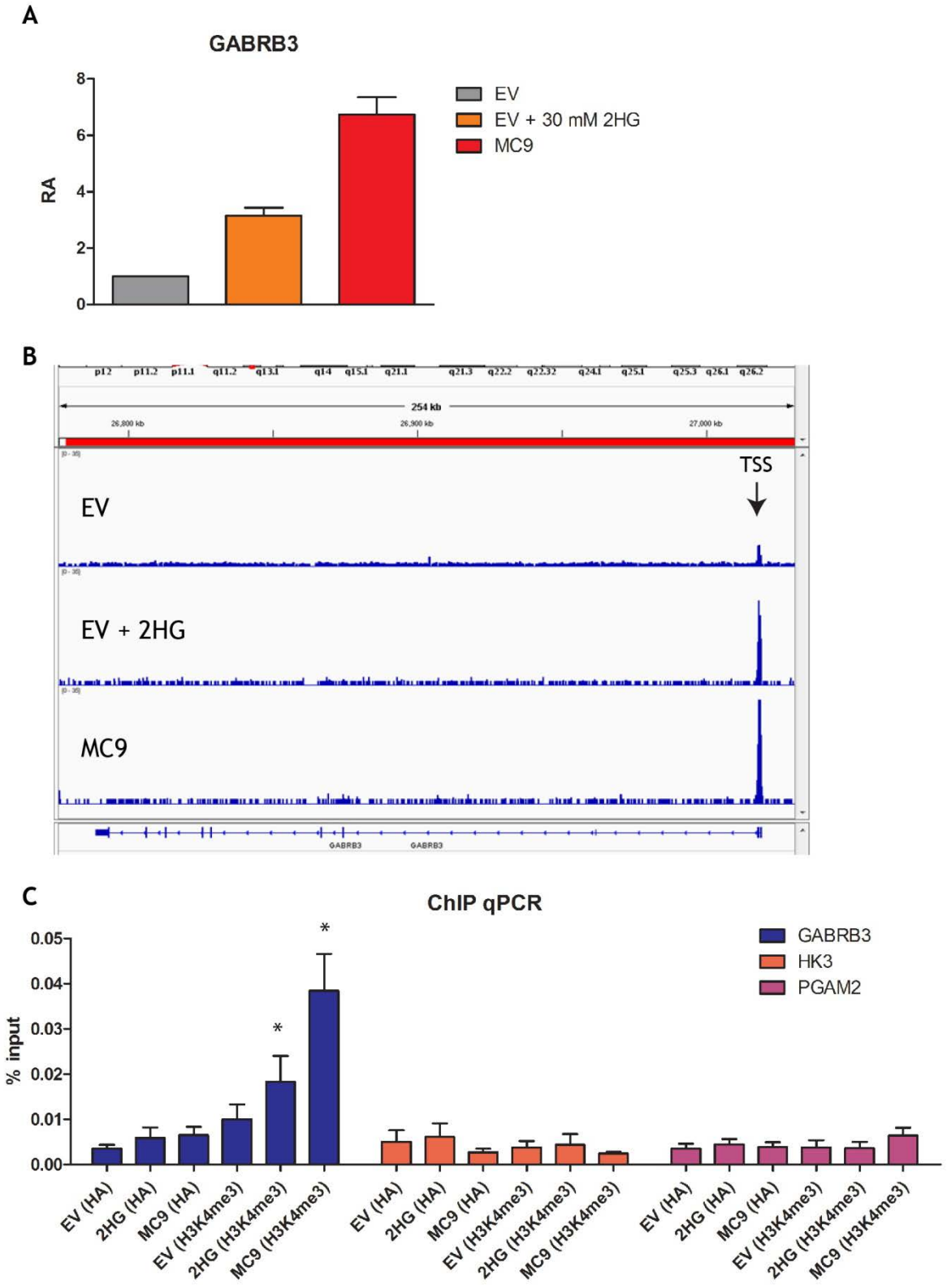

Figure 5-11 Validation of ChIP and RNA Seq data using qPCR

A. mRNA GABRB3 expression in the EV, EV+2HG, and IDH1 mutant MC9 clone. Depicts 3 independent expreiments showing mean +/- SEM. B. Depicts ChIP peaks across the GABRB3 gene. The arrow represents the position of the transcription start site (TSS). C. ChIP qPCR for the GABRB3 gene using pull down for H3K4me3. Haemaglutinin (HA) antibody was used as a negative control. Two other genes (HK3 and PGAM2) with no change in H3K4me3 peaks on ChIP Seq between the EV + 2HG and MC9 clone compared to the EV were used as additional controls. Data were analysed using 2-way ANOVA. * depicts $p \leq 0.01$ compared to EV (H3K4me3).

A

	MC9			EV + 2HG		
Gene	FC	p-value	q-value	FC	p-value	q-value
GABRA1	1.04	6.30E-01	0.754961	1.03	7.06E-01	0.827
GABRA2	1.09	4.99E-01	0.712911	1.09	5.08E-01	0.785
GABRA3	1.40	1.32E-02	0.125609	1.83	2.20E-04	0.017
GABRA4	-1.02	7.95E-01	0.795349	1.02	7.81E-01	0.838
GABRA5	-1.01	8.34E-01	0.803094	1.05	4.48E-01	0.767
GABRA6	-1.06	5.93E-01	0.744661	-1.23	7.43E-02	0.425
GABRB1	-1.09	3.59E-01	0.646763	-1.06	5.17E-01	0.786
GABRB2	-1.03	6.19E-01	0.751955	-1.03	5.73E-01	0.803
GABRB3	1.76	2.55E-04	1.02E-02	1.50	3.34E-03	0.085
GABRD	1.09	1.71E-01	0.48769	1.05	4.27E-01	0.760
GABRE	1.62	1.77E-03	3.59E-02	1.39	1.82E-02	0.220
GABRG1	-1.06	6.37E-01	0.756015	1.00	9.99E-01	0.869
GABRG2	-1.02	7.37E-01	0.783123	1.13	5.01E-02	0.362
GABRG3	-1.10	3.62E-01	0.648607	-1.09	4.04E-01	0.753
GABRP	-1.02	8.21E-01	0.800088	-1.04	6.41E-01	0.816
GABRQ	2.12	2.77E-05	0.003	1.71	5.47E-04	0.029
GABRR1	1.08	3.64E-01	0.649044	-1.06	4.56E-01	0.769
GABRR2	1.01	9.11E-01	0.817631	1.04	5.56E-01	0.798
GABRR3	1.03	7.55E-01	0.786938	-1.10	2.75E-01	0.681

B

	MC9			EV + 2HG		
Gene	FC	p-value	q-value	FC	p-value	q-value
GABRA3	1.41	5.69E-03	0.027	1.78	1.66E-06	2.91E-05
GABRB3	5.21	8.32E-21	9.39E-19	2.36	1.01E-07	2.42E-06
GABRE	1.73	8.03E-08	1.75E-06	1.09	0.498	0.696
GABRQ	3.39	2.08E-33	6.16E-31	2.16	5.56E-14	4.06E-12

Table 5-4 Changes in GABA-A subunits caused by the IDH1 mutation
A. mRNA epression data from Affymetrix microarray depicting fold change (FC) of the IDH1 mutant MC9 clone, and EV + 2HG compared to the EV control for subunits of the GABA-A receptor. B. mRNA epression data from RNA sequencing depicting FC of at least 1.5 for the MC9 or EV + 2HG cells compared to the EV control.

To determine whether the changes in GABA-A receptor subunit gene expression occurred *in vivo*, datasets from Oncomine and the Cancer Genome Atlas (TCGA) were analyzed. In the Oncomine dataset, gene expression for GABRB3 was increased in primary gliomas that are associated with a high incidence of the IDH1 mutation, namely astrocytoma, oligoastrocytoma, and oligodendroglioma. Conversely, GBM, which is associated with a low incidence of the IDH1 mutation, had a reduced expression of the GABRB3 gene (Figure 5-12A). Using TCGA, and focusing on low grade gliomas, there was an increase in both GABRA3 and GABRB3 in IDH mutant compared to IDH wild-type tumours. Conversely, there was a decrease in gene expression of several other GABA-A receptor subunits including GABRA2/3, GABRG3, and GABRQ (Figure 5-12B,C).

A

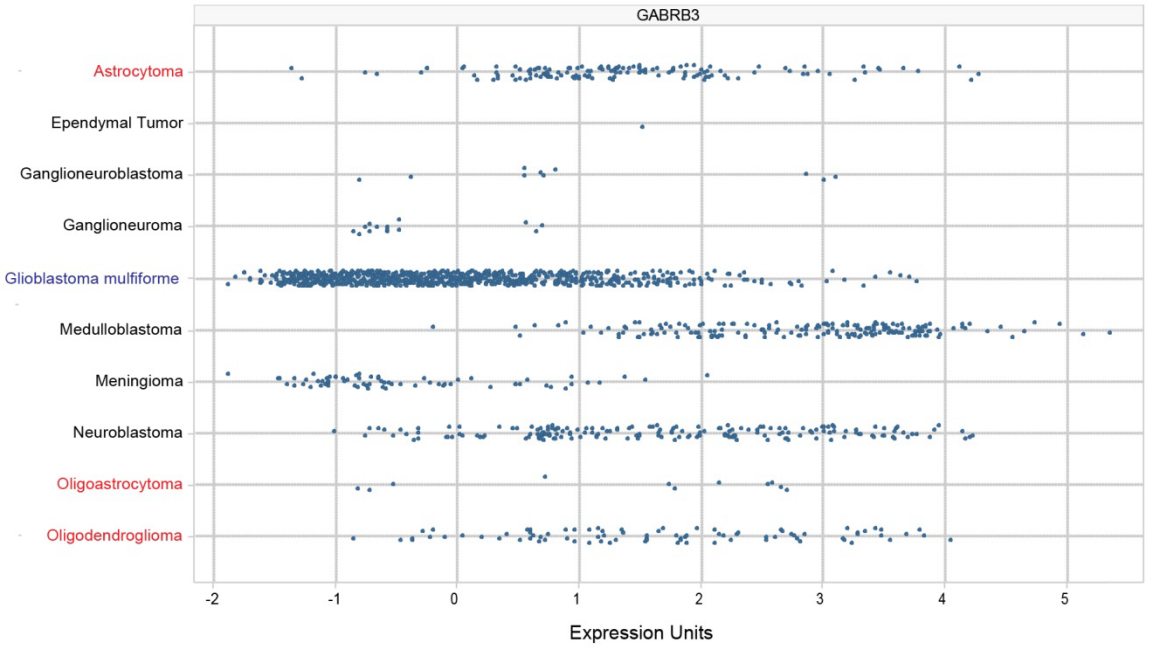

B

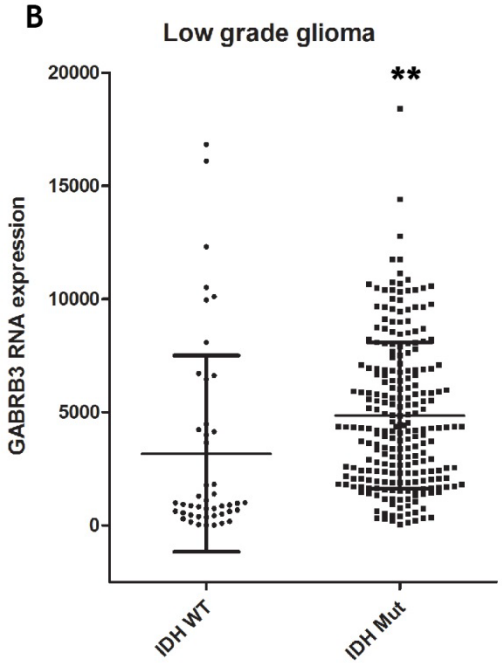

C

Gene	Fold Change	p value	Adj p value
GABRA1	-1.41	0.13	0.19
GABRA2	-2.17	7.27E-05	2.16E-04
GABRA3	1.41	0.02	0.04
GABRA4	-1.53	0.05	0.08
GABRA5	-1.95	1.84E-03	4.13E-03
GABRA6	-1.54	0.09	0.14
GABRB1	1.01	0.95	0.96
GABRB2	-1.41	0.11	0.16
GABRB3	1.51	2.46E-03	0.01
GABRD	1.05	0.78	0.83
GABRE	-2.21	5.19E-07	2.21E-06
GABRG1	-1.39	4.99E-02	0.08
GABRG2	1.03	0.89	0.92
GABRG3	-1.78	0.01	0.02
GABRP	-1.26	0.31	0.38
GABRQ	-1.52	0.01	0.02
GABRR1	-1.23	0.42	0.50
GABRR2	1.18	0.30	0.38
GABRR3	1.01	0.98	0.98

Figure 5-12 Datamining GABRB3 expression from patient samples
A. mRNA expression of GABAB3 in different types of primary brain tumour. Tumours in red are gliomas with a high incidence of IDH1 mutation, while tumours in blue are gliomas with a low incidence of IDH1 mutation. Analysis was done using the Oncomine data base [283]. B. mRNA expression of GABAB3 in cohort of low grade glioma generated by the TCGA Research Network: http://cancergenome.nih.gov/. Statistical analysis was done using Students t-test. ** represents a p value ≤ 0.01. C mRNA expression of different subunits that can constitute the GABA-A receptor using the same TCGA database as B.

To confirm whether these differences in mRNA GABRB3 expression between IDH mutant and IDH wild-type tumours resulted in changes in protein expression *in vivo*, parrafin embedded tumour samples were stained for the presence of the GABRB3 protein using a commercial antibody [284]. 10 IDH1 wild-type and 10 IDH1 mutant tumour samples were used. To quantify the staining for GABRB3, the slides were scanned and analysed using SlidePath Tissue Image Analysis 2.0 (Leica microsystems). To generate a histoscore, the stained area algorithm was used across the whole section of each slide for the GABA-A receptor β3 subunit. There was a trend towards an increase in GABRB3 in the IDH1 mutant tumours but this was not significant (Figure 5-13).

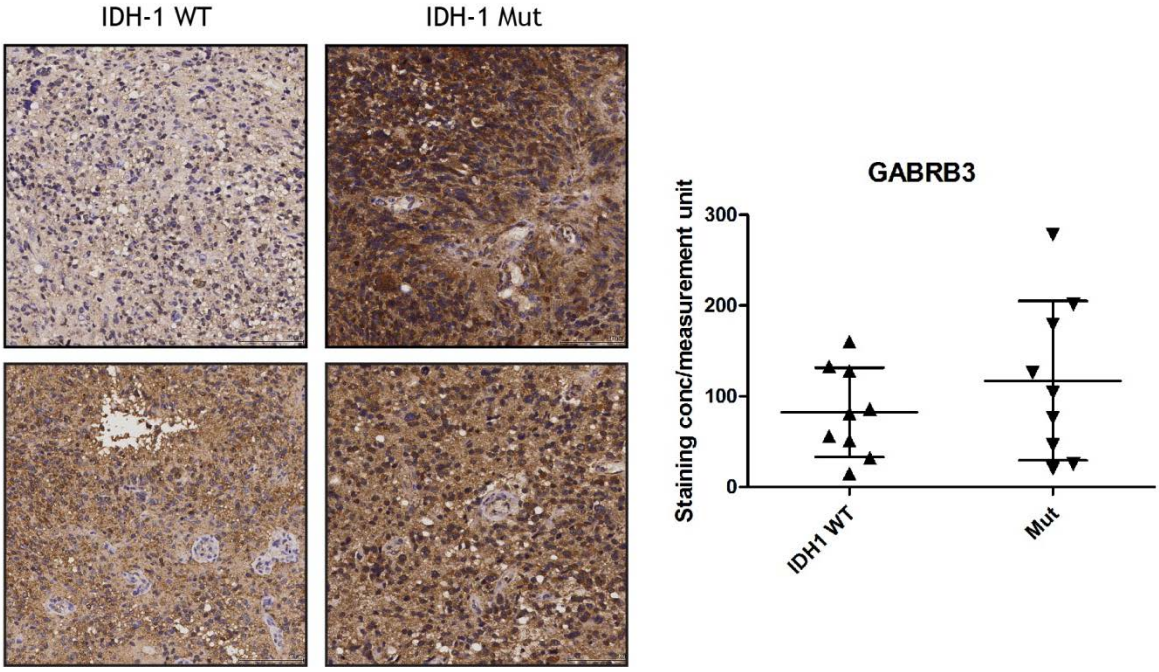

Figure 5-13 GABRB3 expression of clinical GBM samples
Immunohistochemistry for expression of GABAB3 in 10 IDH1 wild-type (WT) and 10 IDH1 mutant (Mut) glioblastoma samples. Representative images of two WT and two Mut samples. Graph depicts quantification of these samples through generation of a histoscore using Leica SlidePathTissue Analysis 2.0. Data were analysed using Students t-test.

To assess whether upregulation of GABRB3 had an effect on cell proliferation and survival, clonogenic assays were carried out comparing the EV control and the MC9 and MC10 IDH1 mutant clones. A GABA-A receptor inhibitor, Bicuculline, in the presence or absence of 0.5 mM GABA, was added to medium. The addition of the GABA-A receptor inhibitor resulted in a 50% reduction in colonies forming for EV and the IDH1 mutant clones. This effect was not reversed by the addition of GABA (Figure-5-14).

To assess whether upregulation of the GABRB3 resulted in changes in cell migration, a scratch assay was used. The reduction in the scratch over 24 hours was measured at hourly intervals using an Incucyte live cell imaging system. There was no difference in cell migration between the PCL, EV and IDH1 mutant MC9 and MC10 clones. There was no effect on cell migration with the addition of Bicuculline or GABA (Figure 5-15).

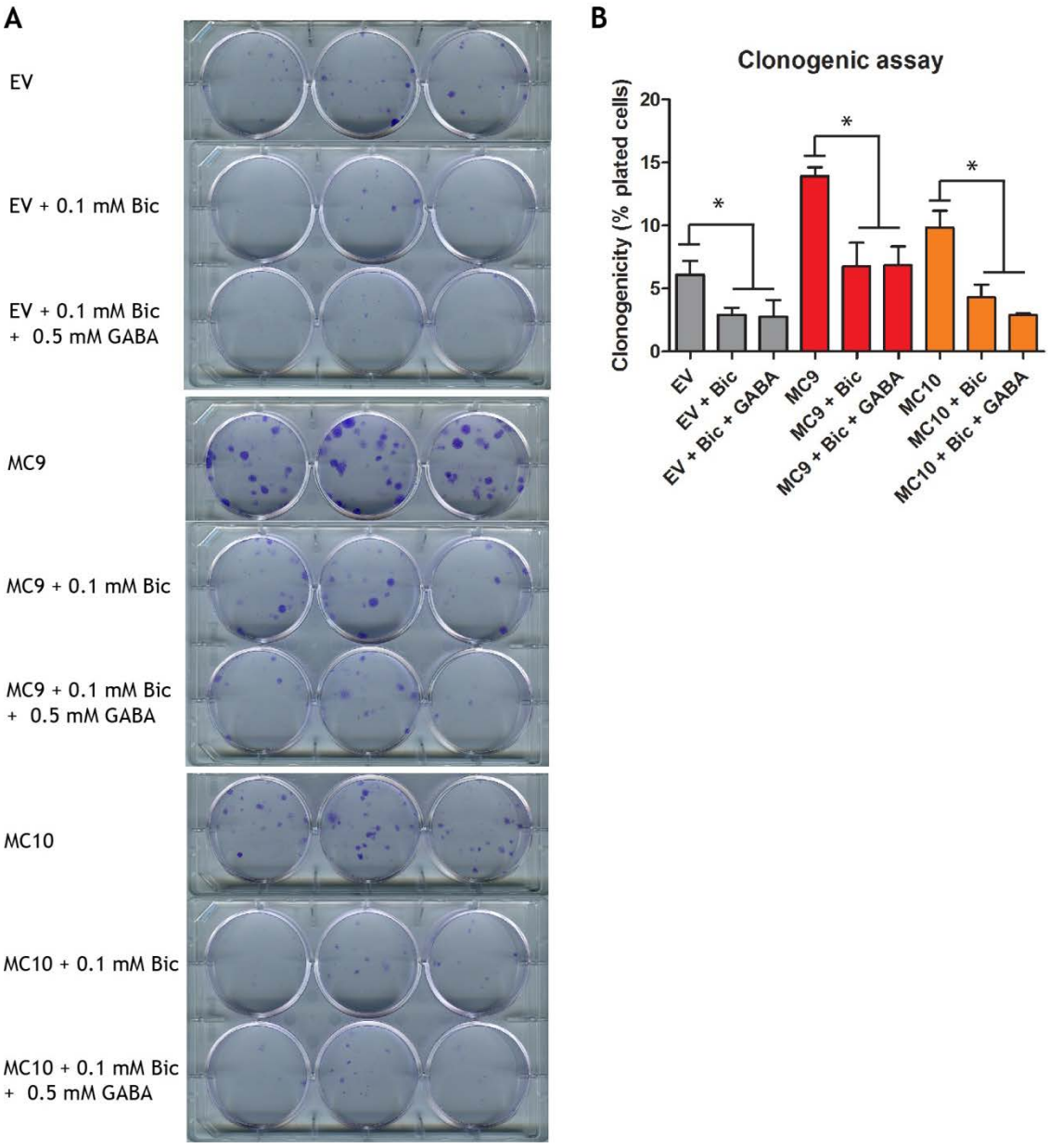

Figure-5-14 Effect of GABA and GABA-A receptor inhibition on clonogenicity
Clonogenic assay of empty vector (EV) or IDH1 mutant MC9 clone, incubated with 0.1 mM Bicuculline (Bic) or 0.1 mM Bic with 0.5 mM GABA. B. Quantification of 3 independent experiments described in A. Statistical analysis was done using 2-way ANOVA. * depicts $p \leq 0.01$

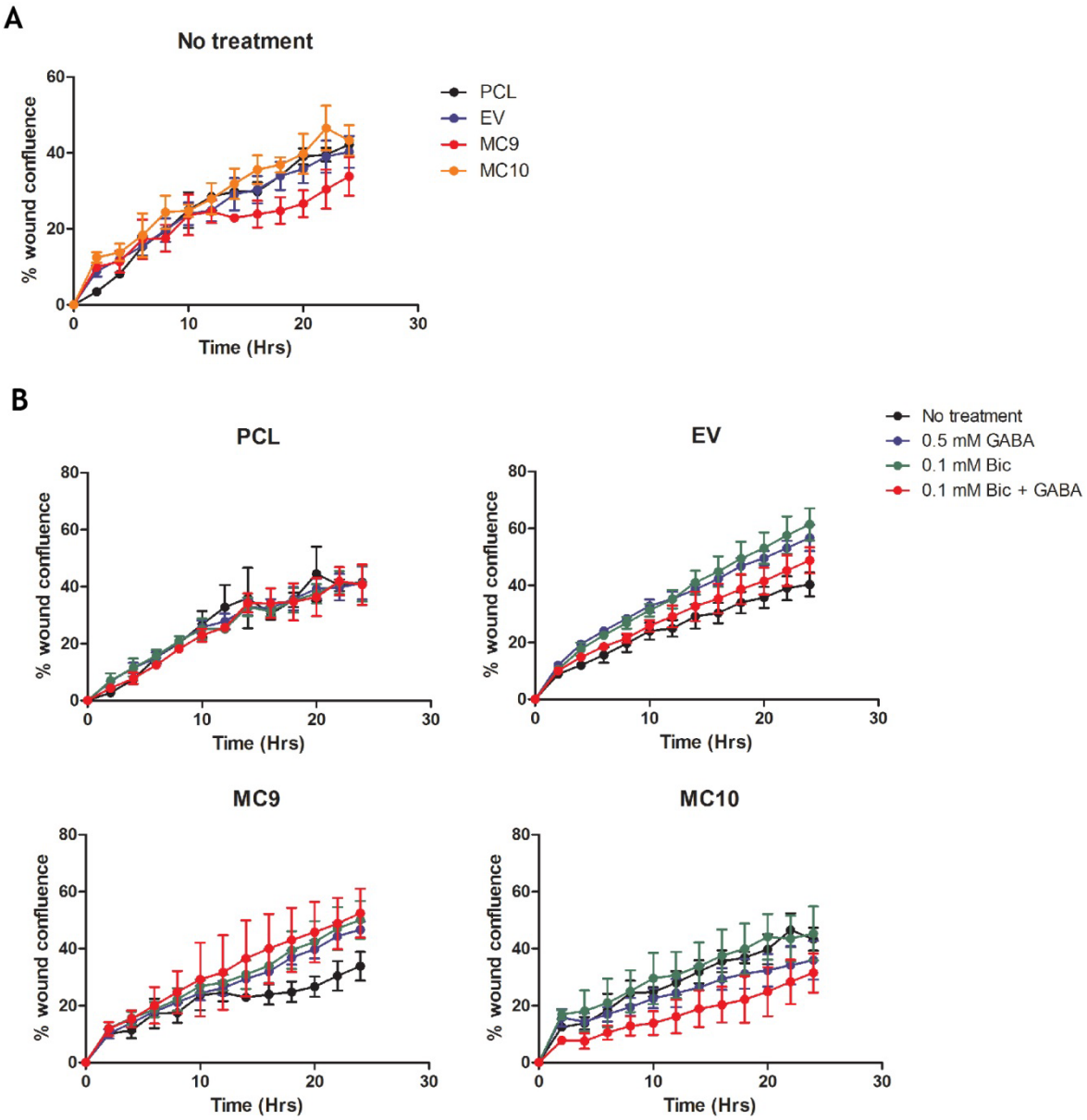

Figure 5-15 Effect of GABA and GABA-A receptor inhibition on cell migration
Scratch assay depicting the% of area filled over 24 hours. A. depicts scratch assay comparing the MOG-GCCM parental cell line (PCL), empty vector (EV), and IDH1 mutant clones MC9 and MC10. B. depicts scratch assay after the addition of 0.5 mM GABA, 0.1 mM Bicuculline (Bic) or both (0.1 mM Bic + GABA). Data from single experiment representative of two independent experiments. Mean +/- SD.

5.3 Discussion

The IDH1 mutation was associated with an increase in intracellular 2HG and a fall in α-KG. This increase in the 2HG/ α-KG ratio was observed in several cell models as well as clinical tumour samples. This large difference in the intracellular 2HG/ α-KG ratio led to the hypothesis that the IDH1 mutation, through the production of 2HG, could result in the inhibition of α-KG-dependent dioxygenases. No effect was observed on PHDs, but there was an increase in histone methylation at some sites on the histone tail. This included H3K4, H3K27 and H4K20, whereas other sites were unaffected. There are numerous JMJ histone demethylases which can demethylate several sites on the histone tail [172]. The variable effect on histone methylation sites and the lack of effect on PHDs by the IDH1 mutation indicates that not all α-KG-dependent dioxygenases are sensitive to inhibition by 2HG. Another group has also shown different effects on histone methylation in oligondendrogliomas, with an increase in H3K9 methylation [261]. This was not observed in our histone methylation screen on an astrocytoma derived cell line and could indicate that the effects of 2HG may be tissue dependent, as well as enzyme specific.

H3K4 methylation is associated with gene activation. The IDH1 mutation resulted in an increase in both H3K4me2 and H3K4me3 across several cell models and in GBM tumour samples. ChIP sequencing of H3K4me2 and H3K4me3 in the MOG-GCCM clones showed an increase in peaks in the IDH1 mutant MC9 clone and EV + 2HG compared to the EV control. This confirmed the effect of 2HG on reducing histone demethylation in these cells at this particular site on the histone tail. In addition, the increase in H3K4me3 was associated with the TSS indicating that these changes could have an effect on gene expression. The H3K4me2 peaks however appeared mostly away from the TSS, which indicates that they may have indirect effects on gene expression. These areas may correspond to regions of non-coding RNA, which may affect gene expression by influencing mRNA translation.

RNA sequencing was performed to assess gene expression in the IDH1 mutant MC9 clone, EV and EV + 2HG cells. When compared to the EV control, the EV + 2HG and MC9 cells had similar changes in gene expression. When these changes in gene expression were aligned to changes in H3K4me3 peaks at the TSS there

was an associated increase in GABRB3, a subunit of the ionotropic GABA-A receptor, which on activation allows for the flow of chloride ions into the cell altering the cell membrane potential. This in turn activates neighbouring calcium channels increasing calcium influx which seems to have a negative effect on cell proliferation [30, 285].

The GABA-A receptor can be formed from a combination of nineteen different subunits. Microarray and RNA seq also showed an increase in GABRA3, GABRE, and GABRQ, in the MC9 and EV + 2HG cells. However, this didn't correspond to changes in H3K4me3, indicating that the increase in gene expression occurred by a mechanism other than hypermethylation of H3K4. H3K27me3 and H4K20me3 were also increased in the IDH1 mutant clones and EV + 2HG, but these are associated with gene repression. It is therefore likely that some of the increases in gene activation may be due to changes in histone methylation at sites not covered by the histone methylation screen, or by other mechanisms of gene regulation.

Data-mining was carried out to identify whether the IDH1 mutation was associated with changes in GABA-A receptor subunits *in vivo*. The GABRB3 and GABRA3 were increased in IDH mutant low grade glioma, but not GABRE or GABRQ. In fact these latter two genes were decreased in the IDH mutant low grade tumours, which was the opposite of what was observed in the microarray and RNA Seq data in the MOG-GCCM cell model. Other GABA-A receptor subunits were also reduced such as GABRA2 and GABRA5. This discrepancy may relate to the differing timescale of epigenetic change caused by the IDH1 mutation. Histone methylation changes seem to occur prior to DNA methylation, which is increased by the inhibitory effect of 2HG on TET2 enzyme [190, 255]. Our cell model was not propagated for more than thirty passages, so additional epigenetic changes caused by the IDH1 mutation may not have developed. The delayed increase in DNA methylation, which acts as a gene repressor, may be the reason why some of the GABA-A receptor subunits had reduced gene expression in vivo, but not in the MOG-GCCM cell model.

Unfortunately, GABRB3 protein changes in IDH1 mutant GBM tumour samples did not replicate the gene expression data. This discrepancy may reflect the small number of clinical samples that were used compared to the number of samples

in the TCGA and Oncomine datasets. However, inhibition of the GABA-A receptor did not have a specific effect on the IDH1 mutant clones on clonogenicity or cell migration when compared to the EV control. This may relate to issues with glioma cell lines in culture. Patch-clamping is a technique that can be used to measure the change in potential across the cell membrane after activation of the GABA-A receptor by GABA. The activity of the GABA-A receptor across a range of glioma cell lines has been measured but no functional activity could be detected. The same effect was also observed in GBM, but not low grade glioma tissue samples which had active GABA-A receptors. This suggests a possible downregulation of the receptor in culture and GBM which may explain why no significant differences were seen in GABRB3 protein expression between the IDH1 wild-type and mutant GBM tumour samples [286]. This would also make it difficult to interpret knockdown experiments if there were no functioning GABA-A receptors in cell culture.

Chapter 6 Conclusions

As described in the previous chapters, the IDH1 mutation leads to production of the "oncometabolite" 2HG from α-KG. Mass spectrometry analysis of clinical samples identified changes in intracellular metabolites in patients bearing IDH1 mutated tumours compared to wild-type tumours, which was confirmed in cell models. Besides the increase in 2HG, a decrease in α-KG, glutamate, and the glutamate derived metabolite GSH was observed. Conversely, there was an increase in GABA, NAA, and NAAG. This was due to an increased flux from α-KG to 2HG, and potentially from malate to NAA and NAAG, and from glutamate to GABA. The metabolic changes caused by the IDH1 mutation led to an increase in the 2HG/α-KG ratio, which resulted in increases in histone methylation, specifically at H3K4. H3K4me3 acts as a transcription activator and was shown to increase expression of GABRB3, a GABA-A receptor subunit.

The suggestion of an increased flux from glutamate to GABA generated the hypothesis that the fall in α-KG due to the IDH mutation may be driving an increased flux through the GABA shunt. In addition, the IDH1 mutation was associated with an increase in GABA uptake compared to wild-type controls, suggesting a benefit from GABA metabolism in IDH1 mutant cells. Increased GABA uptake and metabolism may compensate for the loss of α-KG to 2HG by providing additional carbon to the TCA cycle through the production of succinate. However, the addition of GABA to the MOG-GCCM and immortalised astrocytes did not result in any effect on clonogenicity, and Vigabatrin only had a modest effect. This may reflect the limitations of the cell models that were used. In vivo, astrocytes are essential to the glutamine-glutamate-GABA pathway and normally take up the neurotransmitters glutamate and GABA, metabolise them to glutamine, and secrete them for neuronal uptake and recycling. The MOG-GCCM and immortalised astrocytes both consumed glutamine and secreted glutamate, opposite of what is observed *in vivo*. This could be a consequence of the culture conditions, as these cells have been propagated in medium high in glutamine and without GABA. It would be interesting to see if this effect could be reversed in medium with low glutamine and high glutamate and GABA, and whether this has an effect on clonogenicity in the presence of Vigabatrin. Alternatively, the effect of Vigabatrin could be assessed by propagating IDH1 mutant cell lines in co-culture with GABA secreting neurons.

The large increase in the 2HG/α-KG ratio led to the investigation of how this may affect α-KG-dependent dioxygenases, in particular JMJ histone demethylases. A histone methylation screen was developed which identified an increase in histone methylation status of several histone methylation marks, which included H3K4 and H3K27. However, this screen was limited to five histone methylation sites, whereas over 50 histone methylation sites have been identified across all four histone proteins to date [287]. An alternative method of proteomic analysis using mass spectrometry could be used to increase the scope and range of this screen to potentially identify other histone methylation sites which are altered by the IDH1 mutation and may change gene expression. Mass spectrometry would be able to identify differences in histone mass caused by histone chemical modifications. This technique has the advantage of detecting numerous modifications at the same time as well as being more sensitive in detecting different degrees of methylation at the same site. It also has the ability to accurately quantify changes and identify new sites of histone methylation [287].

Using ChIP and RNA sequencing, increases in H3K4me3 around the TSS were associated with an increase in expression of the GABRB3 subunit, which forms part of the GABA-A receptor. This receptor exists as a pentameric assembly which can be formed from a combination of 19 different subunits (α1-6, β1-3, γ1-3, ρ1-3, δ, ε, θ and π), most commonly consisting of two α, two β, and one γ subunit [29]. The GABA-A receptor functions as an ionotropic receptor which on activation by GABA alters the cell membrane potential via an influx of Cl^- ions [6, 30]. These differences in subunit composition are likely to alter the sensitivity of the receptor to GABA activation, as some subunits are specific to different regions of the brain and to different stages of development [31]. For example, the α3 and β3 subunits, which were increased in EV + 2HG and MC9 cell lines and were found to be increased in glioma patient samples based on data-mining of the TCGA database (chapter 5), are predominantly expressed in the fetal brain and decline after birth [288]. Identifying whether the changes observed in IDH1 mutant cells could result in altered functionality could be achieved by patch clamping. With this technique, the change in voltage across the cell membrane can be measured. The addition of GABA to patch clamped cells from the MOG-GCCM, immortalised astrocytes, and NCH cell lines could

determine whether the IDH1 mutation results in an increased electrophysiological response to GABA via the GABA-A receptor, either through an increased number of receptors or increased sensitivity due to altered subunit composition. Using patch-clamping, functional GABA-A receptors have been identified on grade II and III gliomas, but not GBM [289]. GBM are predominately IDH1/2 wild-type and more aggressive than lower grade predominantly IDH1/2 mutant tumours, suggesting that there may be a growth inhibitory effect of the GABA-A receptor in these cells. An inhibitory growth effect of the GABA-A receptor has been shown in astrocytic stem cells and glioma cells that have been cultured in the presence of GABA secreting neuronal cells [285]. In addition, glioma cells only expressed functional GABA-A receptors when in contact with neurons and not with other glial cells [290]. In fact, increases in a specific microRNA, miR-155, in both primary and secondary GBM has been shown to inhibit the GABRA1 protein resulting in an increase in cell proliferation [291]. A similar effect has also been observed in medulloblastoma, a brain tumour more common in children, where cancer cell survival was decreased by a potent GABRA5 protein agonist [292]. In addition, suppression of GABRB3 protein expression by RNA interference has been shown to increase cell proliferation in embryonic stem cells [293]. This suggests that the GABA-A receptor acts as a negative feedback growth mechanism and may provide an explanation as to why IDH1 mutant gliomas have a slower growth rate than wild-type tumours. However, neurons have also been shown to promote high grade glioma growth through the secretion of neuroligin-3 which induces PI3K-mTOR signalling [294]. This indicates that neurons may have a variable complex effect on glioma growth and may depend on the neuron and tumour sub-type.

GABA can also activate another type of receptor called the GABA-B receptor. These are heterodimeric G-protein coupled receptors which are formed from three major subunits; $GABA_{B1a,}$ $GABA_{B1b,}$ and $GABA_{B2}$. Activation of these receptors leads to an increase in intracellular Ca^{2+} concentration, most likely from intracellular Ca^{2+} stores [32]. Like GABA-A receptors, activation of GABA-B receptors by GABA results in a reduction in cell proliferation [295, 296]. However, only 10% of astrocytes respond to GABA-B receptor stimulation, compared to over 70% of astrocytes to GABA-A receptor stimulation [32]. This suggests that the GABA-A receptor may play a more dominant role in these cells.

The increase in intracellular GABA observed *in vitro* and *in vivo* caused by the IDH1 mutation raises the possibility of autocrine and paracrine activation of the GABA-A receptor in IDH1 mutant tumours. Astrocytes are classically associated with the uptake of GABA from neurons, which they then metabolise to glutamine for secretion. However, astrocytes have also been shown to secrete GABA *de novo*, activating neighbouring GABA-A receptors [297]. This suggests the possibility that glioma cells are also able to activate GABA-A receptors in a paracrine or autocrine fashion. Through this mechanism, cancer cells that are not at the periphery of the tumour and may not be exposed to GABA derived from neurons may be affected by endogenously produced GABA.

The increase in GABA metabolism and the increase in expression of some subunits of the GABA-A receptor may provide a potential target for therapy. A potential increase in flux through GABA-T was identified in one of the IDH1 mutant NCH cell lines compared to the wild-type controls. An increased flux through this pathway may benefit the IDH1 mutant cells by bypassing the IDH1 mutation. Vigabatrin, a GABA transaminase inhibitor, is currently an off patent licensed drug for the treatment of juvenile epilepsy. It works by increasing the concentration of GABA in the brain, thereby utilising the neuroinhibitory effect of the metabolite to increase the threshold for seizures. Vigabatrin could have a negative effect on cell proliferation in IDH1 mutant tumours by both disrupting the catabolism of GABA, and by increasing the GABA concentration in the brain enhancing the negative proliferative effect of the GABA-A receptor. The best way to determine efficacy would be an *in vivo* model. This could be achieved by using an orthotopic mouse model using the IDH1 wild-type and mutant NCH cell lines to assess the effect of Vigabatrin on tumour growth. It would also be interesting to determine whether these same effects occurred with the IDH2 mutation. This enzyme is mitochondrial so it may be more dependent on GABA metabolism to generate succinate and maintain TCA metabolites.

In summary, the IDH1 mutation results in an increase in 2HG production consuming α-KG. There is a corresponding reduction in TCA metabolites and glutamate, but an increase in NAA, NAAG and GABA, the latter possibly due to an increase in flux through the GABA shunt. In addition, IDH1 mutant cells may utilise exogenous GABA as an alternative source of carbon for the TCA cycle. The increase in the 2HG/α-KG ratio results in the inhibition of JMJ histone

demethylases causing an increase in H3K4 methylation. An increase in H3K4me3 around the TSS of GABRB3, a subunit of the GABA-A receptor, results in increased gene expression. This in conjunction with an increased expression of other GABA-A receptor subunits (observed in the TCGA dataset and MOG-GCCM cells, chapter 5) could result in an increase in functional receptors on the cell surface. Activation of the GABA-A receptor could result from exogenous GABA derived from neurons, or endogenous GABA acting in a paracrine or autocrine fashion. GABA transaminase may be a potential therapeutic target as inhibition of the enzyme would reduce flux through the GABA shunt, reduce GABA as a carbon source for the TCA cycle, and increase the concentration of GABA in the brain increasing activation of the GABA-A receptor. All these effects may result in a reduction in cell proliferation and could be tested in an orthotopic mouse model by using Vigabatrin, a specific GABA transaminase inhibitor licensed for use in epilepsy (Figure 6-1).

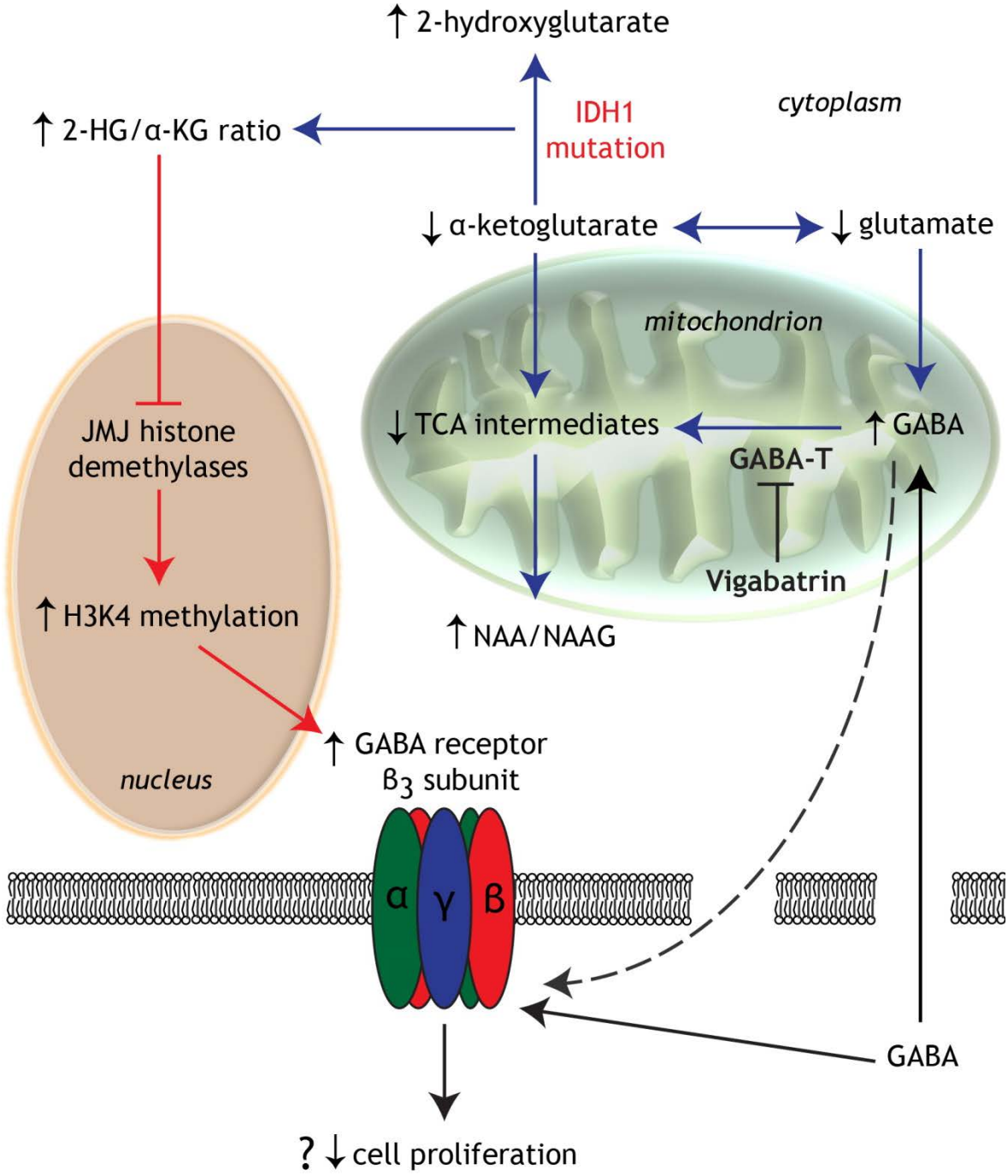

Figure 6-1 Hypothetical model depicting the possible consequences of the metabolic and genetic changes caused by the IDH1 mutation

The IDH1 mutation results in an increase in 2HG production consuming α-KG. There is a corresponding fall in TCA metabolites and glutamate, an increase NAA and NAAG, and an rise in GABA, possibly due to an increased flux through the GABA shunt. In addition, exogenous GABA may also be utilised as an alternative source of carbon for the TCA cycle. The increase in the 2HG/α-KG ratio results in the inhibition of JMJ histone demethylases causing an increase in H3K4 methylation. An increase in H3K4me3 around the TSS of GABRB3, a subunit of the GABA-A receptor, results in increased gene expression. This could result in an increase in GABA-A receptors which could be activated either in an autocrine or paracrine fashion or by exogenous GABA. GABA-A receptor activation is associated with a decrease in cell proliferation so inhibition of GABA-T by Vigabatrin could potentiate this effect by increasing GABA concentration in the brain and reducing the ability of IDH1 mutant cells to metabolise GABA.

List of References

1. Nowicki S & Gottlieb E (2015) Oncometabolites: tailoring our genes. *Febs J* **282**, 2796-2805, doi: 10.1111/febs.13295.
2. Hodgkin AL & Huxley AF (1952) A quantitative description of membrane current and its application to conduction and excitation in nerve. *J Physiol* **117**, 500-544.
3. Virchow R (1856) *Gesammelte Abhandlungen zur wissenschaftlichen Medicin*. Verlag von Meidinger Sohn, Frankfurt a.M.,.
4. Lenhossék M (1893) *Die geschmacksknospen in den blattförmigen papillen der kaninchenzunge*. Stahel, Würzburg,.
5. Weigert C (1895) *Beitra\0308ge zur Kenntnis der normalen menschlichen Neuroglia ... Mit dreizehn Tafeln. Separatabdruck aus den Abhandlungen der Senckenbergischen naturforschenden Gesellschaft*. pp. vi. 65-213. Frankfurt a. M.
6. Kettenmann H, Backus KH & Schachner M (1984) Aspartate, glutamate and gamma-aminobutyric acid depolarize cultured astrocytes. *Neurosci Lett* **52**, 25-29.
7. Verkhratsky A & Steinhauser C (2000) Ion channels in glial cells. *Brain Res Brain Res Rev* **32**, 380-412.
8. Volterra A & Meldolesi J (2005) Astrocytes, from brain glue to communication elements: the revolution continues. *Nat Rev Neurosci* **6**, 626-640, doi: 10.1038/nrn1722.
9. Pankratov Y, Lalo U, Verkhratsky A & North RA (2006) Vesicular release of ATP at central synapses. *Pflugers Arch* **452**, 589-597, doi: 10.1007/s00424-006-0061-x.
10. Tzingounis AV & Wadiche JI (2007) Glutamate transporters: confining runaway excitation by shaping synaptic transmission. *Nat Rev Neurosci* **8**, 935-947, doi: 10.1038/nrn2274.
11. Oberheim NA, Wang X, Goldman S & Nedergaard M (2006) Astrocytic complexity distinguishes the human brain. *Trends Neurosci* **29**, 547-553, doi: 10.1016/j.tins.2006.08.004.
12. Chen Y & Swanson RA (2003) Astrocytes and brain injury. *J Cereb Blood Flow Metab* **23**, 137-149.
13. Cornell-Bell AH, Finkbeiner SM, Cooper MS & Smith SJ (1990) Glutamate induces calcium waves in cultured astrocytes: long-range glial signaling. *Science* **247**, 470-473.
14. Verkhratsky A & Kettenmann H (1996) Calcium signalling in glial cells. *Trends Neurosci* **19**, 346-352.
15. Giaume C & McCarthy KD (1996) Control of gap-junctional communication in astrocytic networks. *Trends Neurosci* **19**, 319-325.
16. Pinto L & Gotz M (2007) Radial glial cell heterogeneity--the source of diverse progeny in the CNS. *Prog Neurobiol* **83**, 2-23, doi: 10.1016/j.pneurobio.2007.02.010.
17. Deng W, Wang H, Rosenberg PA, Volpe JJ & Jensen FE (2004) Role of metabotropic glutamate receptors in oligodendrocyte excitotoxicity and oxidative stress. *Proc Natl Acad Sci U S A* **101**, 7751-7756, doi: 10.1073/pnas.0307850101.

18. Karadottir R, Cavelier P, Bergersen LH & Attwell D (2005) NMDA receptors are expressed in oligodendrocytes and activated in ischaemia. *Nature* **438**, 1162-1166, doi: 10.1038/nature04302.
19. Salter MG & Fern R (2005) NMDA receptors are expressed in developing oligodendrocyte processes and mediate injury. *Nature* **438**, 1167-1171, doi: 10.1038/nature04301.
20. Nimmerjahn A, Kirchhoff F & Helmchen F (2005) Resting microglial cells are highly dynamic surveillants of brain parenchyma in vivo. *Science* **308**, 1314-1318, doi: 10.1126/science.1110647.
21. Aloisi F (2001) Immune function of microglia. *Glia* **36**, 165-179.
22. Raimundo N, Baysal BE & Shadel GS (2011) Revisiting the TCA cycle: signaling to tumor formation. *Trends Mol Med* **17**, 641-649, doi: 10.1016/j.molmed.2011.06.001.
23. Scheffler IE (2008) *Mitochondria*. 2nd ed. edn. Wiley-Liss ; Chichester : John Wiley [distributor], Hoboken, N.J.
24. Satrustegui J & Bak LK (2015) Fluctuations in Cytosolic Calcium Regulate the Neuronal Malate-Aspartate NADH Shuttle: Implications for Neuronal Energy Metabolism. *Neurochem Res* **40**, 2425-2430, doi: 10.1007/s11064-015-1652-8.
25. van den Berg CJ & Garfinkel D (1971) A stimulation study of brain compartments. Metabolism of glutamate and related substances in mouse brain. *Biochem J* **123**, 211-218.
26. Bauer DE, Jackson JG, Genda EN, Montoya MM, Yudkoff M & Robinson MB (2012) The glutamate transporter, GLAST, participates in a macromolecular complex that supports glutamate metabolism. *Neurochem Int* **61**, 566-574, doi: 10.1016/j.neuint.2012.01.013.
27. McKenna MC (2012) Substrate competition studies demonstrate oxidative metabolism of glucose, glutamate, glutamine, lactate and 3-hydroxybutyrate in cortical astrocytes from rat brain. *Neurochem Res* **37**, 2613-2626, doi: 10.1007/s11064-012-0901-3.
28. Rothman DL, De Feyter HM, de Graaf RA, Mason GF & Behar KL (2011) 13C MRS studies of neuroenergetics and neurotransmitter cycling in humans. *NMR Biomed* **24**, 943-957, doi: 10.1002/nbm.1772.
29. Macdonald RL & Olsen RW (1994) GABAA receptor channels. *Annu Rev Neurosci* **17**, 569-602, doi: 10.1146/annurev.ne.17.030194.003033.
30. Nilsson M, Eriksson PS, Ronnback L & Hansson E (1993) GABA induces Ca2+ transients in astrocytes. *Neuroscience* **54**, 605-614.
31. Wisden W & Seeburg PH (1992) GABAA receptor channels: from subunits to functional entities. *Curr Opin Neurobiol* **2**, 263-269.
32. Meier SD, Kafitz KW & Rose CR (2008) Developmental profile and mechanisms of GABA-induced calcium signaling in hippocampal astrocytes. *Glia* **56**, 1127-1137, doi: 10.1002/glia.20684.
33. Chen K, Li HZ, Ye N, Zhang J & Wang JJ (2005) Role of GABAB receptors in GABA and baclofen-induced inhibition of adult rat cerebellar interpositus nucleus neurons in vitro. *Brain Res Bull* **67**, 310-318, doi: 10.1016/j.brainresbull.2005.07.004.
34. Padgett CL & Slesinger PA (2010) GABAB receptor coupling to G-proteins and ion channels. *Adv Pharmacol* **58**, 123-147, doi: 10.1016/S1054-3589(10)58006-2.
35. Hertz L, Wu PH & Schousboe A (1978) Evidence for net uptake of GABA into mouse astrocytes in primary cultures--its sodium dependence and potassium independence. *Neurochem Res* **3**, 313-323.

36. Hearl WG & Churchich JE (1984) Interactions between 4-aminobutyrate aminotransferase and succinic semialdehyde dehydrogenase, two mitochondrial enzymes. *J Biol Chem* **259**, 11459-11463.
37. Schousboe A, Wu JY & Roberts E (1974) Subunit structure and kinetic properties of 4-aminobutyrate-2-ketoglutarate transaminase purified from mouse brain. *J Neurochem* **23**, 1189-1195.
38. Kurz GM, Wiesinger H & Hamprecht B (1993) Purification of cytosolic malic enzyme from bovine brain, generation of monoclonal antibodies, and immunocytochemical localization of the enzyme in glial cells of neural primary cultures. *J Neurochem* **60**, 1467-1474.
39. Patel AB, de Graaf RA, Mason GF, Rothman DL, Shulman RG & Behar KL (2005) The contribution of GABA to glutamate/glutamine cycling and energy metabolism in the rat cortex in vivo. *Proc Natl Acad Sci U S A* **102**, 5588-5593, doi: 10.1073/pnas.0501703102.
40. Fait A, Fromm H, Walter D, Galili G & Fernie AR (2008) Highway or byway: the metabolic role of the GABA shunt in plants. *Trends Plant Sci* **13**, 14-19, doi: 10.1016/j.tplants.2007.10.005.
41. Feehily C & Karatzas KA (2013) Role of glutamate metabolism in bacterial responses towards acid and other stresses. *J Appl Microbiol* **114**, 11-24, doi: 10.1111/j.1365-2672.2012.05434.x.
42. Mamelak M (2012) Sporadic Alzheimer's disease: the starving brain. *J Alzheimers Dis* **31**, 459-474, doi: 10.3233/JAD-2012-120370.
43. Seo JY, Lee CH, Cho JH, Choi JH, Yoo KY, Kim DW, Park OK, Li H, Choi SY, Hwang IK, et al. (2009) Neuroprotection of ebselen against ischemia/reperfusion injury involves GABA shunt enzymes. *J Neurol Sci* **285**, 88-94, doi: 10.1016/j.jns.2009.05.029.
44. Pascual JM, Carceller F, Roda JM & Cerdan S (1998) Glutamate, glutamine, and GABA as substrates for the neuronal and glial compartments after focal cerebral ischemia in rats. *Stroke* **29**, 1048-1056; discussion 1056-1047.
45. Yogeeswari P, Sriram D & Vaigundaragavendran J (2005) The GABA shunt: an attractive and potential therapeutic target in the treatment of epileptic disorders. *Curr Drug Metab* **6**, 127-139.
46. Grant SM & Heel RC (1991) Vigabatrin. A review of its pharmacodynamic and pharmacokinetic properties, and therapeutic potential in epilepsy and disorders of motor control. *Drugs* **41**, 889-926.
47. Hammond EJ & Wilder BJ (1985) Gamma-vinyl GABA. *Gen Pharmacol* **16**, 441-447.
48. Lanctot KL, Herrmann N, Mazzotta P, Khan LR & Ingber N (2004) GABAergic function in Alzheimer's disease: evidence for dysfunction and potential as a therapeutic target for the treatment of behavioural and psychological symptoms of dementia. *Can J Psychiatry* **49**, 439-453.
49. Salminen A, Jouhten P, Sarajarvi T, Haapasalo A & Hiltunen M (2016) Hypoxia and GABA shunt activation in the pathogenesis of Alzheimer's disease. *Neurochem Int* **92**, 13-24, doi: 10.1016/j.neuint.2015.11.005.
50. Michaeli S, Fait A, Lagor K, Nunes-Nesi A, Grillich N, Yellin A, Bar D, Khan M, Fernie AR, Turano FJ, et al. (2011) A mitochondrial GABA permease connects the GABA shunt and the TCA cycle, and is essential for normal carbon metabolism. *Plant J* **67**, 485-498, doi: 10.1111/j.1365-313X.2011.04612.x.
51. Brand MD & Chappell JB (1974) Permeability of mitochondria from rat brain and rat liver to GABA. *J Neurochem* **22**, 47-51.

52. Walsh JM & Clark JB (1976) Studies on the control of 4-aminobutyrate metabolism in 'synaptosomal' and free rat brain mitochondria. *Biochem J* **160**, 147-157.
53. Mehta V & Namboodiri MA (1995) N-acetylaspartate as an acetyl source in the nervous system. *Brain Res Mol Brain Res* **31**, 151-157.
54. Matalon R (1997) Canavan disease: diagnosis and molecular analysis. *Genet Test* **1**, 21-25, doi: 10.1089/gte.1997.1.21.
55. Hershfield JR, Madhavarao CN, Moffett JR, Benjamins JA, Garbern JY & Namboodiri A (2006) Aspartoacylase is a regulated nuclear-cytoplasmic enzyme. *Faseb J* **20**, 2139-2141, doi: 10.1096/fj.05-5358fje.
56. Ariyannur PS, Moffett JR, Madhavarao CN, Arun P, Vishnu N, Jacobowitz DM, Hallows WC, Denu JM & Namboodiri AM (2010) Nuclear-cytoplasmic localization of acetyl coenzyme a synthetase-1 in the rat brain. *J Comp Neurol* **518**, 2952-2977, doi: 10.1002/cne.22373.
57. Wroblewska B, Santi MR & Neale JH (1998) N-acetylaspartylglutamate activates cyclic AMP-coupled metabotropic glutamate receptors in cerebellar astrocytes. *Glia* **24**, 172-179.
58. Schoepp DD, Jane DE & Monn JA (1999) Pharmacological agents acting at subtypes of metabotropic glutamate receptors. *Neuropharmacology* **38**, 1431-1476.
59. Coyle JT (1997) The nagging question of the function of N-acetylaspartylglutamate. *Neurobiol Dis* **4**, 231-238, doi: 10.1006/nbdi.1997.0153.
60. Long PM, Moffett JR, Namboodiri AM, Viapiano MS, Lawler SE & Jaworski DM (2013) N-acetylaspartate (NAA) and N-acetylaspartylglutamate (NAAG) promote growth and inhibit differentiation of glioma stem-like cells. *J Biol Chem* **288**, 26188-26200, doi: 10.1074/jbc.M113.487553.
61. Goldstein FB (1959) Biosynthesis of N-acetyl-L-aspartic acid. *Biochim Biophys Acta* **33**, 583-584.
62. Tyson RL & Sutherland GR (1998) Labeling of N-acetylaspartate and N-acetylaspartylglutamate in rat neocortex, hippocampus and cerebellum from [1-13C]glucose. *Neurosci Lett* **251**, 181-184.
63. D'Adamo AF, Jr., Smith JC & Woiler C (1973) The occurrence of N-acetylaspartate amidohydrolase (aminoacylase II) in the developing rat. *J Neurochem* **20**, 1275-1278.
64. Goldberg RP & Brunengraber H (1980) Contributions of cytosolic and mitochondrial acetyl-CoA syntheses to the activation of lipogenic acetate in rat liver. *Adv Exp Med Biol* **132**, 413-418.
65. Fujino T, Kondo J, Ishikawa M, Morikawa K & Yamamoto TT (2001) Acetyl-CoA synthetase 2, a mitochondrial matrix enzyme involved in the oxidation of acetate. *J Biol Chem* **276**, 11420-11426, doi: 10.1074/jbc.M008782200.
66. Moffett JR, Ross B, Arun P, Madhavarao CN & Namboodiri AM (2007) N-Acetylaspartate in the CNS: from neurodiagnostics to neurobiology. *Prog Neurobiol* **81**, 89-131, doi: 10.1016/j.pneurobio.2006.12.003.
67. Berger UV, Luthi-Carter R, Passani LA, Elkabes S, Black I, Konradi C & Coyle JT (1999) Glutamate carboxypeptidase II is expressed by astrocytes in the adult rat nervous system. *J Comp Neurol* **415**, 52-64.
68. Rothman DL, Sibson NR, Hyder F, Shen J, Behar KL & Shulman RG (1999) In vivo nuclear magnetic resonance spectroscopy studies of the relationship between the glutamate-glutamine neurotransmitter cycle and functional neuroenergetics. *Philos Trans R Soc Lond B Biol Sci* **354**, 1165-1177, doi: 10.1098/rstb.1999.0472.

69. Baslow MH (2000) Functions of N-acetyl-L-aspartate and N-acetyl-L-aspartylglutamate in the vertebrate brain: role in glial cell-specific signaling. *J Neurochem* **75**, 453-459.
70. Ostrom QT, Gittleman H, Farah P, Ondracek A, Chen Y, Wolinsky Y, Stroup NE, Kruchko C & Barnholtz-Sloan JS (2013) CBTRUS statistical report: Primary brain and central nervous system tumors diagnosed in the United States in 2006-2010. *Neuro-oncology* **15 Suppl 2**, ii1-56, doi: 10.1093/neuonc/not151.
71. Ferlay J, Soerjomataram I, Dikshit R, Eser S, Mathers C, Rebelo M, Parkin DM, Forman D & Bray F (2015) Cancer incidence and mortality worldwide: sources, methods and major patterns in GLOBOCAN 2012. *International journal of cancer Journal international du cancer* **136**, E359-386, doi: 10.1002/ijc.29210.
72. Ostrom QT, Bauchet L, Davis FG, Deltour I, Fisher JL, Langer CE, Pekmezci M, Schwartzbaum JA, Turner MC, Walsh KM, et al. (2014) The epidemiology of glioma in adults: a "state of the science" review. *Neuro-oncology* **16**, 896-913, doi: 10.1093/neuonc/nou087.
73. McCormack BM, Miller DC, Budzilovich GN, Voorhees GJ & Ransohoff J (1992) Treatment and survival of low-grade astrocytoma in adults--1977-1988. *Neurosurgery* **31**, 636-642; discussion 642.
74. Ostrom QT, Gittleman H, Liao P, Rouse C, Chen Y, Dowling J, Wolinsky Y, Kruchko C & Barnholtz-Sloan J (2014) CBTRUS statistical report: primary brain and central nervous system tumors diagnosed in the United States in 2007-2011. *Neuro Oncol* **16 Suppl 4**, iv1-63, doi: 10.1093/neuonc/nou223.
75. Ohgaki H, Dessen P, Jourde B, Horstmann S, Nishikawa T, Di Patre PL, Burkhard C, Schuler D, Probst-Hensch NM, Maiorka PC, et al. (2004) Genetic pathways to glioblastoma: a population-based study. *Cancer Res* **64**, 6892-6899, doi: 10.1158/0008-5472.CAN-04-1337.
76. Ferlay J, Steliarova-Foucher E, Lortet-Tieulent J, Rosso S, Coebergh JW, Comber H, Forman D & Bray F (2013) Cancer incidence and mortality patterns in Europe: estimates for 40 countries in 2012. *Eur J Cancer* **49**, 1374-1403, doi: 10.1016/j.ejca.2012.12.027.
77. Cavanagh JB (1970) The proliferation of astrocytes around a needle wound in the rat brain. *J Anat* **106**, 471-487.
78. Jones TR, Bigner SH, Schold SC, Jr., Eng LF & Bigner DD (1981) Anaplastic human gliomas grown in athymic mice. Morphology and glial fibrillary acidic protein expression. *Am J Pathol* **105**, 316-327.
79. Dufour C, Cadusseau J, Varlet P, Surena AL, de Faria GP, Dias-Morais A, Auger N, Leonard N, Daudigeos E, Dantas-Barbosa C, et al. (2009) Astrocytes reverted to a neural progenitor-like state with transforming growth factor alpha are sensitized to cancerous transformation. *Stem Cells* **27**, 2373-2382, doi: 10.1002/stem.155.
80. Bachoo RM, Maher EA, Ligon KL, Sharpless NE, Chan SS, You MJ, Tang Y, DeFrances J, Stover E, Weissleder R, et al. (2002) Epidermal growth factor receptor and Ink4a/Arf: convergent mechanisms governing terminal differentiation and transformation along the neural stem cell to astrocyte axis. *Cancer Cell* **1**, 269-277.
81. Reynolds BA & Weiss S (1992) Generation of neurons and astrocytes from isolated cells of the adult mammalian central nervous system. *Science* **255**, 1707-1710.
82. Eriksson PS, Perfilieva E, Bjork-Eriksson T, Alborn AM, Nordborg C, Peterson DA & Gage FH (1998) Neurogenesis in the adult human hippocampus. *Nat Med* **4**, 1313-1317, doi: 10.1038/3305.

83. Barami K, Sloan AE, Rojiani A, Schell MJ, Staller A & Brem S (2009) Relationship of gliomas to the ventricular walls. *J Clin Neurosci* **16**, 195-201, doi: 10.1016/j.jocn.2008.03.006.
84. (2008) Comprehensive genomic characterization defines human glioblastoma genes and core pathways. *Nature* **455**, 1061-1068, doi: 10.1038/nature07385.
85. Zhu Y, Guignard F, Zhao D, Liu L, Burns DK, Mason RP, Messing A & Parada LF (2005) Early inactivation of p53 tumor suppressor gene cooperating with NF1 loss induces malignant astrocytoma. *Cancer Cell* **8**, 119-130, doi: 10.1016/j.ccr.2005.07.004.
86. Zappone MV, Galli R, Catena R, Meani N, De Biasi S, Mattei E, Tiveron C, Vescovi AL, Lovell-Badge R, Ottolenghi S, et al. (2000) Sox2 regulatory sequences direct expression of a (beta)-geo transgene to telencephalic neural stem cells and precursors of the mouse embryo, revealing regionalization of gene expression in CNS stem cells. *Development* **127**, 2367-2382.
87. Shoshan Y, Nishiyama A, Chang A, Mork S, Barnett GH, Cowell JK, Trapp BD & Staugaitis SM (1999) Expression of oligodendrocyte progenitor cell antigens by gliomas: implications for the histogenesis of brain tumors. *Proc Natl Acad Sci U S A* **96**, 10361-10366.
88. Persson AI, Petritsch C, Swartling FJ, Itsara M, Sim FJ, Auvergne R, Goldenberg DD, Vandenberg SR, Nguyen KN, Yakovenko S, et al. (2010) Non-stem cell origin for oligodendroglioma. *Cancer Cell* **18**, 669-682, doi: 10.1016/j.ccr.2010.10.033.
89. Liu C, Sage JC, Miller MR, Verhaak RG, Hippenmeyer S, Vogel H, Foreman O, Bronson RT, Nishiyama A, Luo L, et al. (2011) Mosaic analysis with double markers reveals tumor cell of origin in glioma. *Cell* **146**, 209-221, doi: 10.1016/j.cell.2011.06.014.
90. Brennan CW, Verhaak RG, McKenna A, Campos B, Noushmehr H, Salama SR, Zheng S, Chakravarty D, Sanborn JZ, Berman SH, et al. (2013) The somatic genomic landscape of glioblastoma. *Cell* **155**, 462-477, doi: 10.1016/j.cell.2013.09.034.
91. Humphrey PA, Wong AJ, Vogelstein B, Zalutsky MR, Fuller GN, Archer GE, Friedman HS, Kwatra MM, Bigner SH & Bigner DD (1990) Anti-synthetic peptide antibody reacting at the fusion junction of deletion-mutant epidermal growth factor receptors in human glioblastoma. *Proc Natl Acad Sci U S A* **87**, 4207-4211.
92. Frattini V, Trifonov V, Chan JM, Castano A, Lia M, Abate F, Keir ST, Ji AX, Zoppoli P, Niola F, et al. (2013) The integrated landscape of driver genomic alterations in glioblastoma. *Nat Genet* **45**, 1141-1149, doi: 10.1038/ng.2734.
93. Singh D, Chan JM, Zoppoli P, Niola F, Sullivan R, Castano A, Liu EM, Reichel J, Porrati P, Pellegatta S, et al. (2012) Transforming fusions of FGFR and TACC genes in human glioblastoma. *Science* **337**, 1231-1235, doi: 10.1126/science.1220834.
94. Parsons DW, Jones S, Zhang X, Lin JC, Leary RJ, Angenendt P, Mankoo P, Carter H, Siu IM, Gallia GL, et al. (2008) An integrated genomic analysis of human glioblastoma multiforme. *Science* **321**, 1807-1812, doi: 10.1126/science.1164382.
95. Yan H, Parsons DW, Jin G, McLendon R, Rasheed BA, Yuan W, Kos I, Batinic-Haberle I, Jones S, Riggins GJ, et al. (2009) IDH1 and IDH2 mutations in gliomas. *N Engl J Med* **360**, 765-773, doi: 10.1056/NEJMoa0808710.
96. Reifenberger J, Reifenberger G, Liu L, James CD, Wechsler W & Collins VP (1994) Molecular genetic analysis of oligodendroglial tumors shows preferential allelic deletions on 19q and 1p. *Am J Pathol* **145**, 1175-1190.

97. Jiao Y, Killela PJ, Reitman ZJ, Rasheed AB, Heaphy CM, de Wilde RF, Rodriguez FJ, Rosemberg S, Oba-Shinjo SM, Nagahashi Marie SK, et al. (2012) Frequent ATRX, CIC, FUBP1 and IDH1 mutations refine the classification of malignant gliomas. *Oncotarget* **3**, 709-722.
98. van den Bent MJ, Brandes AA, Taphoorn MJ, Kros JM, Kouwenhoven MC, Delattre JY, Bernsen HJ, Frenay M, Tijssen CC, Grisold W, et al. (2013) Adjuvant procarbazine, lomustine, and vincristine chemotherapy in newly diagnosed anaplastic oligodendroglioma: long-term follow-up of EORTC brain tumor group study 26951. *J Clin Oncol* **31**, 344-350, doi: 10.1200/JCO.2012.43.2229.
99. Esteller M, Garcia-Foncillas J, Andion E, Goodman SN, Hidalgo OF, Vanaclocha V, Baylin SB & Herman JG (2000) Inactivation of the DNA-repair gene MGMT and the clinical response of gliomas to alkylating agents. *N Engl J Med* **343**, 1350-1354, doi: 10.1056/NEJM200011093431901.
100. Hegi ME, Diserens AC, Gorlia T, Hamou MF, de Tribolet N, Weller M, Kros JM, Hainfellner JA, Mason W, Mariani L, et al. (2005) MGMT gene silencing and benefit from temozolomide in glioblastoma. *N Engl J Med* **352**, 997-1003, doi: 10.1056/NEJMoa043331.
101. Everhard S, Kaloshi G, Criniere E, Benouaich-Amiel A, Lejeune J, Marie Y, Sanson M, Kujas M, Mokhtari K, Hoang-Xuan K, et al. (2006) MGMT methylation: a marker of response to temozolomide in low-grade gliomas. *Ann Neurol* **60**, 740-743, doi: 10.1002/ana.21044.
102. Leu S, von Felten S, Frank S, Vassella E, Vajtai I, Taylor E, Schulz M, Hutter G, Hench J, Schucht P, et al. (2013) IDH/MGMT-driven molecular classification of low-grade glioma is a strong predictor for long-term survival. *Neuro Oncol* **15**, 469-479, doi: 10.1093/neuonc/nos317.
103. Sadones J, Michotte A, Veld P, Chaskis C, Sciot R, Menten J, Joossens EJ, Strauven T, D'Hondt LA, Sartenaer D, et al. (2009) MGMT promoter hypermethylation correlates with a survival benefit from temozolomide in patients with recurrent anaplastic astrocytoma but not glioblastoma. *Eur J Cancer* **45**, 146-153, doi: 10.1016/j.ejca.2008.09.002.
104. von Deimling A, von Ammon K, Schoenfeld D, Wiestler OD, Seizinger BR & Louis DN (1993) Subsets of glioblastoma multiforme defined by molecular genetic analysis. *Brain Pathol* **3**, 19-26.
105. Phillips HS, Kharbanda S, Chen R, Forrest WF, Soriano RH, Wu TD, Misra A, Nigro JM, Colman H, Soroceanu L, et al. (2006) Molecular subclasses of high-grade glioma predict prognosis, delineate a pattern of disease progression, and resemble stages in neurogenesis. *Cancer Cell* **9**, 157-173, doi: 10.1016/j.ccr.2006.02.019.
106. Verhaak RG, Hoadley KA, Purdom E, Wang V, Qi Y, Wilkerson MD, Miller CR, Ding L, Golub T, Mesirov JP, et al. (2010) Integrated genomic analysis identifies clinically relevant subtypes of glioblastoma characterized by abnormalities in PDGFRA, IDH1, EGFR, and NF1. *Cancer Cell* **17**, 98-110, doi: 10.1016/j.ccr.2009.12.020.
107. Noushmehr H, Weisenberger DJ, Diefes K, Phillips HS, Pujara K, Berman BP, Pan F, Pelloski CE, Sulman EP, Bhat KP, et al. (2010) Identification of a CpG island methylator phenotype that defines a distinct subgroup of glioma. *Cancer Cell* **17**, 510-522, doi: 10.1016/j.ccr.2010.03.017.
108. Sturm D, Witt H, Hovestadt V, Khuong-Quang DA, Jones DT, Konermann C, Pfaff E, Tonjes M, Sill M, Bender S, et al. (2012) Hotspot mutations in H3F3A and IDH1 define distinct epigenetic and biological subgroups of glioblastoma. *Cancer Cell* **22**, 425-437, doi: 10.1016/j.ccr.2012.08.024.
109. Brat DJ & Verhaak RG & Aldape KD & Yung WK & Salama SR & Cooper LA & Rheinbay E & Miller CR & Vitucci M & Morozova O, et al. (2015) Comprehensive,

Integrative Genomic Analysis of Diffuse Lower-Grade Gliomas. *N Engl J Med* **372**, 2481-2498, doi: 10.1056/NEJMoa1402121.
110. Wiestler B, Capper D, Sill M, Jones DT, Hovestadt V, Sturm D, Koelsche C, Bertoni A, Schweizer L, Korshunov A, et al. (2014) Integrated DNA methylation and copy-number profiling identify three clinically and biologically relevant groups of anaplastic glioma. *Acta Neuropathol* **128**, 561-571, doi: 10.1007/s00401-014-1315-x.
111. Simpson JR, Horton J, Scott C, Curran WJ, Rubin P, Fischbach J, Isaacson S, Rotman M, Asbell SO, Nelson JS, et al. (1993) Influence of location and extent of surgical resection on survival of patients with glioblastoma multiforme: results of three consecutive Radiation Therapy Oncology Group (RTOG) clinical trials. *International journal of radiation oncology, biology, physics* **26**, 239-244.
112. Gorlia T, Delattre JY, Brandes AA, Kros JM, Taphoorn MJ, Kouwenhoven MC, Bernsen HJ, Frenay M, Tijssen CC, Lacombe D, et al. (2013) New clinical, pathological and molecular prognostic models and calculators in patients with locally diagnosed anaplastic oligodendroglioma or oligoastrocytoma. A prognostic factor analysis of European Organisation for Research and Treatment of Cancer Brain Tumour Group Study 26951. *Eur J Cancer* **49**, 3477-3485, doi: 10.1016/j.ejca.2013.06.039.
113. Jakola AS, Myrmel KS, Kloster R, Torp SH, Lindal S, Unsgard G & Solheim O (2012) Comparison of a strategy favoring early surgical resection vs a strategy favoring watchful waiting in low-grade gliomas. *Jama* **308**, 1881-1888, doi: 10.1001/jama.2012.12807.
114. Chang EF, Potts MB, Keles GE, Lamborn KR, Chang SM, Barbaro NM & Berger MS (2008) Seizure characteristics and control following resection in 332 patients with low-grade gliomas. *J Neurosurg* **108**, 227-235, doi: 10.3171/JNS/2008/108/2/0227.
115. Pignatti F, van den Bent M, Curran D, Debruyne C, Sylvester R, Therasse P, Afra D, Cornu P, Bolla M, Vecht C, et al. (2002) Prognostic factors for survival in adult patients with cerebral low-grade glioma. *J Clin Oncol* **20**, 2076-2084.
116. Diez Valle R & Tejada Solis S (2015) To what extent will 5-aminolevulinic acid change the face of malignant glioma surgery? *CNS Oncol* **4**, 265-272, doi: 10.2217/cns.15.10.
117. Walker MD, Strike TA & Sheline GE (1979) An analysis of dose-effect relationship in the radiotherapy of malignant gliomas. *International journal of radiation oncology, biology, physics* **5**, 1725-1731.
118. Walker MD, Alexander E, Jr., Hunt WE, MacCarty CS, Mahaley MS, Jr., Mealey J, Jr., Norrell HA, Owens G, Ransohoff J, Wilson CB, et al. (1978) Evaluation of BCNU and/or radiotherapy in the treatment of anaplastic gliomas. A cooperative clinical trial. *J Neurosurg* **49**, 333-343, doi: 10.3171/jns.1978.49.3.0333.
119. Salazar OM, Rubin P, Feldstein ML & Pizzutiello R (1979) High dose radiation therapy in the treatment of malignant gliomas: final report. *International journal of radiation oncology, biology, physics* **5**, 1733-1740.
120. Karim AB, Afra D, Cornu P, Bleehan N, Schraub S, De Witte O, Darcel F, Stenning S, Pierart M & Van Glabbeke M (2002) Randomized trial on the efficacy of radiotherapy for cerebral low-grade glioma in the adult: European Organization for Research and Treatment of Cancer Study 22845 with the Medical Research Council study BRO4: an interim analysis. *International journal of radiation oncology, biology, physics* **52**, 316-324.
121. Douw L, Klein M, Fagel SS, van den Heuvel J, Taphoorn MJ, Aaronson NK, Postma TJ, Vandertop WP, Mooij JJ, Boerman RH, et al. (2009) Cognitive and

radiological effects of radiotherapy in patients with low-grade glioma: long-term follow-up. *Lancet Neurol* **8**, 810-818, doi: 10.1016/S1474-4422(09)70204-2.
122. Shaw E, Arusell R, Scheithauer B, O'Fallon J, O'Neill B, Dinapoli R, Nelson D, Earle J, Jones C, Cascino T, et al. (2002) Prospective randomized trial of low- versus high-dose radiation therapy in adults with supratentorial low-grade glioma: initial report of a North Central Cancer Treatment Group/Radiation Therapy Oncology Group/Eastern Cooperative Oncology Group study. *J Clin Oncol* **20**, 2267-2276.
123. Shapiro WR, Green SB, Burger PC, Mahaley MS, Jr., Selker RG, VanGilder JC, Robertson JT, Ransohoff J, Mealey J, Jr., Strike TA, et al. (1989) Randomized trial of three chemotherapy regimens and two radiotherapy regimens and two radiotherapy regimens in postoperative treatment of malignant glioma. Brain Tumor Cooperative Group Trial 8001. *J Neurosurg* **71**, 1-9, doi: 10.3171/jns.1989.71.1.0001.
124. Nelson SJ (2011) Assessment of therapeutic response and treatment planning for brain tumors using metabolic and physiological MRI. *NMR Biomed* **24**, 734-749, doi: 10.1002/nbm.1669.
125. Fine HA, Dear KB, Loeffler JS, Black PM & Canellos GP (1993) Meta-analysis of radiation therapy with and without adjuvant chemotherapy for malignant gliomas in adults. *Cancer* **71**, 2585-2597.
126. Levin VA, Silver P, Hannigan J, Wara WM, Gutin PH, Davis RL & Wilson CB (1990) Superiority of post-radiotherapy adjuvant chemotherapy with CCNU, procarbazine, and vincristine (PCV) over BCNU for anaplastic gliomas: NCOG 6G61 final report. *International journal of radiation oncology, biology, physics* **18**, 321-324.
127. Stupp R, Mason WP, van den Bent MJ, Weller M, Fisher B, Taphoorn MJ, Belanger K, Brandes AA, Marosi C, Bogdahn U, et al. (2005) Radiotherapy plus concomitant and adjuvant temozolomide for glioblastoma. *The New England journal of medicine* **352**, 987-996, doi: 10.1056/NEJMoa043330.
128. Friedman HS, Prados MD, Wen PY, Mikkelsen T, Schiff D, Abrey LE, Yung WK, Paleologos N, Nicholas MK, Jensen R, et al. (2009) Bevacizumab alone and in combination with irinotecan in recurrent glioblastoma. *Journal of clinical oncology : official journal of the American Society of Clinical Oncology* **27**, 4733-4740, doi: 10.1200/JCO.2008.19.8721.
129. Gilbert MR, Dignam JJ, Armstrong TS, Wefel JS, Blumenthal DT, Vogelbaum MA, Colman H, Chakravarti A, Pugh S, Won M, et al. (2014) A randomized trial of bevacizumab for newly diagnosed glioblastoma. *The New England journal of medicine* **370**, 699-708, doi: 10.1056/NEJMoa1308573.
130. Levin VA, Bidaut L, Hou P, Kumar AJ, Wefel JS, Bekele BN, Grewal J, Prabhu S, Loghin M, Gilbert MR, et al. (2011) Randomized double-blind placebo-controlled trial of bevacizumab therapy for radiation necrosis of the central nervous system. *Int J Radiat Oncol Biol Phys* **79**, 1487-1495, doi: 10.1016/j.ijrobp.2009.12.061.
131. Batchelor TT, Mulholland P, Neyns B, Nabors LB, Campone M, Wick A, Mason W, Mikkelsen T, Phuphanich S, Ashby LS, et al. (2013) Phase III randomized trial comparing the efficacy of cediranib as monotherapy, and in combination with lomustine, versus lomustine alone in patients with recurrent glioblastoma. *J Clin Oncol* **31**, 3212-3218, doi: 10.1200/JCO.2012.47.2464.
132. van den Bent MJ, Brandes AA, Rampling R, Kouwenhoven MC, Kros JM, Carpentier AF, Clement PM, Frenay M, Campone M, Baurain JF, et al. (2009) Randomized phase II trial of erlotinib versus temozolomide or carmustine in recurrent glioblastoma: EORTC brain tumor group study 26034. *J Clin Oncol* **27**, 1268-1274, doi: 10.1200/JCO.2008.17.5984.

133. Reardon DA, Egorin MJ, Quinn JA, Rich JN, Gururangan S, Vredenburgh JJ, Desjardins A, Sathornsumetee S, Provenzale JM, Herndon JE, 2nd, et al. (2005) Phase II study of imatinib mesylate plus hydroxyurea in adults with recurrent glioblastoma multiforme. *J Clin Oncol* **23**, 9359-9368, doi: 10.1200/JCO.2005.03.2185.
134. Chang SM, Wen P, Cloughesy T, Greenberg H, Schiff D, Conrad C, Fink K, Robins HI, De Angelis L, Raizer J, et al. (2005) Phase II study of CCI-779 in patients with recurrent glioblastoma multiforme. *Invest New Drugs* **23**, 357-361, doi: 10.1007/s10637-005-1444-0.
135. Chowdhary SA, Ryken T & Newton HB (2015) Survival outcomes and safety of carmustine wafers in the treatment of high-grade gliomas: a meta-analysis. *J Neurooncol* **122**, 367-382, doi: 10.1007/s11060-015-1724-2.
136. Warburg O (1956) On the origin of cancer cells. *Science* **123**, 309-314.
137. Vander Heiden MG, Cantley LC & Thompson CB (2009) Understanding the Warburg effect: the metabolic requirements of cell proliferation. *Science* **324**, 1029-1033, doi: 10.1126/science.1160809.
138. Ward PS & Thompson CB (2012) Metabolic reprogramming: a cancer hallmark even warburg did not anticipate. *Cancer Cell* **21**, 297-308, doi: 10.1016/j.ccr.2012.02.014.
139. Ben-Haim S & Ell P (2009) 18F-FDG PET and PET/CT in the evaluation of cancer treatment response. *J Nucl Med* **50**, 88-99, doi: 10.2967/jnumed.108.054205.
140. Higashi K, Ueda Y, Yagishita M, Arisaka Y, Sakurai A, Oguchi M, Seki H, Nambu Y, Tonami H & Yamamoto I (2000) FDG PET measurement of the proliferative potential of non-small cell lung cancer. *J Nucl Med* **41**, 85-92.
141. Jacob R, Welkoborsky HJ, Mann WJ, Jauch M & Amedee R (2001) [Fluorine-18]fluorodeoxyglucose positron emission tomography, DNA ploidy and growth fraction in squamous-cell carcinomas of the head and neck. *ORL J Otorhinolaryngol Relat Spec* **63**, 307-313, doi: 55764.
142. Avril N, Menzel M, Dose J, Schelling M, Weber W, Janicke F, Nathrath W & Schwaiger M (2001) Glucose metabolism of breast cancer assessed by 18F-FDG PET: histologic and immunohistochemical tissue analysis. *J Nucl Med* **42**, 9-16.
143. Kondoh H, Lleonart ME, Nakashima Y, Yokode M, Tanaka M, Bernard D, Gil J & Beach D (2007) A high glycolytic flux supports the proliferative potential of murine embryonic stem cells. *Antioxid Redox Signal* **9**, 293-299, doi: 10.1089/ars.2007.9.ft-14.
144. O'Neill LA & Hardie DG (2013) Metabolism of inflammation limited by AMPK and pseudo-starvation. *Nature* **493**, 346-355, doi: 10.1038/nature11862.
145. Trabold O, Wagner S, Wicke C, Scheuenstuhl H, Hussain MZ, Rosen N, Seremetiev A, Becker HD & Hunt TK (2003) Lactate and oxygen constitute a fundamental regulatory mechanism in wound healing. *Wound Repair Regen* **11**, 504-509.
146. Christofk HR, Vander Heiden MG, Harris MH, Ramanathan A, Gerszten RE, Wei R, Fleming MD, Schreiber SL & Cantley LC (2008) The M2 splice isoform of pyruvate kinase is important for cancer metabolism and tumour growth. *Nature* **452**, 230-233, doi: 10.1038/nature06734.
147. Dang L, White DW, Gross S, Bennett BD, Bittinger MA, Driggers EM, Fantin VR, Jang HG, Jin S, Keenan MC, et al. (2009) Cancer-associated IDH1 mutations produce 2-hydroxyglutarate. *Nature* **462**, 739-744, doi: 10.1038/nature08617.
148. Jones PA & Baylin SB (2007) The epigenomics of cancer. *Cell* **128**, 683-692, doi: 10.1016/j.cell.2007.01.029.
149. Feinberg AP & Vogelstein B (1983) Hypomethylation distinguishes genes of some human cancers from their normal counterparts. *Nature* **301**, 89-92.

150. Sandoval J & Esteller M (2012) Cancer epigenomics: beyond genomics. *Curr Opin Genet Dev* **22**, 50-55, doi: 10.1016/j.gde.2012.02.008.
151. Toyota M, Ahuja N, Ohe-Toyota M, Herman JG, Baylin SB & Issa JP (1999) CpG island methylator phenotype in colorectal cancer. *Proc Natl Acad Sci U S A* **96**, 8681-8686.
152. Wiench M, John S, Baek S, Johnson TA, Sung MH, Escobar T, Simmons CA, Pearce KH, Biddie SC, Sabo PJ, et al. (2011) DNA methylation status predicts cell type-specific enhancer activity. *Embo J* **30**, 3028-3039, doi: 10.1038/emboj.2011.210.
153. Riggs AD (1975) X inactivation, differentiation, and DNA methylation. *Cytogenet Cell Genet* **14**, 9-25.
154. Holliday R & Pugh JE (1975) DNA modification mechanisms and gene activity during development. *Science* **187**, 226-232.
155. Liang G, Chan MF, Tomigahara Y, Tsai YC, Gonzales FA, Li E, Laird PW & Jones PA (2002) Cooperativity between DNA methyltransferases in the maintenance methylation of repetitive elements. *Mol Cell Biol* **22**, 480-491.
156. Chen T, Ueda Y, Dodge JE, Wang Z & Li E (2003) Establishment and maintenance of genomic methylation patterns in mouse embryonic stem cells by Dnmt3a and Dnmt3b. *Mol Cell Biol* **23**, 5594-5605.
157. Li E, Bestor TH & Jaenisch R (1992) Targeted mutation of the DNA methyltransferase gene results in embryonic lethality. *Cell* **69**, 915-926.
158. Okano M, Bell DW, Haber DA & Li E (1999) DNA methyltransferases Dnmt3a and Dnmt3b are essential for de novo methylation and mammalian development. *Cell* **99**, 247-257.
159. Lorsbach RB, Moore J, Mathew S, Raimondi SC, Mukatira ST & Downing JR (2003) TET1, a member of a novel protein family, is fused to MLL in acute myeloid leukemia containing the t(10;11)(q22;q23). *Leukemia* **17**, 637-641, doi: 10.1038/sj.leu.2402834.
160. Ito S, D'Alessio AC, Taranova OV, Hong K, Sowers LC & Zhang Y (2010) Role of Tet proteins in 5mC to 5hmC conversion, ES-cell self-renewal and inner cell mass specification. *Nature* **466**, 1129-1133, doi: 10.1038/nature09303.
161. Tahiliani M, Koh KP, Shen Y, Pastor WA, Bandukwala H, Brudno Y, Agarwal S, Iyer LM, Liu DR, Aravind L, et al. (2009) Conversion of 5-methylcytosine to 5-hydroxymethylcytosine in mammalian DNA by MLL partner TET1. *Science* **324**, 930-935, doi: 10.1126/science.1170116.
162. Ito S, Shen L, Dai Q, Wu SC, Collins LB, Swenberg JA, He C & Zhang Y (2011) Tet proteins can convert 5-methylcytosine to 5-formylcytosine and 5-carboxylcytosine. *Science* **333**, 1300-1303, doi: 10.1126/science.1210597.
163. He YF, Li BZ, Li Z, Liu P, Wang Y, Tang Q, Ding J, Jia Y, Chen Z, Li L, et al. (2011) Tet-mediated formation of 5-carboxylcytosine and its excision by TDG in mammalian DNA. *Science* **333**, 1303-1307, doi: 10.1126/science.1210944.
164. Liutkeviciute Z, Kriukiene E, Licyte J, Rudyte M, Urbanaviciute G & Klimasauskas S (2014) Direct decarboxylation of 5-carboxylcytosine by DNA C5-methyltransferases. *J Am Chem Soc* **136**, 5884-5887, doi: 10.1021/ja5019223.
165. Jeltsch A & Jurkowska RZ (2014) New concepts in DNA methylation. *Trends Biochem Sci* **39**, 310-318, doi: 10.1016/j.tibs.2014.05.002.
166. Huang H, Sabari BR, Garcia BA, Allis CD & Zhao Y (2014) SnapShot: histone modifications. *Cell* **159**, 458-458 e451, doi: 10.1016/j.cell.2014.09.037.
167. Verrier L, Vandromme M & Trouche D (2011) Histone demethylases in chromatin cross-talks. *Biol Cell* **103**, 381-401, doi: 10.1042/BC20110028.
168. Zhou VW, Goren A & Bernstein BE (2011) Charting histone modifications and the functional organization of mammalian genomes. *Nat Rev Genet* **12**, 7-18, doi: 10.1038/nrg2905.

169. Shi Y, Lan F, Matson C, Mulligan P, Whetstine JR, Cole PA & Casero RA (2004) Histone demethylation mediated by the nuclear amine oxidase homolog LSD1. *Cell* **119**, 941-953, doi: 10.1016/j.cell.2004.12.012.
170. Karytinos A, Forneris F, Profumo A, Ciossani G, Battaglioli E, Binda C & Mattevi A (2009) A novel mammalian flavin-dependent histone demethylase. *J Biol Chem* **284**, 17775-17782, doi: 10.1074/jbc.M109.003087.
171. Kooistra SM & Helin K (2012) Molecular mechanisms and potential functions of histone demethylases. *Nat Rev Mol Cell Biol* **13**, 297-311, doi: 10.1038/nrm3327.
172. Loenarz C & Schofield CJ (2008) Expanding chemical biology of 2-oxoglutarate oxygenases. *Nat Chem Biol* **4**, 152-156, doi: 10.1038/nchembio0308-152.
173. Yap KL & Zhou MM (2010) Keeping it in the family: diverse histone recognition by conserved structural folds. *Crit Rev Biochem Mol Biol* **45**, 488-505, doi: 10.3109/10409238.2010.512001.
174. Huang Y, Fang J, Bedford MT, Zhang Y & Xu RM (2006) Recognition of histone H3 lysine-4 methylation by the double tudor domain of JMJD2A. *Science* **312**, 748-751, doi: 10.1126/science.1125162.
175. Wang J, Hevi S, Kurash JK, Lei H, Gay F, Bajko J, Su H, Sun W, Chang H, Xu G, et al. (2009) The lysine demethylase LSD1 (KDM1) is required for maintenance of global DNA methylation. *Nat Genet* **41**, 125-129, doi: 10.1038/ng.268.
176. Ciccone DN, Su H, Hevi S, Gay F, Lei H, Bajko J, Xu G, Li E & Chen T (2009) KDM1B is a histone H3K4 demethylase required to establish maternal genomic imprints. *Nature* **461**, 415-418, doi: 10.1038/nature08315.
177. Iwamori N, Zhao M, Meistrich ML & Matzuk MM (2011) The testis-enriched histone demethylase, KDM4D, regulates methylation of histone H3 lysine 9 during spermatogenesis in the mouse but is dispensable for fertility. *Biol Reprod* **84**, 1225-1234, doi: 10.1095/biolreprod.110.088955.
178. Takeuchi T, Yamazaki Y, Katoh-Fukui Y, Tsuchiya R, Kondo S, Motoyama J & Higashinakagawa T (1995) Gene trap capture of a novel mouse gene, jumonji, required for neural tube formation. *Genes Dev* **9**, 1211-1222.
179. Hanahan D & Weinberg RA (2011) Hallmarks of cancer: the next generation. *Cell* **144**, 646-674, doi: 10.1016/j.cell.2011.02.013.
180. Baylin SB & Jones PA (2011) A decade of exploring the cancer epigenome - biological and translational implications. *Nat Rev Cancer* **11**, 726-734, doi: 10.1038/nrc3130.
181. Hatziapostolou M & Iliopoulos D (2011) Epigenetic aberrations during oncogenesis. *Cell Mol Life Sci* **68**, 1681-1702, doi: 10.1007/s00018-010-0624-z.
182. You JS & Jones PA (2012) Cancer genetics and epigenetics: two sides of the same coin? *Cancer Cell* **22**, 9-20, doi: 10.1016/j.ccr.2012.06.008.
183. Kandoth C, McLellan MD, Vandin F, Ye K, Niu B, Lu C, Xie M, Zhang Q, McMichael JF, Wyczalkowski MA, et al. (2013) Mutational landscape and significance across 12 major cancer types. *Nature* **502**, 333-339, doi: 10.1038/nature12634.
184. Ley TJ, Ding L, Walter MJ, McLellan MD, Lamprecht T, Larson DE, Kandoth C, Payton JE, Baty J, Welch J, et al. (2010) DNMT3A mutations in acute myeloid leukemia. *N Engl J Med* **363**, 2424-2433, doi: 10.1056/NEJMoa1005143.
185. Trowbridge JJ & Orkin SH (2012) Dnmt3a silences hematopoietic stem cell self-renewal. *Nat Genet* **44**, 13-14, doi: 10.1038/ng.1043.
186. Challen GA, Sun D, Jeong M, Luo M, Jelinek J, Berg JS, Bock C, Vasanthakumar A, Gu H, Xi Y, et al. (2012) Dnmt3a is essential for hematopoietic stem cell differentiation. *Nat Genet* **44**, 23-31, doi: 10.1038/ng.1009.

187. Kanai Y, Ushijima S, Nakanishi Y, Sakamoto M & Hirohashi S (2003) Mutation of the DNA methyltransferase (DNMT) 1 gene in human colorectal cancers. *Cancer Lett* **192**, 75-82.
188. Shen H, Wang L, Spitz MR, Hong WK, Mao L & Wei Q (2002) A novel polymorphism in human cytosine DNA-methyltransferase-3B promoter is associated with an increased risk of lung cancer. *Cancer Res* **62**, 4992-4995.
189. Wu Y, Strawn E, Basir Z, Halverson G & Guo SW (2007) Aberrant expression of deoxyribonucleic acid methyltransferases DNMT1, DNMT3A, and DNMT3B in women with endometriosis. *Fertil Steril* **87**, 24-32, doi: 10.1016/j.fertnstert.2006.05.077.
190. Figueroa ME, Abdel-Wahab O, Lu C, Ward PS, Patel J, Shih A, Li Y, Bhagwat N, Vasanthakumar A, Fernandez HF, et al. (2010) Leukemic IDH1 and IDH2 mutations result in a hypermethylation phenotype, disrupt TET2 function, and impair hematopoietic differentiation. *Cancer Cell* **18**, 553-567, doi: 10.1016/j.ccr.2010.11.015.
191. Tan AY & Manley JL (2009) The TET family of proteins: functions and roles in disease. *J Mol Cell Biol* **1**, 82-92, doi: 10.1093/jmcb/mjp025.
192. Esteller M (2007) Cancer epigenomics: DNA methylomes and histone-modification maps. *Nat Rev Genet* **8**, 286-298, doi: 10.1038/nrg2005.
193. Ocker M & Schneider-Stock R (2007) Histone deacetylase inhibitors: signalling towards p21cip1/waf1. *Int J Biochem Cell Biol* **39**, 1367-1374, doi: 10.1016/j.biocel.2007.03.001.
194. Miremadi A, Oestergaard MZ, Pharoah PD & Caldas C (2007) Cancer genetics of epigenetic genes. *Hum Mol Genet* **16 Spec No 1**, R28-49, doi: 10.1093/hmg/ddm021.
195. Bhaskara S, Knutson SK, Jiang G, Chandrasekharan MB, Wilson AJ, Zheng S, Yenamandra A, Locke K, Yuan JL, Bonine-Summers AR, et al. (2010) Hdac3 is essential for the maintenance of chromatin structure and genome stability. *Cancer Cell* **18**, 436-447, doi: 10.1016/j.ccr.2010.10.022.
196. Slany RK (2009) The molecular biology of mixed lineage leukemia. *Haematologica* **94**, 984-993, doi: 10.3324/haematol.2008.002436.
197. Balgobind BV, Zwaan CM, Pieters R & Van den Heuvel-Eibrink MM (2011) The heterogeneity of pediatric MLL-rearranged acute myeloid leukemia. *Leukemia* **25**, 1239-1248, doi: 10.1038/leu.2011.90.
198. Morin RD, Mendez-Lago M, Mungall AJ, Goya R, Mungall KL, Corbett RD, Johnson NA, Severson TM, Chiu R, Field M, et al. (2011) Frequent mutation of histone-modifying genes in non-Hodgkin lymphoma. *Nature* **476**, 298-303, doi: 10.1038/nature10351.
199. Gui Y, Guo G, Huang Y, Hu X, Tang A, Gao S, Wu R, Chen C, Li X, Zhou L, et al. (2011) Frequent mutations of chromatin remodeling genes in transitional cell carcinoma of the bladder. *Nat Genet* **43**, 875-878, doi: 10.1038/ng.907.
200. Chase A & Cross NC (2011) Aberrations of EZH2 in cancer. *Clin Cancer Res* **17**, 2613-2618, doi: 10.1158/1078-0432.CCR-10-2156.
201. Tsang DP & Cheng AS (2011) Epigenetic regulation of signaling pathways in cancer: role of the histone methyltransferase EZH2. *J Gastroenterol Hepatol* **26**, 19-27, doi: 10.1111/j.1440-1746.2010.06447.x.
202. Varier RA & Timmers HT (2011) Histone lysine methylation and demethylation pathways in cancer. *Biochim Biophys Acta* **1815**, 75-89, doi: 10.1016/j.bbcan.2010.10.002.
203. Rotili D & Mai A (2011) Targeting Histone Demethylases: A New Avenue for the Fight against Cancer. *Genes Cancer* **2**, 663-679, doi: 10.1177/1947601911417976.

204. Seligson DB, Horvath S, Shi T, Yu H, Tze S, Grunstein M & Kurdistani SK (2005) Global histone modification patterns predict risk of prostate cancer recurrence. *Nature* **435**, 1262-1266, doi: 10.1038/nature03672.
205. Barlesi F, Giaccone G, Gallegos-Ruiz MI, Loundou A, Span SW, Lefesvre P, Kruyt FA & Rodriguez JA (2007) Global histone modifications predict prognosis of resected non small-cell lung cancer. *J Clin Oncol* **25**, 4358-4364, doi: 10.1200/JCO.2007.11.2599.
206. Benard A, Goossens-Beumer IJ, van Hoesel AQ, de Graaf W, Horati H, Putter H, Zeestraten EC, van de Velde CJ & Kuppen PJ (2014) Histone trimethylation at H3K4, H3K9 and H4K20 correlates with patient survival and tumor recurrence in early-stage colon cancer. *BMC Cancer* **14**, 531, doi: 10.1186/1471-2407-14-531.
207. Derissen EJ, Beijnen JH & Schellens JH (2013) Concise drug review: azacitidine and decitabine. *Oncologist* **18**, 619-624, doi: 10.1634/theoncologist.2012-0465.
208. Slingerland M, Guchelaar HJ & Gelderblom H (2014) Histone deacetylase inhibitors: an overview of the clinical studies in solid tumors. *Anticancer Drugs* **25**, 140-149, doi: 10.1097/CAD.0000000000000040.
209. Dhanak D & Jackson P (2014) Development and classes of epigenetic drugs for cancer. *Biochem Biophys Res Commun* **455**, 58-69, doi: 10.1016/j.bbrc.2014.07.006.
210. Locasale JW (2013) Serine, glycine and one-carbon units: cancer metabolism in full circle. *Nat Rev Cancer* **13**, 572-583, doi: 10.1038/nrc3557.
211. Wellen KE, Hatzivassiliou G, Sachdeva UM, Bui TV, Cross JR & Thompson CB (2009) ATP-citrate lyase links cellular metabolism to histone acetylation. *Science* **324**, 1076-1080, doi: 10.1126/science.1164097.
212. Yoshii Y, Furukawa T, Yoshii H, Mori T, Kiyono Y, Waki A, Kobayashi M, Tsujikawa T, Kudo T, Okazawa H, et al. (2009) Cytosolic acetyl-CoA synthetase affected tumor cell survival under hypoxia: the possible function in tumor acetyl-CoA/acetate metabolism. *Cancer Sci* **100**, 821-827.
213. Schug ZT, Peck B, Jones DT, Zhang Q, Grosskurth S, Alam IS, Goodwin LM, Smethurst E, Mason S, Blyth K, et al. (2015) Acetyl-CoA Synthetase 2 Promotes Acetate Utilization and Maintains Cancer Cell Growth under Metabolic Stress. *Cancer Cell* **27**, 57-71, doi: 10.1016/j.ccell.2014.12.002.
214. Lee JV, Carrer A, Shah S, Snyder NW, Wei S, Venneti S, Worth AJ, Yuan ZF, Lim HW, Liu S, et al. (2014) Akt-dependent metabolic reprogramming regulates tumor cell histone acetylation. *Cell Metab* **20**, 306-319, doi: 10.1016/j.cmet.2014.06.004.
215. Yang W, Xia Y, Hawke D, Li X, Liang J, Xing D, Aldape K, Hunter T, Alfred Yung WK & Lu Z (2012) PKM2 phosphorylates histone H3 and promotes gene transcription and tumorigenesis. *Cell* **150**, 685-696, doi: 10.1016/j.cell.2012.07.018.
216. Yang W, Xia Y, Ji H, Zheng Y, Liang J, Huang W, Gao X, Aldape K & Lu Z (2011) Nuclear PKM2 regulates beta-catenin transactivation upon EGFR activation. *Nature* **480**, 118-122, doi: 10.1038/nature10598.
217. Ulanovskaya OA, Zuhl AM & Cravatt BF (2013) NNMT promotes epigenetic remodeling in cancer by creating a metabolic methylation sink. *Nat Chem Biol* **9**, 300-306, doi: 10.1038/nchembio.1204.
218. Baysal BE, Ferrell RE, Willett-Brozick JE, Lawrence EC, Myssiorek D, Bosch A, van der Mey A, Taschner PE, Rubinstein WS, Myers EN, et al. (2000) Mutations in SDHD, a mitochondrial complex II gene, in hereditary paraganglioma. *Science* **287**, 848-851.

219. Gimm O, Armanios M, Dziema H, Neumann HP & Eng C (2000) Somatic and occult germ-line mutations in SDHD, a mitochondrial complex II gene, in nonfamilial pheochromocytoma. *Cancer Res* **60**, 6822-6825.
220. Niemann S & Muller U (2000) Mutations in SDHC cause autosomal dominant paraganglioma, type 3. *Nat Genet* **26**, 268-270, doi: 10.1038/81551.
221. Astuti D, Latif F, Dallol A, Dahia PL, Douglas F, George E, Skoldberg F, Husebye ES, Eng C & Maher ER (2001) Gene mutations in the succinate dehydrogenase subunit SDHB cause susceptibility to familial pheochromocytoma and to familial paraganglioma. *Am J Hum Genet* **69**, 49-54, doi: 10.1086/321282.
222. Burnichon N, Briere JJ, Libe R, Vescovo L, Riviere J, Tissier F, Jouanno E, Jeunemaitre X, Benit P, Tzagoloff A, et al. (2010) SDHA is a tumor suppressor gene causing paraganglioma. *Hum Mol Genet* **19**, 3011-3020, doi: 10.1093/hmg/ddq206.
223. Alam NA, Barclay E, Rowan AJ, Tyrer JP, Calonje E, Manek S, Kelsell D, Leigh I, Olpin S & Tomlinson IP (2005) Clinical features of multiple cutaneous and uterine leiomyomatosis: an underdiagnosed tumor syndrome. *Arch Dermatol* **141**, 199-206, doi: 10.1001/archderm.141.2.199.
224. Castro-Vega LJ, Buffet A, De Cubas AA, Cascon A, Menara M, Khalifa E, Amar L, Azriel S, Bourdeau I, Chabre O, et al. (2014) Germline mutations in FH confer predisposition to malignant pheochromocytomas and paragangliomas. *Hum Mol Genet* **23**, 2440-2446, doi: 10.1093/hmg/ddt639.
225. Xiao M, Yang H, Xu W, Ma S, Lin H, Zhu H, Liu L, Liu Y, Yang C, Xu Y, et al. (2012) Inhibition of alpha-KG-dependent histone and DNA demethylases by fumarate and succinate that are accumulated in mutations of FH and SDH tumor suppressors. *Genes Dev* **26**, 1326-1338, doi: 10.1101/gad.191056.112.
226. Selak MA, Armour SM, MacKenzie ED, Boulahbel H, Watson DG, Mansfield KD, Pan Y, Simon MC, Thompson CB & Gottlieb E (2005) Succinate links TCA cycle dysfunction to oncogenesis by inhibiting HIF-alpha prolyl hydroxylase. *Cancer Cell* **7**, 77-85, doi: 10.1016/j.ccr.2004.11.022.
227. Rakheja D, Konoplev S, Medeiros LJ & Chen W (2012) IDH mutations in acute myeloid leukemia. *Hum Pathol* **43**, 1541-1551, doi: 10.1016/j.humpath.2012.05.003.
228. Zou P, Xu H, Chen P, Yan Q, Zhao L, Zhao P & Gu A (2013) IDH1/IDH2 mutations define the prognosis and molecular profiles of patients with gliomas: a meta-analysis. *PLoS One* **8**, e68782, doi: 10.1371/journal.pone.0068782.
229. Borger DR, Goyal L, Yau T, Poon RT, Ancukiewicz M, Deshpande V, Christiani DC, Liebman HM, Yang H, Kim H, et al. (2014) Circulating oncometabolite 2-hydroxyglutarate is a potential surrogate biomarker in patients with isocitrate dehydrogenase-mutant intrahepatic cholangiocarcinoma. *Clin Cancer Res* **20**, 1884-1890, doi: 10.1158/1078-0432.CCR-13-2649.
230. Amary MF, Bacsi K, Maggiani F, Damato S, Halai D, Berisha F, Pollock R, O'Donnell P, Grigoriadis A, Diss T, et al. (2011) IDH1 and IDH2 mutations are frequent events in central chondrosarcoma and central and periosteal chondromas but not in other mesenchymal tumours. *J Pathol* **224**, 334-343, doi: 10.1002/path.2913.
231. Bleeker FE, Atai NA, Lamba S, Jonker A, Rijkeboer D, Bosch KS, Tigchelaar W, Troost D, Vandertop WP, Bardelli A, et al. (2010) The prognostic IDH1(R132) mutation is associated with reduced NADP+-dependent IDH activity in glioblastoma. *Acta Neuropathol* **119**, 487-494, doi: 10.1007/s00401-010-0645-6.
232. Shi J, Zuo H, Ni L, Xia L, Zhao L, Gong M, Nie D, Gong P, Cui D, Shi W, et al. (2014) An IDH1 mutation inhibits growth of glioma cells via GSH depletion and ROS generation. *Neurol Sci* **35**, 839-845, doi: 10.1007/s10072-013-1607-2.

233. Menon SG & Goswami PC (2007) A redox cycle within the cell cycle: ring in the old with the new. *Oncogene* **26**, 1101-1109, doi: 10.1038/sj.onc.1209895.
234. Zhang Z, Leonard SS, Huang C, Vallyathan V, Castranova V & Shi X (2003) Role of reactive oxygen species and MAPKs in vanadate-induced G(2)/M phase arrest. *Free Radic Biol Med* **34**, 1333-1342.
235. Baldewpersad Tewarie NM, Burgers IA, Dawood Y, den Boon HC, den Brok MG, Klunder JH, Koopmans KB, Rademaker E, van den Broek HB, van den Bersselaar SM, et al. (2013) NADP+ -dependent IDH1 R132 mutation and its relevance for glioma patient survival. *Med Hypotheses* **80**, 728-731, doi: 10.1016/j.mehy.2013.02.022.
236. Reitman ZJ, Jin G, Karoly ED, Spasojevic I, Yang J, Kinzler KW, He Y, Bigner DD, Vogelstein B & Yan H (2011) Profiling the effects of isocitrate dehydrogenase 1 and 2 mutations on the cellular metabolome. *Proc Natl Acad Sci U S A* **108**, 3270-3275, doi: 10.1073/pnas.1019393108.
237. Ohka F, Ito M, Ranjit M, Senga T, Motomura A, Motomura K, Saito K, Kato K, Kato Y, Wakabayashi T, et al. (2014) Quantitative metabolome analysis profiles activation of glutaminolysis in glioma with IDH1 mutation. *Tumour Biol* **35**, 5911-5920, doi: 10.1007/s13277-014-1784-5.
238. Wise DR & Thompson CB (2010) Glutamine addiction: a new therapeutic target in cancer. *Trends Biochem Sci* **35**, 427-433, doi: 10.1016/j.tibs.2010.05.003.
239. Seltzer MJ, Bennett BD, Joshi AD, Gao P, Thomas AG, Ferraris DV, Tsukamoto T, Rojas CJ, Slusher BS, Rabinowitz JD, et al. (2010) Inhibition of glutaminase preferentially slows growth of glioma cells with mutant IDH1. *Cancer Res* **70**, 8981-8987, doi: 10.1158/0008-5472.CAN-10-1666.
240. de Groot J & Sontheimer H (2011) Glutamate and the biology of gliomas. *Glia* **59**, 1181-1189, doi: 10.1002/glia.21113.
241. de Groot JF, Liu TJ, Fuller G & Yung WK (2005) The excitatory amino acid transporter-2 induces apoptosis and decreases glioma growth in vitro and in vivo. *Cancer Res* **65**, 1934-1940, doi: 10.1158/0008-5472.CAN-04-3626.
242. van Lith SA, Navis AC, Verrijp K, Niclou SP, Bjerkvig R, Wesseling P, Tops B, Molenaar R, van Noorden CJ & Leenders WP (2014) Glutamate as chemotactic fuel for diffuse glioma cells: are they glutamate suckers? *Biochim Biophys Acta* **1846**, 66-74, doi: 10.1016/j.bbcan.2014.04.004.
243. Navis AC, Niclou SP, Fack F, Stieber D, van Lith S, Verrijp K, Wright A, Stauber J, Tops B, Otte-Holler I, et al. (2013) Increased mitochondrial activity in a novel IDH1-R132H mutant human oligodendroglioma xenograft model: in situ detection of 2-HG and alpha-KG. *Acta Neuropathol Commun* **1**, 18, doi: 10.1186/2051-5960-1-18.
244. Thompson JA, Miles BS & Fennessey PV (1977) Urinary organic acids quantitated by age groups in a healthy pediatric population. *Clin Chem* **23**, 1734-1738.
245. Xu W, Yang H, Liu Y, Yang Y, Wang P, Kim SH, Ito S, Yang C, Xiao MT, Liu LX, et al. (2011) Oncometabolite 2-hydroxyglutarate is a competitive inhibitor of alpha-ketoglutarate-dependent dioxygenases. *Cancer Cell* **19**, 17-30, doi: 10.1016/j.ccr.2010.12.014.
246. van der Knaap MS, Jakobs C, Hoffmann GF, Duran M, Muntau AC, Schweitzer S, Kelley RI, Parrot-Roulaud F, Amiel J, De Lonlay P, et al. (1999) D-2-hydroxyglutaric aciduria: further clinical delineation. *J Inherit Metab Dis* **22**, 404-413.
247. Barth PG, Hoffmann GF, Jaeken J, Wanders RJ, Duran M, Jansen GA, Jakobs C, Lehnert W, Hanefeld F, Valk J, et al. (1993) L-2-hydroxyglutaric

acidaemia: clinical and biochemical findings in 12 patients and preliminary report on L-2-hydroxyacid dehydrogenase. *J Inherit Metab Dis* **16**, 753-761.
248. Van Schaftingen E, Rzem R & Veiga-da-Cunha M (2009) L: -2-Hydroxyglutaric aciduria, a disorder of metabolite repair. *J Inherit Metab Dis* **32**, 135-142, doi: 10.1007/s10545-008-1042-3.
249. Kardon T, Noel G, Vertommen D & Schaftingen EV (2006) Identification of the gene encoding hydroxyacid-oxoacid transhydrogenase, an enzyme that metabolizes 4-hydroxybutyrate. *FEBS Lett* **580**, 2347-2350, doi: 10.1016/j.febslet.2006.02.082.
250. Majmundar AJ, Wong WJ & Simon MC (2010) Hypoxia-inducible factors and the response to hypoxic stress. *Mol Cell* **40**, 294-309, doi: 10.1016/j.molcel.2010.09.022.
251. Isaacs JS, Jung YJ, Mole DR, Lee S, Torres-Cabala C, Chung YL, Merino M, Trepel J, Zbar B, Toro J, et al. (2005) HIF overexpression correlates with biallelic loss of fumarate hydratase in renal cancer: novel role of fumarate in regulation of HIF stability. *Cancer Cell* **8**, 143-153, doi: 10.1016/j.ccr.2005.06.017.
252. Zhao S, Lin Y, Xu W, Jiang W, Zha Z, Wang P, Yu W, Li Z, Gong L, Peng Y, et al. (2009) Glioma-derived mutations in IDH1 dominantly inhibit IDH1 catalytic activity and induce HIF-1alpha. *Science* **324**, 261-265, doi: 10.1126/science.1170944.
253. Williams SC, Karajannis MA, Chiriboga L, Golfinos JG, von Deimling A & Zagzag D (2011) R132H-mutation of isocitrate dehydrogenase-1 is not sufficient for HIF-1alpha upregulation in adult glioma. *Acta Neuropathol* **121**, 279-281, doi: 10.1007/s00401-010-0790-y.
254. Koivunen P, Lee S, Duncan CG, Lopez G, Lu G, Ramkissoon S, Losman JA, Joensuu P, Bergmann U, Gross S, et al. (2012) Transformation by the (R)-enantiomer of 2-hydroxyglutarate linked to EGLN activation. *Nature* **483**, 484-488, doi: 10.1038/nature10898.
255. Turcan S, Rohle D, Goenka A, Walsh LA, Fang F, Yilmaz E, Campos C, Fabius AW, Lu C, Ward PS, et al. (2012) IDH1 mutation is sufficient to establish the glioma hypermethylator phenotype. *Nature* **483**, 479-483, doi: 10.1038/nature10866.
256. Duncan CG, Barwick BG, Jin G, Rago C, Kapoor-Vazirani P, Powell DR, Chi JT, Bigner DD, Vertino PM & Yan H (2012) A heterozygous IDH1R132H/WT mutation induces genome-wide alterations in DNA methylation. *Genome Res* **22**, 2339-2355, doi: 10.1101/gr.132738.111.
257. Wang P, Dong Q, Zhang C, Kuan PF, Liu Y, Jeck WR, Andersen JB, Jiang W, Savich GL, Tan TX, et al. (2013) Mutations in isocitrate dehydrogenase 1 and 2 occur frequently in intrahepatic cholangiocarcinomas and share hypermethylation targets with glioblastomas. *Oncogene* **32**, 3091-3100, doi: 10.1038/onc.2012.315.
258. Letouze E, Martinelli C, Loriot C, Burnichon N, Abermil N, Ottolenghi C, Janin M, Menara M, Nguyen AT, Benit P, et al. (2013) SDH mutations establish a hypermethylator phenotype in paraganglioma. *Cancer Cell* **23**, 739-752, doi: 10.1016/j.ccr.2013.04.018.
259. Losman JA, Looper RE, Koivunen P, Lee S, Schneider RK, McMahon C, Cowley GS, Root DE, Ebert BL & Kaelin WG, Jr. (2013) (R)-2-hydroxyglutarate is sufficient to promote leukemogenesis and its effects are reversible. *Science* **339**, 1621-1625, doi: 10.1126/science.1231677.
260. Chowdhury R, Yeoh KK, Tian YM, Hillringhaus L, Bagg EA, Rose NR, Leung IK, Li XS, Woon EC, Yang M, et al. (2011) The oncometabolite 2-hydroxyglutarate

inhibits histone lysine demethylases. *EMBO Rep* **12**, 463-469, doi: 10.1038/embor.2011.43.
261. Lu C, Ward PS, Kapoor GS, Rohle D, Turcan S, Abdel-Wahab O, Edwards CR, Khanin R, Figueroa ME, Melnick A, et al. (2012) IDH mutation impairs histone demethylation and results in a block to cell differentiation. *Nature* **483**, 474-478, doi: 10.1038/nature10860.
262. Venneti S, Felicella MM, Coyne T, Phillips JJ, Gorovets D, Huse JT, Kofler J, Lu C, Tihan T, Sullivan LM, et al. (2013) Histone 3 lysine 9 trimethylation is differentially associated with isocitrate dehydrogenase mutations in oligodendrogliomas and high-grade astrocytomas. *J Neuropathol Exp Neurol* **72**, 298-306, doi: 10.1097/NEN.0b013e3182898113.
263. Cedar H & Bergman Y (2009) Linking DNA methylation and histone modification: patterns and paradigms. *Nat Rev Genet* **10**, 295-304, doi: 10.1038/nrg2540.
264. Terunuma A, Putluri N, Mishra P, Mathe EA, Dorsey TH, Yi M, Wallace TA, Issaq HJ, Zhou M, Killian JK, et al. (2014) MYC-driven accumulation of 2-hydroxyglutarate is associated with breast cancer prognosis. *J Clin Invest* **124**, 398-412, doi: 10.1172/JCI71180.
265. Fan J, Teng X, Liu L, Mattaini KR, Looper RE, Vander Heiden MG & Rabinowitz JD (2014) Human Phosphoglycerate Dehydrogenase Produces the Oncometabolite d-2-Hydroxyglutarate. *ACS Chem Biol*, doi: 10.1021/cb500683c.
266. Nam H, Campodonico M, Bordbar A, Hyduke DR, Kim S, Zielinski DC & Palsson BO (2014) A systems approach to predict oncometabolites via context-specific genome-scale metabolic networks. *PLoS Comput Biol* **10**, e1003837, doi: 10.1371/journal.pcbi.1003837.
267. Andronesi OC, Rapalino O, Gerstner E, Chi A, Batchelor TT, Cahill DP, Sorensen AG & Rosen BR (2013) Detection of oncogenic IDH1 mutations using magnetic resonance spectroscopy of 2-hydroxyglutarate. *J Clin Invest* **123**, 3659-3663, doi: 10.1172/JCI67229.
268. Bertolino N, Marchionni C, Ghielmetti F, Burns B, Finocchiaro G, Anghileri E, Bruzzone MG & Minati L (2014) Accuracy of 2-hydroxyglutarate quantification by short-echo proton-MRS at 3 T: a phantom study. *Phys Med* **30**, 702-707, doi: 10.1016/j.ejmp.2014.03.002.
269. Rohle D, Popovici-Muller J, Palaskas N, Turcan S, Grommes C, Campos C, Tsoi J, Clark O, Oldrini B, Komisopoulou E, et al. (2013) An inhibitor of mutant IDH1 delays growth and promotes differentiation of glioma cells. *Science* **340**, 626-630, doi: 10.1126/science.1236062.
270. Wang F, Travins J, DeLaBarre B, Penard-Lacronique V, Schalm S, Hansen E, Straley K, Kernytsky A, Liu W, Gliser C, et al. (2013) Targeted inhibition of mutant IDH2 in leukemia cells induces cellular differentiation. *Science* **340**, 622-626, doi: 10.1126/science.1234769.
271. Kernytsky A, Wang F, Hansen E, Schalm S, Straley K, Gliser C, Yang H, Travins J, Murray S, Dorsch M, et al. (2014) IDH2 mutation induced histone and DNA hypermethylation is progressively reversed by small molecule inhibition. *Blood*, doi: 10.1182/blood-2013-10-533604.
272. Bralten LB, Kloosterhof NK, Balvers R, Sacchetti A, Lapre L, Lamfers M, Leenstra S, de Jonge H, Kros JM, Jansen EE, et al. (2011) IDH1 R132H decreases proliferation of glioma cell lines in vitro and in vivo. *Ann Neurol* **69**, 455-463, doi: 10.1002/ana.22390.
273. Tonjes M, Barbus S, Park YJ, Wang W, Schlotter M, Lindroth AM, Pleier SV, Bai AH, Karra D, Piro RM, et al. (2013) BCAT1 promotes cell proliferation through amino acid catabolism in gliomas carrying wild-type IDH1. *Nat Med* **19**, 901-908, doi: 10.1038/nm.3217.

274. Schmidt D, Wilson MD, Spyrou C, Brown GD, Hadfield J & Odom DT (2009) ChIP-seq: using high-throughput sequencing to discover protein-DNA interactions. *Methods* **48**, 240-248, doi: 10.1016/j.ymeth.2009.03.001.
275. Wen PY & Kesari S (2008) Malignant gliomas in adults. *N Engl J Med* **359**, 492-507, doi: 10.1056/NEJMra0708126.
276. Pietschmann S, von Bueren AO, Kerber MJ, Baumert BG, Kortmann RD & Muller K (2015) An individual patient data meta-analysis on characteristics, treatments and outcomes of glioblastoma/ gliosarcoma patients with metastases outside of the central nervous system. *PLoS One* **10**, e0121592, doi: 10.1371/journal.pone.0121592.
277. Siemkowicz E, Hansen AJ & Gjedde A (1982) Hyperglycemic ischemia of rat brain: the effect of post-ischemic insulin on metabolic rate. *Brain Res* **243**, 386-390.
278. Fukami T & Yokoi T (2012) The emerging role of human esterases. *Drug Metab Pharmacokinet* **27**, 466-477.
279. Lee EK, Song KA, Chae JH, Kim KM, Kim SH & Kang MS (2015) GAGE12 mediates human gastric carcinoma growth and metastasis. *Int J Cancer* **136**, 2284-2292, doi: 10.1002/ijc.29286.
280. Besse A, Wu P, Bruni F, Donti T, Graham BH, Craigen WJ, McFarland R, Moretti P, Lalani S, Scott KL, et al. (2015) The GABA transaminase, ABAT, is essential for mitochondrial nucleoside metabolism. *Cell Metab* **21**, 417-427, doi: 10.1016/j.cmet.2015.02.008.
281. Yang B, Zhong C, Peng Y, Lai Z & Ding J (2010) Molecular mechanisms of "off-on switch" of activities of human IDH1 by tumor-associated mutation R132H. *Cell Res* **20**, 1188-1200, doi: 10.1038/cr.2010.145.
282. Buescher JM, Antoniewicz MR, Boros LG, Burgess SC, Brunengraber H, Clish CB, DeBerardinis RJ, Feron O, Frezza C, Ghesquiere B, et al. (2015) A roadmap for interpreting (13)C metabolite labeling patterns from cells. *Curr Opin Biotechnol* **34**, 189-201, doi: 10.1016/j.copbio.2015.02.003.
283. Rhodes DR, Yu J, Shanker K, Deshpande N, Varambally R, Ghosh D, Barrette T, Pandey A & Chinnaiyan AM (2004) ONCOMINE: a cancer microarray database and integrated data-mining platform. *Neoplasia* **6**, 1-6.
284. Fatemi SH, Folsom TD, Rooney RJ & Thuras PD (2013) Expression of GABAA alpha2-, beta1- and epsilon-receptors are altered significantly in the lateral cerebellum of subjects with schizophrenia, major depression and bipolar disorder. *Transl Psychiatry* **3**, e303, doi: 10.1038/tp.2013.64.
285. Liu X, Wang Q, Haydar TF & Bordey A (2005) Nonsynaptic GABA signaling in postnatal subventricular zone controls proliferation of GFAP-expressing progenitors. *Nat Neurosci* **8**, 1179-1187, doi: 10.1038/nn1522.
286. Labrakakis C, Patt S, Hartmann J & Kettenmann H (1998) Functional GABA(A) receptors on human glioma cells. *The European journal of neuroscience* **10**, 231-238.
287. Huang H, Lin S, Garcia BA & Zhao Y (2015) Quantitative proteomic analysis of histone modifications. *Chem Rev* **115**, 2376-2418, doi: 10.1021/cr500491u.
288. Laurie DJ, Seeburg PH & Wisden W (1992) The distribution of 13 GABAA receptor subunit mRNAs in the rat brain. II. Olfactory bulb and cerebellum. *J Neurosci* **12**, 1063-1076.
289. Labrakakis C, Patt S, Hartmann J & Kettenmann H (1998) Functional GABA(A) receptors on human glioma cells. *Eur J Neurosci* **10**, 231-238.
290. Synowitz M, Ahmann P, Matyash M, Kuhn SA, Hofmann B, Zimmer C, Kirchhoff F, Kiwit JC & Kettenmann H (2001) GABA(A)-receptor expression in glioma cells is triggered by contact with neuronal cells. *Eur J Neurosci* **14**, 1294-1302.

291. D'Urso PI, D'Urso OF, Storelli C, Mallardo M, Gianfreda CD, Montinaro A, Cimmino A, Pietro C & Marsigliante S (2012) miR-155 is up-regulated in primary and secondary glioblastoma and promotes tumour growth by inhibiting GABA receptors. *Int J Oncol* **41**, 228-234, doi: 10.3892/ijo.2012.1420.
292. Sengupta S, Weeraratne SD, Sun H, Phallen J, Rallapalli SK, Teider N, Kosaras B, Amani V, Pierre-Francois J, Tang Y, et al. (2014) alpha5-GABAA receptors negatively regulate MYC-amplified medulloblastoma growth. *Acta Neuropathol* **127**, 593-603, doi: 10.1007/s00401-013-1205-7.
293. Andang M, Hjerling-Leffler J, Moliner A, Lundgren TK, Castelo-Branco G, Nanou E, Pozas E, Bryja V, Halliez S, Nishimaru H, et al. (2008) Histone H2AX-dependent GABA(A) receptor regulation of stem cell proliferation. *Nature* **451**, 460-464, doi: 10.1038/nature06488.
294. Venkatesh HS, Johung TB, Caretti V, Noll A, Tang Y, Nagaraja S, Gibson EM, Mount CW, Polepalli J, Mitra SS, et al. (2015) Neuronal Activity Promotes Glioma Growth through Neuroligin-3 Secretion. *Cell* **161**, 803-816, doi: 10.1016/j.cell.2015.04.012.
295. Giachino C, Barz M, Tchorz JS, Tome M, Gassmann M, Bischofberger J, Bettler B & Taylor V (2014) GABA suppresses neurogenesis in the adult hippocampus through GABAB receptors. *Development* **141**, 83-90, doi: 10.1242/dev.102608.
296. Magnaghi V, Ballabio M, Cavarretta IT, Froestl W, Lambert JJ, Zucchi I & Melcangi RC (2004) GABAB receptors in Schwann cells influence proliferation and myelin protein expression. *Eur J Neurosci* **19**, 2641-2649, doi: 10.1111/j.0953-816X.2004.03368.x.
297. Barakat L & Bordey A (2002) GAT-1 and reversible GABA transport in Bergmann glia in slices. *J Neurophysiol* **88**, 1407-1419.